TRAUMATIC BRAIN INJURY: A BINDING CONDITION IN SEARCH OF SOLUTIONS

Maryam Chahin

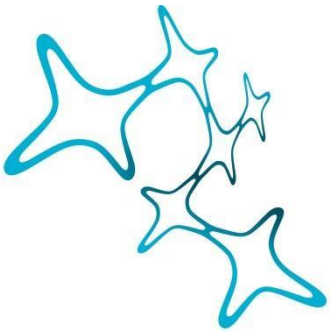

Graduate School of Systemic Neurosciences

LMU Munich

Dissertation der

Graduate School of Systemic Neurosciences der

Ludwig-Maximilians-Universität München

July, 2024

Supervisor
PD. Dr. Florence M. Bareyre
Institute of Clinical Neuroimmunology
Ludwig-Maximilians-Universität München

First Reviewer: PD. Dr. Florence M. Bareyre
Second Reviewer: Prof. Dr. Arthur Liesz
Date of Submission: 02/07/2024
Date of Defense: 14/02/2025

TABLE OF CONTENTS

Abstract

Traumatic brain injury (TBI) is a current economical and societal burden affecting around 70 million individuals worldwide. Traumatic brain injury is categorised in different severity level, being mild, moderate and severe, mild traumatic brain injury (mild TBI) representing 80% of all TBI cases. The heterogeneity displayed by patient undergoing a TBI has made it difficult for the clinician as well as for the scientist to give the appropriate diagnosis and care and develop the adequate therapy and treatment to alleviate the impact of such a trauma.

Moderate and severe TBI, which are invasive injury, are rather straightforward in the display of their repercussion as compared to mild TBI (or concussion) which have displayed no macroscopic changes but rather specific microscopic alterations. Behavioural impairments have also been detected and the extent of the impairments is dependent on the injury severity level. In this thesis, we will tackle different aspects of TBI and investigate the consequences and mechanisms of TBI.

In the first study of this thesis, I introduce an innovative automated analysis tool named Automated Limb Motion Analysis (ALMA), tailored for evaluating locomotion and paw placement in mice afflicted with various neurological disorders. ALMA uses pose estimation derived from DeepLabCut with a user-friendly graphical interface to automate the computation of kinematic parameters, footfall detection, kinematic data analysis, and visualization of gait kinematics. Interestingly, in this study, we used ALMA to analyze, among others, motor dysfunction following TBI. While motor dysfunction is always difficult to quantify following TBI, ALMA allows an in-depth access to gait parameters and can capture small but important impairments and recovery following trauma to the brain.

The second study of my thesis delves into the intricate structural and functional changes occurring in the contralesional cortex following TBI. Despite initial neuronal cell loss and circuit disruption leading to behavioural and cognitive deficits, both clinical observations and animal models indicate a potential for spontaneous recovery, implicating neuronal circuit plasticity. In order to clarify the circuit rearrangements occurring in the contralesional cortex after traumatic brain injury (TBI), the study uses a comprehensive methodology that combines selective labelling of neuronal subpopulations, structural and functional in vivo imaging techniques, and mono-synaptic circuit tracing approaches. Results highlight specific adaptations of callosal neurons and their input circuits, shedding light on the mechanisms underlying cortical plasticity and recovery following TBI. This investigation not only advances our understanding of cortical plasticity but also provides crucial insights into potential therapeutic targets for enhancing recovery mechanisms in TBI patients.

Concussive injuries represent the majority of TBI and pose a significant health risk to the victims. While symptoms often dissipate shortly after a single impact, repetitive concussions, particularly prevalent in sports, lead to enduring acute and chronic deficits. This third and last study

aimed to establish a mouse model of concussive head injury to examine differences in behaviour and anatomy between single and repetitive injuries. Our results demonstrate that the consequences of a single concussion in term of synaptic changes or microglial structure and function are less severe than following repetitive injury. In particular, I showed that repetitive concussions result in a specific cortical and hippocampal loss of excitatory synapses, below the concussion site, associated to a chronic heightened microglial activation and increased engulfment of presynaptic excitatory synapses. These alterations coincide with a temporary deterioration in spatial memory followed by changes in fear and anxiety-related behaviours. This study underscores the significance of concussion repetition in initiating pathological processes affecting excitatory synapses, attributed to enhanced microglial engulfment function.

By integrating the findings from these three studies, my thesis offers a comprehensive understanding of behavioral deficits, cortical plasticity, mechanisms initiating the impairments following different severity of TBIs.

Zusammenfassung

(Übersetzt mit DeepL.com)

Traumatische Hirnverletzungen (TBI) stellen derzeit eine wirtschaftliche und gesellschaftliche Belastung dar, von der weltweit etwa 70 Millionen Menschen betroffen sind. Traumatische Hirnverletzungen werden in verschiedene Schweregrade eingeteilt: leicht, mittelschwer und schwer, wobei 80 % aller Fälle von traumatischen Hirnverletzungen auf leichte Verletzungen entfallen. Die Heterogenität der Patienten, die ein Schädel-Hirn-Trauma erleiden, macht es sowohl dem Arzt als auch dem Wissenschaftler schwer, eine angemessene Diagnose und Behandlung zu stellen und eine geeignete Therapie und Behandlung zu entwickeln, um die Auswirkungen eines solchen Traumas zu lindern.

Mittelschwere und schwere Schädel-Hirn-Traumata, bei denen es sich um invasive Verletzungen handelt, sind im Vergleich zu leichten Schädel-Hirn-Traumata (oder Gehirnerschütterungen), bei denen keine makroskopischen Veränderungen, sondern eher spezifische mikroskopische Veränderungen zu beobachten sind, eher eindeutig in ihrer Auswirkung. Auch Verhaltensstörungen wurden festgestellt, wobei das Ausmaß der Beeinträchtigungen vom Schweregrad der Verletzung abhängt. In dieser Arbeit werden wir uns mit verschiedenen Aspekten von Schädel-Hirn-Traumata beschäftigen und die Folgen und Mechanismen von Schädel-Hirn-Traumata untersuchen.

In der ersten Studie dieser Arbeit stelle ich ein innovatives automatisches Analysewerkzeug namens Automated Limb Motion Analysis (ALMA) vor, das auf die Bewertung der Fortbewegung und der Pfotenplatzierung bei Mäusen mit verschiedenen neurologischen Störungen zugeschnitten ist. ALMA verwendet eine von DeepLabCut abgeleitete Posenschätzung mit einer benutzerfreundlichen grafischen Oberfläche, um die Berechnung kinematischer Parameter, die Erkennung von Tritten, die kinematische Datenanalyse und die Visualisierung der Gangkinematik zu automatisieren. Interessanterweise haben wir in dieser Studie ALMA unter anderem zur Analyse der motorischen Dysfunktion nach einer Schädel-Hirn-Trauma eingesetzt. Während motorische Dysfunktionen nach einem Schädel-Hirn-Trauma immer schwierig zu quantifizieren sind, ermöglicht ALMA einen detaillierten Zugang zu Gangparametern und kann kleine, aber wichtige Beeinträchtigungen und die Erholung nach einem Schädel-Hirn-Trauma erfassen.

Die zweite Studie meiner Dissertation befasst sich mit den komplizierten strukturellen und funktionellen Veränderungen, die im kontraläsionalen Kortex nach einem Schädel-Hirn-Trauma auftreten. Trotz des anfänglichen neuronalen Zellverlusts und der Unterbrechung des Schaltkreises, die zu Verhaltens- und kognitiven Defiziten führen, deuten sowohl klinische Beobachtungen als auch Tiermodelle auf ein Potenzial zur spontanen Erholung hin, was auf die Plastizität des neuronalen Schaltkreises schließen lässt. Die Studie verfolgt einen umfassenden Ansatz, der strukturelle und

funktionelle In-vivo-Bildgebungstechniken, selektive Markierung neuronaler Subpopulationen und Methoden zur monosynaptischen Verfolgung von Schaltkreisen kombiniert, um die im kontraläsionalen Kortex nach einer Schädel-Hirn-Trauma stattfindenden Schaltkreisumstrukturierungen zu klären. Die Ergebnisse heben spezifische Anpassungen der kallosalen Neuronen und ihrer Eingangsschaltkreise hervor und werfen ein Licht auf die Mechanismen, die der kortikalen Plastizität und Erholung nach einer Schädel-Hirn-Trauma zugrunde liegen. Diese Untersuchung trägt nicht nur zu einem besseren Verständnis der kortikalen Plastizität bei, sondern liefert auch wichtige Erkenntnisse über potenzielle therapeutische Ziele zur Verbesserung der Erholungsmechanismen bei Patienten mit Schädel-Hirn-Trauma.

Gehirnerschütterungen machen den Großteil der Schädel-Hirn-Traumata aus und stellen ein erhebliches Gesundheitsrisiko für die Opfer dar. Während die Symptome oft kurz nach einem einmaligen Aufprall abklingen, führen wiederholte Gehirnerschütterungen, die vor allem im Sport vorkommen, zu dauerhaften akuten und chronischen Defiziten. Ziel dieser dritten und letzten Studie war es, ein Mausmodell für Gehirnerschütterungen zu etablieren, um Unterschiede im Verhalten und in der Anatomie zwischen einmaligen und wiederholten Verletzungen zu untersuchen. Unsere Ergebnisse zeigen, dass die Folgen einer einmaligen Gehirnerschütterung in Bezug auf synaptische Veränderungen oder Mikroglia-Struktur und -Funktion weniger schwerwiegend sind als nach wiederholten Verletzungen. Insbesondere konnte ich zeigen, dass wiederholte Gehirnerschütterungen zu einem spezifischen kortikalen und hippocampalen Verlust an erregenden Synapsen unterhalb der Erschütterungsstellen führen, der mit einer chronisch erhöhten Mikrogliaaktivierung und einer verstärkten Verschlingung präsynaptischer erregender Synapsen einhergeht. Diese Veränderungen gehen mit einer vorübergehenden Verschlechterung des räumlichen Gedächtnisses einher, gefolgt von Veränderungen bei Angst und angstbezogenem Verhalten. Diese Studie unterstreicht die Bedeutung der Wiederholung einer Gehirnerschütterung bei der Auslösung pathologischer Prozesse, die exzitatorische Synapsen betreffen und auf eine verstärkte mikrogliale Verschlingungsfunktion zurückzuführen sind.

Durch die Integration der Ergebnisse dieser drei Studien bietet meine Arbeit ein umfassendes Verständnis der Verhaltensdefizite, der kortikalen Plastizität und der Mechanismen, die die Beeinträchtigungen nach unterschiedlichen Schweregraden von Schädel-Hirn-Traumata auslösen.

List of abbreviations

AD	Alzheimer Disease
AI	Artificial Intelligence
ALMA	Automated Limb Motion Analysis
ALS	Amyotrophic lateral sclerosis
AMPA	α-amino-3-hydroxy-5-methyl-4-isoxazolepropionic acid
ASD	Autism spectrum disorders
ATP	Adenosine triphosphate
BBB	Blood Brain Barrier
C1	Complement component 1q
C3	Complement component 3
C3R	Complement component 3 receptor
C4	Complement component 4
CBF	Cerebral Blood Flow
CC	Corpus Callosum
CCI	Controlled Cortical Impact
CCL2	Chemokine (C-C motif) ligand 2
CCL3	Chemokine (C-C motif) ligand 2
CCL5	Chemokine (C-C motif) ligand 5
CCR1	Chemokine receptor type 1
CCR2	Chemokine receptor type 2
CCR5	Chemokine receptor type 5
C/EBP	CCAAT-enhancer-binding proteins
CDC	Centers for Disease Control and Prevention
CD68	Cluster of Differentiation 68
CNS	Central nervous system
CR3	Complement 3 receptor
CSF	Cerebral spinal fluid
CST	Corticospinal tract
CT	Computed tomography
CTE	Chronic traumatic encephalopathy
CX3CL1	Chemokine (C-X3-C motif) ligand 1
CX3CR1	CX3C motif chemokine receptor 1
DAI	Diffuse axonal injury
DLC24	Digital Loudspeaker Cntroller

DNA	Deoxyribonucleic acid
DTW	Dynamic time warping
DTI	Diffusion tensor imaging
EAE	Experimental autoimmune encephalomyelitis
EE	Enriched environment
EPO	Erythropoietin
FPI	Fluid percussion injury
FST	Forced swim test
GABA	Gamma-aminobutyric acid
GCS	Glasgow coma scale
GOAT	The Galveston Orientation and Amnesia Test
GPR56	G protein-coupled receptor 56
ICP	Increased intracranial pressure
ICU	Intensive care unit
IL-10	Interleukine-10
LFPI	Lateral fluid percussion injury model
LOC	Lost of consciousness
MCP-1	Monocyte chemoattractant protein 1
MERTK	Proto-oncogene tyrosine-protein kinase MER
MHC	Major histocompatibility complex molecules
MHCI	Class I major histocompatibility complex molecules
MIP-1	Macrophage inflammatory protein 1
MRI	Magnetic resonance imaging
NFT	Neurofibrillary tangles
NLR	NOD-like receptor
NMDA	*N*-methyl-D-aspartate
NMJ	Mammalian neuromuscular junction
NOD	Nucleotide oligomerization domain
NP1	Nociceptor and pruriceptor 1
NP2	Nociceptor and pruriceptor 2
NSS	Neurological severity score
OFT	Open field test
P2RY12	Purinergic Receptor P2Y12
PAMP	Pathogen-associated molecular patterns
PCS	Post-concussive syndrome
PD	Parkinson disease

PNS	Peripheral nervous system
PRR	Pattern recognition receptors
PSD	Post-synaptic density
PTA	Post traumatic amnesia
PU.1	Transcription factor PU.1
RANTES	Regulated upon activation, normal T cell expressed and secreted
ROI	Region of interest
SER	Smooth endoplasmic reticulum
SNRI	Serotonin and norepinephrine re-uptake inhibitors
SSRI	Selective serotonin reuptake inhibitors
STED	Stimulated emission depletion
SZ	Schizophrenia
TAM	Tumour associated macrophages
TBI	Traumatic brain injury
TGF	Transforming growth factor
TLR	Toll-like receptors
TNF	Tumor necrosis factor
TPM	Two-photon microscope
TREM2	Triggering receptor expressed on myeloid cells 2
TST	Tail suspension test
TWEAK	TNF-weak inducer of apoptosis
VEGF	Vascular endothelial growth factor
VGAT	Vesicular GABA transporter
VGLUT	Vesicular glutamate transporter
WDI	Weight-drop injury
WPTAS	Westmead Post-traumatic Amnesia Scale
YMT	Y-maze test

Introduction

I. Traumatic brain injury

I.A. Definition and epidemiology of Traumatic brain injury (TBI)

Traumatic brain injury (TBI) is considered as a leading cause of morbidity and mortality worldwide (Rubiano et al., 2015; Ghajar, 2000). Traumatic brain injuries (TBIs) are defined as *"induced structural injuries and/or physiological disruptions of brain function as a result of an external force*" (Silver et al., 2018; McKee & Daneshvar, 2015; Menon et al., 2010), the external forces being a blow to the head or an acceleration/deceleration injury type. It includes penetrating injuries (with the rupture of brain parenchyma through the fracture of the skull and a breach of the dura) and closed head/blunt injuries (displaying no apparent damage of the skull and the dura) (Santiago et al., 2012). TBI can be classified according to its severity, from concussion and mild to severe injury and can have a range of short- and long-term consequences, including behavioural changes as cognitive impairments and physical disabilities.

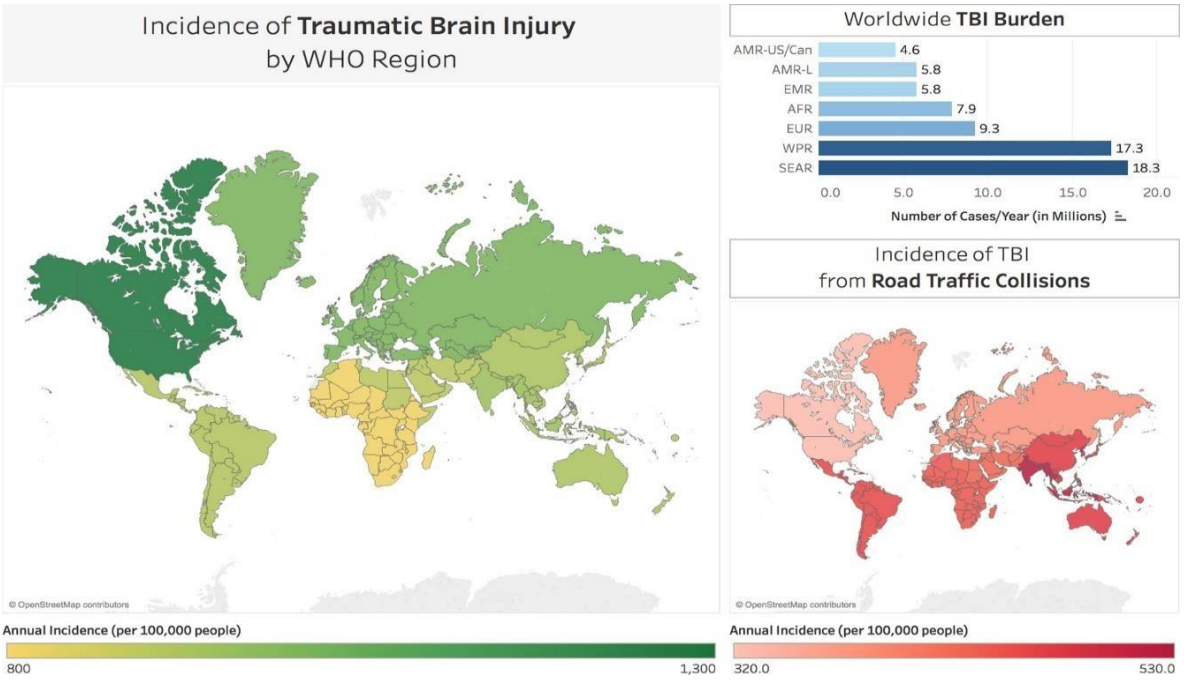

Figure 1. Worldwide incidence of TBI
Left**:** *Map illustrating the incidence of TBI cases per 100,000 people) across various WHO regions.* Upper right: *Bar graph depicting the estimated annual volume of TBI cases across the similar regions.* Lower right: *incidence of TBI resulting from traffic collisions across WHO region. Regarding the maps, reproduced with permission from OpenStreetMap Contributors, CC BY-SA 2.0 (http://www.openstreetmap.org/copyright). Figure is available in color online only. (Reprinted from the Journal Of Neurosurgery, Dewan et al., 2019. Copyright © 2019 by the American Association of Neurological Surgeons)*

Worldwide, TBI affects an average of 69 million individual yearly (Dewan et al., 2019), representing in total 295 per 100000 person-years (Nguyen et al., 2016). “10 million deaths and/or hospitalizations annually and worldwide are directly attributable to TBI” (Xiong et al., 2013). The incidence of TBI varies depending on the population studied, gender or ethnicity, the social and economic background and the methods used to collect data (Roozenbeek et al., 2013). In the United States, the Centers for Disease Control and Prevention (CDC) estimates that TBI results in approximately 2.5 million emergency department visits, 282,000 hospitalizations, and 52,000 deaths each year (Taylor et al., 2017). It has been shown that in middle and low-income countries TBI cases have increased due, in particular to an increase of motor vehicle and lack of safety (Fig1.). In Europe, across all TBI severity and ages, the crude incidence was varying from 47.3 to 694 per 100 000 population per year (per country). The mortality rate varying from 9 to 28,1 per 100 000 population per year (Bražinová et al., 2021). Overall, in Europe, TBI contribute to 37% of all injury-related death (Sivčo et al., 2023). However, these numbers probably understate the actual prevalence of TBI, as many cases go undiagnosed or unreported.

The principal cause of traumatic brain injury, across all severity levels, is falls and traffic accident that account for the main emergencies reports among young and old individuals (above 65 years) (Fig1.) (Bražinová et al., 2021). However younger individuals are the main population to be concerned and exposed to potential TBI. This is likely due to the higher levels of physical activity and risk-taking behaviour among them. Other common causes include motor vehicle accidents, struck by/against an object, and assaults (Mollayeva et al., 2018).

Men are most likely to engage in dangerous activities such as certain contact sports (american football, boxing, hockey, soccer) as well as their higher enrolment and participation to military missions. Coexisting illnesses such as alcoholism contribute to a greater chance of TBI exposition and worse long-lasting consequences (Mollayeva et al., 2018; Nikoo et al., 2017).

Both individuals and the society, as a whole, may be significantly impacted by TBI. Indeed, traumatic brain injury symptoms include headache, nausea, dizziness as well as amnesia (Blennow et al., 2016). The duration of the amnesia is a criterion used to categorised patient within one of the three severity level following TBI (Blennow et al., 2016). Those symptoms can, in some instances, last longer than some days and up to some months. The short- and long-term consequences of TBI can include cognitive impairment, behavioural changes, and physical disabilities, which can result in an increased healthcare costs and a decreased quality of life (Langlois et al., 2006). Sixty billion dollars represent yearly the financial burden brought by traumatic brain injury in the US only (Langlois et al., 2006). The lack of appropriate care and the difficulties to monitor longitudinally patients imply the absence of proper therapies development. Therefore, it is important to identify strategies for preventing TBI and improving outcomes for individuals who have experienced it. This may entail initiatives such as enhancing safety measures, promoting the use of protective equipment, and developing targeted therapies for TBI.

I.B. Classification of TBI and diagnosis

As previously addressed, TBI is categorised according to three main severity levels, being mild, moderate and severe (Blennow et al., 2016). Concussion as well as sub-concussive injury has risen lately as a specific closed head injury category, distinguished from mild TBI (McCrory et al., 2013). The different severity levels are based on the type of injury that the patient underwent, from macroscopic to microscopic lesions leading to brain alterations. TBI patients, after being admitted to the hospital, sustain a series of test to attest and define the level of their injury. The tests include the assessment of post-traumatic amnesia (PTA), the loss of consciousness (LOC) and the attribution to a score based on the Glasgow Coma Scale (GCS) (Blennow et al., 2016). Those three main tests can be, if necessary, implemented with diagnostic imaging techniques including magnetic resonance imaging (MRI) with diffusion tensor imaging (DTI) and computed tomography (CT) (McKee & Daneshvar, 2015). The imaging techniques bring a macroscopic visualisation of the integrity of the brain parenchyma following TBI and is usually useful for establishing moderate and severe cases.

As previously mentioned, the diagnostic of the different categories of traumatic brain relies on a batteries of test, essential for the appropriate clinical care of the patient. The table (Table 1.) above list all the criteria that are applied to each test to define the precise type of the injury:

	Mild TBI	**Moderate TBI**	**Severe TBI**
Structural brain imaging	Normal	Normal or abnormal	Normal or abnormal
Loss of consciousness (duration)	0 - 30 minutes	30 minutes to 24 hours	Up to 24 hours
Altered mental state (duration)	Inferior or equal to 24 hours	Superior to 24 hours	Superior to 24 hours
Post-trauma amnesia (duration)	Inferior or equal to 1 day	1 – 7 days	Superior to 7 days
Glasgow Coma Scale score	13 – 15	9 – 12	Inferior to 9

Table 1. Classification of the different severity level of traumatic brain injuries (TBIs) and its criteria. *Patient entering hospital care after undergoing a traumatic brain injury is tested in order to categorise the level of the injuries. If the patient fits in different criteria, the higher severity level will be retained. Figure inspired and modified from the US Department of Veterans Affairs and the US Department of Defense concussion or mild TBI Working Group (Adapted from Nature Reviews Disease Primers, Blennow et al., 2016. Copyright © 2016 by Springer Nature)*

- Post traumatic amnesia

Post-traumatic amnesia (PTA) is assessed according to a series of scale such as the The Westmead Post-traumatic Amnesia Scale (WPTAS) or The Galveston Orientation and Amnesia Test (GOAT) (Spiteri et al., 2020). PTA is the period of time after a brain damage during which a person has trouble acquiring new knowledge. When the patient is orientated and continuous memories are recovered,

PTA is over (Rosen & Gerring, 1986). The test is conducted repetitively until disappearance of PTA. Moreover, the duration of PTA also plays a role in defining the severity level of the injury; mild injury are those that last less than a day (≤ 1), moderate last one to seven days (1-7 days) and severe more than seven days (>7days) (Table 1.) (Blennow et al., 2016).

- Loss of consciousness

Loss of consciousness is evaluated through the Glasgow Coma Scale (GCS) (Teasdale et al., 2014). The Loss of consciousness (LOC) duration is also required to scale the severity of the trauma undergone by the patient. The Glasgow Coma scale, a 50-year-old established and useful procedure for monitoring impairment of conscious level, integrate the LOC dimension (Aguilar-Fuentes et al., 2024). The scale was designed to determine the level of consciousness, as previously mentioned, by including three components, each being “assessed by standardised approach”. Those three components include Eye opening (E), Verbal response (V), best Motor response (M) (Jain & Iversond, 2023). Each individual component will be attributed a score. The evaluation of the components will be repeated, if needed, spaced by one to two hours in between each test until complete consciousness recovery of the patient (GCS score of 15) (Blennow et al., 2016). Thereafter all three component scores will be summed to give the Glasgow Coma Score of the patient. This will allow the clinicians to characterise the injury level. The lower the score, the worst the response is. Severely affected patients will usually get a score inferior to 9, moderate patients are assigned a score between 9 to 12 and mild injuries are categorised with a score laying in between 13 to 15 (Table 1.) (Blennow et al., 2016). Nonetheless, the cutoff established out of pragmatic application of the scale could reveal some limitations. For example, the GCS is not suitable for patients intubated or in a sedated state, as they are incapable of performing some test and therefore give inconclusive results (Blennow et al., 2016). Other subscales are then used by clinician in order to evaluate the patient state in the most accurate way (Blennow et al., 2016). Mild traumatic injured patients may share similar component scores; however, the scale can turn out to be restrictive in precisely defining the different levels of risks, and particularly the long-lasting complication. The level of consciousness is hence an essential clinical feature of the brain injury’s severity (Gabbe et al., 2003).

Considering the different tools provided to characterise the severity level of a brain injury, it is, however, complicated to keep track of all the cases and their complexity, as some go unreported. This is notably the case for mild traumatic brain injury. Therefore, focusing on the pathophysiologic features of patients will allow for a substantial understanding of the various patient’s groups and appliance of a better care.

I.C. Biophysical mechanisms and pathology

Traumatic brain injury has been shown to be one of the most invasive types of injury, as well as one of the most complex. TBI pathogenesis causes neurological impairments being transient or permanent (Galgano et al., 2017). The nature of the injuries is very diverse as well as the physical forces causing them (Blennow et al., 2016). The injuries can result from linear and/or rotational acceleration as well as from impact deceleration. The anterior-posterior movement of the head resulting from the impact is attributed to linear acceleration forces, also referred as translational acceleration forces (Blennow et al., 2016). Rotational, or angular, acceleration happens when external forces cause the head to turn sideways, for example, from a blow to one side of the head (Blennow et al., 2016). When a patient undergoes a fall leading to an impact of the head to a surface, the impact is usually abruptly interrupted causing a spontaneous deceleration of the head, referred as impact deceleration (Blennow et al., 2016). Taken together, those mechanics leadings to head injuries can happen simultaneously (Blennow et al., 2016). As we know, the brain is imprisoned in the cranium or cranial cavity filled with cerebrospinal fluid (CSF) which serves as “a damper”. The forces implied, however, can overcome this “cushioning effect” and trigger “gradient intracranial pressure” responsible for axonal shearing causing what is known as Diffusive axonal Injury (DAI), which will be discussed subsequently (Gennarelli et al., 1982; Blennow et al., 2016). The consequences are different according to each brain regions. Regions with more axonal tracts/bundles will be more prone to axonal shearing and therefore DAI, which is substantially representative of the outcome of the injuries and their severity level (Medana & Esiri, 2003). Here is another way to categorise an impact: blast, blunt and penetrating (Rule et al., 2015).

Penetrating trauma, as its name implies, involves the direct disruption of the scalp, the skull and the brain parenchyma. When a weapon is involved, the depth, the angle of entry, as well as the power applied is also important to consider when making the right diagnosis and avoid complications (Nolan, 2005). Those injuries are mostly alluded to moderate and severe trauma/TBI. Gunshots, for instance, are considered as the cause of the highest mortality rate in penetrating brain injuries in the US, according to the Centre for Disease Control and Prevention, National Centre for Injury Prevention and Control’s data. Overall, the consequences of penetrating impact depend on the weight, the velocity and the cross-sectional area of the involved object (Rule et al., 2015).

In case of Blast’s impact, the nature of the injury is rather mixed. It can involve penetrating injury, non-penetrating injury or a combination of both respectively. Overpressure triggered by a blast are responsible of TBI first injuries through “blast wave energy transfer” to the head, “accelerative motion” and from any direct impacts (Rule et al., 2015). As previously mentioned, blast triggers very unique injuries. All depends on the explosive’s materials, the positioning of the individuals as well as the safety level taken by the individual being exposed to the blast (Nyein et al., 2008; Elder, Mitsis, Ahlers, & Cristian, 2010). The effect of blast revealed to be very specific to brain region. Indeed, blast injuries

can hold some similarities with penetrating trauma type as tissue strains causing DAI, intracranial pressure due to the inertia of the brain and contusions at the brain's site of the coup/contrecoup (this notion will be clarified in the next paragraph) (Taylor, Ludwigsen, & Ford, 2014). Therefore, it is important to better understand the power applied by the impact onto the brain, in order to characterise the blasts consequences. And for this reason, computational model was developed or are under-development in order to help further the existing knowledge by providing insights into the propagation of the blast's energy onto the brain (Zhu et al., 2012). Blasts are responsible for the whole severity range of TBI, from mild to severe injuries. It is said that blunt impact to the brain comes from objects with high mass and low velocity as well as their cross-sectional (Rule et al., 2015). Similarly to the blast, the consequences of such an impact led to increased intracranial pressure leading to axonal shearing causing DAI, coup and contrecoup contusions resulting from rotational or/and linear deceleration/acceleration, adding to the distortion of the skull and some scalp tearing (Post & Hoshizaki, 2012; Hardy, Khalil, & King, 1994; King, 2000). The contusion resulting from the coup/contrecoup effect can also be caused by the head quick acceleration. Those impairment has been shown to not only be focal but also diffusive. Rotational accelerations blunt impact has been primarily held accountable for the diffuse injuries (Adams, Graham, & Gennarelli, 1981; Ommaya, Thibault, & Bandak, 1994). Current consensus suggests that brain injuries arise from a blend of translational and rotational motion, causing both direct contusions and intracranial pressure effects. Therefore, depending on the mechanical force applied during the impact and their occurrence, it is essential for the care giver to have a better understanding of the mechanistic behind the injury. In addition to its mechanism, TBI injuries can be categorised as primary or secondary injury.

The injury that subsequent the initial impact, engendering the direct disruption of the brain parenchyma, is called primary injury. The energy, resulting from the impact, is conveyed though the brain and triggers what is called a "coup" (directly beneath the impact) and triggers as well a "contrecoup" (opposite to the site of the impact) (Nolan, 2005). This initial injury leads to immediate intracranial disruption of brain entities, starting in some cases with skull fracture. Brain parenchyma disruptions such as lacerations, shearing of brain white matter tracts, contusions as well as hematomas and oedemas are largely attributed to the primary injury. Neurons and glial cells damages leading potentially to their death, increased intracranial pressure (ICP) and swelling accelerating the overall vascular damages, and risks of haematoma and haemorrhage are additional primary injuries that will instigate the further development of persisting secondary injuries (Sande & West, 2010) within minutes, days lasting months to years. The severity of the primary injury is very variable and therefore its level relies on the occurrence or not of skull fracture, on top of potential direct disruption of the brain parenchyma. Hence, the subsequent injuries are variables among patients.

The secondary injury, as it implies, occurs subsequently to the primary injury. It results from pathophysiological responses through cascade of molecular, metabolic as well as cellular processes,

leading to further tissue damages and degeneration (Xiong et al.,2013; Fehlings et al., 2017; Nolan, 2005).

Neuronal and glial cells impairments implying ions homeostasis disturbances, rise of free radicals and lipid peroxidation leading to apoptosis or necrosis, diffuse axonal injury (DAI), white matter degeneration and overall systemic injury in the form of hypoxia constitute a non-exhaustive list of detrimental events leading to potential permanent physical, cognitive and societal impairments following TBI. Globally, inflammatory mechanism and cytotoxicity following primary injury, usually resulting from ischemia, establish the main factor accountable for the secondary injury (Gaetz., 2004). As such, an increase of glutamate release and a lack of its uptake activate a panel of receptors causing cell membrane depolarisation followed by an influx of Ca2+. The influx of Ca2+ participates to the exacerbation of the glutamate neurotoxicity (Choi, 1988; Gennarelli, 1993). Oedema is considered, as well, as a critical element related to the secondary injury, resulting from a plethora of pathological processes (Gaetz., 2004). Divided into different categories, vasogenic and cytotoxic, oedema is essentially a “swelling of the brain” (Nehring et al., 2023). Vasogenic oedemas, commonly observed, is responsible for the blood brain barrier (BBB) disruption as opposed to the cytotoxic ones also called cellular oedemas to which the BBB remains intact (Fishman, 1975). The BBB is considered as an essential structure that controls the movement of chemicals from the blood to the brain. Vasogenic oedemas leads to the disruption of the white matter though the diffusion of proteins and other macromolecules, such as glutamate, vascular endothelial growth factor (VEGF), subsequently to the loss of tight junction from endothelial cells, increasing the BBB’s permeability (Nehring et al., 2023). Cytotoxic oedemas imply swelling of cells, through the deficiency of the adenosine triphosphate (ATP) dependent Na+ K+ pump. Consequently, the injury resulting in an ischemic episode leads to Na+ accumulating within cells following the failure of these pumps. Through osmotic pressure created by the influx of Na+, water is drawn into the cells (Bullock et al., 1991; Gaetz, 2004). Extracellular accumulation of neurotransmitter such as glutamate or glycine have been shown to lead, as well through the same process, to cells swelling. Mechanical traumas have demonstrated to also consequently trigger oedema by creating disruptive K+ influx in the extracellular matrix causing swelling in the grey and white matter, particularly in astrocytes end feet (Bullock et al., 1991). Altogether, adding to the brain parenchyma integrity deterioration, neurometabolic disruption are observed as secondary injury following brain injury.

Primary and secondary injury classification of TBI, as previously shown, depend on the injury onset and is representative of the outcomes. Nonetheless, TBIs can also be classified in two different categories, based on the “distribution of the structural damages” and their mechanical aspect: focal and diffusive injuries (Andriessen et al., 2010; Povlishock & Katz, 2005). Injuries defined as focal are usually resulting from forces impacting the cranium in a localised manner. This can lead to the compression of the brain at the site of the collision (coup) or on the opposite side (named contre-coup), as previously mentioned, which participate to an increased morbidity rate. Considering the

location and severity level of the collision, focal injuries are the main cause of moderate and severe TBI neurological impairments. Intra or extra axial tampering of the brain, implying epidural and subdural haematomas, intracranial and subarachnoid haemorrhages resulting from contusions constitute focal injuries (Andriessen et al., 2010; McGinn & Povlishock, 2016; Gaetz, 2004).

In another vein, diffuse brain injuries are considered as damages occurred over a more extended area as opposed to focal injuries being more confined (Nolan S., 2005). Two main types of diffuse injuries have been identified being concussion and scattered axonal injury also referred as DAI. Spread vascular damages, oedemas and possible hypoxic ischemic episodes are to be attributed to the diffused injuries (Andriessen et al., 2010; McGinn & Povlishock, 2016). As previously mentioned, the extent of the damages is dependent, as seen in focal injury, on the mechanical forces implied (McGinn & Povlishock, 2016). Frontal and temporal cortex are the most inclined to develop cerebral contusion (Nolan, 2005). Shearing, inertial forces and shaking are the main component of diffuse injuries. Yet radiographic technics such as computerised tomography (CT) encounter some limitation in the characterisation of those injuries. Microscopic alterations within the brain parenchyma have been associated to DAI or cerebral contusion, however the CT do not have the capacity to view them (Nolan, 2005). Therefore, post-mortem studies of the human brain have risen overtime and have shown that DAI was a consistent component in the increased morbidity among TBI patients, affecting site as subcortical white matter systems or corpus callosum (CC) (Adams et al., 1989). DAI has been initially characterised as axonal swelling and axonal disconnection, however further studies have described the implication of cytoskeletal disruption inducing destructive processes. Unmyelinated axons demonstrated to be the most vulnerable to exposed mechanical forces (T. Reeves et al., 2005). The diffusive injuries, observed in the context of TBI, have helped to pinpoint TBI as a brain network disorder (Fig2.) whose severity is correlated with the injury itself. A reduced proportion of axonal degeneration is observed for milder types however the consequences are not minor.

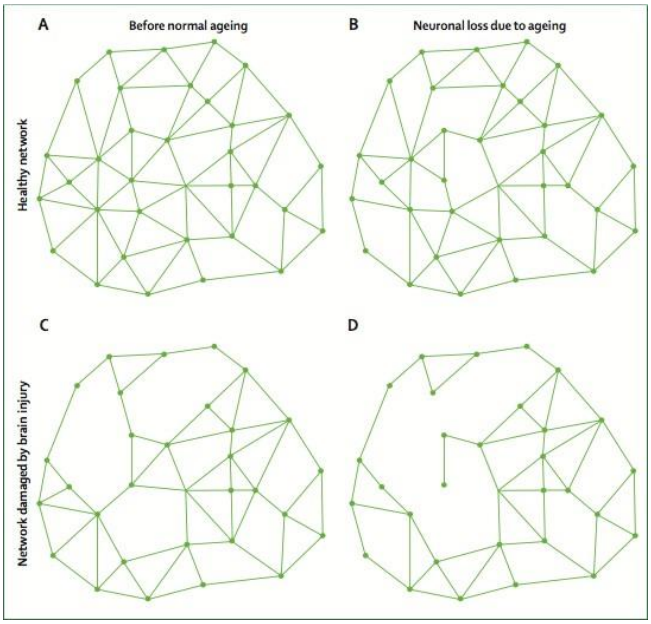

Figure 2. Impact on the neuronal networks of brain injury before and after normal ageing brain
The combination of traumatic brain injury and the natural aging process of the brain can lead to a higher risk of worsened cognitive decline. (A) A healthy neural network. (B) Normal ageing brain display some loss of neuronal connections. (C) Following TBI, a few nodes networks have disappeared. (D) In the context of normal ageing, the brain remains unaffected by the loss of networks seen in a normal ageing brain. TBI affects network damages introducing significant impairments along the aging process. (Reprinted from the Lancet Neurology, Moretti et al., 2012. Copyright © 2012 by Elsevier)

Over the years, a large number of studies have established links between traumatic brain injury (TBI) and neurodegenerative pathologies, including amyotrophic lateral sclerosis (ALS), Parkinson's disease (PD), Alzheimer's disease (AD), and chronic traumatic encephalopathy (CTE), which is the result of recurrent mild TBI.

I.D. Neuropathological consequences

As previously mentioned, the primary injury leads to initial acute impairments depending on the level of the injury. However, the secondary injuries, resulting from the primary injuries, are disastrous, regardless of the severity, and are shown to be long lasting. The chronic effect of TBI has been shown to exacerbate the development of misfolded, aggregated proteins such as ß-amyloid, tau protein or α- synuclein, responsible for neurological degeneration.

Usually, the symptoms resulting from a mild traumatic brain injury resolve within a week. However, when the symptoms persist (over 3 months), patients sustain post concussive syndrome also known as post-concussion disorder (Silverberg & Iverson, 2011). It concerns 10-15% of the patient sustaining a concussion, however the symptoms are quite heterogeneous which makes it complicated to have a proper estimation of the prevalence (Blennow et al, 2016; Silverberg & Iverson, 2011).

Chronic traumatic encephalopathy (CTE) is a neuropathological condition uncovered postmortem in patients exposed to repetitive mild TBI (including concussion and sub-concussive head impacts). It has been identified, in majority of the cases, among athletes practising contact sports and soldiers (Blennow et al, 2016). CTE is characterised by the widespread accumulation of aggregated phosphorylated tau (P-tau) protein in neurons and glial cells, particularly seen at the perivascular level as well as the depths of cortical sulci (Blennow et al, 2016; Fesharaki-Zadeh, 2019). In 1928, a condition observed among retired boxers was described and referred to as the “punch drunk syndrome” (Martland, H. S., 1928). It was the first attempt at bridging the practice of a sport to a neurological condition. Thereafter, the terminology evolved to “dementia pugilistica”, where neurofibrillary tangles (NFTs) were found in the brain of boxers, to finally referring to as CTE in 1949 (Fesharaki-Zadeh A., 2019). NFTs were later found to contain aggregates of paired helical filament-tau. In 2005, CTE was first seen and described in a retired american football player which then led to the identification of similar symptomatology in further contact sports (Omalu et al., 2005). Amyloid-β (Aβ) plaques have been spotted in half of CTE cases, marker of multiple neurodegenerative diseases. Abnormal Tau proteins are mainly seen at the very superficial layer of the frontal and temporal cortex (Blennow et al, 2016). CTE reveals also macroscopic changes implying the enlargement of ventricles and of the cavum septum pellucidum visible using neuroimaging procedures. A further study has been able to identify the importance of mild TBI repetition in the development of CTE (Bieniek et al., 2015).

However, limitations encountered to study CTE makes it complicated, to this day, to establish to this day an ante mortem diagnosis. Taking into consideration the other TBI severity level, the late neuropathological impacts remain unclear, given the prevalence of severe and moderate cases.
Prevention, as wearing a helmet or the seatbelt, is the only way to avoid the occurrence of TBI and therefore the primary injury (Xiong et al., 2013). Therefore, the focus is brought to improve our understanding of the heterogeneity and the ethology of the mechanism leading to long-term impairments following TBI, and therefore the secondary injury. Caregivers apply the nomenclature established for a better anticipation of the secondary injuries. Whether it is focal or diffusive, adding the characteristic of the primary injury, the injury's severity coupled with its location, the individual's age and gender that contribute to the complexity of the pathophysiology, all are responsible to traumatic brain injury's sequelae (Nolan, 2005; Prins et al., 2013). In traumatic brain injuries (TBIs), understanding the underlying mechanism of injury is crucial for providing optimal patient care (Nolan, 2005). However, numerous limitations are still anchored as for the establishment of proper and appropriate care of patients. Hence, the development of post clinical studies and the democratisation of the matter, notably within the taboo around mild TBI in the context of sports, have helped in the development of tools and strategies to gain further knowledge.

II. Experimental treatment and multifactorial neuroprotective strategies

As previously discussed, TBI revealed to be a very complex, multi-step process resulting in primary and secondary injuries, leading to transient and/or long-term neurological impairments. The heterogeneity of sustained TBI considering the patient's sex, age, habits and medical backgrounds makes it particularly difficult to address effective treatment solutions for each severity level. So far, none of the preclinical studies have established promising therapies. Considering the primary injury resulting from mechanical damages, treatments modalities are very limited. Therefore, most of the focus is on attempting to tackle the cellular and molecular mechanisms ensuing the secondary injury cascade (Galgano et al., 2017). However, a series of measures can be provided to adapt the approach to effectively treat the patient's symptoms.

II.A. Clinical management of the acute phase of TBI

Following the accident, patients sustaining a TBI will usually be taken care of, and the severity of their injuries will be assessed (Blennow et al., 2016), as mentioned previously with scoring systems (GCS) or radiographic imaging. The aim of the emergency care is to stabilise the patient state by checking their vital signs. Usually, two distinct groups of patients are identified, based upon the necessity of a surgical intervention. The severe and moderate cases would, for most of them, require

direct surgical procedures directly after TBI, to fixe skull fractures and relieve intracranial pressure (ICP). ICP is usually resulting from hematoma, haemorrhage or/and contusion leading to significant compression of the brain. (National Institute of Neurological Disorders and Stroke & National Institutes of Health. (n.d.). Traumatic brain injury. In *Hope Through Research*, 2020). The hematomas as well as the contusions can and are advised, if vital, to be relieved through surgery such as bilateral decompressive craniotomy (Bohman & Schuster, 2013; Plesnila, 2007). In case of patients that may not require operations, they will be closely monitored to see how contusions and hematomas are evolving or enlarging. In the context of hematomas enlargement, patients will then require an emergency surgery (Bohman & Schuster, 2013; Plesnila, 2007).

Considering patients that sustained mild TBI or concussion, care provided is usually dependent on the individual that sustain the injury and its GCS score (Blennow et al., 2016). In most of the cases, rest is highly advised. It mainly concerns athletes, as they are highly exposed to new head impacts, and is referred as “recovery phase” (Blennow et al., 2016). For non-athlete’s patients, a resting phase is also applied. Risks of relapses are also to be expected, depending on the patient habits, sexe, age, which can extend and slow down the recovery phase, as well as introducing long-term impairments (National Institute of Neurological Disorders and Stroke & National Institutes of Health. (n.d.). Traumatic brain injury. In *Hope Through Research*, 2020). Unlike the sports players, the other patients are provided with some management guidance by the emergency department after being discharged. However, no further follow-up on their physical and mental conditions is applied (Blennow et al., 2016). Also, difficulties in defining accurately what “rest” is and its duration introduce hurdles into the creation of the proper paradigm to alleviate acute TBI symptoms as well as long term ones (Thomas, Apps, Hoffmann, McCrea, & Hammeke, 2015; Blennow et al., 2016).

Further acute medical interventions are also in use to address the acute consequences of TBI. As an example, elevating the head of a traumatic brain-injured patient is carried in order to decrease the intracranial pressure (Galgano et al., 2017). The hyperosmolar therapy is a therapeutic approach involving the use of a bolus of a hyperosmolar agent, such as mannitol or hypertonic saline, leading to a reduction of elevated ICP through the reduction of blood viscosity and the decrease of the Cerebral Blood Flow (CBF) (Galgano et al., 2017; Knapp, 2005). Hyperventilation has proven to lower ICP and finally therapeutic cooling technic, bearing mixed opinion, has been shown to lessen oxidative stress resulting from the secondary effect of TBI (Bayır et al., 2009; Galgano et al., 2017). Nevertheless, some of the acute symptoms of TBI appeared to be refractory to some of the approaches. Therefore, additional pharmacological procedures are being developed to substitute some of those approaches, carrying, however, some limitation (Tani, Wen, Hu, & Sung, 2022). After admission to the intensive care unit (ICU), patients are usually administered sedative and anaesthetic compounds to lower the ICP, at the very acute phase of the injury (Tani, Wen, Hu, & Sung, 2022). However, this should be carefully monitored for secondary effects such as lower body temperature and considerable decrease of blood pressure, degrading even more the state of the patient (Tani,

Wen, Hu, & Sung, 2022; Roberts & Sydenham, 2012). Other drugs such as Heparin, against thromboembolism (Margolick et al., 2018), or antipyretic (Puccio et al., 2009) can also be used. Cases of epileptic episodes have been observed, with the incidence correlating with the severity level of the TBI (Frey, 2003). Therefore, epileptic treatments have been dispensed to reduce the early seizure incidence without averting completely late term seizures (Annegers, Hauser, Coan, & Rocca, 1998; Tani, Wen, Hu, & Sung, 2022).

II.B. Chronic treatments following TBI

As priorly stated, TBI leads to anatomical and functional impairments to the brain. The initial treatments are applied to patients to relieve them from the consequences of the first/primary injury. However, yet, the treatments revealed to be not conclusive. Further investigations have been and are still being conducted in order to focus on the secondary injury part of TBI, responsible for the establishment of persisting symptoms and impairments as neurodegeneration and neuropsychiatric changes (Galgano et al., 2017; Tani, Wen, Hu, & Sung, 2022). More emphasis is made in uncovering treatments that boost the recovery and restore brain's functions (Xiong, Mahmood, & Chopp, 2013; Galgano et al., 2017). Many treatment paths have been taken, involving the intervention of pharmaceutical compounds such as selective serotonin reuptake inhibitors (SSRI) and serotonin and norepinephrine re-uptake inhibitors (SNRIs) both used to treat post-TBI depression (Ashman et al., 2009). Buspirone (a serotonin receptor partial agonist) has been shown to reduce anxiety level in brain injured patient, as well as agitation behaviour (Levy et al., 2005). To improve functional and cognitive recovery, amantadine (dopamine agonists acting as an antagonist of the NMDA-type glutamate receptor) has been shown to be effective (Meythaler, Brunner, Johnson, & Novack, 2002; Sawyer, Mauro, & Ohlinger, 2008; Tani, Wen, Hu, & Sung, 2022). Other clinical trials have demonstrated that erythropoietin (EPO) carry a neuroprotective effect when administered to TBI patients. EPO, responsible for the stimulation of red blood cell production (Suresh, Rajvanshi, & Noguchi, 2020), shows pro-anti-inflammatory and antioxidant as well as reduced excitotoxicity effects after TBI (Bramlett et al., 2016; Ponce, Navarro, Ahmed, & Robertson, 2013). The use of glibenclamide has emerge as a potential approach to reduce and prevent oedemas (Walcott et al., 2012). The recent growing interest for the use of stem cell as a recovery-based or regenerative therapy has led scientists to consider it as a potential way to improve outcomes following TBI, notably by enhancing pro-regenerative and neuroprotective chemokines and growth factors (Galgano et al., 2017; Blennow et al., 2016). An ongoing phase I clinic implying the use of bone marrow mononuclear cells in severe TBI is believed to release intracranial pressure (Liao et al., 2015).

In regard of mild TBI and more specifically concussion, the increasing recognition of the importance of those impacts and their repetition on one's health has allowed to uncover acute and chronic impairment attributed to those injuries. Considering players of contact sports undergoing decades of

those repetitive concussions and developing later cognitive impairments, clinicians would caution them to withdraw from their career, especially in case of sustained concussions. However, the potential risk taken by those athletes to develop neurodegenerative disorder is usually dependent on them (Blennow et al., 2016; Montenigro et al., 2017). The extent and severity of the symptoms is also dependent on the longevity of their career. Therefore, several approaches are being investigated to alleviate the consequences of repetitive concussion (Blennow et al., 2016). The accumulation of cis P-tau protein disrupting microtubules integrity can be counter using monoclonal antibody against cis P-tau, lowering its spread and damping the bad outcomes (Kondo et al., 2015). Hyperthermia occurs following concussion leading to later cognitive decline. Therefore, a quick regulation of the body temperature reveals to prevent those impairing effects (Titus et al., 2015). Current increasing evidence assess of the importance of rehabilitation approaches, currently being investigated as a potential method to assist in the recovery of individuals with traumatic brain injuries (Galgano et al., 2017). The process of neurorehabilitation is essential for helping TBI survivors reintegrate into the everyday life, especially given the common occurrence of long-lasting depression and memory impairment among them (Galgano et al., 2017). Research involving animals placed in enriched environments (EE), where they have access to larger living spaces and increased opportunities for social interaction and sensory stimulation, has yielded promising outcomes in terms of both behaviour and brain structure improvement (Sozda et al., 2010). These interventions have shown effectiveness in various models of neurological injuries, including TBI, cerebral ischemia, and spinal cord injury (Dunkerson et al., 2014; Nudi et al., 2015). Furthermore, there is evidence suggesting that exposure to enriched environments before injury could provide preventive advantages (Döbrössy & Dunnett, 2004). These findings indicate that implementing EE interventions in clinical settings for humans could significantly contribute to neurorehabilitation, especially for TBI patients who are susceptible to depression (Galgano et al., 2017).

Although significant progress has been made, investigations of TBI and more specifically mild TBI/concussion, post-concussion syndrome (PCS), and chronic traumatic encephalopathy (CTE) are still in their initial phases, leaving numerous knowledge gaps to be addressed (Blennow et al., 2016). The heterogeneity found in each TBI cases makes it complicate to address the most adequate care. Therefore, biomarkers could be used in giving appropriate diagnosis and prognosis, assessing the severity of the TBI and defining the suitable return-to-play period of contact sports athletes (Blennow et al., 2016). Although there are currently no known biomarkers in bodily fluids like saliva or urine, cerebrospinal fluid (CSF), serum, and plasma are relevant for identifying fluid biomarkers in TBI patients. According to Blennow et al., the optimal TBI biomarkers should precisely depict the underlying pathophysiological processes (Blennow et al., 2016).

The multiplicity of the TBI cases due to the different causes makes it a model complicated to study. Therefore, it is necessary to expand the pre-clinical research, in that domain, to find appropriate therapies and treatment to alleviate or repair the burdens created by those trauma (O'Connor et al.,

2011). And for this the development in the recent years of the different animal model of traumatic brain injuries has been crucial to better understand the consequences and reaction waves triggered within the brain. Unfortunately, these experimental studies have not been successfully translated into clinical therapies. Many questions have been raised through these years such as whether we fully understand the pathological dynamics after TBI and whether TBI models are clinically relevant (O'Connor et al., 2011).

III. Animal models of TBI

The complexity and heterogeneity of traumatic brain injuries has led scientists to develop several animal models that would reflect and represent, to their best, human TBI. Hence, the pathological features of the injury such as the onset (primary or secondary) as well as the pattern and the distribution of the structural damages (focal or diffuse) are to be distinguished (Andriessen et al., 2010). The initial collision leads to the compression of the brain into the skull at the impact point (coup) and on the opposite side of the blunt impact site (contre-coup) characteristic of focal brain injuries. They are characterised by contusion at the level of the impact, as previously mentioned, leading to hematoma (O'Connor et al., 2011). Diffusive injuries are defined as damages to the axons and blood vessels, leading to hypoxic and ischemic condition (Rauchman et al., 2023), as well as diffusive axonal injury (DAI) (O'Connor et al., 2011). Different model of TBI have been developed to represent the different severity level of the injury. But first, it is important to mention that a variety of species were used to model TBI, including non-human primate, swine, cat, rodents (rat, mouse), zebrafish, drosophila and others. There are pros and cons for the use of certain species. The non primates as well as the swine or the cat present a gyrencephalic cortical structure, whereas rodents are lacking this structural similarity to human. However, the life span of those "larger animal", the ethical concerns as well as their care cost makes it complicated for researcher to carry experiment upon their use. The shorter life span, the lower cost and the ability to manipulate them genetically make rodents a more viable alternative to further operate. The elaboration of those model is an opportunity to further our understanding on the pathophysiology of TBI and explore potential therapies. In this context, we have chosen to work with mice and only TBI models using this specific specie will be mentioned. Each individual models can be calibrated to regulate the severity of the injury.

III.A. Fluid percussion model

The fluid percussion injury (FPI) model has been initially described in 1965 by Lindgren and Rinder on a rabbit model (Lindgren & Rinder, 1965). FPI is considered as the most characterised and commonly used TBI model. It involves the trepanation/craniotomy of the selected species exposing

the brain and the intact dura. The insult is triggered by striking, with a pendulum, the piston of a reservoir filled with a fluid (in most of the case a saline solution) directly onto the exposed dura as well as the epidural space in a concentric manner from the injection site (Wahab et al., 2015). The brain distorts as a result of the hit, and the extent of the damage depends on the pulse pressure, which is controlled by the pendulum's height. The position of the craniotomy is as well very important and needs to be considered regarding the severity of the injury about to be inflected. A more focal injury requires a trepanation positioned on the lateral side of the sagittal fissure, onto one of the hemispheres between bregma and lambda, which will be called lateral fluid percussion injury model (LFPI). Whereas a diffuse injury is inflected when the craniotomy is positioned onto the midline (O'Connor et al., 2011). The use of FPI allows the reproduction of the symptoms seen in human TBI, without a proper skull fracture and provide a model with an extensible and reproducible injury severity (O'Connor et al., 2011). It implies the development of oedemas, intracranial haemorrhage, brain swelling, axonal shearing and further degeneration of the grey matter (Xiong et al.,2013). However, FPI encompasses some disadvantages as how close the model translates a human traumatic brain injury and therefore constitutes a model not properly suited for a further analysis of the biophysical mechanism of the injury.

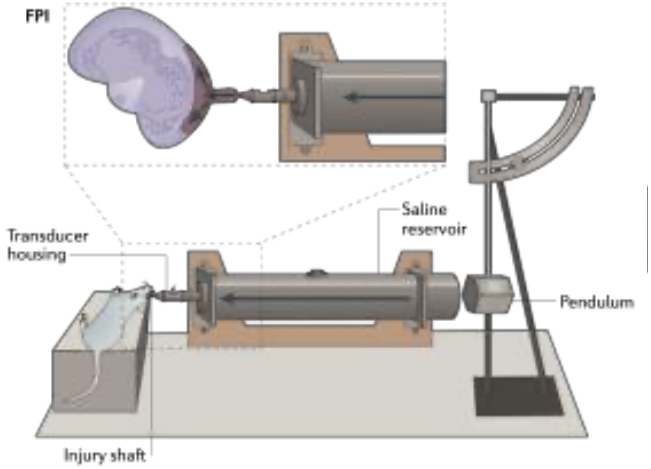

Figure 3. Fluid percussion injury (FPI) model
(Reprinted from Nature Reviews Neuroscience, Xiong et al., 2013. Copyright © 2013 by Springer Nature)

III.B. Weight drop injury model

The weight-drop injury model (WDI) is considered as a pioneering model of TBI. This model uses the gravitational force produced by "a free-falling direct weight onto the head of a mouse" to trigger an impact (Xiong et al.,2013). The weight's mass and the height at which it is dropped determine how serious the damages are. (Xiong et al.,2013). In some cases, a craniotomy is applied which correspond to Feeney's weight-drop paradigm (Feeney et al., 1981). In this model, the brain of the mouse with the intact dura is directly exposed to the falling weight, causing a cortical contusion and haemorrhage with damages to the blood brain barrier (BBB) (Xiong et al.,2013; Ma et al., 2019).

Thereafter, in 1988, Shapira et al. adapted the WDI to maintain the head fix during the impact to avoid any acceleration and sustain a certain reproducibility of the model (Ma et al., 2019; Morales et al., 2005). In the late 20st century, Shohami et al suggested a new closed head injury model involving WDI by triggering an impact on one side of the exposed skull. Similar pathophysiology as Feeney's

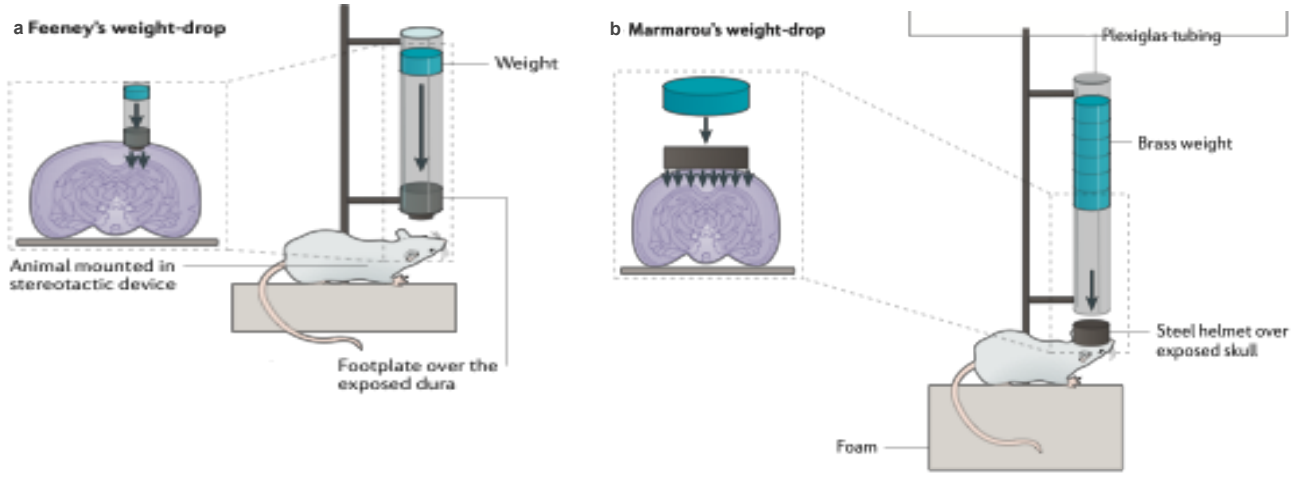

Figure 4. Weight drop injury model
a: Feeney's weight-drop model imply a free dropped weight onto the exposed dura.
b: Marmarou's weight-drop model entail a similar system as the Feemey's model, however, in the Marmarou model, a metal disk is placed onto the rodent head unlike the Feemey's model.
(Reprinted from Nature Reviews Neuroscience, Xiong et al., 2013. Copyright © 2013 by Springer Nature)

paradigm was observed such as BBB breakage, gliosis and neurological impairments evaluated using the neurological severity score (NSS). The injury generates simultaneously a focal and diffusive injury; however, the diffusive aspect of the injury remains on the ipsilateral hemisphere of the impact. Hence, Marmarou et al., in 1994, presented a model of closed head injury that translated to the closest, the diffuse aspect of human traumatic brain injury (Marmarou et al., 1994). Their model consisted of a mounted stainless-steel glue to the exposed skull between bregma and lambda, to avoid any skull fracture and similar to the previous model, a free-falling weight placed at a certain height. The position of the steel disc onto the midline has been shown to impact and propagate to sub-ventricular areas such as the hippocampus. However, certain levels of dysfunction of the model lead to a lack of consistency and reproducibility notably through a possible rebound of the weight in some cases. The model is poorly characterised, therefore further investigations will be required.

III.C. Controlled Cortical Impact (CCI) model to different severity level

Controlled cortical impact has been described as an invasive model, due to the implication of a craniotomy triggering a direct brain deformation. It was initially developed in the late 90s for ferret and has been later expended to other species model (Lighthall, 1988). CCI was adapted from previously developed experimental model that were focusing on spinal cord injury. It implies the use of a rigid impactor, driven by an electromagnetic or pneumatic device, that generate a mechanical

force delivered to the intact dura after a craniotomy in a unilateral manner. The animal heads are kept restrained throughout the whole process. The CCI model triggers cortical damages leading to necrotic tissue, axonal diffused injuries, haematoma, blood brain barriers (BBB) disruption, decline in cerebral blood flow and cognitive impairments (Kochanek et al., 2002). According to a thorough neuropathological investigation of the CCI model, the concomitant damages revealed to be extensive and include thalamic, hippocampal, and acute cortical degeneration (Hall et al., 2005).

The conveyance of experiment using this TBI model has proven to overcome certain drawbacks carried by other TBI models. One of the main advantages includes the possibility to administer a controlled, reproducible, and specified severity level of brain damages through setting parameters such as the velocity, the dwell time and the depth of the impact. Moreover, this model was able to subvert the risk of rebound seen in the weight drop models.

III.D. Animal model of repetitive concussion/ mild traumatic brain injury (mTBI)

An important number of TBI models were developed and have succeeded to characterise the molecular and cellular consequences of severe/moderate TBI at acute and chronic stages. In order to recreate a particular pathophysiology and mimic specific clinical situations, some of the previously described models have been readapted. This was the case for concussions/single mild traumatic brain injuries notably, as well as their repetition paradigm. In order to replicate mild TBI, one strategy that has been tackled was to scale parameters used to inflict the impact (Bolton-Hall et al., 2019). The site of the impact and how the impact is triggered are as well crucial to adjust the severity level, conditioning then the histopathological consequences and mouse's response to the injury.

A series of studies have shown the expansion and the reliability of methods reconfigured to generate closed-head injuries. Those methods englobed the previously described ones, namely LFPI, CCI and WDI. Nevertheless, LFPI or CCI models, due to their configuration (implying a craniotomy), have been found to translate the least the injury observed in humans after mild TBI repetition.

In 2020, Chen, Hao and Liang et al. have contributed to the development and the improvement of a mild TBI model resulting to a more representative pathophysiology of the human TBI. They implemented a model applying both a linear and rotational head acceleration system (K. Chen et al., 2020).

Already in 2012, Kane and Mariana et al. readapted the Marmarou weight drop model to recreate repetitive concussion seen in human. The mice did not undergo any surgery leaving the head of the animal intact. One important aspect of this method is the delivery, to an unrestrained subject, of an impact onto its skull (Kane et al., 2012). This way allows to reproduce the rapid acceleration of the head and the high impact speed observed among the athletes of contact sports. The impact can be repeated (for up to 2 times a day) and leads to a more diffusive injury without any cranial fracture and no internal bleeding (Kane et al., 2012). This was made possible by changing the impactor tip by

adding rubber or silicone, which prevented skull fractures from being caused by direct impact (Bolton-Hall et al., 2019).

Behavioural and neurological impairments exhibit distinct characteristics and often improve over time. And rodent's brain histological examination has shown a pathophysiology similar to the one observed in postmortem human's brain that underwent multiple concussion or mild TBI. Fluid percussion injury model delivered at the midline is chosen in order to replicate diffusive axonal damages observed in clinical instances. Additionally, focal invasive brain contusion is highly represented in lateral FPI, CCI and WDI models (Bolton-Hall et al., 2019). However, the multiplicity and the diversity of the symptomatology portrayed in repetitive and single mild TBI depend on the site of the impact as well as the occurrence of the impact. Although rodents have been used to reproduce the pathophysiology seen in humans, improvements in understanding the clinical outcomes are yet still very limited.

As the primary focus was on model operating impactor, the list of TBI animal models remain partial. Stab wound model is as well used to recreate a certain severity level observed in TBI patients. To reproduce the TBI seen among soldiers, a blast TBI model has also been developed (Sundaramurthy et al., 2012). Head injuries reveal to be very unpredictable, and no proper animal model can replicate the complete spectrum of pathological changes observed in human after TBI (O'Connor et al., 2011). Therefore, it is crucial to select the appropriate model capable of providing accurate and reproducible data (O'Connor et al., 2011).

IV. Behavioural impairments assessment following TBI

Due to the increased life span seen in the population over the past two decades, the prevalence of neurodegenerative diseases as well as impairments of specific brain functions following head injuries, as the memory, is constantly increasing and constitute a global concern (Logroscino & Tortelli, 2015). Public health institutions are worried by the evolution of the situation as most of the cases are sporadic (Logroscino & Tortelli, 2015). To understand better this increasing concern, the development and the use of animal model and behavioural test are paramount to overcome this current challenge.

A range of significant cognitive and sensorimotor impairments in human have been seen following TBI. Accordingly, a growing number of research studies extensively assess behavioural correlates in animal models (Fujimoto et al., 2004). The multiplicity and diversity of rodent's behaviour implies the establishment of different tests to assess different aspects of their behaviours, such as sensory-motor function, cognitive function, anxiety and depressive-like behaviours as well as social interactions (Hånell & Marklund, 2014).

IV.A. Motoric tests

Motor functions are managed by intricate neuronal networks starting in the cortex and expanding to the spinal cord through the brainstem. Those neuronal tracts connect with motor neuron that innervate the skeletal muscle (Fujimoto et al., 2004).
TBI motor deficits-induced would results from damages onto those tracts. The current behavioural tests are overall sensorimotor by nature and therefore are more prone to assess or uncovers sensorimotor impairments rather than purely motor tasks (Fujimoto et al., 2004).

IV.A.1. Righting reflex

The Righting reflex test is a simple way to assess behavioural responsiveness of rodents, especially in mouse model, as well as their locomotion abilities (El-Khodor et al., 2008). This method was initially described in 1939 by Warkentin and Carmichael as air-righting reflex in cat and rabbit (Warkentin & Carmichael, 1939). It was later on applied on rodents in a 1975 experiment by Altman and Sudarshan (Altman & Sudarshan, 1975). The mouse is put on its back (supine position) on a flat surface and the time taken by the mice to get back to its prone position is measured (Franks, 2006). Mice undergoing anaesthesia tend to lose their protective ability to get back on their four paws. Therefore, evaluating the loss of righting reflex is an essential way to determine the level of consciousness (Wasilczuk et al., 2018).

IV.A.2. Treadmill/Kinematic test

Locomotion is a rhythmic behaviour aimed at moving the whole body in space (Bouët et al., 2003). As for kinematic, it refers to the movement dynamics (Newell et al., 1983). In their 2019 paper, Cardoso Diogo et al. define kinematic techniques as “any method that describes and quantifies the movement of the whole body or body segments relative to each other and/or to an external frame of reference" (Diogo et al., 2019).
The treadmill is a motorised runway establishing an accessible and standard system to assess the impact of exercising on the physical and cognitive state of the rodent. It was initially reported in 1965 by Robert James Andrews who adapted the previous circular treadmill version into a horizontal form (Andrews, 1965). The treadmill can be operated at varying speeds and inclination of the runway belt, determined by the experimenter. Multiple animals can be monitored simultaneously due to the multiple lane configuration of the treadmill. It is, as well and primarily, a device that forces animals to exercise and trigger them a motor pattern for long periods of time. This has proven to alleviate rodents’ health by reducing their body fat and improving their cardiovascular function leading to a potential enhanced brain plasticity (Kolb & Whishaw, 1998).

As such, it pertains to endurance rather than coordination. The use of treadmill has mainly focused on hindlimb movement's dynamic in physiological and impairment condition. As of the gait evaluation, the treadmill test is implemented with kinematic techniques that involves the placement of labels at strategic point of the limb, mainly on the joints from the animal being monitored (Pereira et al., 2006). The animal is recorded for series of treadmill and the recorded movement of the labels offer a collection of numerous measurements along with temporal measurements. Such parameters as cycle duration and velocity are essential for the gait assessment. As previously mentioned, the treadmill constitutes a very structured, standardised device, due to its motorised feature, providing fixed applied settings essential for tests (Pereira et al., 2006). Kinematic treadmill test demonstrates the sensitivity of the kinematic approach in raising the smallest difference in between groups and particularly characterising functional impairments. Improvements, following injury or pathophysiological condition, can be as well tracked after therapies or treatments. This has been shown in the study carried by Lail et al in a stroke mouse model (Lai et al., 2014). As mentioned, kinematic analysis is implemented to the recorded treadmill test. Its analysis allows a three-dimensional assessment of limbs motricity (Ueno & Yamashita, 2011). This can be done manually; however, over the past years, a new era of deep learning-based tools as well as machine learning approaches, mimicking the human made kinematic system, have proven more reliability and consistency compared to the human eye (Arac et al., 2019).

IV.A.3. Ladder rung test

Ladder rung test belongs to the motor coordination and balance test category, involving the grid stepping paradigm. The test enables the assessment of fore- and hindlimbs performance, coordination and placement (Metz & Whishaw, 2009) as well as very fine chronic motor disturbances, describing the overall rodent walking skills (Farr et al., 2006). The principle of the test lays on placing a rodent on a horizontal ladder in which the rodent will travel through by grasping the rung with the use of its fore- and hindlimbs. The rungs can be regularly or irregularly spaced and periodically changed in order to vary the level of difficulty, for the rats or mice, to cross the ladder. Therefore, this adjustment adds a layer of sensitivity to the test and enable to characterise the locomotion and coordination of the rodent's limb (Brooks & Dunnett, 2009). It also prevents the animal to compensate its impairments by learning the position of the rungs. Time taken to cross the apparatus, numbers of footfall and slips, foot placement as well as digits arrangement constitute a series of variables that can be measured from the test's recording (Metz & Whishaw, 2009). Ladder rung test is regarded as one of the most used tests for locomotion due to its many advantages such as the spontaneous walking paradigm that it allows, and the many parameters that can be extracted, notably with the current development of deep-learning tools (Aljovic et al., 2022; McVea & Pearson, 2009). Considering the irregular rung condition, rodents are being challenge in their gait pattern, their

learning capabilities, requiring from them adjustment of their weight support, the position of their paws and their stride length. Lastly, the rung walking test form a prominent test to assess functions decline or gain following traumatic brain injuries.

IV.A.4. Rotarod test

Originated from the work achieved by Dunham and Miya in 1957 (Dunham & Miya, 1957), the rotarod test is one of the oldest tests employed to evaluate the impact of a drug and/or genetic effects on motor coordination on animal behaviour (Bohlen et al., 2009). It has also been implemented to evaluate rodents motor coordination besides their balance/gait (Shi et al., 2021), therefore displaying testing abilities similar to the ladder rung test.

The rotarod comprises a beam that can rotate at a fixed or accelerating speed (Jones & Roberts, 1968; Bohlen et al., 2009). Mice are placed on the beam and their latency to fall, in different timed trials series, provides a measurement of their motor coordination (Brooks & Dunnett, 2009). Thereafter, the test has been designed to automatically evaluate rodent motors behaviour deficits and recovery following injuries. Additionally, it has demonstrated sensitivity in detecting cerebellar impairments (Shiotsuki et al., 2010). Moreover, several animals can be evaluated simultaneously, being separated from one another by walls. However, there is a certain restriction in the assessment of the rodents' coordination with the use of an increased speed. The rodents may alternatively show signs of exhaustion instead of translating the effect of their injuries (Monville et al., 2006; Brooks & Dunnett, 2009). Additionally, a few variables, including learning, cardiopulmonary endurance and motor coordination might affect how well a rodent does on the rotarod (Shiotsuki et al., 2010). However, as the other motor tests, the rotarod should be accompanied or completed by extra tests that will further the initial screening.

IV.B. Cognitive tests

The contribution of motor behaviours test on TBI model is paramount to improve our comprehension of the ensuing deficits and for the development of targeted treatment. However, in humans, TBI often promotes the development of cognitive impairments (Xiong et al.,2013). Cognition relies on the ability to focus and grant full attention, to learn, to develop memory and being capable of decision-making (Kiely, 2014). Following TBI, those characteristics are usually disrupted and lead to a hampered cognition level (Hölter et al., 2015). Therefore, a series of test, usually very simple to set, have allowed scientist to evaluate the level of those cognitive impairments. Furthermore, it is crucial to take the mouse strain into account. Indeed, some mouse strains have been described with very little exploratory drive which would not be of the best fit for exploratory test such an open field test (Crusio, 2012).

IV.B.1. Open field test

Patients that sustained TBI have often endured heavy cognitive behaviours impairments as well as anxiety, depression and motor dysfunctions. The open field test (OFT) has been conceived to evaluate the exploratory behaviour and the general activity of the rodent. In a 1932 publication, Hall et al. firstly introduced the OFT (C. Hall & Ballachey, 1932; Walsh & Cummins, 1976; Hall, 1934). Hall is extensively recognised for the establishment of the OFT, that were originally investigated in rats and transferred to mice ulteriorly (Gould et al., 2009).

It consists of an "enclosure, generally square, rectangular, or circular in shape with surrounding walls that prevent escape" (Gould et al., 2009). The distance travelled, the rearing, the motility periods are amid the numerous variables that can be measured. A particular set of measurements can, in some cases, translate into some emotional state of the rodent such as anxiety. Hence, OFT was and is used to evaluate, for instance, the efficacy of anxiety compounds/treatments (Gould et al., 2009). The OFT has been used for different reasons and in different TBI contexts (Shultz et al., 2012; Tucker et al., 2016; Tucker et al., 2017). In 2017, Jamnia et al. used the test to investigate both locomotion and anxiety level of rats following closed head injury (Jamnia et al., 2017). Similarly, in 2016, McAteer et al. solely evaluate the anxiety of rats following mild TBI by monitoring their exploration time and pattern (McAteer et al., 2016). Beyond assessing locomotion, the OFT evaluates a range of other behaviours aspects as well. The test has also been implemented or fused with other test such as Novel object recognition, used for to assess rodents at various stages of learning and memory (Lueptow, 2017).

However, the reliability of OFT to measure some emotional features has been argued. Therefore, a series of complementary tests can be used, instead, to compensate for the limitations and evaluate, with more precision, individual facets of rodent behaviour.

IV.B.2. Y-maze test

Similarly to the OFT, Y-Maze test (YMT) gauge rodent's memory and spatial learning by observing their exploratory behaviour. Originally brought up by Spence and Lippitt in a 1946 publication, YMT, as the name implies, refers to a maze in a "Y" shape, thus displaying 3 arms with walls high enough to avoid any escape from the rodent (Spence & Lippitt, 1946). Interestingly, different configurations and paradigms of the test are being used. The spontaneous alternation test and the recognition memory test, also known as the spatial reference memory test, are two types of tests that can be performed independently. Spontaneous alternation test is used to measure the short-term spatial working memory of rodents (Prieur & Jadavji, 2019). "An alternation is defined as consecutive entries into all three arms" (Kraeuter et al., 2018). As an example, entries in these orders: 1, 2, 3 or 1, 3, 2 and repeated in those same orders will be considered as an alternation.

However, if the entries are following, for example, this order 1, 2, 1, no alternation is then observed. Regarding the recognition memory test, the time spent by the rodent in a novel or known arm is measured. The principle of this test lies on the restriction of one of the three arms, in a primary test phase, leaving the rodent to explore only two of them. In a second test phase, the three arms are free to be explored. Mice instinctively tend to directly explore new things/areas and in this case the new arm (initially restrained), by spending most of the time as opposed to the initially explored arms. All the subcategories of the YMT allow the assessment of different aspects of the rodent memory such as spatial working memory, exploration behaviours and learning abilities. Comparable to the OFT, the YMT can be readapted and merged with tests such as object recognition/novel object recognition test.

IV.B.3. Tail suspension test

Conceived in the mid-80s, the tail suspension test (TST) was inspired by the forced swim test (FST), a test engaging a mouse in a cylinder filled with water. The mouse is then found in an inescapable situation, thus triggering some level of stress. Both tests were initially used to screen for antidepressant in mice (Steru et al., 1985) and was thereafter used for purposes other than depression related behaviours (Can et al., 2011). However, FST has proven to create a more sever physiological imbalance in rodents as compared to the TST, causing risk of hypothermia and revealing to be more stressful for the animal than the TST (Thierry et al., 1986). The TST is described as followed: Mice are being hanged by their tail in such a way that they cannot escape nor hold onto element or surfaces surrounding them. The time spent being hanged is around six minutes. During this trial period, the behaviour adopted by the mice is scrutinized. The mice, undergoing this situation, reacted by adopting a stressed behaviour pattern like wriggling as well as episodes of immobility (Cryan et al., 2005). In FST context, Porsolt (1978) suggested that this “immobility” posture endorsed by the mice translate as a desperation feeling to escape from the situation (Porsolt et al., 1978). With the development of the investigation on the subject, the interpretation of the behaviour adopted by those mice have evolved and led to various conclusion and outcomes.

However, the complexity of the paradigm does not cover the broad range of occurring consequences through a single model. Each of them describes a particular aspect of TBI (Albert-Weißenberger & Sirén, 2010).

V. Neuron and its dendritic spines, synapses and plasticity

V.A. Spine dynamism in development and healthy paradigm

The brain has proven to constitute one of the most complex organs of the human body. This intricate organ encompasses around 10^{11} neurons creating a complex and cohesive network also known as the neuronal circuit. Implemented to the multiplicity of those circuits are glial cells that represent a major part in the maintenance and the proper function of the brain. Looking closely to the elaboration of the neuronal circuitry has led to uncover the underlying process used by and for neuron's communication. It was suggested for the first time in 1881 by Ramon y Cajal (y Cajal, 1888; Runge et al., 2020). Small protrusions were shown to originate along chickens cerebellar purkinje neurons' dendrites. Dendrites are defined as "appendages projecting directly from the neuron soma and branching largely" (Kapalka, 2010; Dharani, n.d.) These protrusions have been found to participate in neuronal communication and were thereafter named "spines". Thus far, the definition that is given of "spines" is: "protrusions from the dendrites, forming points of contact between neurons. The spines constitute the postsynaptic element of the majority of excitatory neuron" (Runge et al., 2020). Further investigations have shown a heterogeneity of spines distribution on a single dendrite, dependent on the neuron location itself, the cortical layer and region of the central nervous system (Knott & Holtmaat, 2008). More than 10^{13} spines are found in the brain (Nimchinsky et al., 2002) and around ten thousand of them on an individual dendrite (Gipson & Olive, 2016). Given their ability to alter both their density and morphology, dendritic spines have shown to be extremely dynamic entities (Gipson & Olive, 2016). In fact, with the development of high-resolution microscopic techniques and the improvement of reconstructive analysis tools, spine display a striking heterogeneity in their morphology and in the associated measurements (Gipson & Olive, 2016). Despite the versatility that dendritic spine shape presents, ranging from thin to thick and short to long, they have been categorised into three different main groups. Considering that a spine consists of a head of differential size connected to the dendritic shaft by a neck, in 1970, Peters & Kaiserman-Abramof have introduced a new way of characterising spines based on established metrics, commonly used nowadays (Peters & Kaiserman-Abramof, 1970). The spine nomenclature comprises stubby, mushroom and thin type. The filopodia type was added more recently.

Mushroom shaped spines present a large head and a slender neck unlike the thin spines that hold this distinctive head and neck configuration with a substantially smaller diameter and presenting a longer neck (Gipson & Olive, 2016). Mushroom spines are considered as mature, functional and stable spines, connected to synaptic boutons. However, thin spines appear to be the opposite and display a more transient state, allowing them to maintain a certain structural flexibility and translate, if needed, into a more mature state, the mushroom type ((Holtmaat et al., 2005; Runge et al., 2020).

On cortical and hippocampal neurons from the adult brain, 25% of spine are categorised as mushroom whereas more than 65% are “thin” (Harris et al., 1992; Peters & Kaiserman-Abramof, 1970; Berry & Nedivi, 2017).

Stubby spines, constituting another category from the dendritic “protrusions nomenclature”, are shorter, devoid of a discernible neck and are mostly sessile (Gipson & Olive, 2016; Berry & Nedivi, 2017). Nevertheless, in 2014, Tonnesen *et al.* were able to challenge the initial assumption by proving, with the use of stimulated emission depletion (STED), that stubby do in contrary own a neck part and could be therefore “mushroom” shaped spine (Tønnesen et al., 2014). Lastly, filopodia, protrusion from dendritic shaft described as the thinnest spine structure from whole categories, happened to be very motile and develop within seconds to minutes (Ozcan, 2017). In general, caution must be exercised when applying this arbitrary categorisation. Indeed, the recent evolution of imaging techniques has unravelled some inconsistencies with the previous findings and has consequently helped to further our understanding on dendritic spine. In addition, this categorisation minimises significantly the complexity of spine morphology and their perpetual dynamism (Gipson & Olive, 2016; Tønnesen et al., 2014).

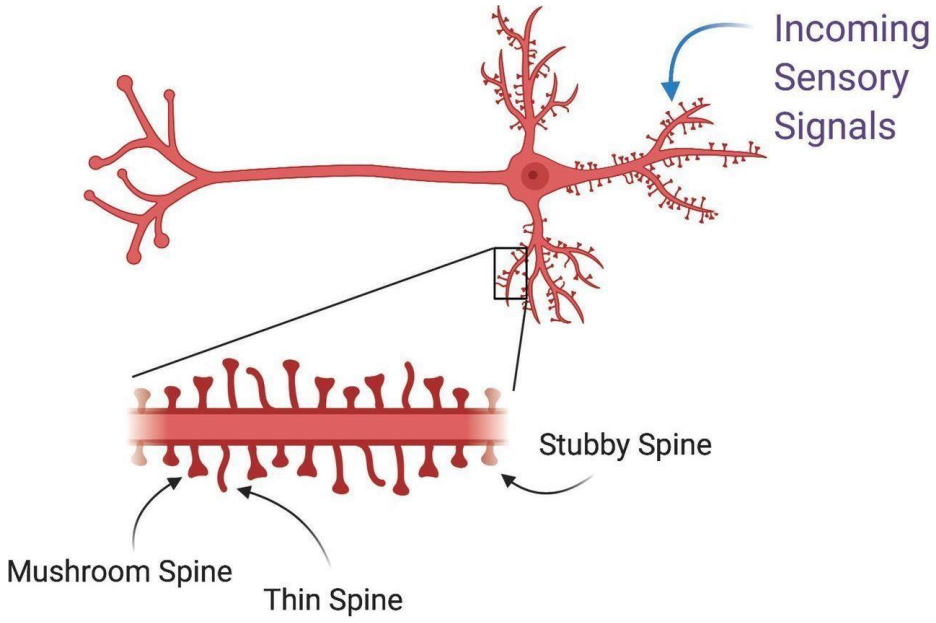

Figure 5. Illustration of the morphological classification of each dendritic spine
(Figure extracted and modified from Stratton & Khanna, 2020. License CC-BY- NC 4.)

Unlike the adult brain, early neuronal growth occurs primarily on the dendritic shaft of pyramidal neurons, where initial synapses are found. As spines start to appear, excitatory synapses relocate from the dendritic shaft to the newly formed spine (Yuste & Bonhoeffer, 2004; Berry & Nedivi, 2017). And as previously mentioned, most of the contacted spine are by excitatory neurons (Kawaguchi et al., 2005; Kuhlman & Huang, 2008). Thus far, inhibitory synapses onto spine have been shown to be

very minor. The cell body, axon initial segment and the dendritic shaft are among the main sub-cellular domains on which inhibitory synapses are often directly formed (Markram et al., 2004).

At the beginning of synaptogenesis, a continuous bulging and retraction from the dendrite is observed from a specific category of spine, the filopodia (Ziv & Smith, 1996; Fiala et al., 1998; Hering & Sheng, 2001). From those observations, emerging filopodia-shaped protuberances have been considered as precursor of dendritic spines. Over the first post-natal week, filopodia start drastically to increase. In the following weeks, these spines are gradually replaced by stubby spines and dendritic shaft synapses (Fiala et al., 1998; Hering & Sheng, 2001). Subsequently, thin and mushroom-shaped spines remain in the further developed rodent brain. Harris and colleagues suggested then that filopodia spine attract the pre-synapses to the dendritic shaft to create a contact that will then lead to the emergence of mature spine (Harris K. M. et al., 1999). However, in 2000, Parnass and colleagues demonstrated that spines could also, reversely, become filopodia (Parnass et al., 2000). The paradigm associated with the creation and the function of dendritic spines has been suggested by Ramon y Cajal, stating that neurons through their dendrites create spines to increase “their receptive surface” to form synapses (Gipson & Olive, 2016). Synapses constitute the mean through which neurons communicate with each other, using chemical signals transmitted from neuron to neuron,

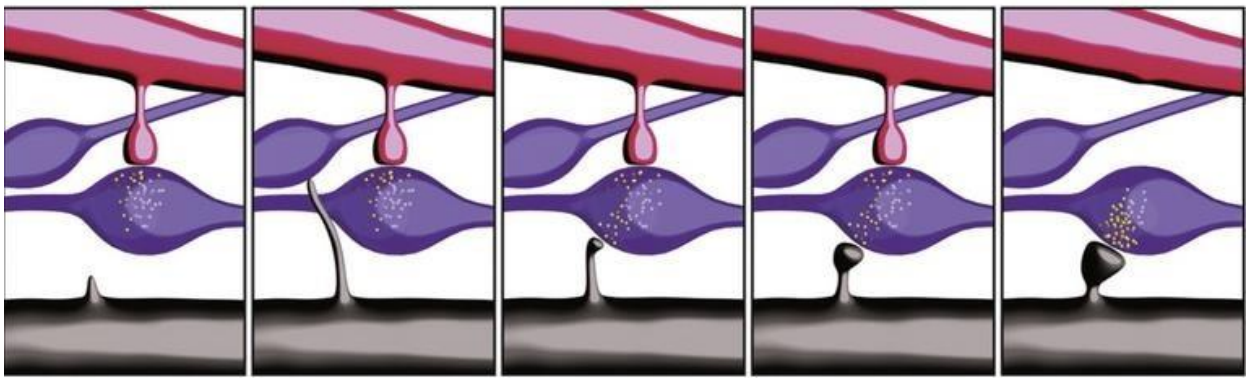

Figure 6. Dynamic Evolution of Dendritic Spines: a visual narrative
The figure illustrates the stepwise development of a dendritic spine. Firstly, a filopodia (depicted in grey) emerges and contacts an existing axonal bouton (shown in blue) already interacting with the dendritic spine (depicted in red). Following this initial contact, the filopodia establishes a synaptic connection and gradually enlarges in size. Thereafter, the initial spine diminishes, resulting in a solitary synapse bouton connected to the newly formed spine. (Reprinted from Brain Research Reviews, Knott & Holtmaat, 2008. Copyright © 2008 by Elsevier)

“one cell talks, the other listens” (*How Neurons Talk to Each Other* by Reinhard Jahn, 2016).

Therefore, spine can be considered as the central nervous system's (CNS) strategy to lay the foundations of neurons interplay and later their structural plasticity (Gipson & Olive, 2016; Hering & Sheng, 2001; Knott & Holtmaat, 2008).

Numerous studies have demonstrated the diversity of spines’ functions. Given their specific conformation, spines form a micro-compartment enclosing postsynaptic chemical signalling allowing them to operate semi-independently from the dendritic shaft. Calcium level for instance can be regulated locally and independently. Interestingly, this principal asset of the dendritic spines relies on their morphology and more specifically on their neck geometry, sign of their own stability (Hering &

Sheng, 2001; Gipson & Olive, 2016; Crick 1982; Koch & Zador, 1993; Lee et al., 2012; Shepherd, 1996; Yuste & Majewska, 2001). Spines are highly plastic entities. According to the conformation they adopt, they can display a more or less stable status, disclosing their maturity level. However, an older brain does not necessarily go hand in hand with stability and strengthening of neuron communication. In the contrary, numerous studies have shown that there is a non-negligible dendritic spine turnover (protrusion, maturation and elimination) maintained overtime, with thinner spines disappearing over few days and mushroom spines persisting over month (Bourne & Harris, 2008; Gipson & Olive, 2016). Mushroom spines, as previously described, foster most of the stable synapses, also referred to as "mature" synapses. The maturity level of those spine depends in particular on their post-synaptic density (PSD). The PSD is associated to the spines head membrane and is aligned with the presynaptic zone to allow smooth synaptic transmission. It consists of an assemblage of receptors, ions channels, cytoskeletal and signalling protein constructs (Nimchinsky et al., 2002). Therefore, synaptic strengthening could potentially correlate with the size of the spine head, determined by the number of receptors, as well as the surface covered by PSD (Hering & Sheng, 2001). Among the molecular systems presented by the PSD, the metabotropic glutamate receptors, α-amino-3-hydroxy-5-methyl-4-isoxazolepropionic acid (AMPA)- and *N*-methyl-D-aspartate (NMDA)-receptors are to be found. Additionally, voltage channels such as calcium, potassium and sodium channels, and polyribosomes are found within the spine. A smooth endoplasmic reticulum (SER) is also contained in dendritic spines, important for the maintenance and the regulation of endogenous Ca^{2+} level (Bourne & Harris, 2008; Nimchinsky et al., 2002). The SER and some cytoskeletal elements, such as the actin filament or microtubules, establish the spine apparatus. Found in a subpopulation of dendritic spines, the spine apparatus is most likely to be found in larger spine rather than thinner ones. Within spines, F-actin filaments are mostly seen compared to microtubules that happened to be very sparse. This suggests that the developmental and maturation/stability level of dendritic spines is due to the cytoskeletal organisation and their calcium management notably (Nimchinsky et al., 2002; Hering & Sheng, 2001). In addition to the listed elements, PSD-95, a scaffold protein that binds to NMDA receptor, is also present in spines and is important for the modulation and maturation of the post synaptic function (Cane et al., 2014). In the healthy developing brain, filopodia type of spine do not present a PSD. As for thin spines, they present a very small PSD area containing NMDA receptors and a minority of AMPA receptors, mainly responsible for the creation of action potential and therefore the synaptic transmission. Thin spines tend to maintain a certain structural flexibility that allow them to adjust or not to a more mature/stable form during the learning process and participate to the structural remodelling of the neuronal network (Bourne & Harris, 2008).

Looking at mushroom spines, they are highly enriched in polyribosomes, AMPA and NMDA receptors as well as actin filaments (Nimchinsky et al., 2002), which make them the most stable spine structure.

V.B. Disruption of spine dynamism and plasticity in neuropathology

With the development of advanced visualization techniques, such as two-photon microscopy (TPM), and certain transgenic animal lines, dendritic spines have proven to be highly dynamic entities, sustaining a certain balance between their formation and elimination rate over both short and long time periods (Hering & Sheng, 2001). Their dynamic is regulated through neuronal activity, development and experiences-dependent processes, involving particularly learning (Grutzendler et al., 2002; Cane et al., 2014; Zuo et al., 2005). This is well observed during the developmental phase of the brain. The neurons present in the young brain have been shown to display a much higher dendritic spine density than in adult brain (Duan et al., 2003), which point toward an endogenous process which mediate neuronal network over synaptic elimination, also referred as synaptic pruning. In a physiological context, the synapse elimination plays a role in the neuronal network reorganisation and the refinement of existing circuits across the different brain regions (Bhatt et al., 2009). However, the disbalance of spine dynamics has constantly been attributed the development of neurological disorders as neurodegenerative disease or psychiatric abnormalities such as schizophrenia, fragile X syndrome, autism and Alzheimer's disease (Glausier & Lewis, 2013; He & Portera-Cailliau, 2013; Leuner & Shors, 2013; Van Spronsen & Hoogenraad, 2010). As for TBI, dendritic spines degenerate leading to functional and structural impairments, attributed to the primary and secondary injuries (Xiong et al., 2013). Overall, dendritic spines have been able to demonstrate the important place they hold within the connectome, thanks to their plasticity and their dynamism. Their ability to modulate their morphology makes them an important entity for the acquisition and the storage of information to build memory (Bhatt et al., 2009). Nevertheless, the mechanism leading to the dysregulation of dendritic spines, contributing, or resulting from the development of diseases, remain pending.

V.B.1. The synapse; its genesis and function

In the early nineteenth century, living organism were shown to be built out of an abundance of unitary elements called cell. The central nervous system displayed a certain organisational complexity leading scientist to conclude that the nervous system was similarly constituted. However, the lack of adequate technicality hindered neurobiologists delving into the characteristic of this neuronal unit. The shape was assimilated as a vast intertwined network connected by protoplasmic links, which was the foundation of the "reticular theory" brought by Camillo Golgi (G. Shepherd & Erulkar, 1997). The advent and expansion of microscopy led to the rise of another concept called the "neuron doctrine". In the early twentieth century, Santiago Ramón y Cajal as well as Charles Sherrington described neuron as independent entities communicating with junctions which Sherrington named "synapses" (G. Shepherd & Erulkar, 1997). A synapse consists in a pre- and post-synaptic terminal communicating with each other through a gap called the synaptic cleft (Caire et al.,

2023). The synaptic cleft can be more or less large depending on the type of transmission they adopt. Neurons have been shown to communicate with one another across the whole CNS, also referred as synaptic transmission. Their communication has been described in two different ways: the transmission of electrical signalling/current, via gap junction, named electrical synapse and/or through neurotransmitters delivery, being the prominent way for neurons to communicate also known as chemical synapse (Purves, n.d.). Neurons adopt different types of “conversation” according to their specific morphology. The number of contacts depends on the intricacy of neurons’ dendrites. One to 100 000 synaptic inputs can be made on a single neuron (Caire et al., 2023).

Neurons morphology range from very bushy dendrite displaying a rich arborization to a very simplified one. Synaptic connections made onto neurons are categorised according to their contact sit: “axodendritic (presynaptic axon to postsynaptic dendrite), axosomatic (presynaptic axon to postsynaptic cell body), and axo-axonic (axon to axon)” (Caire et al., 2023).

Not only neurons, due to their dendrite’s aspect, influence the synaptic connection, the synapse itself adopts a certain phenotype that apply to their shape, their structure and the neurotransmitters delivered. Synapses can be assigned to two different categories, based upon those neurotransmitters: excitatory or inhibitory (Caire et al., 2023). During development, the synapse formation is associated with neuronal faith. After neurons form and develop their different features including their axon and dendrites, a group of gene allocated to the creation of synaptic protein become functional. This will lead to the establishment of the synaptic complex and the development of its dynamism, implying the transport of neurotransmitters the axonal terminal (Waites et al., 2005). At developmental stage, the synapses are initially very abundant and volatile due to neurons first attempt to communicate. Throughout time, synapses can stabilise or get eliminated according to their activity level. The same procedure is occurring in adults, at later stages (Grutzendler et al., 2002).

V.B.2. Synapse elimination: pruning and engulfment

As previously mentioned, during brain development, the number of synapses is beyond the one seen in mature brains, with 15% more than the remaining ones in adulthood (Sakai, 2020). Synaptic pruning, in human CNS, mainly happens during the first two post-natal years and during adolescence/puberty (Riccomagno & Kolodkin, 2015). At the premises of post-natal development, an abundant subset of synapses is formed throughout the entire nervous system, central and peripheral. As the development phase progresses, synapses are being eliminated through a process defined as "synaptic pruning” (Faust, Gunner, & Schafer, 2021). In humans, the first two years after birth and adolescence are the two key developmental stages when most of the synaptic pruning takes place (Faust, Gunner, & Schafer, 2021). In a synchronous manner, the remaining synapses are maintained into a mature and self-tuned circuit. In brief, a post-synaptic element receives multiple potential connections from neurons, as pre-synaptic elements. However, only one pre-synaptic input will

remain, resulting from the pruning process (Hua & Smith, 2004). The remaining synapses have been characterized as strong synapses and have been linked to their activity level. This paradigm has been demonstrated by Wiesel and Hubel declaring that “changes in neuronal activity can elicit developmental rewiring of the central nervous system (CNS)” (Faust, Gunner, & Schafer, 2021). Therefore, the Connectome, based upon those synapses, will get refined overtime, thus engaging in synaptic plasticity. The tuning process triggers as well morphological changes helping in the reinforcement and the maintenance of the remaining synapses (Schafer et al., 2012; Hua & Smith, 2004; Hubel, Wiesel, & Stryker, 1977). The reason underlying the targeted removal of certain synapses, involved in the network remodeling process, is still poorly understood at a cellular and molecular level, but as mentioned previously, some studies advocate for synaptic activity being paramount for synapses own stability and the removal of the “weaker ones”. Interestingly, the approach taken by the central and peripheral nervous system to operate as such has been demonstrated by Barth et al in 2015 to be the most efficient strategies (Navlakha, Barth, & Bar-Joseph, 2015). “Network that are constructed through overabundance and then pruning are much more robust and efficient than networks that are constructed through other means” (Sakai, 2020). The investigation of peripheral nervous system (PNS) mammalian neuromuscular junctions (NMJ) (Sanes & Lichtman, 1999) has furthered our understanding in the process of synaptic pruning, also shown to occur in the CNS in the retinogeniculate system (C. Chen & Regehr, 2000). The importance of synaptic activity in the pruning process has been shown when blocked neural activity led to the disruption of pruning (Shatz, 1990). Strength of a synapse has been determined as “the average amount of current or voltage excursion produced in the postsynaptic neuron by an action potential in the presynaptic neuron” (Murthy, 1998). Not only neural activity has been linked to synapse removal and synapses strengthening, but there is also neuron-intrinsic immune based mechanism responsible for the elimination of synapses. Certain molecules involved in the immune system of the CNS are also present in the body immune system and revealed to be essential for synaptic pruning (Faust et al., 2021). The discovery of class I major histocompatibility complex molecules (MHC class I), being an important mediator in the antigen presentation of the adaptive immune response, participate in the synaptic pruning but also help maintaining the physiological balance of synapses (Faust et al., 2021). MHC class I knock-out leads to an increased in spine density and is present during the first steps of the CNS connections (Glynn et al., 2011). Continuing with the implication of the immune system in synaptic pruning, pentraxins, a protein involved in the innate immune response, is expressed in neuron under two different forms, NP1 and NP2/Narp. They have been responsible for the regulation of AMPA receptor clustering and influenced synaptic plasticity (Faust et al., 2021). NP1 knockdown shows increase in synapse density (Figueiro-Silva et al., 2015). Some studies hypothesized on the interaction of pentraxins and the complement proteins, and more specifically complement component 1q (C1q), in the mediation of synaptic pruning (Kovács et al., 2021). In the central nervous immune system, the complement cascade is also present and evolve cooperatively with microglial cells in the

pruning process of synapses, microglia being the resident macrophages of the CNS (Stevens et al., 2007). As an essential element of innate immunity, the complement system is in charge of identifying pathogens or stressed cells, which triggers the migration of immune cells with scavenger capabilities—in this case, microglia (Alawieh et al., 2018; Faust et al., 2021). The mechanistic undertaken by the complement cascade is very specific. It implies the deposition of complements opsonin [complement component 1q (C1q) and C3 components] to bind on the synapses. Initiated by C1q, the complement cascade led to the formation of C3 convertase, activating C3. C1q and C3 are present at the retinogeniculate synapses during developmental pruning. The synapses are pruned by microglia via complement 3 receptor (CR3) (Schafer et al., 2012; Stevens et al., 2007). Mice presenting a lack of C1q, C3 or CR3 display impairments in eye-specific segregation by failing to engulf synapses to refine the circuit (Schafer et al., 2012; Stevens et al., 2007). In CNS, microglial cells reveal to be major contributor of C1q components (Fonseca et al., 2017). As for astrocytes, they are a source of complement components being C3. Astrocytes were also proven to participate in the synaptic pruning by carrying Megf10 receptors, highly represented on astrocytes, and MerTK receptors which is found as well on microglia (Chung et al., 2013; Faust et al., 2021). Apart from synaptic pruning, astrocyte secrete specific factors which come into play in the engulfment process, such as Hevin, a factor influencing the elimination of excess synapses (Faust et al., 2021; Risher et al., 2014). Furthermore, microglia-astrocyte crosstalk coordinates microglia's engulfment though molecular player such as TGF-ß and IL-33. Vis versa, studies have suggested that microglia influence astrocytic pruning via triggering receptor expressed on myeloid (TREM2) in the hippocampus (Jay et al., 2019). The fractalkine receptor CX3CR1 was shown to be present on microglia and highly influence their phagocytic properties (Paolicelli et al., 2011). In 2011, a study has shown the implication of microglia in synaptic pruning by disrupting fractalkine and observing an immature network in adult mouse (Paolicelli et al., 2011). In 2012, Stevens et al uncovered the implication of a particular group of protein involved in a process called the complement cascade, highly implicated and relevant during CNS immune reaction, as an essential intermediate between microglia and the pruned synapse (Stevens et al., 2007). Other factors, besides any immune signaling, are as well responsible or promotes synaptic pruning. The activation of cell death marker, such Caspase-3, plays a role in dendritic spine pruning. Studies revealed that knockout mice lacking caspase-3 displayed impaired pruning of hippocampal spines in live experiments. Furthermore, calcineurin, a calcium-dependent protein phosphatase, participates in the activity-dependent degradation of PSD-95, contributing to the elimination of dendritic spines (Faust et al., 2021). Lastly, externalization of Phosphatidylserine (PtdSer), following caspase activation, constitute a key factor facilitating clearance of apoptotic cells. PtdSer bound to tumor associated macrophages (TAM) receptor complexes such as MerTK, present on phagocytes (Zagórska et al., 2014; Scott-Hewitt et al., 2020). Additional immune molecules linked to synaptic pruning, including Triggering receptor expressed on myeloid cells 2 (TREM2), G protein-coupled receptor 56 (GPR56), and C1q, also bind to PtdSer.

(Païdassi et al., 2008; Li et al., 2021; Lemke & Burstyn-Cohen, 2010). Overall, Pro-apoptotic caspase pathways have been shown to lead to “degeneration-like pruning” processes (Nikolaev et al., 2009; Olsen et al., 2014; Riccomagno & Kolodkin, 2015). A variety of intrinsic and extrinsic components engage in the process of synaptic pruning with a close internal monitoring in the development of a functional and organized network (Riccomagno & Kolodkin, 2015).

V.C. Aberrant synaptic pruning in the alteration of brain networks

A functional and adaptive brain is based on its precise and restricted wiring paradigm sharpened through synaptic pruning (Faust et al., 2021). This mature neuronal network depends on the elimination of the excess of synapses and dendrites initially formed during the CNS development. Synaptic pruning represents a significant developmental process for the nervous system and is a major contributor in the structural plasticity of the CNS. Neural activity is implicated in this process, in addition to recently identified functions for chemicals involved in cell death and immunological signalling. These mechanisms, intrinsic to neurons or driven by glia, contribute to synapse removal and maintenance of the proper brain function (Faust et al., 2021). However, any defects in synaptic pruning during those period leads to a misbalance in synaptic density during and underlie neurodevelopmental disorders and abnormal brain connectivity. This statement was already suggested in the early 80s by the psychiatrist Irwin Feinberg (Feinberg, 1982), which led scientist to carry investigation in order to understand the potential detrimental role of pruning dysregulation. Schizophrenia (SZ) and autism spectrum disorders (ASD) are two different conditions, diagnosed at different time periods which led Researchers to question whether an inconsistence in synaptic pruning would be the reason to their genesis (Fig7.). Schizophrenic patients are described having less synapses in their brain as compared to a normal brain (Sellgren et al., 2019; Watson & Tang, 2022; Feinberg, 1982). As a result, a more severe synaptic pruning may be the root of it, and according to Feinberg, the first initial diagnosis and the excess synaptic pruning occur throughout adolescence (Feinberg, 1982). Therefore, a more pronounced synaptic pruning could be the cause of it and the timeline of the first diagnosis and the synaptic pruning coincide, which is during adolescence (Feinberg, 1982). Further investigations have even led to identify a gene that would be responsible for an excessive synaptic pruning in schizophrenic patient. A gene variant of the complement cascade element C4 as well as other gene variant that would promote C4 increased expression are held responsible for a higher risk to develop schizophrenia (Sekar et al., 2016). The increased synaptic pruning was demonstrated by Sellgren et al in a 2019 publication, reporting an increase in synaptic elements within microglia from schizophrenic patient (Sellgren et al., 2019). Conversely, ASD has shown an overabundance of synapses which may suggest a deficiency in the synaptic pruning (Hutsler & Zhang, 2010; Tang et al., 2014). Synaptic pruning happens at early stages of post-

development and during adolescence. An impairment in this process, as demonstrated previously, leads to neurodevelopmental disorders, revealing the central role of synaptic elimination in the development of a functional brain. During adulthood and later in life, several studies have uncovered the maintenance or the development of synaptic pruning processes, however the purpose remains elusive. As seen with the neurodevelopmental disorders, synaptic pruning could also lead to neurodegenerative disease. When it comes to Alzheimer disease (AD), an extensive number of risk genes have been observed to be overexpressed by microglia (Sudwarts & Thinakaran, 2023). Therefore, microglia have been defined as one major player in the incidence of AD.

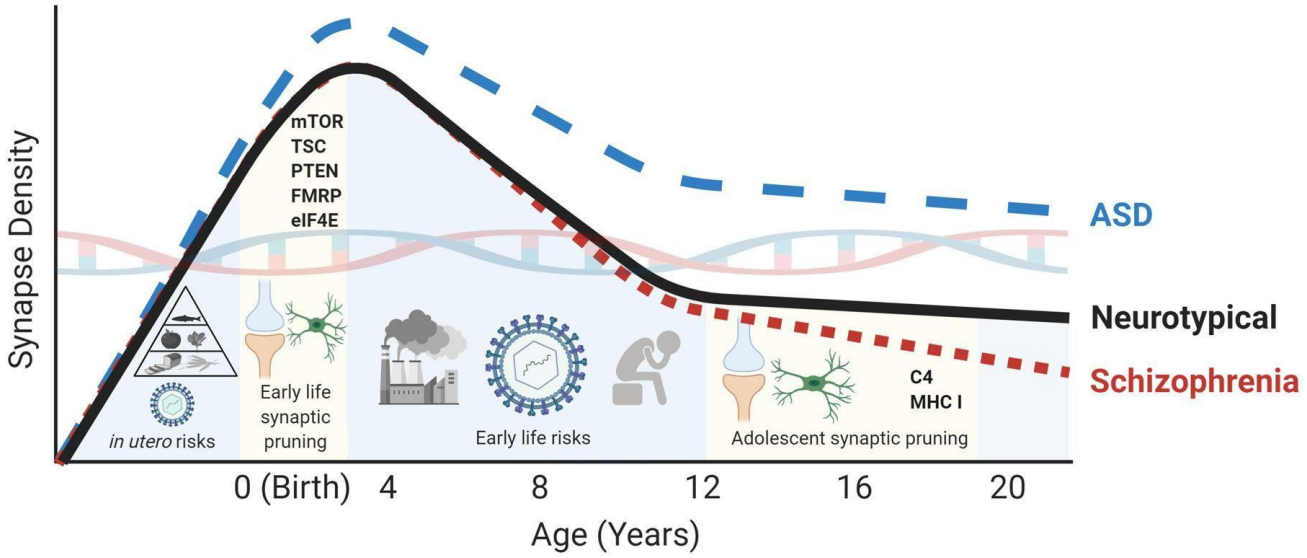

Figure 7. Insights into Synaptic Pruning and Neurodevelopmental Disorders: A Comprehensive Overview
The figure presents a synthesis, drawn from research results regarding alterations in synapse density throughout brain development in neurotypical individuals versus those diagnosed with autism spectrum disorders (ASD) or schizophrenia (SZ). Mammalian target of rapamycin (mTOR), tuberous sclerosis (TSC), phosphatase and tensin homolog (PTEN), fragile X mental retardation protein (FMRP), eukaryotic translation initiation factor 4E (eIF4E), major histocompatibility complex class I (MHC I), complement 4 (C4). (Reprinted from Nature Reviews Neuroscience, Faust et al., 2021. Copyright © 2021 by Springer Nature)

There is evidence that traumatic brain damage increases the risk of strokes, Parkinson's disease (PD), dementia, and other conditions (Gorgoraptis et al., 2019; Fann et al., 2018; Gardner et al., 2018; Chen, Kang, & Lin, 2011). Even in the early stages of Alzheimer's disease, there is a correlation between the loss of synapses and the reduction in cognitive function (Scheff et al., 2006; Sultana et al., 2010). Conversely, repeated traumatic brain injuries, such as those commonly experienced by boxers and football players, can lead to chronic traumatic encephalopathy (CTE), characterized by abnormal tau protein accumulation (Stern et al., 2013). Given that synapses loss is implicated in the progression of Alzheimer's disease due to the spread of pathological tau, it prompts the question of whether similar synaptic mechanisms contribute to neurodegeneration following traumatic brain injury. Interestingly, studies employing a controlled cortical impact (CCI) model have demonstrated little neuronal loss but a marked decrease in synaptic density in the hippocampus region soon after

damage. These findings collectively highlight the swift occurrence of synapse loss following TBI, particularly within the hippocampus adjacent to the injury.

Similarly to fractalkine, the interruption of the complement cascade leads to the maintenance of an immature network in the adulthood. The paradigm involving the complement cascade as a synaptic pruning mechanism lies in the complement protein targeting low-activity synapses that will further be pruned by microglia. However, Gross observes a particular behaviour adopted by the microglia at the time of the pruning (Weinhard et al., 2018; Paolicelli et al., 2011). He assesses that microglia do not completely engulf the entire synapse but nibble a part, which is called trogocytosis. He then confirmed that the entire mechanism is not entirely understood and clear at this stage (Weinhard et al., 2018). Therefore, further investigations on the pruning role of microglia are central in understanding the origine of synapse loss and establishing, in the future, the right target for a better maintenance of the homeostatic pruning.

VI. Glial cells – Microglia

Accounting for 10–20% of all brain cells, microglia are the native macrophages of the central nervous system (Soulet & Rivest, 2008). In the early 20th century, Pío del Río Hortega, a Spanish neuroscientist, discovered this multifactorial entity, that will during the 100 years following the discovery, show its primary role in brain development and pathological condition (Pérez-Cerdá et al., 2015; Prinz et al., 2019).

VI.A. History and ontology

As previously mentioned, microglia represent the primary immune cells of the central nervous (CNS), along with perivascular macrophages (Perry & Teeling, 2013). In the brain parenchyma, microglia represent the largest immune cells' population from the CNS (Sevenich, 2018). Microglia were formerly believed to have a neuroectodermal origin, similar to other glial cells and neurons seen in the CNS (van Furth et al., 1972; Prinz et al., 2019). However, it has since been determined that these cells are macrophages, suggesting that they are related to the immune system (van Furth et al., 1972; Prinz et al., 2019). Macrophages, including microglia, can arise from three distinct developmental pathways in mice (Ginhoux and Guilliams, 2016). Microglia originates from c-KitloCD41lo progenitors in the yolk sac around embryonic day 7.25 (Prinz et al., 2019; Ginhoux et al., 2010). Those cells present a unique embryonic origin and migrate to the developing brain during foetal development (Ginhoux et al., 2010; Prinz et al., 2019). The BBB is thereafter formed which leads to a complete shutdown of the migration of further macrophages. Microglia as well as meningeal and perivascular macrophages are described as the remaining macrophages that persist through life as byproducts of the early primitive haematopoiesis (Prinz et al., 2019; Ginhoux et al., 2010).

Although the life expectancy of a single microglia is very limited, changes in their density is mitigated by their self-regeneration capacity in absence of any precursor's inputs (Ajami et al., 2007; Prinz et al., 2014). This led to a maintenance of microglia's density in a region-specific manner. Microglia, together with other CNS macrophages, persist throughout adulthood without major contribution from hematopoietic stem cell (HSC)-derived cells (Ajami et al., 2011). The complexity of microglia's development and maturation, also known as microglial ontogeny, involves a series of steps that are regulated by various genetic and environmental factors (Bennett et al., 2018). Also, microglia display distinct transcriptomes and epigenomes, shaped by local tissue-specific factors during development (Lavin et al., 2014).

During early development, erythro-myeloid progenitors migrate to the CNS and differentiate into microglia under the influence of various growth factors and signalling pathways (Ginhoux et al., 2010; Kierdorf et al., 2013). Transcription factor PU.1, considered as one of the key regulator of microglia development is essential for the proper differentiation and maturation of microglia (Kierdorf et al., 2013; Bennett et al., 2018). The transcription factor CCAAT-enhancer-binding proteins alpha (C/EBPα) is crucial for the formation of the microglial lineage from myeloid progenitors. Research have also demonstrated that C/EBPα is involved in the maturation and specifically in the polarization of microglia (Ren et al., 2008). Both factors are regulated by colony-stimulating factor-1 (CSF-1) or interleukin (IL)-34 secreted by astrocytes and neurons (Ginhoux et al., 2010; Kierdorf et al., 2013 However, Buttgereit et al. raised the possibility that the transcriptional repressor Sall1 is essential for preserving the microglia core signature (Buttgereit et al., 2016).

Microglia's diverse functions have since been elucidated, including synaptic tagging and elimination during development, as well as continuous monitoring and rapid response to injuries throughout life. (Stevens et al., 2007; Schafer & Stevens, 2010; Paolicelli et al., 2011; Schafer et al., 2012; Davalos et al., 2005; Nimmerjahn et al., 2005). They were shown to play key roles in regulating neuronal numbers, phagocytosing apoptotic cells, and responding to CNS insults. (Paolicelli et al., 2011). In disease, microglia can exhibit either damaging or restorative behaviours. (De Lucia et al., 2016; Krasemann et al., 2017). Recent research has uncovered microglial involvement in synaptic plasticity, highlighting their multifaceted roles. (Tremblay et al., 2010; Miyamoto et al., 2016; Sipe et al., 2016)

Exploring microglial self-renewal and homeostasis in the adult brain has become a topic of increasing interest and will help better understand the stake represented by microglia in the maintenance of brain homeostasis (Zhan et al., 2019; Zhan et al., 2020; Mendes et al., 2020). These findings would contribute to developing therapeutic strategies targeting microglia-related disorders.

VI.B. The role of Microglia in developmental processes

During the embryonic and early postnatal stages, microglia in the developing brain exhibit a distinct morphology compared to adult microglia. Unlike their ramified counterparts in the adult brain adopting then a surveillance feature of their environment, these cells display an amoeboid morphology mainly seen among macrophages, indicating their active implication in phagocytic processes and tissue remodelling (Lawson et al., 1990; Matcovitch-Natan et al., 2016). Furthermore, some studies indicate a significantly higher proliferation rate of microglia during development as compared to adulthood (Askew et al., 2017; Bennett et al., 2018; Kierdorf et al., 2013; Varol et al., 2017).

Microglia play crucial roles in shaping the neuronal network of the CNS during its development (Frost and Schafer, 2016). Their involvement in building a functional network imply the control of neuronal density notably using engulfment processes, the removal of dead cells as shown in zebrafish with the engulfing neuronal progenitor cells (NPC) and monitoring neuronal faith (Ashwell, 1990; Marín-Teva et al., 2004; Sedel et al., 2004). Similar procedures happen, as well, into young adulthood, where microglia participate in shaping neuronal network by removing apoptotic neurons in specific brain regions such as the hippocampus (Sierra et al., 2010). Additionally, microglia support neurogenesis by promoting the survival, proliferation, and maturation of NPCs and neurons, with factors like the CX3CR1 chemokine receptor and insulin-like growth factor 1 (IGF-1) playing crucial roles (Ueno et al., 2013). However, the precise coordination and balance of these activities and their regional specificity remain subjects for further investigation (Prinz et al., 2019).

During postnatal development, microglia are extensively interacting with synapses, potentially playing an active role in remodeling synaptic circuits. They are implicated in the removal of non-functional synapses and the modulation of synaptic connectivity, with observations of synaptic defects in animals lacking microglial CX3CR1 (Paolicelli et al., 2011). Recent studies suggest that microglial synapse engulfment may involve the complement cascade rather than CX3CR1 engagement (Stevens et al., 2007; Schafer et al., 2012). Moreover, microglial expression of the purinergic receptor P2Y12 and the CD47-SIRPα signaling axis have been shown to influence synaptic pruning, highlighting the complex regulatory mechanisms involved (Sipe et al., 2016; Lehrman et al., 2018). Additionally, microglia are implicated in modulating neuronal wiring and axonal outgrowth during brain development, impacting the positioning of various neuronal subsets (Squarzoni et al., 2014). Not only microglial cells play a critical role among neurons, but they also support other cells from the CNS and the development of the vasculature structures. They contribute as well to the creation and maintenance of the BBB. They are critical for myelinogenesis and remyelination processes, interacting with oligodendrocytes and their progenitors during the postnatal period (Hagemeyer et al., 2017; Wlodarczyk et al., 2017). Additionally, microglia contribute to developmental angiogenesis by promoting vessel fusion, although the underlying mechanisms are still unclear (Fantin et al., 2010). Additional investigations are required to clarify the specific molecular players and mechanisms underlying microglial interactions with other

glial cells and endothelial cells as well as understanding the mechanisms underpinning microglial ontogeny and function during development, despite their significance.

VI.C. Microglia integrity and morphology

Microglia in both developing and adult brains are recognized for their distinctive morphologies, appearing as either amoeboid or ramified cells. These structural variations most likely indicate that different microglial populations are at different activation stages (Lawson et al., 1992). Besides displaying morphological differences, in distinct region of the brain, the distribution of microglia cells remains consistent (Stopper et al., 2018). However, looking globally at the brain, microglia's' features and density differ (Kongsui et al., 2014). One of the key features of microglial morphology is their highly branched, tree-like appearance. Microglia have a small cell body with numerous processes that extend outwards, allowing them to surveil their surroundings and respond to various stimuli (Tremblay et al., 2011; Nimmerjahn, 2012). Due to their dynamic nature, these systems have the ability to expand and retract in response to various cues. For example, when microglia encounter a pathogen or other stimulus, such as damage-associated molecular patterns (DAMPs), they retract their processes and adopt a larger, more voluminous cell body in order to embrace a phagocytic phenotype or release pro-inflammatory cytokines, leading to a final morphology state being amoeboid (Huang et al., 2015; Colonna & Butovsky, 2017). The amoeboid shape usually refers to a large, rounded shape which provide to the microglia the ability to migrate quick and easily, and to m phagocyte entities (Doorn et al., 2013). Therefore, microglia hold the significant ability to undergo quick morphological changes, allowing their migration to injury sites and the phagocytosis of pathogens and debris (Davalos et al., 2005; Nimmerjahn et al., 2005; Tremblay et al., 2011). Within the spectrum of microglial morphology, ranging from ramified to amoeboid shapes, microglia exhibit diverse transition states. These transitional morphologies may denote disease-specific functional states of the cells, yet their precise spatial organization and role in diseased or damaged brains remain ambiguous (Stence et al., 2001; Fumagalli et al., 2013; Salamanca et al., 2019). Recent investigations have unveiled a previously unrecognized morphology of microglia in mice, termed "rod-like microglial cells." (Nissl, 1899). This morphology, first described by Franz Nissl in 1899, is characterized by the absence of planar processes, reduced secondary branching, and narrowing of the cell and soma (Nissl, 1899; Ziebell et al., 2012; Taylor et al., 2014).

Microglia have a variety of surface receptors in addition to their distinctive morphology, which enables them to recognize and react to a range of stimuli. These receptors also participate in shaping microglia morphology. They include complement receptors (which are activated by the complement system) and toll-like receptors (TLRs), which are triggered by pathogen-associated molecular patterns (PAMPs). TLRs are a crucial part of the innate immune system, and their activation can cause the production of cytokines that promote inflammation as well as other immune mediators

(Lehnardt, 2009). Complement receptors, on the other hand, play a vital role in the humoral immune response by activating the complement system (Stevens et al., 2007; Schafer et al., 2012).
The phagocytosis of waste and injured cells by microglia is a crucial feature of their morphology. Microglia are equipped with a range of phagocytic receptors that allow them to recognize and engulf debris, including opsonin such as complement proteins and antibodies. In addition, microglia can also express phagocytic receptors that recognize specific types of debris, such as amyloid plaques in the brain. This process, known as microglial phagocytosis, is essential for maintaining brain homeostasis and protecting against injury and infection. Furthermore, new research indicate that microglia differ morphologically and phenotypically in various brain regions, at various ages, and during illnesses (Mendes & Majewska, 2021).

Overall, microglial morphology plays a crucial role in their function as immune cells of the CNS. By expressing surface receptors, phagocytosing debris, and extending and retracting their processes to screen the extracellular space in the brain, microglial cells are able to maintain brain homeostasis and protect against injury and infection.

VI.D. Microglia in synapse engulfment and pruning

For the CNS to mature and operate properly, redundant and unnecessary synapses must be removed through a process known as "synapse pruning." By engulfing and destroying synapses through a process known as phagocytosis, microglia have demonstrated to play a significant part in this process (Liu et al., 2020). The human brain experiences rapid synapse production and growth during development, followed by synapse pruning (Schafer, Lehrman, & Stevens, 2012). This procedure enables the brain to improve its connectivity and remove unused or excessive synapses, which is crucial for the CNS's healthy maturation and operation. Neuronal activity, genetics, and environmental factors are some of the factors that are hypothesized to control synapse pruning (Katz & Shatz, 1996; Hua & Smith, 2004). Numerous components of the signalling network, many of which are found at the synapse, are essential for both innate and adaptive immunity and control the complex interactions between microglia and neurons. (Eyo & Wu, 2013; Sun & Barres, 2016). This positioning enables microglia to actively regulate the development and plasticity of neural circuits (Mendes & Majewska, 2021). Mounting evidence suggest that a variety of variables, including neuronal activity, inflammatory signals, and epigenetic changes, may govern microglial-mediated synapse pruning. Altering retinal activity or exposure to light affects how neurons and microglia physically interact in the visual cortex, consequently affecting the phagocytic activity of microglia (Wake et al., 2009; Tremblay et al., 2010). Similarly, manipulation of retinogeniculate projections impacts the preferential elimination of less active presynaptic inputs by microglia (Schafer, Lehrman, Kautzman, et al., 2012). Furthermore, the activation of dendritic NMDA receptors on neurons by exogenous ATP or seizure induction triggers the recruitment of microglia to synapses (Eyo et al., 2014). Microglial pathways

involved in synaptic modulation across different stages of life provides valuable insights into the mechanisms governing microglial regulation of synaptic dynamics and their contributions to neural circuit development and plasticity. Fractalkine is one of them main candidate pathway.

Synaptic activity plays a crucial role in regulating the phagocytic activity of microglia. In the hippocampus, the removal of synapses through phagocytosis is reliant on fractalkine signalling. The chemokine fractalkine, release by neuron in an activity-dependent way, plays a major role in synaptic pruning, impacting dendritic spine density and maturation deficits (Paolicelli et al., 2011; Gunner et al., 2019). This signaling pathway, mediated by the fractalkine receptor, CX3CR1 and CX3CL1, is crucial for synaptic connections refinement during development through direct interactions between neurons and microglia (Schecter et al., 2017; Lowery et al., 2017). However, fractalkine signaling is not universally required for synaptic plasticity, indicating context-dependent roles in microglial function (Paolicelli et al., 2011; Gunner et al., 2019; Hoshiko et al., 2012; Schafer et al., 2012; Lowery et al., 2017; Schecter et al., 2017).

Purinergic signaling, mediated by ATP and ADP and their receptors, regulates synaptic development and transmission (Sipe et al., 2016; Haynes et al., 2006; Mildner et al., 2016). The purinergic receptor P2Y, more precisely P2Y12, primarily expressed by microglia, facilitates synaptic remodeling and plasticity through ATP-mediated communication. Its disruption impairs, for instance, ocular dominance plasticity, highlighting its essential role in microglial dynamics and synaptic refinement (Sipe et al., 2016; Davalos et al., 2005).

Noradrenergic neurons modulate microglial function throughout the brain, impacting synaptic plasticity during development and adult stage, and vigilance states (Heneka et al., 2010; Liu et al., 2019; Stowell et al., 2019). Noradrenaline (NE), also known as norepinephrine, holds anti-inflammatory properties and enhances microglial phagocytosis, particularly in the context of Alzheimer’s disease (AD) (Mendes & Majewska, 2021). Noradrenaline-mediated signaling, particularly through β2 adrenergic receptors expressed by cortical microglia, influences microglial surveillance and their interactions with dendritic spines, vital for the visual cortex's experience-dependent plasticity (Heneka et al., 2010; O’Donnell et al., 2012). Furthermore, it's probable that receptors like P2Y12 and β2 adrenergic receptors cooperate to regulate microglial roles in neurotransmission (Mendes & Majewska, 2021). Both receptors are G-protein coupled, activating opposing downstream pathways (Gyoneva & Traynelis, 2013).

A complex signaling pathway called the complement cascade is composed of several proteins that are activated by partial cleavage (Carroll, 2004). Many different organs and cell types, including brain cells like astrocytes, microglia, and even neurons, have a large distribution of complement ligands and receptors. Previously, it was thought that complement was mostly expressed in immune cells (Stephan et al., 2012). This general representation implies that the complement cascade's roles in clearing debris and defending the immune system are maintained in both peripheral and central tissues (Mendes & Majewska, 2021). The complement cascade plays a vital role in microglial-

mediated synaptic engulfment and elimination, particularly during early development. Complement proteins tag weak synapses for removal, contributing to synaptic refinement and circuit organization (Schafer et al., 2012; Stevens et al., 2007). In the developing central nervous system (CNS), complement proteins are widely distributed, with the classical complement cascade significantly involved in microglia-mediated synaptic engulfment (Schafer et al., 2012; Wu et al., 2015). C1q and downstream complement protein C3 have been identified, by immunohistochemistry studies, on dendrites and axons in the postnatal brain. These proteins are especially important for active synaptic circuit remodeling by microglia and astrocytes in the early postnatal stages (Stevens et al., 2007; Tremblay et al., 2010; Paolicelli et al., 2011). For instance, complement regulation facilitates the remodeling and elimination of transient connections between retinal ganglion cells (RGCs) and relay neurons in the dorsal lateral geniculate nucleus (dLGN) during early development (Schafer et al., 2012). Genetic deficiencies in key complement proteins such as C1q and C3 result in synaptic refinement deficits, affecting synaptic connectivity in the mature brain (Stevens et al., 2007). Notably, microglia play a pivotal role in this process, expressing both the initiating molecule of the complement cascade, C1q, and the complement receptor CR3 (Ransohoff & Perry, 2009). Although the involvement of the complement cascade in early synaptic refinement is well-established, its direct roles in physiological synaptic remodeling beyond early development remain ambiguous. However, sustained defects in synaptic connectivity observed in adult mice deficient in C3 or CR3 imply a potential long-term impact of complement signaling on synaptic organization (Schafer et al., 2012). Uncovering the precise processes behind complement-mediated synaptic refinement throughout the CNS's developing and mature stages will require additional research.

Phosphatidylserine and CD47 signaling pathways regulate microglial phagocytosis of synapses, with phosphatidylserine, similarly to the complement pathway, acting as a signal for synaptic refinement by tagging the weak synapses and CD47-SIRPα signaling protecting active synapses from elimination. Their dynamic interplay determines the balance between synapse preservation and pruning (Scott-Hewitt et al., 2020; Lehrman et al., 2018).

And lastly microglial-derived brain-derived neurotrophic factor (BDNF) modulates synaptic plasticity, synaptogenesis, impacting spine formation and motor learning task, in case of a lack of BDNF expression by microglia (Mendes & Majewska, 2021). Its widespread expression suggests a crucial role in the local regulation of synapses (Parkhurst et al., 2013).

Overall, microglia are important for the synapse pruning process, which is necessary for the CNS to mature and operate properly. The processes behind microglial-mediated synapse pruning are still poorly understood, and it is unclear how this process is controlled. This will be crucial for creating targeted treatments for neurological conditions and disorders that entail aberrant synapse growth or function.

VI.E. Microglia activation and neuroinflammation

Microglia are responsible for maintaining brain homeostasis and protecting against injury and infection (Wolf et al., 2017). They can be initiated by a variety of triggers, such as neuronal injury, the presence of infections, and exposure to toxins. Activated microglia undergo a number of morphological and functional changes, such as an increase of surface receptors, an increase in phagocytic activity, and the creation of pro-inflammatory cytokines (Szalay et al., 2016). This procedure, known as microglial activation, is crucial for the clearance of damaged tissue and the elimination of pathogens. Microglia are equipped with specific pattern recognition receptors (PRRs) designed to detect microbial molecules, such as highly conserved pathogen-associated molecular patterns (PAMPs) (Kierdorf & Prinz, 2017; Wolf et al., 2017).

Conversely, prolonged or excessive activation of microglia can lead to neuroinflammation, a process implicated in various neurological illnesses and disorders (Lull & Block, 2010). According to an increasing amount of evidence, neuroinflammation has a role in the development of Alzheimer's disease, a progressive neurodegenerative condition marked by the buildup of tau protein aggregates and amyloid plaques in the brain (Heneka et al., 2015). Neuroinflammation has been associated with various neurological conditions, including multiple sclerosis, which is characterized by inflammation-induced damage to myelin, the protective sheath surrounding neurons (Compston & Coles, 2002). Furthermore, post-stroke impairment can arise due to neuroinflammation-induced tissue damages and scarring in affected brain regions (Iadecola & Anrather, 2011).

Developing tailored therapies for such disorders requires investigating the processes behind microglial activation and how it affects CNS function, given the pivotal role microglia play in maintaining brain homeostasis and contributing to neuroinflammation (Ransohoff, 2016). Targeting pathways or receptors involved in microglial activation offer good prospects for managing neuroinflammatory reactions and improving outcomes in individuals with neurological ailments and conditions (Ransohoff, 2016).

Chemokines, a family of small proteins secreted by various cells, are crucial for immune cell activation and recruitment, including microglia (Ransohoff, 2009). Among these, chemokine (C-C motif) ligand 2 (CCL2), CCL3, and CCL5 are frequently associated with microglial activation (Banisadr et al., 2005). Particularly, CCL2, also known as monocyte chemoattractant protein-1 (MCP-1), is produced by neurons and astrocytes, serving as a key attractant for microglia through its interaction with the CCR2 receptor (Banisadr et al., 2005).

Another chemokine implicated in microglial recruitment to injury sites is CCL3, also called macrophage inflammatory protein-1 (MIP-1). This chemokine is secreted by neurons, astrocytes, and other cell types, acting through the CCR1 receptor on microglia to facilitate their migration to the injury site (Banisadr et al., 2005).

CCL5, also known as regulated on activation normal T-cell expressed and secreted (RANTES), is another chemokine involved in microglial recruitment to injury sites. Produced by neurons, astrocytes, and activated microglia, CCL5 interacts with microglial receptors CCR1 and CCR5, crucial for the recruitment of microglia to the injury site (Babcock et al., 2003).

CX3CL1, commonly referred as "Fractalkine," is another chemokine associated with microglial activation. Fractalkine functions both as a soluble and transmembrane protein and plays a role in the activation and migration of microglia (Cardona et al., 2006).

Apart from the complement cascade and pattern recognition receptors (PRRs) like toll-like receptors (TLRs) and NOD-like receptors (NLRs), microglial activation involves diverse signalling pathways essential for recruiting and activating microglia (Kierdorf & Prinz, 2013).

Recent research has shown that microglia can undergo various stages of activation depending on the extent of damage. In the past, scientists have divided activated microglia into several phenotypes according to several factors, such as physiological traits, surface marker expression, and cellular shape (Prinz et al., 2019). One proposed classification system is the M1-M2 dichotomy, which categorizes microglial activation into classical M1 and alternative M2 states in experimental models (Franco and Fernández-Suárez, 2015). Classical M1 microglia often express higher amounts of cellular markers such CD16, CD86, iNOS, and MHC class II and display pro-inflammatory and neurotoxic behaviours. (Orihuela et al., 2016). Conversely, alternative M2 microglia exhibit phenotypic markers including as CD163, CD206, Arg-1, Ym-1, and FIZZ-1, and they participate in several processes such tissue remodelling, debris clearing, and suppression of inflammation. (Mecha et al., 2016). M2 microglia are therefore characterized as anti-inflammatory. Moreover, microglia in the M1 state facilitate synaptic loss through the release of various signalling molecules, such as cytokines and chemokines, which initiate synaptic pruning. However, excessive pruning resulting in the loss of synapses and neuronal connections may worsen cognitive deficits (Schafer et al., 2012). Microglia in the M2 state are marked by the secretion of anti-inflammatory molecules such as IL-10 and TGF-β, which contribute to dampening inflammation and facilitating tissue repair (Colonna and Butovsky, 2017). However, in traumatic brain injury (TBI), the balance between M1 and M2 microglia is often skewed towards M1 activation, leading to increased inflammation and cognitive deficits (Morganti et al., 2016). Further research is needed to determine the molecular and cellular mechanisms underlying microglial formation as well as how these pathways are regulated.

VII. Aim of the thesis

Traumatic brain injury revealed to be a very complex and intriguing study case for the neuroscientific community. The understanding of the mechanism underlying the ongoing processes following TBI has been very limited, and studies struggle to establish potential commonalities. Indeed, the representation of TBI in an animal model, in this case mouse model, is very scattered, even within a severity level and is dependent on each research group. However, a common pathophysiological pattern is usually found within each individual severity level, being neuroinflammation and the re organisation of the neuronal network pattern after TBI. The overall aim of this PhD was to investigate the different severity level of TBI and further our knowledge on a condition responsible for the development of neurodegenerative features and comprehend the role of glial cells in the neuroinflammatory processes taking place, the neuronal loss and deficiency, and the resulting behaviour impairments.

This investigation presents three distinct studies focusing on different aspects of brain injuries and the structural and functional impairments implied.

Firstly, the aim of this first study was to develop an automated tool, named ALMA, to assess accurately the paw placement and the locomotion of mice affected by moderate TBI; as we already know, it is rather delicate to retrieve locomotion impairment from TBI mouse model. We also aimed at creating a cost-efficient and user-friendly tool that can be widely used by any lab. Therefore, we sought to answer the following questions:

- Can ALMA accurately assess locomotion and paw placement in mice afflicted with neurological disorders?
- How does ALMA compare to conventional evaluation strategies in terms of cost, time, and expertise required?
- Does ALMA facilitate precise analysis of locomotor deficits in various neurological conditions, including traumatic and inflammatory brain diseases?

On a different note, moderate TBI, as previously mentioned, triggers structural and functional changes in the brain. Amongst the loss of neurons and the interruption of neuronal circuit in the brain leading to behavioural deficits, signs of potential spontaneous recovery through neuronal plasticity have been demonstrated by previous studies. However, the precise mechanisms underlying this cortical response remain unclear. Therefore, we decided to study the transcallosal neurons, a particular set of neurons which link the two hemispheres through the corpus callosum. The specificity of this bundle of neurons had allowed us to investigate the effect of the ipsilesional hemisphere on the contralesional side, spared from any injury. In order to clarify the circuit rearrangements that take place in the contralesional cortex after traumatic brain injury (TBI), structural and functional in vivo

imaging techniques, selective labeling of neuronal subpopulations, and circuit mono-synaptic tracing approaches are employed. The goal is to shed light on the intricate mechanisms underlying cortical plasticity and recovery after traumatic brain injury (TBI) by grasping the specific structural and functional adaptations of callosal neurons and their input pathways.
Here are the questions we tried to answer:

- How do callosal neurons from the contralesional cortex adjust both structurally and functionally following TBI?
- What role do these adaptations play in the restoration of circuit connectivity and activity patterns?

Lastly, the third and last study shifts to the mild version of TBI and most specifically, the concussions sub-category. The investigation aspires to uncover the cellular mechanisms underlying physiological brain dysfunction following repetitive concussions, a common consequence of TBI associated with long-term cognitive and mood impairments. Not only did the study focused on the repetitive concussions, but it also brought a comparative point of view of a single versus repetitive concussion on synaptic changes and microglial function. We also aimed at exploring their behavioural and anatomical differences. Using a mouse model of repetitive concussion to mimic human brain injury, the fate of glial and neuronal cells in the cortex and hippocampus is examined, highlighting the importance of targeting this novel mechanism for potential treatment strategies. The following questions were intended to be addressed:

- How do single and repetitive concussive head injuries affect synaptic changes and microglial function in mice?
- Are there discernible differences in behaviour and anatomy between mice subjected to single versus repetitive concussive head injuries?
- What particular alterations in synaptic changes and microglial function are observed following repetitive concussive head injuries?
- Do repetitive concussive head injuries lead to specific patterns of synaptic loss and microglial activation in affected brain regions?

Results

Study 1

A deep learning-based toolbox for Automated Limb Motion Analysis (ALMA) in murine models of neurological disorders

Almir Aljovic, Shuqing Zhao*, **Maryam Chahin**, Clara de la Rosa, Valerie Van Steenbergen, Martin Kerschensteiner & Florence M. Bareyre*

** These authors contributed equally to the manuscript*

Aim of Study 1

The primary objective of this investigation is to create an automated analysis tool, called Automated Limb Motion Analysis (ALMA), specifically designed for evaluating locomotion and paw placement in mice afflicted with neurological disorders. ALMA utilizes pose estimation derived from DeepLabCut and incorporates a graphical user interface to automate kinematic parameter computation, footfall detection, kinematic data analysis, and gait kinematics visualization. The aim is to develop a tool that is cost-effective, time-efficient, and user-friendly, enabling accurate monitoring of locomotor deficits in a variety of neurological conditions, including traumatic and inflammatory brain and spinal cord diseases. The study showcases the efficacy of ALMA in accurately delineating specific locomotor function parameters for tracking injuries and predicting disease onset in mouse models.

My contribution to this publication in detail:

For this paper, I was involved in generating mice model of moderate traumatic brain injury and in the performance of all required surgical procedures. To be more specific, I carried the anaesthesia of those mice, the craniotomy, the brain injury using an impactor directly onto the brain parenchyma, the awakening, and the monitoring of the mice subsequently to the injury.

The paper has been published in Communication Biology (2022)

DOI: https://doi.org/10.1038/s42003-022-03077-6

communications biology

ARTICLE

https://doi.org/10.1038/s42003-022-03077-6 OPEN

A deep learning-based toolbox for Automated Limb Motion Analysis (ALMA) in murine models of neurological disorders

Almir Aljovic[1,2,3,5], Shuqing Zhao[1,2,3,5], Maryam Chahin[1,2,3], Clara de la Rosa[1,2,3], Valerie Van Steenbergen[1,2], Martin Kerschensteiner[1,2,4] & Florence M. Bareyre[1,2,4]✉

In neuroscience research, the refined analysis of rodent locomotion is complex and cumbersome, and access to the technique is limited because of the necessity for expensive equipment. In this study, we implemented a new deep learning-based open-source toolbox for Automated Limb Motion Analysis (ALMA) that requires only basic behavioral equipment and an inexpensive camera. The ALMA toolbox enables the consistent and comprehensive analyses of locomotor kinematics and paw placement and can be applied to neurological conditions affecting the brain and spinal cord. We demonstrated that the ALMA toolbox can (1) robustly track the evolution of locomotor deficits after spinal cord injury, (2) sensitively detect locomotor abnormalities after traumatic brain injury, and (3) correctly predict disease onset in a multiple sclerosis model. We, therefore, established a broadly applicable automated and standardized approach that requires minimal financial and time commitments to facilitate the comprehensive analysis of locomotion in rodent disease models.

[1] Institute of Clinical Neuroimmunology, University Hospital, LMU Munich, 81377 Munich, Germany. [2] Biomedical Center Munich (BMC), Faculty of Medicine, LMU Munich, 82152 Planegg-Martinsried, Germany. [3] Graduate School of Systemic Neurosciences, Ludwig-Maximilians-Universitaet Munich, 82152 Planegg-Martinsried, Germany. [4] Munich Cluster of Systems Neurology (SyNergy), 81377 Munich, Germany. [5] These authors contributed equally: Almir Aljovic, Shuqing Zhao. ✉email: florence.bareyre@med.uni-muenchen.de

Research into neurological conditions often attempts to uncover how the structural and functional deficits of individual neurons and circuits relate to behavioral outcomes[1]. Over the years, a number of elaborate tools based on chemogenetics, optogenics, and connectomics have been designed to manipulate and record the structure and function of individual circuits and circuit elements[2–6]; nevertheless, a full understanding of the consequences of such interventions can only be achieved using refined behavioral analysis.

To this extent, a wide range of behavioral tests have been developed that can detect specific aspects of behavior in a range of neurological conditions[7–9]. Although such tests have substantially improved our ability to selectively monitor deficits, for example in motor function, the evaluation tools are still hampered by a number of limitations. These include a lack of automatization, which makes such tests both highly time-consuming or susceptible to observer bias. For example, the use of the open field[10] to assess locomotor behavior in rodents requires two independent investigators trained to distinguish between the subtle paw and tail positions that could be prone to interpretation. Another limitation is often the high costs of recording and analysis equipment[11], which often restricts access to a few specialized labs. Such limitations also affect the evaluation of locomotion that plays a central role in disease-related neuroscientific research, as many common neurological conditions caused by trauma, ischemia, or inflammation prominently affect walking abilities.

Unraveling the complexity of locomotion is best approached via the generation of gait parameters based on the precise position of the limbs. Since Hildebrand's early description of the notion of gait[12], several tests have been designed to evaluate limb motion and paw placement. Early work relied on collecting footprints[13–15] from an animal after inking the paws, but the data that could be retrieved were often incomplete due to rapid drying of the ink, and analysis was cumbersome to perform. Later systems, including the use of the commercial automated Catwalk® system, which uses foot placement to derive a range of gait parameters that reflect locomotion on a static ramp, offered important improvements[16,17]. The Catwalk® system has proven quite useful in the analysis of gait parameters in rodents subjected to genetic manipulation or injuries[18,19]. However, this system also has some limitations, as the tracking of light-furred rodents can be difficult, and potential mistakes in the tracking of footprints need to be manually corrected by the experimenter. In addition, the system is static and does not allow the locomotion speed to be controlled. The gait can also be recorded at variable speeds while the animal is running on a treadmill using three-dimensional video recordings coupled with a kinematic tracing system[15] or using the well-established motion-capture system VICON with eight infrared cameras[20–22]. Both require reflective markers to be manually and bilaterally attached at key joints (for example, iliac crest, lateral malleolus, the tip of the toe, etc.), and use of the latter system is further limited by the cost of the acquisition[23]. Therefore, recent new advances have been made to improve and facilitate locomotion tracking. A key step has been the development of the DeepLabCut (DLC) method that provides a markerless approach to labeling and tracking moving joints (DeepLabCut[24]) and, thereby, facilitates the kinematic analysis of gait as well as arm movements in animals and humans[25–28]. However, even this approach requires substantial specialized expertise and processing times to translate the limb coordinates into kinematic profiles and parameters that quantify the distinct aspects of locomotion.

Here, we describe how we overcame this final challenge by developing an open-source computational "toolbox", Automated Limb Motion Analysis (ALMA), which provides a fully automated and comprehensive analysis of locomotion and fine paw placement in mice with minimal costs, time requirements, and previous expertise. This toolbox which is based upon pose estimation obtained from deep lab cut (DLC) and includes a graphical user interface (GUI) with functionalities for automated kinematic parameter computation and automated footfall detection, kinematic data analysis with random forest classification and principal component analysis, and visualization of the gait kinematics. To make it amenable to as many users as possible, we used only inexpensive equipment (custom-made ladders and a commercial treadmill) and a single standard high-speed action camera. We applied this toolbox to mouse models of common traumatic and inflammatory diseases of the brain and spinal cord to demonstrate its capability to robustly and sensitively monitor the evolution of locomotor deficits in a broad range of neurological conditions. Notably, our results show that such an automated comprehensive analysis can delineate the specific parameters of the locomotor function that are best suited to track injuries of the brain or spinal cord or are sensitive enough to predict disease onset during the prodromal phase of a multiple sclerosis model.

Results

Pipeline for automated limb motion analysis: DLC markerless labeling, model training, and automated kinematic analysis and footfall detection in mice. In this paper, we present a new open-source toolbox for the analysis of gait kinematic parameters of locomotion and fine paw placement in mice. To do so, we focused on two behavioral tasks that were applied to mice: walking on a treadmill (Fig. 1a) to determine gait kinematic parameters and walking along ladders (Fig. 1b) with regularly or irregularly spaced rungs to analyze fine paw placement. All tasks were filmed with a GoPro 8 camera positioned parallel to and at a fixed distance and angle from the treadmill and ladder. We used DLC to perform markerless limb tracking of six hindlimb joints (toe, metatarsophalangeal joint (MTP), ankle, knee, hip, and iliac crest) for treadmill kinematic analysis, and of limb extremities for the ladder rung paradigm. (Fig. 1a, b). For both analyses, we focused only on the hindlimb trajectories.

We then trained the neural network model for body part coordinate extraction For each behavioral paradigm, 2D body part coordinates were obtained using a deep residual network model (ResNet-50), which was trained and refined using DLC (Fig. 1a, b). By choosing the most representative frames through k-means clustering, we were able to obtain a finetuned deep residual network model that can reliably detect body part coordinates using only up to 450 manually labeled frames, as described in the methods. We then performed automated kinematic analysis on the coordinate data obtained from the treadmill task and extracted a selection of 44 kinematic parameters that best reflected the locomotion of the hindlimbs according to the literature[20,29], which could also easily be expanded depending on the study goal. We grouped those parameters into five main categories: joint angles, spatial variability, the temporal feature of gait, limb endpoint trajectories, and dragging (Fig. 1a and Supplementary Table 1). These parameters could then be classified and compared using random forest and principal component analyses (PCA) to extract the most important parameters (Fig. 1a). Our toolbox also allows via a scree plot the visualization of the percentage of explained variance for all components of the PCA. For the ladder rung analysis, we performed automated detection of hindlimb footfalls (Fig. 1b), which were manually validated. Three parameters were then extracted, the number, depth, and duration of footfalls (Fig. 1b).

Tracking locomotion after spinal cord injury with the ALMA toolbox. We first tested the applicability of our toolbox for analyzing overground locomotion following spinal cord injury (SCI) (Fig. 2a). To do so, mice walking on a treadmill were

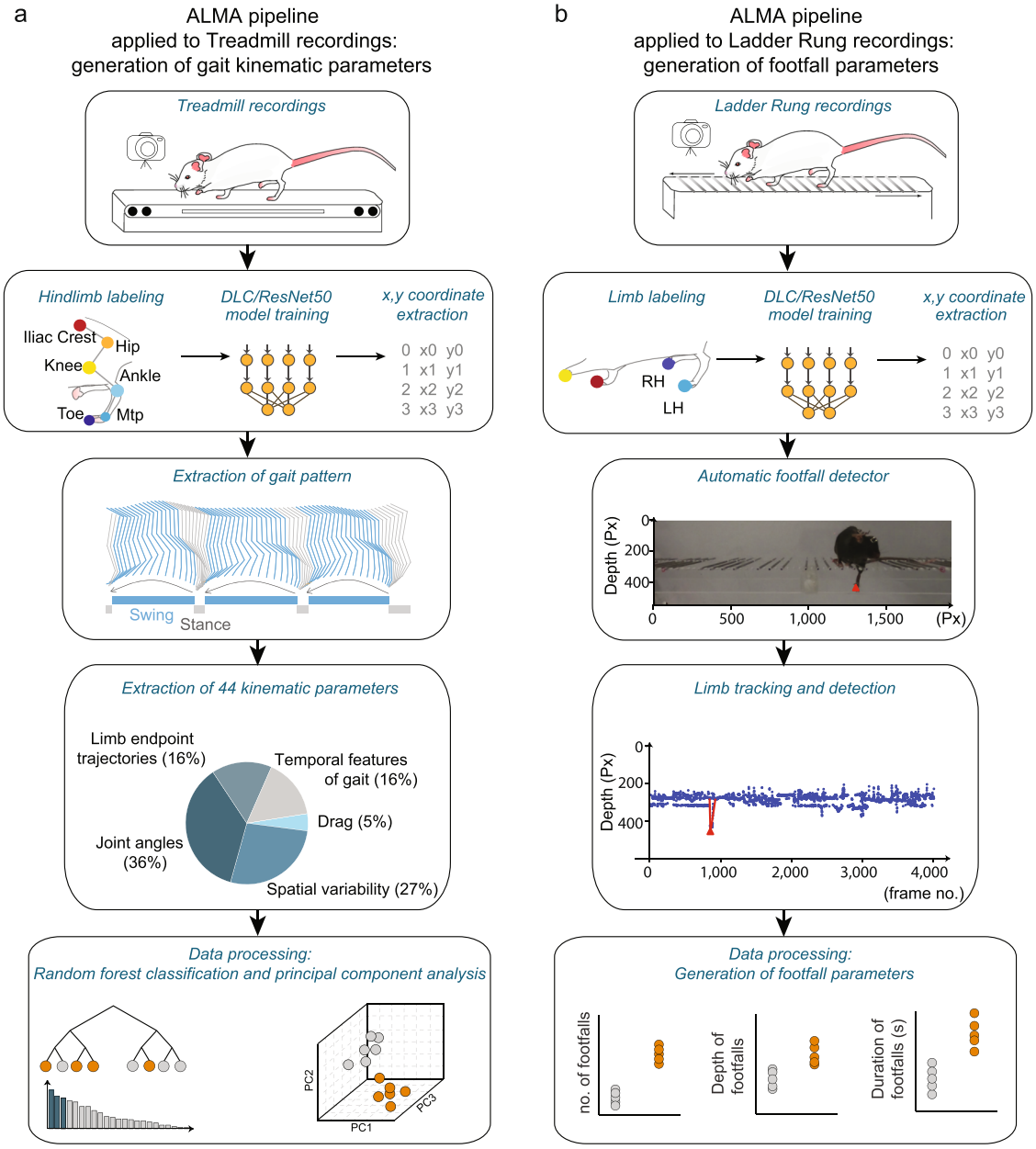

Fig. 1 Automated behavioral analysis using ALMA toolbox. a Schematic of ALMA toolbox application to treadmill recordings for the generation of gait kinematic parameters. First, treadmill videos were recorded with a GoPro 8 camera placed parallel to the treadmill. Then, markerless limb labeling and modeling was trained and refined using ResNet-50 and DeepLabCut (DLC) and coordinates were extracted. Coordinates were tracked for six hindlimb joints (toe, metatarsophalangeal (MTP) joint, ankle, knee, hip, and iliac crest) in the treadmill kinematic paradigm, and the coordinates were processed using the toolbox to generate hindlimb trajectories. This allowed the generation of 44 kinematic parameters that represented joint angles, spatial variability, limb endpoint trajectories, temporal features of gait, and dragging. Data processing was conducted in ALMA to obtain principal component analysis and random forest classification of the parameters. **b** Schematic of ALMA toolbox application to the ladder rung recordings for the generation of footfall parameters. First, ladder rung videos were recorded with a GoPro 8 camera placed parallel to the ladder. Then, markerless limb labeling and modeling was trained and refined using ResNet-50 and DLC, and coordinates were extracted. Coordinates could be tracked for all four paws. The toolbox used the automated footfall detector to extract limb tracing and footfall detection. The on- and off-set of locomotor errors (footfalls) were estimated using signal processing methods and subjected to manual validation. Three parameters, the number, depth, and duration of the footfalls, were extracted. Px pixels.

recorded with a GoPro 8 camera (Fig. 2b), and we used DLC to perform markerless labeling of the six hindlimb joints as described above (Fig. 2c and Supplementary Video 1). The ALMA toolbox then automatically detected the treadmill speed and adjusted the body part coordinates accordingly. The adjusted body part coordinate data were then used to extract stride onsets and offsets, as well as to distinguish the stance and swing phases (Fig. 2d and Supplementary Fig. 1). This procedure enabled automated kinematic parameter extraction for each stride (Fig. 2d). We validated the reliability of the extracted data with baseline recordings to check the reproducibility of the 44 parameters measured. To do so, we tested and re-tested mice on consecutive days on the treadmill task at baseline (e.g., before injury), and we found that reliability was excellent for all parameters measured (Fig. 2e; $r = 0.9985$, $P < 0.0001$, Pearson's correlation) between the initial test and the re-test conditions.

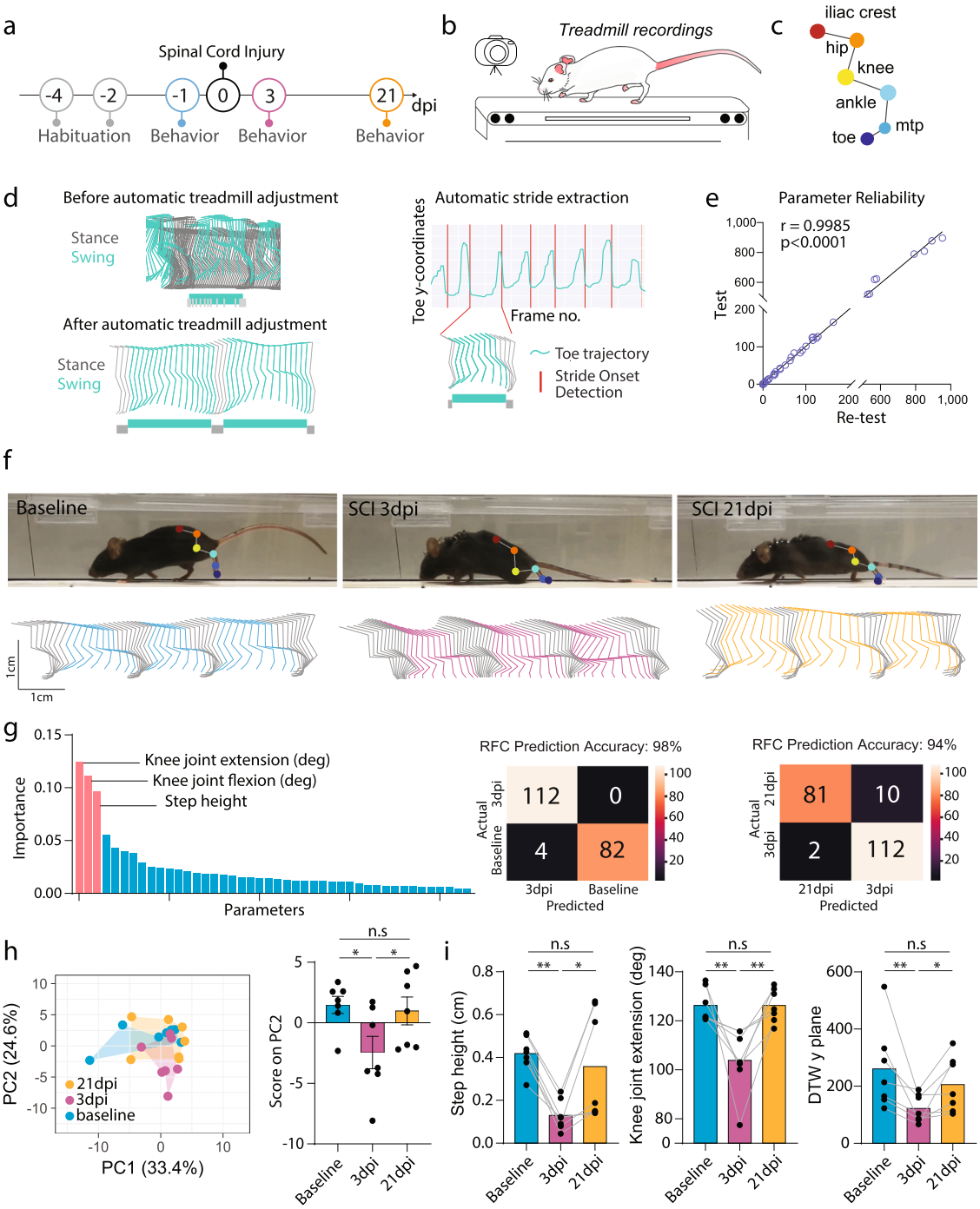

For the SCI experiment, we used mice that were first tested in the Basso Mouse Scale (BMS)[10] and showed at least one point of recovery over time (BMS score baseline 9 ± 0; BMS score 3 days post-injury (dpi) 3.86 ± 1.08 and BMS score 21 dpi 6.29 ± 0.81). We then analyzed the treadmill recordings collected before spinal cord injury and at 3 and 21 days following SCI in these mice and generated the adjusted hindlimb trajectories (Fig. 2f). Those trajectories were profoundly altered in SCI mice at 3 days post-injury (dpi) but had partially recovered by 21 dpi (Fig. 2f). We applied random forest classification to the data for the animals based on the 44 extracted parameters, and we could predict the injury status to a 98% accuracy when we compared baseline to animals at 3 dpi, and the recovery status to a 94% accuracy when we compared 3 dpi to 21 dpi animals. The step height, knee joint flexion, and knee joint extension showed the highest Gini impurity-based feature importance (Fig. 2g). We then compared the gait of the mice before and after spinal cord injury using principal component analysis of our 44 kinematic parameters and determined that the data for injured mice at 3 dpi clustered separately from those of the mice at baseline, while mice at 21 dpi were clustered in between, again indicating incomplete recovery of locomotor function (Fig. 2h). PC1 and PC2 together represented 58% of the variance, with PC2 better reflecting the between-group differences (Fig. 2h). After calculating the factor loadings, we identified three parameters that best-represented PC2 and were, thus, most likely to track SCI-related differences (Fig. 2h). Step height, knee joint extension, and dynamic time warping (DTW) demonstrated significant alterations at 3 dpi, and recovered over time until they were no longer significantly different from baseline (Fig. 2h and Supplementary Table 2).

Fig. 2 ALMA analysis of gait changes in spinal cord injured mice tested on the treadmill. **a** Timeline of the traumatic spinal cord injury (SCI) experiment. **b** Schematic of the treadmill system used to record the behavior of mice during the SCI experiment. **c** Schematic of DeepLabCut (DLC) markerless joint labeling. Six joints were labeled: iliac crest, hip, knee, ankle, metatarsophalangeal joint (MTP), and toe. **d** Representation of hindlimb trajectories (left panel) before the adjustment in ALMA (top; green, swing; gray, stance) and after adjustment with ALMA (bottom; green, swing; gray, stance). Note, that after adjustment, swing and stance were efficiently separated. Representation of automatic stride extraction from the toe coordinates and frame number (right panel). **e** Quantification of parameter reliability; baseline data were tested and re-tested and demonstrated a high correlation coefficient ($r = 0.9985$, $P < 0.0001$; Pearson's correlation coefficient). **f** Photographic images (top) of mice running on the treadmill showing the markerless labeling of hindlimb joints using DLC at baseline, 3 dpi, and 21 dpi, and hindlimb trajectories for baseline (cyan), 3 dpi (fuchsia), and 21 dpi (orange). **g** Random forest classification (RFC) of 44 parameters extracted from the ALMA toolbox for the analysis of gait following spinal cord injury and accuracy injury status prediction based on the 44 parameters using confusion matrices for 3 dpi vs. 21 dpi (Gini impurity-based feature importance for RFC: knee joint extension, 0.125; knee joint flexion, 0.112; step height, 0.097. RFC prediction accuracy: baseline vs. 3 dpi 98% and 3 dpi vs. 21 dpi 94%, tested in $n = 84$–92 step cycles). **h** Principal component analysis of data obtained on the treadmill and processed with the ALMA toolbox for spinal cord injury, and plot of scores of PC2 that represent 22.3% of the variability (principal component analysis, PC1 36.1%, PC2 22.3%, repeated-measures one-way ANOVA followed by Tukey's test; baseline vs. 3 dpi [$P = 0.022$]; baseline vs. 21 dpi [$P = 0.920$], 3 dpi vs. 21 dpi [$P = 0.044$]; $n = 7$). **i** Quantitative evaluation of parameters associated with PC2, such as step height, knee joint extension, or dynamic time warping (DTW) *y* plane, at baseline, 3 dpi, and 21 dpi. Repeated-measures one-way ANOVA followed by Tukey's test was used to analyze knee joint extension (baseline vs. 3 dpi, $P = 0.005$; baseline vs. 21 dpi, $P > 0.999$; 3 dpi vs. 21 dpi, $P = 0.005$; $n = 7$), Friedman and Dunn tests were used for DTW *y* plane (baseline vs. 3 dpi, P = 0.004; baseline vs. 21 dpi, $P > 0.999$; 3 dpi vs. 21 dpi, $P = 0.049$; $n = 7$), Repeated-measures one-way ANOVA followed by Tukey's test was used to analyze step height (baseline vs. 3 dpi, $P = 0.063$; baseline vs. 21 dpi, $P = 0.012$; 3 dpi vs. 21 dpi, $P > 0.999$; $n = 6$). In all panels, data are presented as mean ± SEM; $^{*}P < 0.05$; $^{**}P < 0.01$; $^{***}P < 0.001$. Px pixels.

Our analysis thus suggests that these kinematic parameters are best suited to monitor locomotor deficits resulting from an incomplete spinal cord injury. In addition, we validated a subset of kinematic parameters by manually labeling the different joints and the onset of step cycle detection, and found no significant differences with the parameters obtained through the automatic method (Supplementary Fig. 2). Importantly, those changes are specific of SCI as our toolbox could not pick up any gait kinematic changes following sham injury (Supplementary Fig. 3).

Tracking skilled paw placement after spinal cord injury with the ALMA toolbox. While overground locomotion strongly depends on the function of intraspinal circuits, skilled paw placement requires supraspinal input and is, thus, commonly used to assess the regeneration and remodeling of descending motor tracks, including corticospinal projections. We, therefore, assessed whether the ALMA toolbox could also be used to monitor skilled paw placement following spinal cord injury (Fig. 3a). To this end, we recorded mice walking on a horizontal ladder with regularly or irregularly spaced rungs. Similar to the overground locomotion experiment, all videos were recorded using a single GoPro 8 camera, and we used DLC to perform markerless labeling of the hind paws (Fig. 3b and Supplementary Video 2). We then applied ALMA to determine footfall characteristics with a peak detection algorithm (Fig. 3c, d and Supplementary Fig. 4). The parameters extracted from ALMA showed that spinal cord injury caused an increase in the mean number and depth of footfalls at 3 dpi, while the mean duration of the footfalls was only slightly increased, for the ladder with regularly spaced rungs (Fig. 3e). Those parameters remained altered over a prolonged period so that they remained different from baseline at 21 dpi (Fig. 3e). Similarly, in the ladder with irregular rungs experiment, the mean number of footfalls and duration of footfalls were found to increase at 3 dpi and remained elevated till 21 dpi. However, the mean number of footfalls significantly recovered from 3 to 21 dpi. The mean depth of footfalls was, in this case, unchanged throughout the study period (Fig. 3f). We also calculated the total duration and total depth of the footfalls on the ladders with regularly and irregularly spaced rungs and observed a significant increase in the total depth and total duration at 3 dpi and 21 dpi (Fig. 3g). Finally, we compared the ALMA automated detection of the number of footfalls using a deviation algorithm with (i) the semi-automatic detection (that includes a manual correction provided by the GUI) and (ii) a fully manual count of the mistakes. In both cases, we found a highly significant correlation (Fig. 3h) confirming that the ALMA toolbox can provide precise quantification of skilled paw placement. While there is a slight overestimation through the fully automated detection (see "Methods"), the fully manual quantification and the semi-automated quantifications with ALMA are similar (Fig. 3h).

The ALMA toolbox can reveal behavioral consequences of traumatic brain injury. Next, we wanted to determine whether our toolbox, which was initially designed to reveal motor abnormalities related to spinal cord pathology, was also capable of detecting the locomotor changes induced by neurological conditions primarily affecting the brain. This is of particular importance for traumatic brain injuries, as it has often been challenging to detect and reliably quantify motor deficits arising from such insults, in particular in the acute injury phase[30,31]. We, therefore, induced moderate brain injury in mice using a traumatic brain injury (TBI) impactor and recorded the locomotion and paw placements of mice walking on the treadmill and ladders, respectively, before and 1 day and 10 days after traumatic brain injury (Fig. 4a). We applied the ALMA toolbox as described above and initially analyzed the treadmill recordings (Fig. 4b, c). The findings showed that the limb trajectories were strongly affected at 1 dpi and had partially recovered by 10 dpi (Fig. 4d). We applied random forest classification to all animals at baseline and 1 dpi based on the 44 extracted parameters, and we were able to demonstrate the parameters with the highest Gini impurity-based feature importance (step height, hip joint, hip joint amplitude, and hip joint flexion) and predict the injury status with 83% accuracy. This indicates that our toolbox makes it possible to robustly detect even the subtle locomotor changes induced by a moderate TBI (Fig. 4e). We then used principal component analysis to reduce the dimensionality of our data and determine the individual movement parameters that best identified differences between the groups. We found that data for mice at baseline clustered closer to the data for the mice at 10 dpi than to those at 1 dpi, indicating that the injury and recovery effects can be ascertained based on the kinematic parameters (Fig. 4f). As PC1 represented almost 40% of the variance, we plotted the principal component analysis scores and demonstrated the above-mentioned effects at 1 dpi (Fig. 4f). Based on PC1, we identified the top three parameters that contributed to the differences: step height, stride length, and DTW distance. These parameters showed significant

changes at 1 dpi and later recovery at 10 dpi, indicating that our toolbox can also detect changes in locomotion following brain lesions (Fig. 4g and Supplementary Table 3).

We then analyzed the ladder task recordings using the ALMA toolbox (Fig. 4h). We extracted the three footfall parameters described previously and demonstrated that mice with brain injuries displayed an increased number of footfalls in the regular-rung ladder task, which returned to baseline at 10 dpi (Fig. 4i). In contrast, the irregular-rung ladder performance was unaffected by moderate traumatic brain injury. Taken together, these results indicate that the ALMA toolbox can be applied to assess neurological conditions of the brain and is capable of sensitively

Fig. 3 ALMA analysis of fine paw placement in spinal cord injured mice in the ladder rung test. a Timeline of the traumatic spinal cord injury experiment. **b** Schematic of the ladder rung system used to record the fine paw placement of mice during the spinal cord injury experiment indicating the DeepLabCut (DLC) markerless paw labeling (yellow, red, dark blue and light blue dots). **c** Photographic image of a mouse running on the treadmill showing the automatic detection of footfall, as predicted in time and space by the toolbox. **d** Automated detection algorithm used to predict footfalls in space and time. **e** Quantitative parameters extracted from ALMA for the regular walk showing the mean number, mean depth, and mean duration of footfalls for all time points (cyan, baseline; purple, 3 dpi; and orange, 21 dpi). Repeated one-way ANOVA followed by Tukey's test was used to the analyze the regular ladder rung results (mean no. footfalls, baseline vs. 3 dpi [$P = 0.0002$], baseline vs. 21 dpi [$P = 0.021$], 3 dpi vs. 21 dpi [$P = 0.223$]; mean depth, baseline vs. 3 dpi [$P = 0.003$], baseline vs. 21 dpi [$P = 0.013$], 3 dpi vs. 21 dpi [$P = 0.612$]; and mean duration, baseline vs. 3 dpi [p = 0.053], baseline vs. 21 dpi [$P = 0.131$], 3 dpi vs. 21 dpi [$P = 0.838$]; $n = 6$). **f** Quantitative parameters extracted from ALMA for the regular walk showing the mean number, mean depth, and mean duration of footfalls for all time points (cyan, baseline; purple, 3 dpi; and orange, 21 dpi). Repeated one-way ANOVA followed by Tukey's test was used to the analyze the irregular ladder rung results (mean no. footfalls, baseline vs. 3 dpi: [$P < 0.0001$], baseline vs. 21 dpi [$P < 0.0001$], 3 dpi vs. 21 dpi [$P = 0.002$]; mean depth, baseline vs. 3 dpi [$P = 0.745$], baseline vs. 21 dpi [$P > 0.999$], 3 dpi vs. 21 dpi [$P > 0.999$]; and mean duration, baseline vs. 3 dpi, $P = [0.028]$, baseline vs. 21 dpi [$P = 0.028$], 3 dpi vs. 21 dpi [$P > 0.999$]; $n = 6$). **g** Quantitative evaluation of the total depth and total duration of footfalls for all time points (cyan, baseline; purple, 3 dpi; and orange, 21 dpi). Repeated one-way ANOVA followed by Tukey's test was used to analyze total footfall depth on regular ladder rungs (baseline vs. 3 dpi, $P = 0.0047$; baseline vs. 21 dpi, $P = 0.043$; and 3 dpi vs. 21 dpi, $P = 0.175$; $n = 6$), total depth on irregular ladder rungs (baseline vs. 3 dpi, $P < 0.0001$; baseline vs. 21 dpi, $P < 0.0001$; 3 dpi vs. 21 dpi, $P = 0.0039$; $n = 6$), total duration on regular ladder rungs (baseline vs. 3 dpi, $P = 0.0042$; baseline vs. 21 dpi, $P = 0.173$; 3 dpi vs. 21 dpi, $P = 0.101$; $n = 6$), and total duration on irregular ladder rungs (baseline vs. 3 dpi, $P < 0.0001$; baseline vs. 21 dpi, $P = 0.004$; 3 dpi vs. 21 dpi, $P = 0.041$; $n = 6$). **h** Correlation between the ALMA automatic detection of the number of footfalls using the deviation algorithm and a fully manual detection (left panel; $r = 0.9845$, $P < 0.0001$; Pearson's correlation coefficient) and between the ALMA semi-automatic detection of the number of footfalls using the deviation algorithm and a fully manual detection (left panel; $r = 0.9989$, $P < 0.0001$; Pearson's correlation coefficient). In all panels, data are presented as mean ± SEM; $^{*}P < 0.05$; $^{**}P < 0.01$; $^{***}P < 0.001$. Px pixels, dpi days post-injury.

tracking both alterations in locomotor kinematics and foot placement after TBI.

The ALMA toolbox can monitor disease symptoms and predict disease onset in a multiple sclerosis model. Finally, we sought to investigate the applicability of our toolbox for assessing neurological conditions with a less predictable disease course, such as those caused by CNS inflammation. Therefore, we induced a commonly used mouse model of multiple sclerosis, experimental autoimmune encephalomyelitis (EAE), by immunizing mice with the myelin oligodendrocyte glycoprotein (MOG). We then recorded the locomotion of the mice on the treadmill at baseline, disease onset (defined as the first day with clinical symptoms), disease peak (3 or 4 days after onset), and recovery (10 or 11 days after onset; Fig. 5a, b). As expected, as the disease progressed, the mice developed ascending paresis and paralysis that strongly altered their hindlimb trajectories at the peak of the disease (and precluded the use of the ladder tests). While the hindlimb trajectories recovered slightly over the next few days, they remained clearly distinct from the baseline pattern (Fig. 5c). The principal component analysis confirmed that the data formed distinct clusters at the onset, peak, and recovery of disease compared to baseline (Fig. 5d). As PC1 represented 76.1% of the variability, we plotted the scores in PC1 to recapitulate the evolution of motor systems (Fig. 5e) and extracted the key parameters clustering with PC1. Those parameters (stride length, stride height, toe–crest distance, and dragging percentage) all showed significant changes at the peak of the disease and tended towards a later recovery, indicating that our toolbox is well suited to monitoring the locomotor alterations resulting from the formation and resolution of inflammatory lesions (Fig. 5f and Supplementary Table 4).

We next examined whether this refined analysis of locomotion kinematics is sufficiently sensitive to pick up the prodromal stages of the disease, which are not apparent in classical EAE scoring (based on simple observations of mouse mobility). In this context, we were particularly interested in whether we could detect the more subtle locomotor alterations associated with the initial formation of the lesions, which can predict the subsequent onset of overt disease symptoms (defined as the first day of detectable symptoms in the EAE score; often seen as tail paralysis). This would be useful, as it is often important to precisely initiate interventions, e.g., pharmacological treatment, when CNS lesions first start to form, as, once initiated, the CNS inflammatory process can self-perpetuate. Therefore, we used the ALMA toolbox to analyze the treadmill recordings starting 3 days prior to disease onset (defined by the EAE score). Using random forest classification, we found we could predict whether and when the mice would subsequently show EAE symptoms with 75% accuracy 3 days before onset, with 78% accuracy 2 days before onset, and with 86% accuracy 1 day before onset (Fig. 5g). This illustrated the ability of our toolbox to accurately predict whether an immunized mouse will develop overt disease symptoms in the prodromal disease phase and even predict the day of onset. This renders the initial formation phase of CNS lesions amenable to study.

Discussion

The quantitative assessment of locomotor performance is critical in the analysis of physiological gait patterns and their perturbations in neurological diseases. Conventional evaluation strategies often rely on resource-intensive and time-demanding observation and analysis setups. Together with the specialized expertise required to operate these setups, these demands currently prevent the broad application of refined locomotor analyses in basic and clinical neuroscience. In this study, we used deep-learning strategies to implement ALMA, an open-source toolbox that facilitates refined analysis of overground locomotion and skilled paw placement at a fraction of the cost of specialized behavioral setups. ALMA is fully automated, saving time and preventing observer bias, and it can be used without previous expertise through its user-friendly interface. Therefore, ALMA makes a comprehensive analysis of locomotion accessible to every research group interested in revealing the behavioral consequences of nervous system dysfunction and disease.

The use of machine-learning approaches to the study of behavior in both rodents and humans has dramatically increased in the last 5 years[24–27,32]. An important step in this process was the development, by Mathis and colleagues, of a markerless method (DLC[24]) to label the joints and follow their motion reliably over time. Here, we made use of this method to mark important joints in mice and import the DLC coordinates to track locomotion and fine paw placements. Alternatively, our toolbox can also be efficiently used with coordinates generated through other techniques, such as VICON, the newly published DANNCE[28] methods or any other

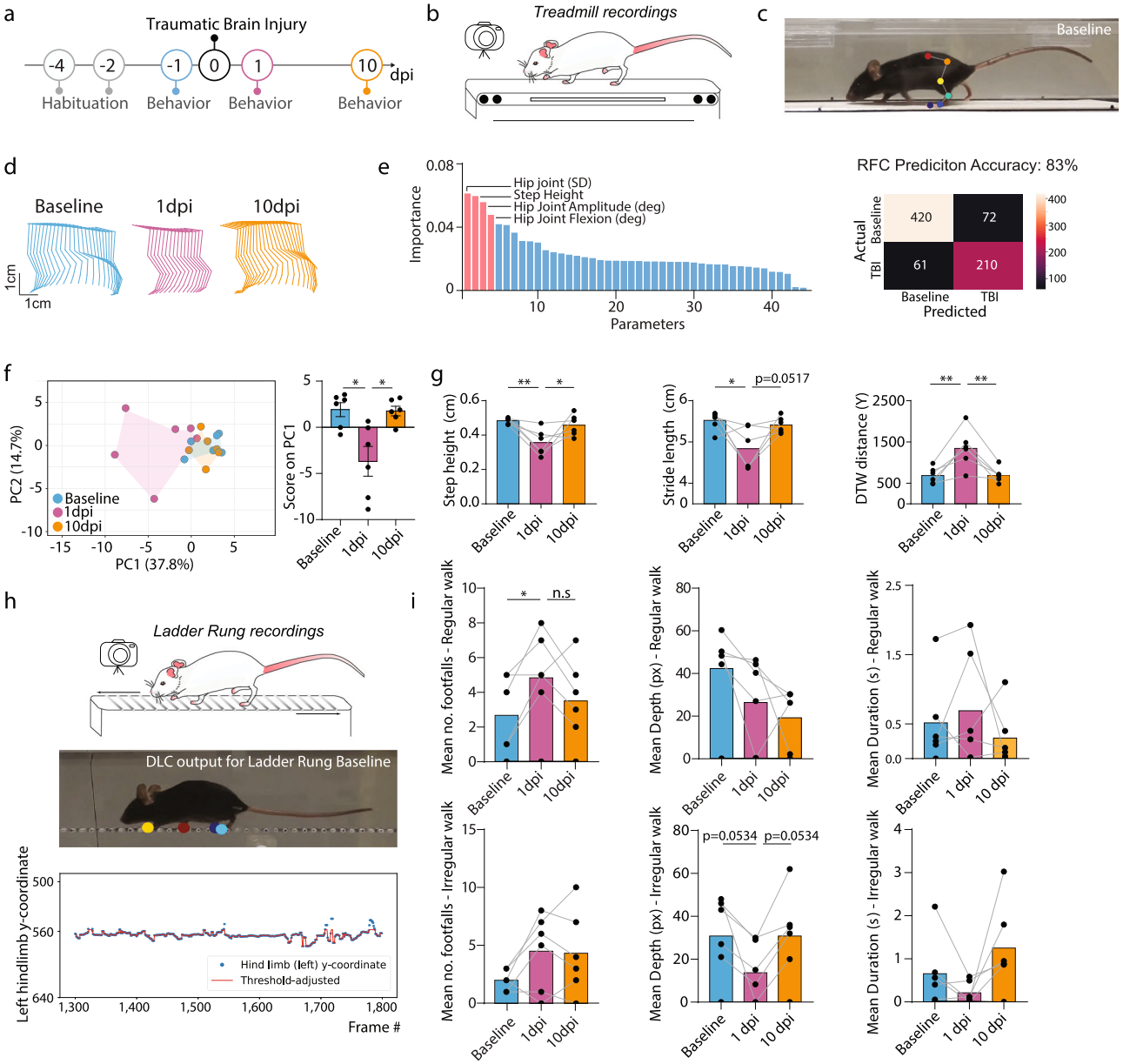

excellent pose estimation platforms such as SLEAP (sleap.ai[33]), MARS[34], and DeepPoseKit[35].

To translate these limb and joint coordinates into locomotor patterns on a treadmill or horizontal ladder and to subsequently extract the parameters of gait and footfall, we used model training. In healthy mice, this allowed us to define a list of 44 hindlimb parameters— validated with almost perfect re-test reliability ($r = 0.9985$)—that best represent gait features but can also be increased or made more comprehensive to meet one's needs. It is remarkable that this highly robust kinematic analysis can not only be achieved with a fully automated analysis pipeline but also that it can be achieved with the use of an affordable single-action camera. Particularly as, to date, scientists have had to rely on the use of high-end cameras and software modules to manually extract gait cycles and parameters in the analysis of kinematic behavior. Previous techniques came with several pitfalls, including high software costs, limited troubleshooting support, and cumbersome and time-consuming post-experimental processing. In contrast, the ALMA toolbox simply requires the import of DLC output using a GUI and allows the extraction of the final gait kinematic parameters. Another important aspect of our approach is that the ALMA toolbox allows the tracking of locomotor patterns based on side-view camera recordings, which, while harder to model, provide much more gait parameters compared with the bottom-view recordings used in the catwalk approach or in recent automated approaches[19,27]. As demonstrated here, 2D side-view tracking and analysis provides important information on each joint angle, step height, and body support, which is missing in top- or bottom-view recordings of gait analysis.

In addition to kinematic analysis, the ALMA toolbox offers the first automated analysis of the number, duration, and depth of footfalls on regularly and irregularly spaced ladder rungs. This is an important improvement for those investigating skilled paw placement, as it replaces a cumbersome analysis protocol that had to be performed frame by frame[36,37]. The analysis of skilled paw placement is complementary to the obtention of kinematic parameters, as it provides a readout of the damage and recovery of supraspinal circuits[18,38]. Finally, it should be noted that while we focused our analysis on both the gait and footfall aspects of mouse hindlimb movements, the ALMA toolbox should (with minor modifications) be equally suitable for the analysis of

Fig. 4 ALMA monitoring of gait changes and differences in fine paw placement in brain-injured mice. **a** Timeline of the traumatic brain injury experiment. **b** Schematic of the treadmill system used to record the behavior of the mice during the traumatic brain injury experiment. **c** Photographic images of the mice running on the treadmill showing markerless labeling of hindlimb joints using DeepLabCut (DLC) at baseline. **d** Hindlimb trajectories for baseline (top, cyan), 1 dpi (middle, purple), and 10 dpi (bottom, orange). **e** Random forest classification (left) of the 44 parameters extracted from the ALMA toolbox for the analysis of gait following traumatic brain injury, and confusion matrix (right) for determining prediction accuracy of the injury status based on the 44 parameters (Gini impurity-based feature importance for RFC: hip joint, 0.061; step height, 0.059; hip joint amplitude, 0.056; hip joint flexion, 0.047: RFC prediction accuracy: baseline vs. 1 dpi 83%; tested in $n = 282$–481 step cycles). **f** Principal component analysis of data obtained from the treadmill task and processed with the ALMA toolbox, and plot of PC1 scores that represent 37.8% of the variability and associated factor loadings (principal component analysis, PC1 37.8%, PC2 14.7%; repeated one-way ANOVA followed by Tukey's test, baseline vs. 1 dpi [$P = 0.012$], baseline vs. 10 dpi [$P = 0.665$], 1 dpi vs. 10 dpi [$P = 0.014$]; $n = 6$). **g** Quantitative evaluation of factors associated with PC1, i.e., step height, stride length, and dynamic time warping (DTW) distance, at baseline, 1 dpi, and 10 dpi. Repeated one-way ANOVA followed by Tukey's test was used to analyze step height (baseline vs. 1 dpi, $P = 0.0095$; baseline vs. 10 dpi, $P = 0.730$; 1 dpi vs. 10 dpi, $P = 0.033$; $n = 6$), stride length (baseline vs. 1 dpi, $P = 0.0214$; baseline vs. 10 dpi, $P = 0.855$; 1 dpi vs. 10 dpi, $P = 0.0517$; $n = 6$), and DTW distance (baseline vs. 1 dpi, $P = 0.001$; baseline vs. 10 dpi, $P = 0.9943$; 1 dpi vs. 10 dpi, $P = 0.0012$; $n = 6$). **h** Schematic of the ladder rung system used to record the behavior of mice during the traumatic brain injury experiment, and photographic images of a mouse running on the treadmill showing markerless labeling of hindlimb paws using DLC at baseline and showing the algorithm detection of footfall. **i** Quantitative evaluation of three parameters extracted from ALMA for footfalls at baseline, 1 dpi, and 10 dpi. Friedman followed by Dunn's test was used to analyze the regular ladder rung mean no. footfalls (baseline vs. 1 dpi, $P = 0.0315$, baseline vs. 10 dpi, $P = 0.2557$; 1 dpi vs. 10 dpi, $P = 0.1583$), mean depth (baseline vs. 1 dpi, $P = 0.1299$; baseline vs. 10 dpi, $P = 0.0628$; 1 dpi vs. 10 dpi, $P > 9999$), and mean duration (baseline vs. 1 dpi, $P > 0.9999$; baseline vs. 10 dpi, $P > 0.9999$; 1 dpi vs. 10 dpi, $P > 9999$; $n = 6$) and the irregular ladder rung mean no. footfalls (baseline vs. 1 dpi, $P = 0.3371$; baseline vs. 10 dpi, $P = 0.9370$; 1 dpi vs. 10 dpi, $P > 0.9999$; $n = 6$), mean depth (baseline vs. 1 dpi, $P = 0.0534$, baseline vs. 10 dpi, $P > 0.9999$; 1 dpi vs. 10 dpi, $P = 0.0534$; $n = 6$) and mean duration (baseline vs. 1 dpi, $P > 0.9999$; baseline vs. 10 dpi, $P = 0.9370$; 1 dpi vs. 10 dpi, $P = 0.3371$; $n = 6$). In all panels, data are presented as mean ± SEM; $^{*}P < 0.05$; $^{**}P < 0.01$; $^{***}P < 0.001$. Px pixels, dpi days post-injury.

forelimb function, forelimb–hindlimb coordination, or the tracking of locomotor function in larger rodents such as rats.

We further showed that the ALMA toolbox can be applied to a range of neurological conditions and enables the automated tracking of locomotor deficits in mice with traumatic and inflammatory injuries of the brain and spinal cord. Using spinal cord injury models, we confirmed that tracking of locomotor deficits is robust, as demonstrated by the high reproducibility and the correct prediction of injury status. As spinal cord injuries lead to pronounced locomotor deficits, a large number of studies have used behavioral testing strategies to assess the functional outcomes of genetic or therapeutic modulations[20,21,39–45]. Importantly, using ALMA, we find profound disturbances in gait and fine paw placement at acute time points following incomplete spinal cord injury and demonstrate a recovery at more chronic time points. This is similar to previous reports that use similar spinal cord injury models[18,20,29,38,46,47]. The application of the ALMA toolbox in such models should both improve the reliability of the analysis (as observer and selection biases are removed) and provide a more refined view of locomotor disturbance and recovery, as it allows the operator to precisely determine which component or components of locomotor function are regulated by a specific circuit modulation or therapeutic intervention.

The locomotor deficits observed after spinal cord injury are pronounced compared with the less obvious deficits resulting from mild-to-moderate brain injuries. It has often been challenging to detect and reliably monitor locomotor deficits following such brain injuries in mice, particularly in the early phase when the effects are subtle[30,31]. Our findings showed that the kinematic tracking of gait parameters, in particular, step height, stride length, and DTW (which measures the similarity between two step sequences), allowed us to sensitively reveal both the emergence of locomotor deficits (1 day after injury) and their recovery (by 10 days after injury). Interestingly, while pronounced abnormalities of locomotion were observed at the initial recording after injury, the animals later recovered a movement pattern almost identical to the pattern observed at baseline. This is clearly distinct from the comparably incomplete recovery process observed after spinal cord injury and may indicate that the persistence of intraspinal circuits is critical for re-establishing the "original" physiological movement pattern, while the reorganization of intraspinal (but not supraspinal) circuits results in a compensatory adaption of the movement pattern.

In comparison to studies of the injured brain and spinal cord, only a few attempts have been made to apply refined behavioral testing to models of inflammatory CNS damage, such as the EAE model[48–50]. One limitation has been, that, due to the disseminated nature of inflammatory infiltration, which results in variable neuronal tracking systems being affected in different mice, inter-individual differences in the pattern of locomotor changes are to be expected. For this purpose, targeted EAE models have been developed that allow inflammatory lesions to be directed to a predetermined anatomical location in the brain or spinal cord[51–53]. However, the stereotactic injection procedure required for the induction of such models limits their application, e.g., for studying disease initiation. Here we were able to show that the comprehensive kinematic analysis generated by the ALMA toolbox allows for the refined monitoring of locomotor deficits, even in classical disseminated EAE models. While such locomotor symptoms can also be tracked by the classical EAE scoring scale, which is based on visual inspection of the walking abilities of mice, kinematic analysis provides a number of advantages. First, the ALMA toolbox allows for fully automated and standardized analyses, removing observer bias and, thereby, making behavioral assessments more comparable between different observers and labs. Second, it stands to reason that the quantitative assessment of 44 distinct gait parameters should be more sensitive to differences in locomotor function compared with visual inspection. This is particularly important when evaluating the behavioral consequences of therapeutic manipulations targeting neuronal protection and repair[54] that are expected to lead to more subtle changes in locomotor function. Third, and related to the latter, our current analysis showed that the ALMA toolbox is able to accurately predict the onset of overt motor symptoms up to 3 days before the onset of disease can be detected by conventional EAE scoring. This indicates that even subtle motor symptoms that arise during this stage[55], which are presumably related to the formation of the first CNS lesions, can be detected by the ALMA toolbox. Our toolbox thus facilitates studies of the prodromal stage of the disease and its targeted modulation by therapeutic interventions.

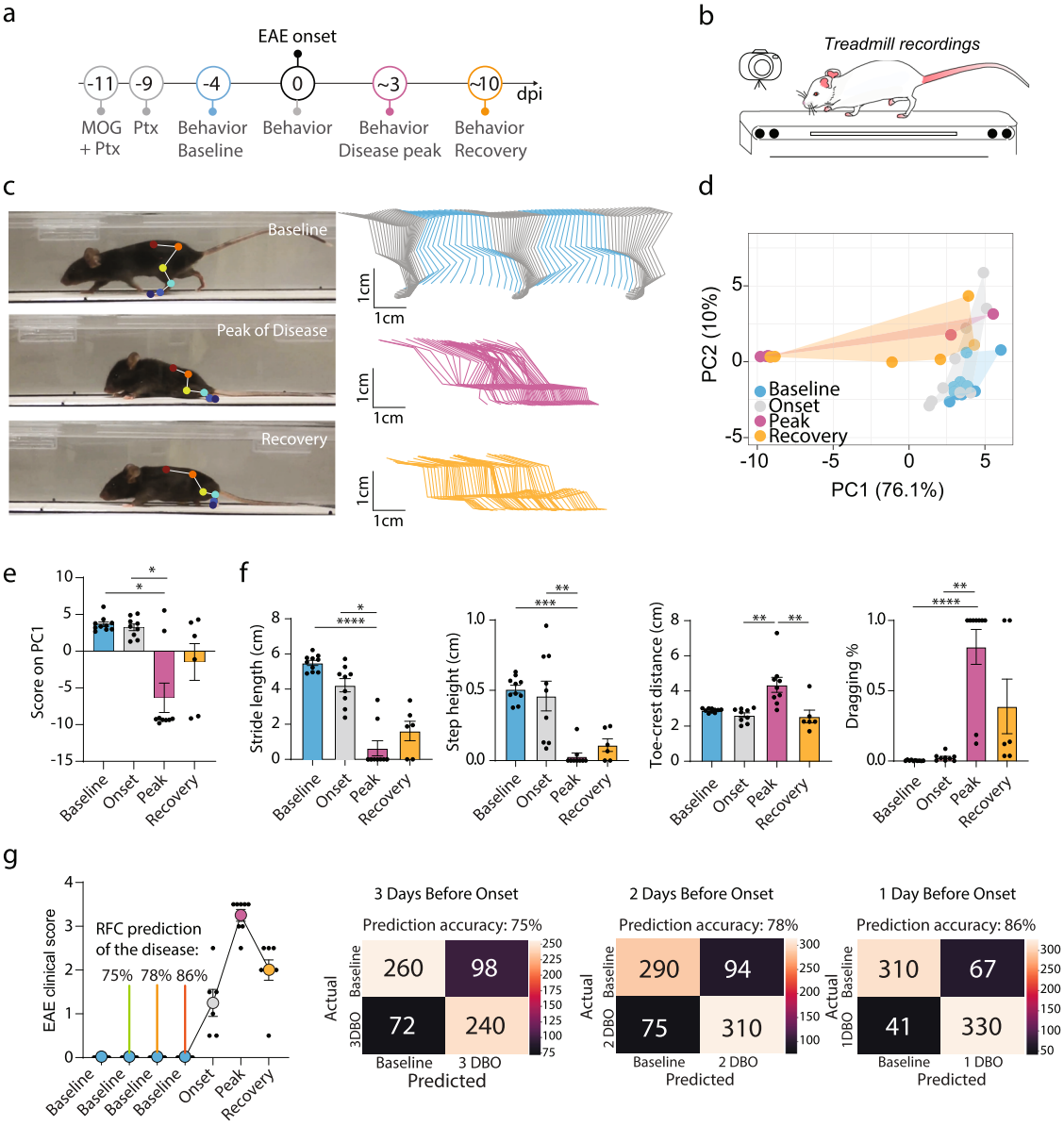

Fig. 5 ALMA monitoring of locomotor changes in mice that developed experimental autoimmune encephalomyelitis and accurate prediction of disease development during the prodromal phase. **a** Timeline of the EAE experiment. **b** Schematic of treadmill system used to record the behavior of the mice during the EAE experiment. **c** Photographic images of mice running on the treadmill (left) showing markerless labeling of hindlimb joints using DeepLabCut (DLC) at baseline (top), onset of disease (middle), and disease recovery (bottom), and hindlimb trajectories (right) for baseline (top), onset of disease (middle), and disease recovery (bottom). **d** Principal component analysis of data obtained on the treadmill and processed with the ALMA toolbox. **e** Plot of the PC1 scores that represent 76.1% of the variability and associated factor loadings (Kruskal–Wallis followed by Dunn's test; baseline vs. peak, $P = 0.0104$; onset vs. peak, $P = 0.0418$; baseline vs. recovery, $P = 0.9806$; peak vs. recovery, $P > 0.9999$). **f** Quantitative evaluation of factors associated with PC1, i.e., stride length, step height, toe-crest distance, and dragging, at baseline and different stages of EAE (Kruskal–Wallis followed by Dunn's test; stride length, baseline vs. peak [$P < 0.0001$], onset vs. peak [$P = 0.0231$], baseline vs. recovery [$P = 0.0019$], peak vs. recovery [$P > 0.9999$]; $n = 6$; step height, baseline vs. peak [$P = 0.0002$], onset vs. peak [$P = 0.0020$], baseline vs. recovery, [$P = 0.0382$], peak vs. recovery [$P > 0.9999$]; toe-crest distance, baseline vs. peak [$P = 0.0737$], onset vs. peak [$P = 0.0036$], baseline vs. recovery [$P = 0.0382$], peak vs. recovery [$P = 0.7374$]; and dragging (%), baseline vs. peak [$P < 0.0001$], onset vs. peak [$P = 0.0082$], baseline vs. recovery [$P = 0.0039$], peak vs. recovery [$P > 0.9999$]; $n = 6$). **g** EAE clinical score and prediction of the disease onset based on random forest classification in the prodromal phase (3, 2, and 1 days before onset) using ALMA. In all panels, data are presented as mean ± SEM; $^*P < 0.05$; $^{**}P < 0.01$; $^{***}P < 0.001$. Px pixels, dpi days post-injury.

While we have outlined the real advantages of using ALMA to analyze gait and fine paw placements in the context of CNS damage, ALMA also comes with inherent limitations. For example, gait analysis was, in this paper, performed only on hindlimbs. This can be easily circumvented by further using pose estimation to label the forelimb joints which would allow the generation of gait parameters for the forelimb and the generation of coupling data between forelimbs and hindlimbs. Likewise, ALMA currently provides the investigators with the two main components of the PCA following analysis. Using a scree plot (also provided in the toolbox), more components can be visualized and studied. For the determination of mistakes in the ladder rung test, we used a "deviation peak detection" algorithm that slightly overestimates the raw number of mistakes. This can be

circumvented, as we describe in the paper, by manual validation of the number of mistakes within the GUI in our semi-automatic detection. Alternatively, other algorithms (also implemented in the toolbox) could be used such as the "threshold" or "baseline correction" algorithms but pose additional constraints on recording set-ups.

Taken together, we provide a user-friendly open-source toolbox that requires minimal time and resource commitments; is applicable to a wide range of neurological conditions affecting the brain and spinal cord; and provides an unbiased, robust, and comprehensive assessment of locomotion.

Methods

ALMA toolbox. This research aimed to provide a toolbox for the analysis of gait and footfall in mouse models of neurological disorders. This toolbox includes a graphical user interface (GUI) with functionalities for (i) automated kinematic parameter computation, (ii) automated footfall detection, (iii) data analysis of the computed kinematic parameters with random forest classification and principal component analysis, and (iv) visualization of gait kinematics. The ALMA toolbox is an open-source Python repository for the automatic processing of DLC coordinates, gait cycle detection, and kinematic parameter extraction. Parameters extracted from ALMA include joint angles, limb endpoint trajectories, drag, temporal features of gait, and spatial variability. This last category represents a range of pairwise dynamic time warping (DTW) parameters that measure similarity between limb endpoint trajectories despite different duration and speede[32]. Following kinematic parameter extraction, the ALMA toolbox enables the use of machine-learning algorithms, such as random forest classification and principal component analysis, to reduce dimensionality and identify the most relevant kinematic parameters in the scope of health and disease. In addition to automated kinematic analysis, the toolbox GUI provides a code for the accurate detection of footfalls during fine motor tasks (e.g., traversing ladder rungs) for manual validation of each footfall. Details and the open-source toolbox can be found at https://github.com/sollan/alma.

Feature labeling and model training. To train the DLC model, we used ~450 image frames from different disease models (spinal cord injury, traumatic brain injury, and EAE) and time points. To predict hindlimb kinematic positions, we manually labeled six different body parts (toe, MTP joint, ankle, knee, hip, and iliac crest) in all ~450 image frames. The model was trained for up to 650,000 iterations using a deep residual network structure (ResNet-50), based on the pretrained model weights from DLC. To detect footfalls in the ladder rung test, we manually labeled all four paws on ~200 image frames for different mouse models (see above) and time points. The ResNet-50 model was trained for 400,000 iterations, based on the pretrained model weights from DLC. To train our models, we used a computer with 64 GB RAM, AMD Ryzen 9 3900 × 12-Core Processor x 24, and GeForce RTX 2080 Ti 11 GB graphics card. Our trained models for kinematic and footfall analyses are publicly available.

To perform random forest (RF) classification following gait analysis, we used scikit-learn[56]. To build the classifiers, ALMA provides several built-in functions such as outlier removal, assignment of group labels to the single gait cycle kinematic data, and concatenation of the kinematic data from different groups into a single data frame. For the random forest hyperparameters, we followed the default from the random forest classifier function in sklearn, which was sufficient for learning the mapping[57]. Specifically, we used 100 decision trees in each RF classifier, with Gini impurity as the splitting criterion. We did not set a maximum depth for the trees and allowed an unlimited number of leaf nodes. The individual trees were built with samples from the entire training dataset. Importantly, we created new classifiers for each assay (i.e., one RF classifier for healthy vs. 3 dpi, another for healthy vs. 21 dpi, and so on). We used a 75%/25% split of training and testing data. As there was roughly an equal amount of data from the healthy/disease conditions, we based the splitting on random selection. The accuracy results presented in this paper were based on test data not included in the training set to demonstrate the generalizability of the models.

Animals. We used C57bl6 female mice of 2–4 months of age. The mice were kept in our animal facility under a regular day/night cycle (12 h/12 h). Animals had constant access to food and water. All animal experiments were carried out in accordance with the German animal welfare guidelines and previously authorized by the local regulatory committees (Regierung von Oberbayern).

Spinal cord injury. Mice were anesthetized with MMF (medetomidin 0.5 mg/kg, Orion Pharma; midazolam 5.0 mg/kg, Ratiopharm; fentanyl 0.05 mg/kg, B. Braun). Once the mice presented no reflex reaction from paw pinching, their backs were shaved and a laminectomy was performed at T8 levels. The dura was exposed, and a dorsal hemisection was performed using irridectomy scissors[38,58] (Bradley et al.[58]; Loy et al.[59]). After the hemisection, the wound was closed, and the skin was sutured. An antagonist mix was given (atipamezole 2.5 mg/kg, flumazenil 0.5 mg/kg, and naloxon 1.2 mg/kg), and mice were kept on a heating pad until completely awake. Mice received meloxicam (Metacam, 1.5 mg/ml oral suspension) at 12, 24, and 48 h following the injury.

EAE. Active EAE was induced in female mice by subcutaneous injection of 400 µg of purified recombinant MOG (N1-125) in complete Freund's adjuvant (freshly made by adding 10 mg/mL *Mycobacterium* tuberculosis H37 Ra, Sigma-Aldrich). Then, 400 ng of pertussis toxin (Sigma-Aldrich) were administered intraperitoneally (i.p.) on days 0 and 2 after immunization[60]. The mice were weighed daily and scored for neurological deficits according to the following EAE scores: 0, no clinical signs; 0.5, partial tail weakness; 1, tail paralysis; 1.5, gait instability or impaired righting ability; 2, hindlimb paresis; 2.5, hindlimb paresis with dragging of one foot; 3, total hindlimb paralysis; 3.5, hindlimb paralysis and forelimb paresis; 4, hindlimb and forelimb paralysis; 5, death.

Stages of the disease were defined as follows: disease onset was defined as the first day with clinical symptoms in the EAE score, disease peak occurred 3 or 4 days after onset, and recovery occurred 10 or 11 days after onset).

Traumatic brain injury. Mice were anesthetized by intraperitoneal MMF injection. Once the mice presented no reflex reaction from paw pinching, they were put on a stereotaxic frame (Precision Systems & Instrumentation, LLC). A skin incision was made followed by the drilling of a window on the right skull hemisphere, which was positioned rostrocaudal, between the bregma and lambda and under the sagittal suture. Mice were then placed on the TBI-0310 impactor (Precision Systems & Instrumentation, LLC) to undergo traumatic brain injury (TBI). The tip of a 3-mm diameter steel rod was used to induce injury to the somatosensory cortex according to the following settings: 6 m/s, 150 ms dwell time, 0.5 mm depth[61]. Mice were removed from the impactor, the skull window was repositioned and sealed with Vetbond glue (3 M Vetbond, 3 M United States), and the skin was stitched. Mice were placed on a heating pad and injected with the antagonist mix before receiving a subcutaneous glucose injection (glucose 5% B. Braun Infusionslösung).

Behavior setup for kinematics. Mice were recorded using a GoPro 8 camera at 120 frames per second while running on a treadmill (Harvard Apparatus; speed varying from 2 cm/s to 25 cm/s depending on the disease model; Supplementary Fig. 1). The distance between the treadmill and camera was 14.5 cm, and the camera was placed equidistant from the two ends of the treadmill. We chose this camera position to obtain comprehensive information on joint angles, spatial variability, and limb endpoint trajectories, which are missing from bottom recordings of gait analysis. Each mouse was recorded for at least 1 min to sample enough step cycles. Every incomplete step cycle was automatically excluded by the toolbox. To extract meaningful datasets, a minimum number of 1200 frames were captured, i.e., 10 s of recording. One prerequisite to accurate data extraction was the blind selection of frames with representative step cycles (no pause in animal locomotion, no grooming, no back turns etc.). When the animal's limbs are completely dragging, our algorithm will only compute parameters that are independent to the step cycles. All preprocessing and processing steps undertaken by the ALMA toolbox can be found in Supplementary Fig. 1. We tested the validity of the automated kinematic analysis methods of ALMA by computing a selection of temporal and spatial kinematic parameters through manual labeling and quantification, based on a subset of the video data recorded at baseline (Supplementary Fig. 2). The manual validation was done using a custom-written Python script using OpenCV (openCV.org). An experienced observer labeled the body parts used for markerless pose estimation (toe, MTP, ankle, knee, hip, iliac crest) in more than 200 frames from a video recording at baseline (120 fps, treadmill speed 30 cm/s). We then calculated the Euclidean distance between the body part coordinates generated by manual labeling and markerless tracking from DLC. We then computed a number of kinematic parameters for up to seven-step cycles based on manually determined step onsets, using both manually labeled coordinates and automatically detected coordinates.

Behavior setup for a ladder rung. Mice were recorded using a GoPro 8 camera at 120 frames per second while making four consecutive runs on our custom-made ladders. In this test, the animals had to cross 1-m horizontal ladders, and footfalls were recorded. We evaluated the rhythmic locomotion in the regular walking task on a ladder with evenly spaced rungs and the animal's fine coordination paw placement ability using irregularly spaced rungs (irregular walking task). The camera was placed 17.5 cm distant from the ladder equidistant from the two ends. Animals were habituated on a ladder with regularly spaced rungs before any experiment was performed (2/3 habituations each for a total max. time of 3 min). We used DLC to perform markerless labeling of the hind paws and then applied ALMA to determine footfall characteristics with a peak detection algorithm. In the toolbox, we included three preprocessing algorithms that accommodate a range of different recording conditions and can be chosen by the experimenter. Here we chose to use a preprocessing procedure based on the deviation algorithm that shows a great correlation with manual counting. In particular, we used the "deviation" algorithm in automated ladder rung analysis, based on peak detection applied to the raw *y*-coordinate signal output from markerless pose estimation

methods, to determine mistakes. In order to avoid missed footfalls, we set a low prominence (footfall depth) threshold in the peak detection step, leading to a slightly higher number of false positives due to the signal-noise ratio. To reduce the number of false positives while using the "deviation" algorithm, we then adjusted the prominence threshold in the peak detection function. The data generated by ALMA in this paper include a manual validation step using the graphic interface provided in ALMA. We also validated fully manually all datasets obtained using ALMA by manually counting all mistakes made by the animals. To do so, we only analyzed consecutive steps of the hindlimbs. Therefore, the last step before or after any interruptions were not scored. Placements were considered a mistake when mice either totally missed a rung or if they slipped from a rung (deep or slight slip). Placements were considered as correct when the mice correctly placed all the feet or only a portion of the foot on the rungs. Then the number of mistakes over a standard distance was calculated quantitatively. All data preprocessing and analysis steps undertaken by the ALMA toolbox can be found in Supplementary Fig. 3.

Basso mouse scale. All mice with SCI were evaluated preoperatively and at 7 and 21 dpi. The scores regarding the locomotor ability of mice were given according to the original paper[10] by fully trained observers.

Statistics and reproducibility. All results are given as mean ± standard error of the mean (SEM) in the figures. In the expanded tables, data are given as mean ± standard deviation (SD). Statistical analysis and the construction of the graphs for data illustration were carried out on GraphPad Prism 8.4.3 for Windows (GraphPad Software). All datasets were tested for normality using the Shapiro–Wilk test. Parametric data from the SCI and TBI experiments were analyzed using repeated-measures ANOVA and Tukey's post hoc test. Nonparametric datasets from the SCI and TBI experiments were analyzed using the Friedman test followed by the Dunn post hoc test. Datasets from the EAE experiments were analyzed with the Kruskal–Wallis test followed by the Dunn post hoc test, as they were distributed non-normally. To determine correlation, we used Pearson's correlation coefficient. In order to classify animals we used random forest classification, based on individual step cycles. Feature importance in the Random Forest Classification was determined by Gini impurity-based feature importance which ranged between 0 and 1. Statistical significance levels are indicated as follows: $*P < 0.05$; $**P < 0.01$; $***P < 0.001$.

Reproducibility. All experiments in this study include at least five biological replicates. The number of replicates (ns) is mentioned in the text or figure legend.

Reporting summary. Further information on research design is available in the Nature Research Reporting Summary linked to this article.

Data availability

All data generated and analyzed in this study are included in this published article or are publicly available on Figshare repository[62].

Code availability

We have provided the code for the ALMA toolbox at https://github.com/sollan/alma and Zenodo[63].

Received: 26 July 2021; Accepted: 21 January 2022;
Published online: 15 February 2022

References

1. Krakauer, J. W., Ghazanfar, A. A., Gomez-Marin, A., Maciver, M. A. & Poeppel, D. Perspective neuroscience needs behavior: correcting a reductionist bias. https://doi.org/10.1016/j.neuron.2016.12.041 (2017).
2. Boyden, E. S., Zhang, F., Bamberg, E., Nagel, G. & Deisseroth, K. Millisecond-timescale, genetically targeted optical control of neural activity. *Nat. Neurosci.* **8**, 1263–1268 (2005).
3. Armbruster, B. N., Li, X., Pausch, M. H., Herlitze, S. & Roth, B. L. Evolving the lock to fit the key to create a family of G protein-coupled receptors potently activated by an inert ligand. *Proc. Natl Acad. Sci. USA* **104**, 5163–5168 (2007).
4. Wickersham, I. R., Finke, S., Conzelmann, K. K. & Callaway, E. M. Retrograde neuronal tracing with a deletion-mutant rabies virus. *Nat. Methods* **4**, 47–49 (2007).
5. Fenno, L., Yizhar, O. & Deisseroth, K. The development and application of optogenetics. *Annu. Rev. Neurosci.* **34**, 389–412 (2011).
6. Roth, B. L. DREADDs for neuroscientists. *Neuron* **89**, 683–694 (2016).
7. Crawley, J. N. Behavioral phenotyping strategies for mutant mice. *Neuron* **57**, 809–818 (2008).
8. Brooks, S. P. & Dunnett, S. B. Tests to assess motor phenotype in mice: a user's guide. *Nat. Rev. Neurosci.* **10**, 519–529 (2009).
9. Fonio, E., Golani, I. & Benjamini, Y. Measuring behavior of animal models: faults and remedies. *Nat. Methods* **9**, 1167–1170 (2012).
10. Basso, D. M. et al. Basso mouse scale for locomotion detects differences in recovery after spinal cord injury in five common mouse strains. *J. Neurotrauma* **23**, 635–659 (2006).
11. Merriaux, P., Dupuis, Y., Boutteau, R., Vasseur, P. & Savatier, X. A study of vicon system positioning performance. *Sensors* **17**, 1591 (2017).
12. Hildebrand, M. Vertebrate locomotion: an introduction: how does an animal's body move itself along? *Bioscience* **39**, 764–765 (1989).
13. Metz, G. A. S., Dietz, V., Schwab, M. E. & Van de Meent, H. The effects of unilateral pyramidal tract section on hindlimb motor performance in the rat. *Behav. Brain Res.* **96**, 37–46 (1998)..
14. Fouad, K., Metz, G. A. S., Merkler, D., Dietz, V. & Schwab, M. E. Treadmill training in incomplete spinal cord injured rats. *Behav. Brain Res.* **115**, 107–113 (2000).
15. Ueno, M. & Yamashita, T. Kinematic analyses reveal impaired locomotion following injury of the motor cortex in mice. *Exp. Neurol.* **230**, 280–290 (2011).
16. Hamers, F. P. T., Lankhorst, A. J., Van Laar, T. J., Veldhuis, W. B. & Gispen, W. H. Automated quantitative gait analysis during overground locomotion in the rat: Its application to spinal cord contusion and transection injuries. *J. Neurotrauma* **18**, 187–201 (2001).
17. Bhimani, A. D. et al. Functional gait analysis in a spinal contusion rat model. *Neurosci. Biobehav. Rev.* **83**, 540–546 (2017).
18. Jacobi, A. et al. FGF 22 signaling regulates synapse formation during post-injury remodeling of the spinal cord. *EMBO J.* **34**, 1231–1243 (2015).
19. Hamers, F. P. T., Koopmans, G. C. & Joosten, E. A. J. CatWalk-assisted gait analysis in the assessment of spinal cord injury. *J. Neurotrauma* **23**, 537–548 (2006).
20. Takeoka, A., Vollenweider, I., Courtine, G. & Arber, S. Muscle spindle feedback directs locomotor recovery and circuit reorganization after spinal cord injury. *Cell* **159**, 1626–1639 (2014).
21. Courtine, G. et al. Recovery of supraspinal control of stepping via indirect propriospinal relay connections after spinal cord injury. *Nat. Med.* **14**, 69–74 (2008).
22. Huang, R. et al. Machine learning classifies predictive kinematic features in a mouse model of neurodegeneration. *Sci. Rep.* **11**, 1–16 (2021).
23. Pfister, A., West, A. M., Bronner, S. & Noah, J. A. Comparative abilities of Microsoft Kinect and Vicon 3D motion capture for gait analysis. *J. Med. Eng. Technol.* **38**, 274–280 (2014).
24. Mathis, A. et al. DeepLabCut: markerless pose estimation of user-defined body parts with deep learning. *Nat. Neurosci.* **21**, 1281–1289 (2018).
25. Arac, A., Zhao, P., Dobkin, B. H., Carmichael, S. T. & Golshani, P. Deepbehavior: a deep learning toolbox for automated analysis of animal and human behavior imaging data. *Front. Syst. Neurosci.* **13**, 20 (2019).
26. Zimmermann, C., Schneider, A., Alyahyay, M., Brox, T. & Diester, I. FreiPose: a deep learning framework for precise animal motion capture in 3D spaces. Preprint at *bioRxiv* https://doi.org/10.1101/2020.02.27.967620 (2020).
27. Fiker, R., Kim, L. H., Molina, L. A., Chomiak, T. & Whelan, P. J. Visual Gait Lab: a user-friendly approach to gait analysis. *J. Neurosci. Methods* **341**, 108775 (2020).
28. Dunn, T. W. et al. Geometric deep learning enables 3D kinematic profiling across species and environments. *Nat. Methods* https://doi.org/10.1038/s41592-021-01106-6 (2021).
29. Wenger, N. et al. Spatiotemporal neuromodulation therapies engaging muscle synergies improve motor control after spinal cord injury. *Nat. Med.* **22**, 138–145 (2016).
30. Liu, N. K. et al. A semicircular controlled cortical impact produces long-term motor and cognitive dysfunction that correlates well with damage to both the sensorimotor cortex and hippocampus. *Brain Res.* **1576**, 18–26 (2014).
31. Bondi, C. O. et al. Found in translation: Understanding the biology and behavior of experimental traumatic brain injury. *Neurosci. Biobehav. Rev.* **58**, 123–146 (2015).
32. Nica, I., Deprez, M., Nuttin, B. & Aerts, J. M. Automated assessment of endpoint and kinematic features of skilled reaching in rats. *Front. Behav. Neurosci.* **11**, 255 (2018).
33. Pereira, T. D. et al. SLEAP: Multi-animal pose tracking. Preprint at https://doi.org/10.1101/2020.08.31.276246 (2020).
34. Segalin, C. et al. The Mouse Action Recognition System (MARS) software pipeline for automated analysis of social behaviors in mice. *Elife*. **10**, e63720 (2021).
35. Graving, J. M. et al. DeepPoseKit, a software toolkit for fast and robust animal pose estimation using deep learning. *eLife* **8**, e47994 (2019).
36. Metz, G. A. & Whishaw, I. Q. Cortical and subcortical lesions impair skilled walking in the ladder rung walking test: a new task to evaluate fore- and hindlimb stepping, placing, and co-ordination. *J. Neurosci. Methods* **115**, 169–179 (2002).

37. Metz, G. A. & Whishaw, I. Q. The ladder rung walking task: a scoring system and its practical application. *J. Vis. Exp.* https://doi.org/10.3791/1204 (2009).
38. Loy, K. et al. Semaphorin 7A restricts serotonergic innervation and ensures recovery after spinal cord injury. *Cell. Mol. Life Sci.* **78**, 2911–2927 (2021).
39. Silver, J. & Miller, J. H. Regeneration beyond the glial scar. *Nat. Rev. Neurosci.* **5**, 146–156 (2004).
40. Bareyre, F. M. et al. The injured spinal cord spontaneously forms a new intraspinal circuit in adult rats. *Nat. Neurosci.* **7**, 269–277 (2004).
41. Ueno, M., Hayano, Y., Nakagawa, H. & Yamashita, T. Intraspinal rewiring of the corticospinal tract requires target-derived brain-derived neurotrophic factor and compensates lost function after brain injury. *Brain* **135**, 1253–1267 (2012).
42. Lai, S. et al. Quantitative kinematic characterization of reaching impairments in mice after a stroke. *Neurorehabil. Neural Repair* **29**, 382–392 (2015).
43. Maier, I. C. et al. Differential effects of anti-Nogo-A antibody treatment and treadmill training in rats with incomplete spinal cord injury. *Brain* **132**, 1426–1440 (2009).
44. Chen, K. et al. Sequential therapy of anti-Nogo-A antibody treatment and treadmill training leads to cumulative improvements after spinal cord injury in rats. *Exp. Neurol.* **292**, 135–144 (2017).
45. Hanlon, L. A., Huh, J. W. & Raghupathi, R. Minocycline transiently reduces microglia/macrophage activation but exacerbates cognitive deficits following repetitive traumatic brain injury in the neonatal rat. *J. Neuropathol. Exp. Neurol.* **75**, 214–226 (2016).
46. Brown, A. R. & Martinez, M. Chronic inactivation of the contralesional hindlimb motor cortex after thoracic spinal cord hemisection impedes locomotor recovery in the rat. *Exp. Neurol.* **343**, 113775 (2021).
47. Jacobs, B. Y. et al. The Open Source GAITOR suite for rodent gait analysis. *Sci. Rep.* **8**, 1–14 (2018).
48. Peruga, I. et al. Inflammation modulates anxiety in an animal model of multiple sclerosis. *Behav. Brain Res.* **220**, 20–29 (2011).
49. de Bruin, N. M. W. J. et al. Multiple rodent models and behavioral measures reveal unexpected responses to FTY720 and DMF in experimental autoimmune encephalomyelitis. *Behav. Brain Res.* **300**, 160–174 (2016).
50. Herold, S. et al. CatWalk gait analysis in a rat model of multiple sclerosis. *BMC Neurosci.* **17**, 1–13 (2016).
51. Kerschensteiner, M. et al. Remodeling of axonal connections contributes to recovery in an animal model of multiple sclerosis. *J. Exp. Med.* **200**, 1027–1038 (2004).
52. Merkler, D., Ernsting, T., Kerschensteiner, M., Brück, W. & Stadelmann, C. A new focal EAE model of cortical demyelination: multiple sclerosis-like lesions with rapid resolution of inflammation and extensive remyelination. *Brain* **129**, 1972–1983 (2006).
53. Jafari, M. et al. Phagocyte-mediated synapse removal in cortical neuroinflammation is promoted by local calcium accumulation. *Nat. Neurosci.* **24**, 355–367 (2021).
54. Faissner, S., Plemel, J. R., Gold, R. & Yong, V. W. Progressive multiple sclerosis: from pathophysiology to therapeutic strategies. *Nat. Rev. Drug Discov.* **18**, 905–922 (2019).
55. Zhan, J. et al. High speed ventral plane videography as a convenient tool to quantify motor deficits during pre-clinical experimental autoimmune encephalomyelitis. *Cells* **8**, 1439 (2019).
56. Pedregosa Fabianpedregosa, F. et al. Scikit-learn: machine learning in Python Gaël Varoquaux Bertrand Thirion Vincent Dubourg Alexandre Passos PEDREGOSA, VAROQUAUX, GRAMFORT ET AL. *Matthieu Perro. J. Mach. Learn. Res.* **12**, 2825–2830 (2011).
57. Hsu, A. I. & Yttri, E. A. B-SOiD, an open-source unsupervised algorithm for identification and fast prediction of behaviors. *Nat. Commun.* **12**, 1–13 (2021).
58. Bradley, P. M. et al. Corticospinal circuit remodeling after central nervous system injury is dependent on neuronal activity. *J. Exp. Med.* **216**, 2503–2514 (2019).
59. Loy, K. et al. Enhanced voluntary exercise improves functional recovery following spinal cord injury by impacting the local neuroglial injury response and supporting the rewiring of supraspinal circuits. *J. Neurotrauma.* **35**, 2904–2915 (2018).
60. Locatelli, G. et al. Mononuclear phagocytes locally specify and adapt their phenotype in a multiple sclerosis model. *Nat. Neurosci.* **21**, 1196–1208 (2018).
61. Littlejohn, E. L., Scott, D. & Saatman, K. E. Insulin-like growth factor-1 overexpression increases long-term survival of posttrauma-born hippocampal neurons while inhibiting ectopic migration following traumatic brain injury. *Acta Neuropathol. Commun.* **8**, 1–15 (2020).
62. Aljovic, A. et al. Data used in this publication. https://doi.org/10.6084/m9.figshare.17212856.v1 (2021).
63. Zhao S. & Aljovic A. sollan/alma: first major release. https://doi.org/10.5281/zenodo.5767422 (2021).

Acknowledgements

The authors would like to thank Luca Fabbio for animal handling as well as Dana Matzek and Bianca Stahr for animal husbandry. Work in F.M.B.'s lab is supported by grants from the Deutsche Forschungsgemeinschaft (DFG, SFB 870 Project ID 118803580, TRR274 Project ID 408885537), by the Munich Center for Neurosciences (MCN) and the Institute for Research on Paraplegia (IRP). F.M.B. is also supported by the Munich Center for Systems Neurology (DFG, SyNergy; EXC 2145/ID 390857198). V.V.S. is supported by a post-doctoral fellowship from the Humboldt foundation.

Author contributions

F.B., A.A., and S.Z. designed the experiments. A.A., C.R., and M.C. performed all surgical procedures. A.A., S.Z., and V.V. collected and analyzed the data. F.B., A.A., S.Z., and M.K. wrote the manuscript. All authors approved the final version of the paper.

Funding

Open Access funding enabled and organized by Projekt DEAL.

Competing interests

The authors declare no competing interests.

Additional information

Supplementary information The online version contains supplementary material available at https://doi.org/10.1038/s42003-022-03077-6.

Correspondence and requests for materials should be addressed to Florence M. Bareyre.

Peer review information *Communications Biology* thanks Ronaldo Ichiyama and the other, anonymous, reviewers for their contribution to the peer review of this work. Primary Handling Editor: Luke R. Grinham. Peer reviewer reports are available.

Reprints and permission information is available at http://www.nature.com/reprints

Publisher's note Springer Nature remains neutral with regard to jurisdictional claims in published maps and institutional affiliations.

Study 2

Selective plasticity of callosal neurons in the adult contralesional cortex following murine traumatic brain injury

Laura Empl, Alexandra Chovsepian*, **Maryam Chahin**, Wing Yin Vanessa Kan, Julie Fourneau, Valérie Van Steenbergen, Sanofer Weidinger, Maite Marcantoni, Alexander Ghanem, Peter Bradley, Karl Klaus Conzelmann, Ruiyao Cai, Alireza Ghasemigharagoz, Ali Ertürk, Ingrid Wagner, Mario Kreutzfeldt, Doron Merkler, Sabine Liebscher & Florence M. Bareyre*

** These authors contributed equally to the manuscript*

Aim of Study 2

The objective of this study is to investigate the structural and functional changes occurring in the contralesional cortex following traumatic brain injury (TBI). Despite the initial neuronal cell loss and circuit disruption resulting in behavioural and cognitive deficits, both clinical observations and animal models suggest a potential for spontaneous recovery, indicating the involvement of neuronal circuit plasticity. Specifically, the contralesional cortex has been implicated in the recovery process, with reports suggesting plastic reorganization and alterations in neuronal activity levels in this region. However, the precise mechanisms underlying this cortical response remain unclear. Therefore, this study employs a combination of structural and functional in vivo imaging techniques, selective labelling of neuronal subpopulations, and circuit mono-synaptic tracing methods to elucidate the circuit rearrangements occurring in the contralesional cortex post-TBI. The focus is on understanding the selective structural and functional adaptations of callosal neurons and their input circuits in response to contralateral brain injury, shedding light on the intricate mechanisms of cortical plasticity and recovery following TBI.

My contribution to this publication in detail:

For this paper, I was involved in designing experiments as well as contributing to the surgical procedures, inducing moderate traumatic brain injuries on mice through a craniotomy and the placement of cranial windows. I did stereotaxic brain viral tracer injection to label transcallosal neuron and CST neurons. The injured mice also underwent chronic in vivo recording with the use of two-photon microscope in order to document dendritic spine dynamic. I also performed the analysis of the dendritic spine morphology using NeuronStudio. Apart from data collection, I contributed to analysis and data quantifications. The data collection consisted of sacrificing the mice that underwent injuries as well as their controls to extract their brain. I participated in the brain tissue processing that was used for immunohistochemistry, notably to evaluate the lesion volume following moderate TBI. With

the generation of calcium imaging two-photon recording of mice after moderate TBI, I analysed, using a custom-written matlab code, the calcium intensity within intact neurons using manually drawn regions of interest (ROIs).

The paper has been published in Nature Communication (2022)

DOI: https://doi.org/10.1038/s41467-022-29992-0

nature COMMUNICATIONS

ARTICLE

https://doi.org/10.1038/s41467-022-29992-0 OPEN

Selective plasticity of callosal neurons in the adult contralesional cortex following murine traumatic brain injury

Laura Empl[1,2,9], Alexandra Chovsepian[1,2,9], Maryam Chahin[1,2,3], Wing Yin Vanessa Kan[1,2,3], Julie Fourneau[1,2], Valérie Van Steenbergen[1,2], Sanofer Weidinger[1,2], Maite Marcantoni[1,2], Alexander Ghanem[4], Peter Bradley[1,2], Karl Klaus Conzelmann[4], Ruiyao Cai[5,6], Alireza Ghasemigharagoz[5,6], Ali Ertürk[5,6,7], Ingrid Wagner[8], Mario Kreutzfeldt[8], Doron Merkler[8], Sabine Liebscher[1,2,7] & Florence M. Bareyre[1,2,7]✉

Traumatic brain injury (TBI) results in deficits that are often followed by recovery. The contralesional cortex can contribute to this process but how distinct contralesional neurons and circuits respond to injury remains to be determined. To unravel adaptations in the contralesional cortex, we used chronic in vivo two-photon imaging. We observed a general decrease in spine density with concomitant changes in spine dynamics over time. With retrograde co-labeling techniques, we showed that callosal neurons are uniquely affected by and responsive to TBI. To elucidate circuit connectivity, we used monosynaptic rabies tracing, clearing techniques and histology. We demonstrate that contralesional callosal neurons adapt their input circuitry by strengthening ipsilateral connections from pre-connected areas. Finally, functional in vivo two-photon imaging demonstrates that the restoration of pre-synaptic circuitry parallels the restoration of callosal activity patterns. Taken together our study thus delineates how callosal neurons structurally and functionally adapt following a contralateral murine TBI.

[1] Institute of Clinical Neuroimmunology, University Hospital, LMU Munich, 81377 Munich, Germany. [2] Biomedical Center Munich (BMC), Faculty of Medicine, LMU Munich, 82152 Planegg-Martinsried, Germany. [3] Graduate School of Systemic Neurosciences, Ludwig-Maximilians-Universitaet Munich, 82152 Planegg-Martinsried, Germany. [4] Max von Pettenkofer-Institute, Virology, Faculty of Medicine, & Gene Center, LMU Munich, 80336 Munich, Germany. [5] Institute for Tissue Engineering and Regenerative Medicine (iTERM), Helmholtz Zentrum München, Neuherberg, Germany. [6] Institute for Stroke and Dementia Research (ISD), Ludwig-Maximilians-Universität (LMU), Munich, Germany. [7] Munich Cluster of Systems Neurology (SyNergy), 81377 Munich, Germany. [8] Department of Pathology and Immunology, Division of Clinical Pathology, CMU, University & University Hospitals of Geneva, Rue Michel-Servet, 1211 Geneva, Switzerland. [9] These authors contributed equally: Laura Empl, Alexandra Chovsepian. ✉email: florence.bareyre@med.uni-muenchen.de

Moderate traumatic brain injury (TBI) is often followed by regional neuronal cell loss and disruption of neuronal circuits that result in behavioral and cognitive deficits. Both in humans and in animal models, the functional deficits can be followed by spontaneous recovery, suggesting that plasticity of the neuronal circuits disrupted by the injury can compensate for the lost function[1–3]. One region that has been implicated in the recovery process following traumatic or ischemic cortical lesions, is the homotopic contralesional cortex[1,3–10]. Both clinical and experimental studies point to plastic reorganization and changes in neuronal activity levels in the contralesional cortex[9,11–18]. Interestingly, several reports indicate different anatomical sites of plasticity including the formation of new axonal projections from the cortex to neighboring areas or to subcortical areas[6,19–24]. While these observations suggest that the contralesional cortex and its efferent fibers can in principle contribute to recovery[25] or to the emergence of compensatory behavioral strategies[26], it is worth noting that in some settings plasticity and increased activity in the contralesional cortex could also be detrimental and increase injury-mediated deficits[27,28]. These findings indicate that a more refined understanding of the cortical response pattern and in particular of the specific neuronal populations and circuits that adapt to a contralateral lesion is needed.

Recently, it was reported that anatomically connected areas undergo microstructural changes in response to cortical ischemic injuries[16] and that contralesional cortical areas take over the lost function following amputation via adaptive remodeling of callosal inputs[17]. It is thus tempting to speculate that neuronal networks connecting the two hemispheres such as transcallosal connections could play a critical role in the response to cortical injury[29,30]. This is important as, while some higher order information processing, such as attention and language, is lateralized to a region in one hemisphere, correlation of activity between homotopic regions of the two hemispheres is important for sensorimotor processing and hence recovery[31,32]. Thus in this study, we used structural and functional in vivo imaging, selective labeling of neuronal subpopulations as well as circuit mono-synaptic tracing techniques to monitor the circuit rearrangements that take place in the contralesional cortex following TBI. Here, we reveal the selective structural and functional adaptation of callosal neurons and their input circuits to a contralateral brain injury.

Results

In vivo two-photon imaging reveals an early general loss of spines and changes in spine dynamics of contralesional cortical neurons following TBI. We induced TBI unilaterally in the sensorimotor cortex of mice using a controlled cortical impactor (TBI-0310 Impactor, precision Systems and Instrumentations, LLC; Fig.1a) which produced hemicortical lesions that spanned the ipsilateral primary somatosensory cortex (mean lesion volume $7.063 \pm 0.603\ mm^3$, $n = 4$; Supplementary Fig. 1a) and produced righting reflex and apnea recovery consistent with a moderate injury[33–35] (Supplementary Fig.1b). We first investigated the sensorimotor changes triggered by this brain injury over time using the irregular ladder rung, which allows us to appreciate skilled walking while minimizing the ability of the mice to compensate for impairments through learning. In this test, we observed that acutely following TBI, there is a marked increase in the number of mistakes made by the animals which then recovers over the following weeks (up to day 21 after TBI; Fig. 1b; $^{***}p = 0.0001$ 3d vs Baseline; $^{*}p = 0.0481$ 7d vs Baseline;$^{\#}p = 0.0044$ at 14d, 21d vs 3d;.Friedman test followed by uncorrected Dunn's test). This established that, in our model, remodeling processes in the first few weeks after injury are likely critical for functional recovery. Such remodeling processes are likely to take place throughout the CNS and include corticospinal and intraspinal rewiring. Here we wanted to focus on changes that occur in the contralesional cortex so we first examined whether there were apparent changes to the cortical microanatomy. Our results indicated, however, that cortical thickness, neuronal density and soma size contralateral to the lesion were not different between control and injured mice at any time points investigated (Supplementary Fig. 2). As contralesional cortical neurons do neither die nor suffer from atrophy following TBI, we concentrated on analyzing changes to the morphology of individual neurons and in particular their dendritic spines. To do so we used GFP-M mice[36], which sparsely express eGFP in a subset of pyramidal neurons mainly in layer V of the cortex, and performed in vivo two photon imaging of the contralesional sensorimotor cortex before (baselines 1 and 2) and after injury (Fig. 1c). We were able to image and follow 81 dendritic stretches from 4 animals (Fig. 1d) and a total of 10,191 spines throughout the experiment. With two-photon imaging we could show that TBI induced a strong and significant reduction of the spine density that can be detected as early as 3 days following TBI and persisted throughout the study-period (Fig. 1e; $^{***}p = 0.0001$ B1 vs 3dpi and $^{***}p < 0.0001$ B1 vs all other time points; one-way repeated measure (RM) Anova followed by Dunnett's test). To assess whether the reduction in spine density was due to a pronounced loss of spines or a lack of newly formed spines, we then followed the fate of the spines and determined the proportion of stable spines, lost spines or newly formed spines (Fig. 1f and Supplementary Fig.3). We found that while the rate of stable spines remained around 80% (Supplementary Fig.3) during the entire study period, the rate of formation and elimination of spines fluctuated over time following injury (Fig. 1f). In particular, the elimination rate of spines was significantly increased compared to the formation rate at 3d post-injury ($^{*}p = 0.0146$ Two-way RM Anova and Tukey test) while the formation rate was significantly increased compared to the elimination rate between days 12 and 18 ($p = 0.0287$ 12–15d and $p = 0.0146$ 15–18d Two-way RM Anova and Tukey test). This argues that adaptive structural plasticity can restore spine density and prompted us to perform additional experiments to determine the neuronal populations involved in these adaptations and the specific time course of these changes following TBI.

The decrease in spine density is specific to callosal neurons. To determine whether changes in dendritic spine density can be found in all contralesional neurons or are specific to a given population of neurons, we used GFP-M mice and used retrograde tracing with fluorogold. We injected fluorogold into the ipsilesional area prior to TBI to retrogradely label and analyze spine density of callosal neurons located homotopically[37] in the contralesional hemisphere (Fig.2a). Non-callosal neurons (not retrogradely-labeled with fluorogold but whose location was overlapping with the retrogradely-labeled callosal neurons in the contralesional hemisphere) were investigated as controls. We focused on layer II/III and layer V neurons and analyzed spine density in the proximal dendrite, distal dendrite (only for layer V neurons) and apical tufts. We observed that following brain injury dendritic spine density in the apical tufts of callosal neurons is decreased at 7 and 14d (layer II/III 7d $p = 0.0124$, 14d $p = 0.0303$; layer V 14d $p = 0.0329$ One-Way Anova and Dunnett's test) and subsequently recovers to control values by 42d (Fig. 2b–d; *left panel*). In contrast, dendritic spine density of the apical tufts of non-callosal layer II/III and layer V neurons remained unchanged over the study period (Fig. 2e, f, *left panels*). We then investigated changes in spine density of proximal

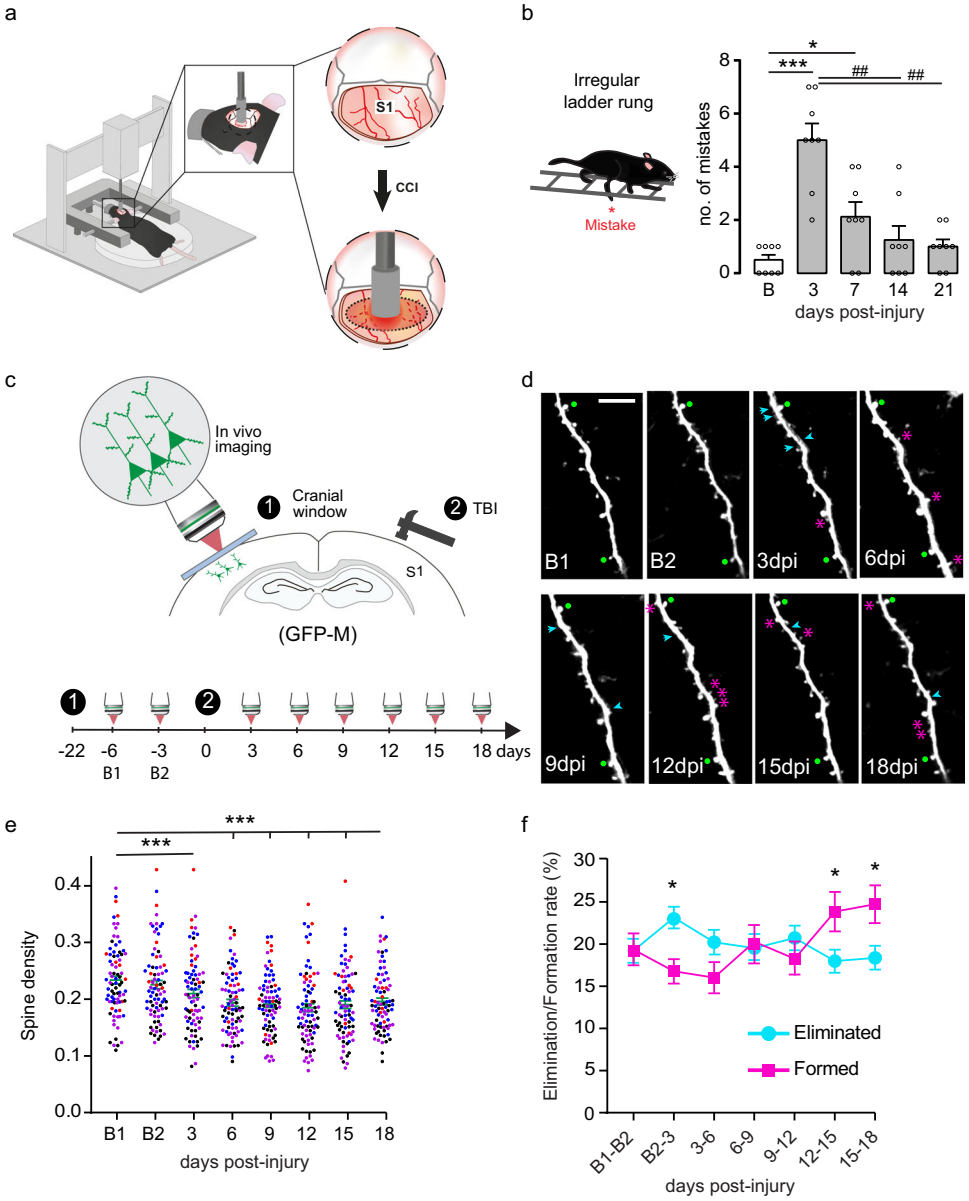

Fig. 1 Traumatic brain injury triggers a contralesional decrease in spine density and time-dependent variations of the rate of eliminated /formed spines on dendrites of GFP-M mice analyzed using two-photon in vivo imaging. a Scheme of the moderate brain injury depicting the flat-edged impactor used to lesion the brain (S1: primary somatosensory cortex; CCI: controlled cortical impact). **b** Scheme of the irregular ladder rung test used to evaluate sensorimotor recovery following traumatic brain injury and quantification (mean ± SEM) of the number of mistakes at baseline and following the injury. Data are analyzed with a Friedman test followed by uncorrected Dunn's test. ***:$p = 0.0001$ 3d vs Baseline; *:$p = 0.0481$ 7d vs Baseline; $^{\#\#}p = 0.0044$ at 14d, 21d vs 3d. **c** Scheme of the experimental design and timeline of the two-photon in vivo imaging. **d** Representative timelapse series of an apical dendrite from a layer V neuron in GFP-M mice assessed at the indicated experimental time point and followed up to 18d post-injury. B: Baseline; Scale bar: 10 µm. Cyan arrowhead indicates the position of a lost spine, green dot indicate stable spines present throughout the entire investigational period, and fushia asterisk indicates gained spines. **e** Quantification (mean ± SEM) of spine density at different time points post-injury (dendrites are color-coded per animal). Data are analyzed with one-way RM Anova followed by Dunnett's test. ***$p = 0.0001$ 3 dpi vs B1; ***$p < 0.0001$ 6, 9, 12, 15, 18dpi vs B1. **f** Average of elimination and formation rate of spines in GFP-M mice. Data in (**e** and **f**) come from 81 dendritic stretches, 10,191 spines followed over time and $n = 4$ animals. Data are presented as mean ± SEM and analyzed with two-way RM Anova followed by Tukey test. *$p = 0.0146$ 3 dpi vs B2 eliminated vs formed; *$p = 0.0287$ 12 dpi vs 15 dpi eliminated vs formed; *$p = 0.0146$ 15 dpi vs 18 dpi eliminated vs formed. Source data are provided as a Source Data file. B1: Baseline 1; B2: Baseline 2.

dendrites of callosal and non-callosal neurons (Fig. 2b–d, *right panels* and Fig. 2e,f *right panels*). We found a decrease in spine density at 14d in layer II/III callosal neurons ($p = 0.0288$) and a decrease in spine density at 7d ($p = 0.0286$) and 14d ($p = 0.0288$) in layer V callosal neurons while no such changes were observed in layer II/III and layer V non-callosal neurons (One-Way Anova and Dunnett's test for all comparisons). Finally we examined the spine density of distal dendritic segments of layer V callosal neurons (Fig. 2d, *middle panel*) and could observe a significant albeit transient decrease in spine density at 7d post-injury ($p = 0.0341$ One-Way Anova and Dunnett's test). In contrast, similarly to the apical tufts, no changes in spine density could be seen on the distal compartment of the dendritic trunk of layer V non-callosal neurons (Fig. 2f, *middle panel*). To confirm that the

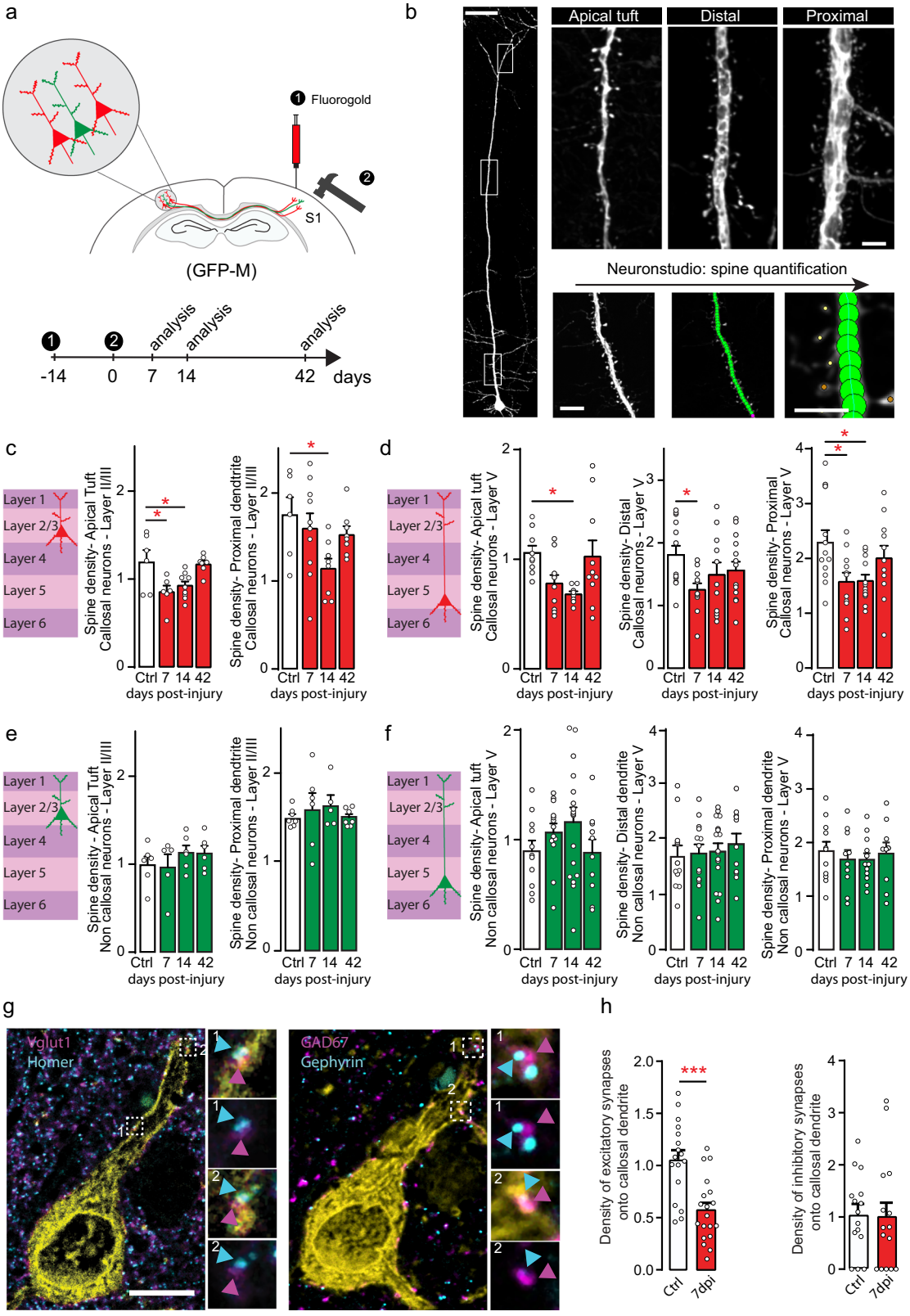

observed changes are indeed selective for neurons that project to the lesioned hemisphere we also examined corticospinal tract (CST) neurons, which were retrogradely labeled from the spinal cord. Here, no differences in spine density could be seen in CST neurons before and 7d after injury (proximal: 2.11 ± 0.22 vs 1.95 ± 0.12; distal: CST 2.1 ± 0.14 vs 2.19 ± 0.12; apical: CST 1.00 ± 0.07 vs 0.96 ± 0.07/µm) or between non-callosal and corticospinal neurons before and 7d after injury (proximal control: CST 2.11 ± 0.22 vs NC 2.28 ± 0.23; distal control: CST 2.1 ± 0.14 vs NC 1.75 ± 0.15; apical control: CST 1.00 ± 0.07 vs NC 0.94 ± 0.09; proximal 7d: CST 1.95 ± 0.12 vs NC 1.86 ± 0.10; distal 7d: CST 2.19 ± 0.12 vs NC 2.02 ± 0.11; apical 7d: CST 0.96 ± 0.07 vs NC 1.06 ± 0.08/µm). Finally, we investigated how the balance of excitatory and inhibitory inputs onto callosal

Fig. 2 The decrease in spine density is specific to contralesional neurons directly connected to the lesion site (callosal neurons). a Scheme of the experimental design and timeline of the confocal ex vivo imaging (red: retrogradely-labelled neurons; green: GFP positive neurons). **b** Confocal images of a layer V cortical neuron (left) and magnification of the dendritic parts boxed in the left images (right) and representative example illustrating the spine quantification using Neuronstudio. Scale bars: 150 µm (left panel), 5 µm (top panels and bottom right panel) and 10 µm (bottom middle panels). **c** Scheme of layer II/III callosal cortical neuron and dendritic spine density (mean ± SEM) of layer II/III callosal population in the apical tuft (left) and proximal dendrite (right) in control (white column) and injured mice (red column) at several time points following injury. $n = 6$–9 independent dendritic stretches from 4 to 5 mice for Apical and $n = 6$–9 independent dendritic stretches from 4 to 5 mice for Proximal. Apical: $p = 0.0124$ and $p = 0.0303$ Ctrl vs 7d and Ctrl vs 14d respectively one-way Anova and Dunnett's test. Proximal: $p = 0.0288$ Ctrl vs 14d one-way Anova and Dunnett's test. **d** Scheme of layer V callosal cortical neuron and dendritic spine density (mean ± SEM) of layer V callosal population in the apical tuft (left), distal dendrite (middle) and proximal dendrite (right) in control (white column) and injured mice (red column) at several time points following injury. $n = 8$–10 independent dendritic stretches from 4 to 5 mice for Apical, $n = 11$–14 independent dendritic stretches from 4 to 5 mice for Distal, $n = 11$–12 independent dendritic stretches from 4 to 5 mice for Proximal. Apical: $p = 0.0329$ Ctrl vs 14d. Distal: $p = 0.0341$ Ctrl vs 7d. Proximal: $p = 0.0286$ Ctrl vs 7d and $p = 0.0288$ Ctrl vs 14d. One-way Anova and Dunnett's test for all. **e** Scheme of layer II/III non callosal cortical neuron and mean ± SEM dendritic spine density of layer II/III non callosal population in the apical tuft (left) and proximal dendrite (right) in control (white column) and injured mice (green column) at several time points following injury. $n = 5$–6 independent dendritic stretches from 4 to 5 mice for Apical and $n = 5$–7 independent dendritic stretches from 4 to 5 mice for Proximal. **f** Scheme of layer V non callosal cortical neuron and dendritic spine density (mean ± SEM) of layer V non callosal population in the apical tuft (left), distal dendrite (middle) and proximal dendrite (right) in control (white column) and injured mice (green column) at several time points following injury. $n = 10$–17 independent dendritic stretches from 4 to 5 mice for Apical, $n = 11$–17 independent dendritic stretches from 4 to 5 mice for Distal, $n = 9$–12 independent dendritic stretches from 4 to 5 mice for Proximal. **g** Confocal images of a retrogradely labeled callosal neuron (Yellow) in the contralesional cortex stained with the excitatory presynaptic marker Vglut1 and the excitatory post-synaptic marker Homer (left panel) and with the inhibitory pre-synaptic marker GAD67 and the inhibitory post-synaptic marker Gephyrin (right panel). Insets show co-localization of pre and post-synaptic marker pairs in contact with the callosal dendrite that we evaluated. Scale bar equals 10 µm. **h** Quantification (mean ± SEM) of the density of excitatory and inhibitory synaptic pairs co-localizing with callosal dendrites. $n = 15$–19 dendritic segments per group from 4 to 5 animal per group. Data are analyzed using unpaired two-tailed *t*-test. $p = 0.0001$ for excitatory synapses and $p = 0.8605$ for inhibitory synapses control (Ctrl) vs TBI. Source data are provided as a Source Data file.

neurons changes following brain injury. To do so, we identified excitatory synapses based on the co-localization of the pre-synaptic marker Vglut1 and the post-synaptic marker Homer and inhibitory synapses based on the co-localization of the pre-synaptic marker GAD67 and the post-synaptic marker Gephyrin on thin paraffin-embedded sections. We found that the density of excitatory inputs but not of inhibitory inputs onto the dendrites of callosal neurons was significantly decreased at 7 days after TBI ($p = 0.0001$ unpaired two-tailed *t*-test; Fig. 2g, h).

The decrease in spine density is accompanied by alterations of spine morphology. To further characterize the changes triggered by TBI to contralesional dendritic spines we then characterized the spine morphology as an indicator of the degree of spine maturation. We divided spines into three types: mushroom, thin and stubby spines (Fig. 3a) with mushroom spines generally considered as the most stable and mature structures[38,39]. We investigated spine morphology in the apical tuft of control and injured contralesional callosal layer II/III and layer V neurons in GFP-M mice. We found that, the proportion of the more stable mushroom spines decreased acutely following the injury (layer II/III: $p = 0.0040$ at 7d, $p = 0.0102$ at 14d; layer V: $p = 0.0271$ at 7d and $p = 0.0015$ at 14d; One-Way Anova and Dunnett's test) and partially recovered by 42d in the apical tuft of contralesional callosal neurons. In parallel, the proportion of stubby spines transiently increased at 14d in the apical tufts of layer V neurons ($p = 0.0026$; One-Way Anova and Dunnett's test) before returning to baseline levels at 42d (Fig. 3b,c) arguing for a shortening of the neck. The proportion of thin spines did not change overtime following TBI (Fig. 3b, c). We then investigated spine morphology in the distal and proximal dendrites of callosal neurons in GFP-M mice. Overall, we did not find any changes in the proportion of mushroom, thin and stubby spines following injury in the distal or proximal dendrites of layer II/III and layer V contralesional callosal neurons (Fig. 3b, c). In contrast to callosal neurons, non-callosal neurons do not demonstrate any changes of spine morphology following TBI even on apical tufts (Fig. 3d, e). To complement our spine analysis of contralesional callosal neurons, we also investigated the response of the callosal axons to injury. To do so, we quantified axons branches of callosal neurons as an indicator of the axonal response to TBI. Both at acute (7d) and chronic (42d) time points, we could see no differences to control animals (0.34 ± 0.05au in control animals vs 0.28 ± 0.04au 7d post-injury vs 0.35 ± 0.05au 42d post-injury). This suggests that the response of contralesional callosal neurons primarily involves dendritic remodeling with an initial loss and later recovery of pre-synaptic input to those neurons.

Newly formed spines on callosal neurons after TBI are more stable that those that form on non callosal neurons. As the spine density of callosal neurons recovers at later timepoints, we wanted to investigate the contribution of spines that form newly after injury to this process. To do so we used two-photon in vivo imaging to track the fate of the newly formed spines of callosal neurons as well as of corticospinal projection neurons (CST neurons), which are located in a similar anatomical location but do not project to the injured cortex. To selectively visualize these neuronal populations, we injected a retrograde adeno-associated virus expressing EGFP (retroAAV-EGFP) either in the ipsilesional cortex (to label callosal neurons, Fig. 4a–c) or in the spinal cord (to label CST neurons, Fig. 4d–f). Using this approach we could follow 23 apical dendrite stretches (8724 spines followed at each time points) for callosal neurons and 13 apical dendrite stretches (4376 spines followed at each time points) for CST neurons. We then analyzed the persistence of pre-existing (spines present before the injury) and newly formed spines and first confirmed that spines that already exist (both on callosal and CST neurons) before the injury are significantly more stable than newly formed spines ($p < 0.0001$; Mann–Whitney test, Fig. 4g). When we specifically compared the stability of the spines that form after injury on callosal neurons to non callosal neurons (CST neurons) we found that the persistence index was significantly higher for newly formed spines on callosal neurons ($p < 0.0001$, Mann–Whitney test, Fig. 4g). This indicates that an increased survival of newly formed spines on callosal neurons can contribute to the recovery of spine density after injury and

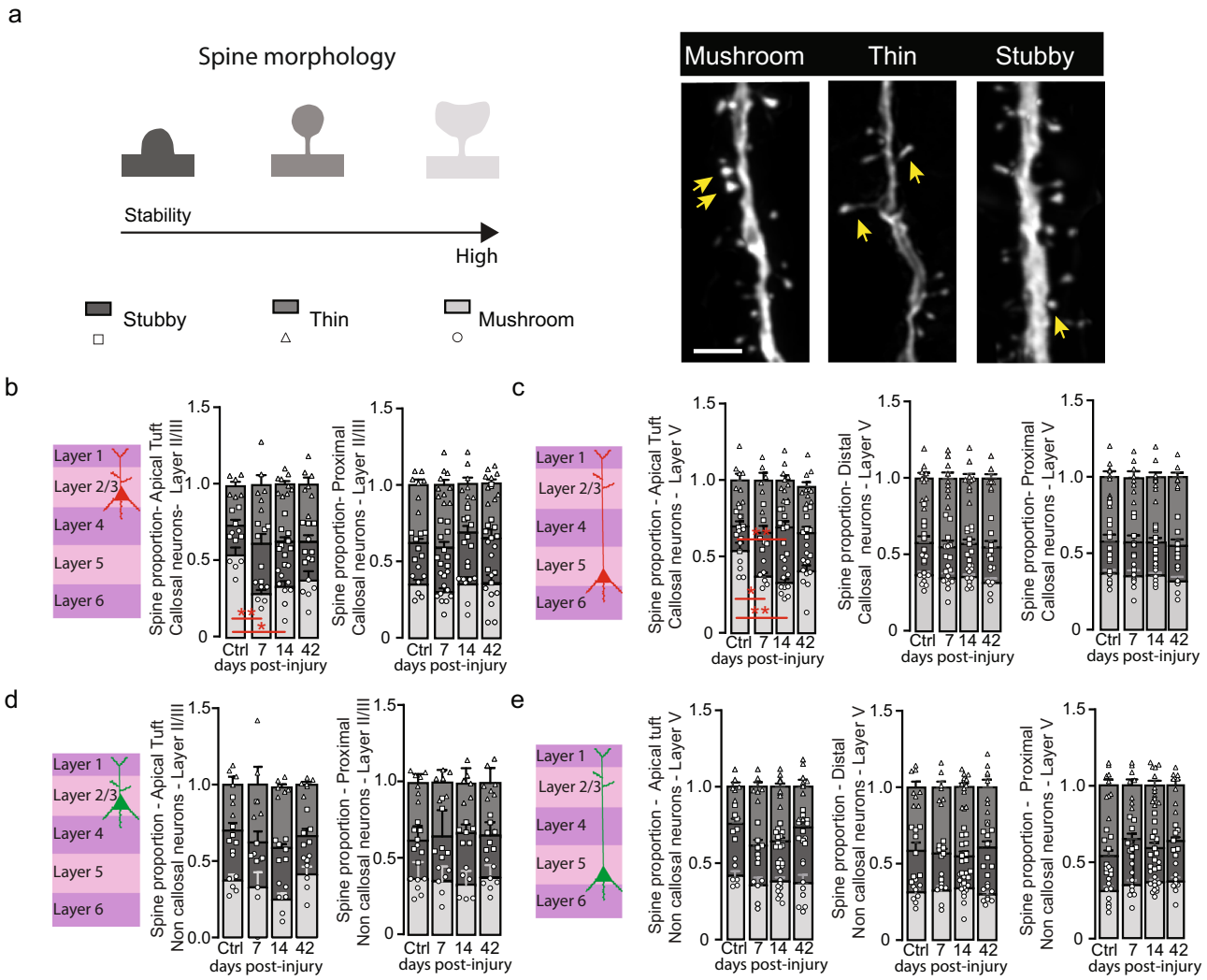

Fig. 3 Callosal neurons display changes in spine morphology following TBI. a Schematic representation of spine morphology and confocal images of mushroom, thin and stubby spines. Yellow arrows represent the examples of the respective spine type. Scale bar: 5 µm. **b** Scheme of layer II/III callosal cortical neuron and quantification (mean ± SEM) of the fraction of mushroom, thin and stubby spines on apical tuft and proximal dendrites of layer II/III callosal neurons. $n = 6$–9 independent dendritic stretches from 4 to 5 mice for Apical and $n = 7$–10 independent dendritic stretches from 4 to 5 mice for Proximal. Apical mushroom spines: $p = 0.0040$ Ctrl vs7d and $p = 0.0102$ Ctrl vs 14d. One way-ANOVA and Dunnett's test. **c** Scheme of layer V callosal cortical neuron and quantification (mean ± SEM) of the fraction of mushroom, thin and stubby spines on apical tuft, distal and proximal dendrites of layer V callosal neurons. $n = 7$–10 independent dendritic stretches from 4 to 5 mice for Apical, $n = 7$–10 independent dendritic stretches from 4 to 5 mice for Distal, $n = 6$–10 independent dendritic stretches from 4 to 5 mice for Proximal. Apical mushroom spines: $p = 0.0271$ Ctrl vs7d and $p = 0.0015$ Ctrl vs 14d. One way-Anova and Dunnett's test. Apical stubby spines: $p = 0.0026$ Ctrl vs 14d. One way-Anova and Dunnett's test. **d** Scheme of layer II/III non callosal cortical neuron and quantification (mean ± SEM) of the fraction of mushroom, thin and stubby spines on apical tuft and proximal dendrites of layer II/III non callosal neurons. $n = 5$–6 independent dendritic stretches from 4 to 5 mice for Apical and $n = 6$–7 independent dendritic stretches from 4 to 5 mice for Proximal. **e** Scheme of layer V non callosal cortical neuron and quantification (mean ± SEM) of the fraction of mushroom, thin and stubby spines on apical tuft, distal and proximal dendrites of layer V non callosal neurons. (light gray: mushroom spines, dark gray: stubby spines, medium gray: thin spines). $n = 6$–12 independent dendritic stretches from 4 to 5 mice for Apical, $n = 7$–13 independent dendritic stretches from 4 to 5 mice for Distal, $n = 8$–12 independent dendritic stretches from 4 to 5 mice for Proximal. Statistical p values are always compared to control (Ctrl) values. Source data are provided as a Source Data file.

underlines the functional significance of the associated rewiring of the callosal input circuitry.

Callosal neurons adapt their input circuitry by re-establishing ipsilateral connections from pre-connected areas following TBI. The observation that callosal neurons can remodel their input connections prompted us to study how the input circuitry of callosal neurons evolves after TBI. To answer this question, we first implemented retrograde mono-synaptic tracing using rabies virus[40,41] (Fig. 5a) combined with tissue clearing[42] (Fig. 5b). We first verified that the mono-synaptic tracing was specific and does not show any leakage by injecting either the rabies virus in absence of the complementing G and EnvA proteins as well as the cre recombinase or either injecting the AAV expressing the envA and G proteins (AAV1-synP-DIO-sTpEpB-eGFP) without rabies virus. Trans-synaptic retrograde tracing and tissue clearing allowed us to identify the general location of presynaptic inputs of callosal neurons before and following injury (Fig. 5c). This approach allowed us to determine that the major presynaptic input of contralesional callosal neurons is located in the

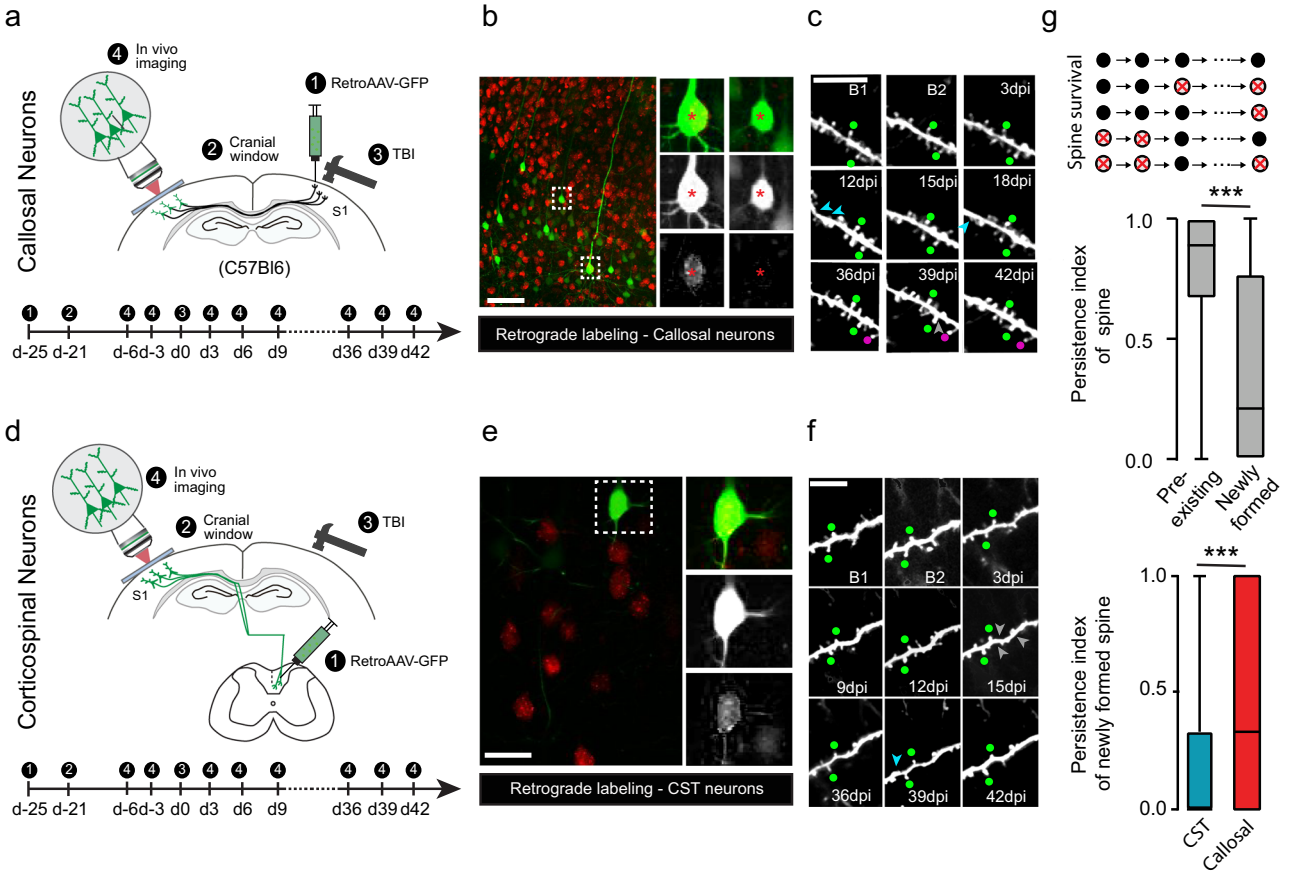

Fig. 4 Differential stability of newly generated spines formed on callosal and non callosal neurons following traumatic brain injury. a Scheme of the experimental design with retroAAV injected in the lesion area and timeline of the two-photon in vivo imaging. **b** Confocal images of retrogradely labeled callosal neurons in the cortex (Green: retroAAV-EGFP; red: NT435). Insets are four times magnified (top raw overlay; middle raw: retroAAV-EGFP; bottom raw: NT435).Scale bar equals 50 µm. **c** Representative timelapse series of an apical dendrite from a callosal neuron retrogradely-labeled with retroAAV-EGFP. Each image shows the same dendrite stretch at a specific experimental time point before and up to 42d post-injury (23 independent dentritic stretches and 8724 spines were followed). Cyan arrowheads indicate disappearing pre-existing spines. Gray arrowheads indicate disappearing newly-formed spines. Green dot indicate stable pre-existing spines. Magenta dots indicate stable newly-formed spines. B1: Baseline 1; B2: Baseline 2; Scale bar: 10 µm. **d** Scheme of the experimental design with the retroAAV injected in the spinal cord and timeline of the two-photon in vivo imaging. **e** Confocal images of retrogradely labeled CST neurons in the cortex (Green: retroAAV-EGFP; red: NT435). Insets are two times magnified (top raw overlay; middle raw:retroAAV-EGFP; bottom raw: NT435). Scale bar equals 50 µm. **f** Representative timelapse series of an apical dendrite from a CST neuron retrogradely-labeled with retroAAV-EGFP. Each image shows the same dendrite stretch at a specific experimental time point before and up to 42d post-injury (13 independent dentritic stretches and 4376 spines were followed). Cyan arrowheads indicate disappearing pre-existing spines. Gray arrowheads indicate disappearing newly-formed spines. Green dot indicate stable pre-existing spines. Magenta dots indicate stable newly-formed spines. B1: Baseline 1; B2: Baseline 2; Scale bar: 10 µm. **g** Quantifications comparing the persistence of all pre-existing spines ($n = 377$ spines analyzed) to all newly formed spines ($n = 187$ spines analyzed) (top panel) and the persistence of newly formed spines on callosal ($n = 134$ spines from nine dentritic stretches from four animals) and CST neurons ($n = 55$ spines analyzed from eight dendritic stretches from four animals) (bottom panel). All data (top and bottom) are analyzed using two-tailed Mann–Whitney test ($p < 0.0001$ in both cases) and presented as box plots (top panel: Pre-existing spines: minima:0, maxima:1,median = 0.8889; 25% percentile = 0.6667; 75% percentile = 1; newly formed spines: minima:0, maxima:1; median = 0.2111; 25% percentile = 0; 75% percentile = 0.7708 - bottom panel: CST: minima:0, maxima:1, median = 0; 25% percentile = 0; 75% percentile = 0.3333; Callosal: minima:0, maxima:1,median = 0.3333; 25% percentile = 0; 75% percentile = 1) Source data are provided as a Source Data file.

contralesional somatosensory cortex and showed that presynaptic cortical areas that are strongly connected were largely similar between control and TBI mice, with only subtle changes (Supplementary movie and Fig. 5c). As only presynaptic cells could be visualized and starter cells could not be detected using clearing techniques, we complemented this analysis using conventional immunohistological approaches. We sectioned, stained and analyzed the entire mouse brain and obtained connectivity ratios by normalizing the counted number of presynaptic cells to the number of starter cells (Fig.5d, e). Starter neurons (mCherry + / GFP +) were located exclusively within the injected area in the somatosensory cortex (Fig. 5e) and were surrounded by many mCherry + -only, monosynaptic input neurons (Fig. 5e). We analyzed more than 20 brain regions and identified the areas that provide input to callosal neurons in controls, in both ipsilesional and contralesional cortices (Fig. 5f), with the somatosensory cortex exhibiting the highest connectivity ratio. Other cortical inter-areal connectivity included afferents from the motor cortex, from the auditory area, the retrosplenial area or the posterior parietal association area, among others (Fig. 5f). Subcortical inter-areal connectivity included mostly the thalamus and at much lower ratios the hypothalamus and caudate putamen (Fig. 5f). Importantly, all of these regions have been found to project to the somatosensory cortex before[43] and we detected no aberrant input.

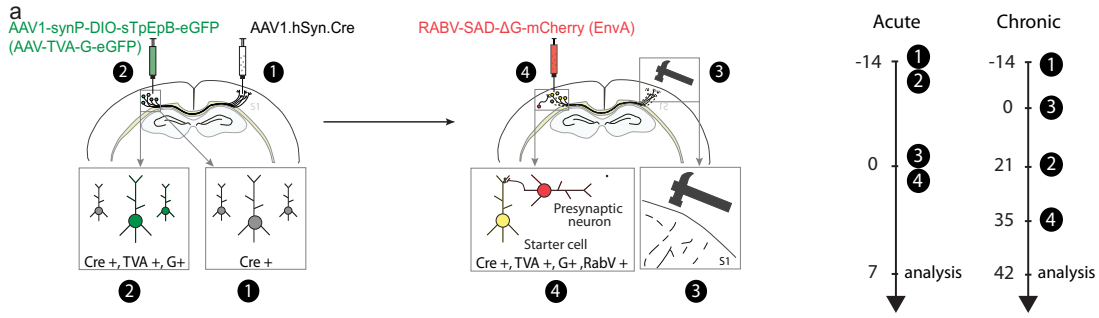

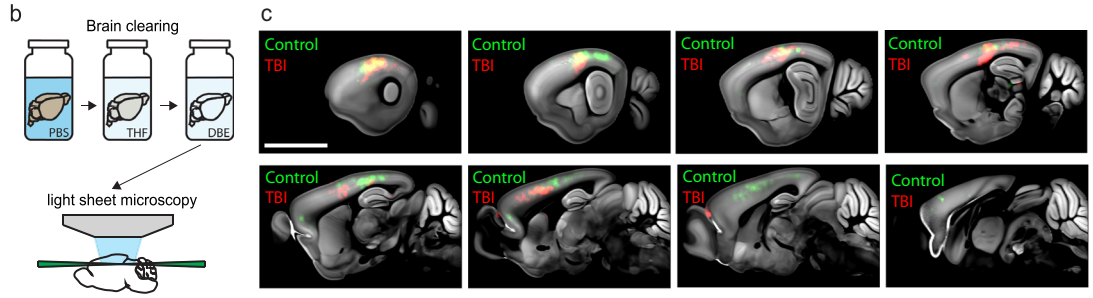

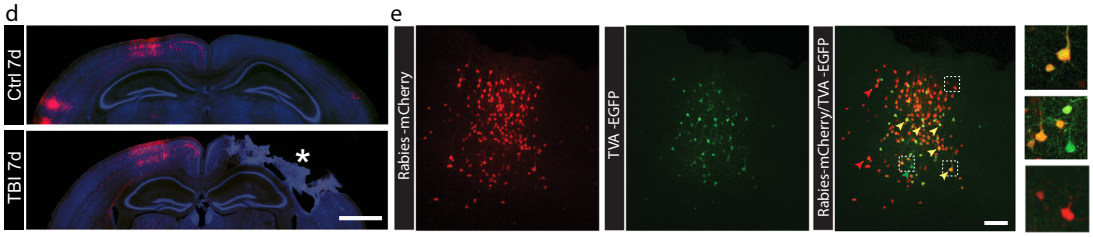

f

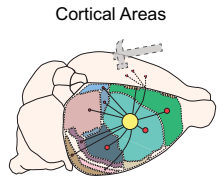

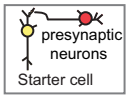

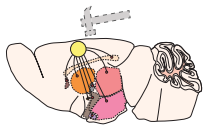

0 2
Connectivity ratios

	Connectivity ratios Acute			Connectivity ratios Chronic		
Contralesional cortical areas	Control 7d	7d TBI		Control 42d	42d TBI	
Somatosensory	1.952±0.201	1.532±0.361		1.250±0.098	1.056±0.139	
Auditory	1.001±0.192	0.297±0.062	**	0.706±0.130	0.552±0.067	
Motor	0.842±0.206	0.386±0.046	*	0.448±0.065	0.393±0.078	
Retrosplenial	0.527±0.108	0.291±0.063	*	0.510±0.075	0.411±0.083	
Posterior Perietal association	0.462±0.123	0.521±0.097		0.468±0.058	0.468±0.078	
Anterior Cingulate	0.096±0.020	0.086±0.035		0.156±0.055	0.076±0.012	
Visual	0.0652±0.018	0.081±0.015		0.089±0.016	0.062±0.015	
Temporal association	0.025±0.009	0.006±0.002	p=0,05	0.019±0.010	0.020±0.004	
Perirhinal	0.001±0.0004	0.001±0.0006		0±0	0±0	
Enthorinal	0.0003±0.0003	0±0		0±0	0.0003±0.0003	
Visceral	0±0	0.0013±0.0010		0±0	0.0009±0.0008	
Ipsilesional cortical areas						
Somatosensory	0.154±0.059	0±0	**	0.016±0.005	0±0	**
Retrosplenial	0.0172±0.007	0±0	*	0.027±0.004	0.003±0.002	***
Motor	0.030±0.008	0.0001±0.0001	***	0.008±0.003	0.0007±0.0005	**
Auditory	0.020±0.010	0±0	*	0.017±0.008	0.0000	*
Posterior Perietal association	0.008±0.005	0±0		0.022±0.011	0.0000	*
Anterior Cingulate	0.0008±0.0006	0.0001±0.0001		0.0019±0.0011	0.0010±0.0004	
Contralesional subcortical areas	Control 7d	7d TBI		Control 42d	42d TBI	
Thalamus	0.295±0.060	0.294±0.054		0.330±0.034	0.293±0.039	
Hypothalamus	0.016±0.004	0.021±0.007		0.016±0.002	0.021±0.007	
Caudate putamen	0.016±0.008	0.025±0.010		0.005±0.003	0.006±0.002	
Diagonal band nucleus	0.009±0.004	0.004±0.002		0.012±0.003	0.009±0.003	
Pallidium	0.010±0.003	0.011±0.005		0.006±0.002	0.009±0.002	
Claustrum	0.0005±0.0003	0±0		0.0022±0.0022	0.0003±0.0003	

Acutely (7d) following the lesion we observed a general reduction in connectivity within the contralesional somatosensory area, motor area ($p = 0.0419$), retrosplenial area ($p = 0.0405$), the auditory cortex ($p = 0.0021$) and temporal association area ($p = 0.0503$), in particular (all two-tailed t-test, Fig. 5f). Additional contralesional areas, albeit whose connectivity ratio was lower initially showed no significant change (anterior cingulate area, visual and perirhinal cortices). All areas located in the ipsilesional cortex fully dropped in connectivity, as expected, as this is the site of the brain injury. At chronic time points, 42d post TBI, these ispilesional areas remained low in connectivity. Remarkably, during the chronic phase following TBI, we observed a pronounced recovery of the connectivity in the contralesional hemisphere with a normalization of input from the

Fig. 5 Circuit connectivity is adaptive following traumatic brain injury. a Scheme of trans-synaptic circuit tracing, clearing and experimental timelines for acute and chronic connectivity. **b** Schematic of brain clearing and light-sheet fluorescence microscopy. **c** Serial light-sheet fluorescence microscopy images of cleared brain demonstrating the location of presynapstic neurons in control (green) and injured (red) mice. Scale bar: 5 mm. **d** Representative images of Rabies labeling in the cortex (red: presynaptic cells). Scale bar: 1 mm. **e** Confocal images of starter cells and presynaptic cells in the cortex (green: neurons infected with TVA-GFP; red: neurons infected with rabies-mcherry and yellow: starter neurons). Scale bar: 100 µm. **f** Scheme of the connectivity between the somatosensory cortex and contralesional cortical (upper) and subcortical (lower) areas and tables of contralesional and ipsilesional connectivity ratios (mean ± SEM) in controls 7d, controls 42d, and TBI 7d and TBI 42d. The connectivity ratios are color-coded and significance from matching controls is reported. All data were analyzed with two-tailed *t*-test. Auditory: $p = 0.0021$ Ctrl 7d vs TBI 7d; Motor: $p = 0.0419$ Ctrl 7d vs TBI 7d; Retrosplenial: $p = 0.0405$ Ctrl 7d vs TBI7d; Temporal association: $p = 0.0503$ Ctrl 7d vs TBI 7d; Ipsilateral somatosensory: $p = 0.0047$ Ctrl 7d vs TBI 7d; $p = 0.0024$ Ctrl 42d vs TBI 42d; Ipsilateral Retrosplenial: $p = 0.02$ Ctrl 7d vs TBI 7d; $p < 0.0001$ Ctrl 42d vs TBI 42d; Ipsilateral Motor: $p = 0.0008$ Ctrl 7d vs TBI 7d; $p = 0.0019$ Ctrl 42d vs TBI 42d; Ipsilateral Auditory: $p = 0.0492$ Ctrl 7d vs TBI 7d; $p = 0.0152$ Ctrl 42d vs TBI 42d; Ispilateral Posterior Perietal association:$p = 0.0294$ Ctrl 42d vs TBI 42d. $n = 6$–12 regions of interest from 6 to 8 independent animals per group. Source data are provided as a Source Data file.

motor, auditory, retrosplenial and temporal association areas (all two-tailed *t*-test, Fig. 5f) when injured animals at 42d were compared to their matching controls. Subcortical areas, which had originally low connectivity ratios with the examined contralesional somatosensory cortex, demonstrated relatively minor changes both acutely and chronically following TBI (Fig. 5f). Our in situ analysis therefore underscores that callosal neurons restore their pre-synaptic connectivity largely by strengthening ipsilateral connections from pre-connected areas and is therefore largely homeostatic in nature, thereby restoring hitherto lost connections.

TBI causes a widespread, transient reduction in neuronal activity in the contralesional cortex. As we have shown that TBI causes dendritic remodeling of callosal neurons that include the loss of excitatory inputs early after lesion, we then asked whether these changes might also translate into alterations of neuronal function. To address this question, we longitudinally assessed neuronal activity in vivo using two-photon calcium imaging using the genetically encoded calcium indicator GCaMP6m in callosal and non-callosal neurons in the contralesional cortex (Fig. 6a, b). Callosal neurons were retrogradely labelled by the injection of retroAAV-tdTomato into the lesion area prior to brain trauma (Fig. 6a). At the level of the proportion of active cells a clear decrease was detected 10 days after the injury for both neuronal populations (Fig. 6c, baseline (B) vs 10d: callosal neurons $p = 0.029$; non-callosal neurons $p = 0.015$, two-tailed *t*-test). The fraction of active cells normalized after 42d both in callosal as well as in non-callosal neurons (Fig. 6c, 10d vs 42d: callosal neurons $p = 0.027$, non-callosal $p = 0.047$, two-tailed *t*-test) and were not significantly different from the baseline recording anymore. When we followed the same neurons over time we found that TBI also caused a pronounced reduction of neuronal activity in both callosal and non-callosal neurons 10 days after injury (Fig. 6d, baseline vs 10d: callosal neurons $p = 0.013$, non-callosal neurons $p < 10^{-10}$, KS test). After 42 days we observed a recovery in activity levels primarily in non-callosal neurons (10d vs 42d: callosal neurons $p = 0.23$, non-callosal neurons $p = 0.012$, KS test). The activity levels, however, were still reduced compared to the baseline recordings in non-callosal ($p < 10^{-4}$, KS test). More specifically, the activity of cells active at baseline was strongly reduced 42 days after injury for both non-callosal and callosal neurons (Fig. 6e, callosal neurons $p < 10^{-5}$, non-callosal neurons $p < 10^{-12}$, two-tailed *t*-test). The initial activity levels were also determining the likelihood of remaining active until at least 42 days after the injury. Neurons with a baseline activity level of ≥1 transient per minute ('high') were significantly more likely to remain active as opposed to neurons with a lower activity level (<1 transient/min, 'low') (Fig. 6f, callosal neurons $p < 0.05$, non-callosal neurons $p < 0.05$, nonparametric bootstrapping). We further investigated the fate of neurons initially active at baseline. This investigation revealed that a larger fraction of callosal compared to non-callosal neurons went silent at 10d after TBI ($p < 0.05$, nonparametric bootstrapping), while the fraction of persistently active neurons or neurons that regained activity after 42d, or those turning silent only at d42 did not differ between the two populations (Fig. 6g). When investigating the history of cells active at day 42, we found that a large majority of these cells only became active after TBI ('newly active') both in callosal as well as in non-callosal neurons (Fig. 6h). Only ~20% of cells active at day 42 were persistently active cells, while 24 and 29%, in callosal and non-callosal neurons regained activity after turning silent at day 10 (p = ns; Fig. 6h).

Discussion

The adaptation of contralesional cortex following brain injury is an important paradigm that has been studied to understand how the adult brain responds to damage. However, if and how such adaptive responses contribute to functional recovery is not entirely resolved[26,28] and the specific neuronal populations and circuits that underlie these responses have not been identified. In this study, we used a combination of techniques ranging from retrograde viral labeling, in vivo timelapse two-photon imaging of spine turnover, trans-synaptic circuit tracing, tissue clearing and in vivo calcium imaging to reveal the specific adaptation of contralesional cortical callosal neurons directly connected to the injury site following TBI (Table 1). We find, using two-photon longitudinal imaging over 18 days that there is a strong early decrease in spine density over at least 2 weeks with signs of recovery thereafter. The plasticity of contralesional areas following brain injury has been established previously thanks to observations in patients[44–46] and in animal models[47–51]. In particular changes in neurotransmitters[52], dendritic growth and synapse formation have been described[53,54]. Reports also point out changes in neuronal activity in the contralesional cortex that are correlated with functional impairments in the acute and subacute phases following injury[10,18,55–57]. In our study, we find, among others, that callosal neurons, which homotopically connect both cortical hemispheres, show a unique vulnerability and adaptation following TBI with a homeostatic reintegration into existing circuits. Recent clinical observations reported a specific vulnerability of remote brain regions directly connected to ischemic brain lesion[16,58]. Likewise, recent experimental work indicates a specific and profound plasticity of callosal input following peripheral injury that underlies cortical takeover[17]. In line with this view, our study now reveals the selective adaptation of callosal neurons and their input circuits after a contralateral brain injury. Interestingly, clinical observations following visual cortical damage that leads to blindness also point toward a similar compensatory mechanism in which areas in the visual cortex of

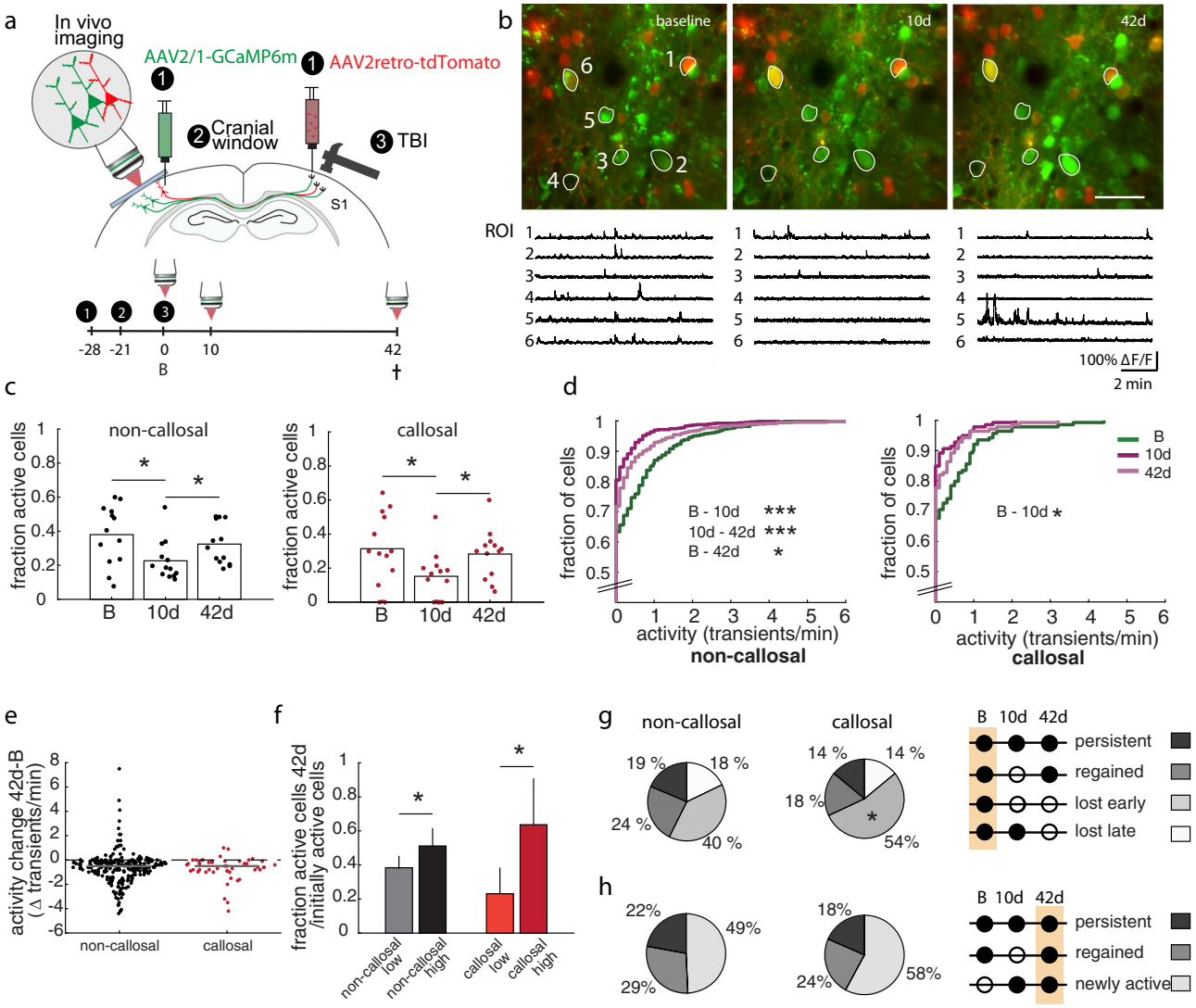

Fig. 6 Contralesional neurons display dynamic alterations of spontaneous activity levels following traumatic brain injury. a Scheme of functional in vivo imaging experiments investigating contralesional neurons using AAV-GCaMP6m. **b** Average projection of a representative field of view (FOV) showing neurons transduced with AAV-GCaMP6m in the contralesional hemisphere (green) and retrogradely transduced with retroAAV-CAG-tdtomato (red) at different time points following traumatic brain injury (B – baseline). Bottom: Calcium traces of example neurons marked within the FOV images. Scale bar equals 50 µm. **c** Fraction of active cells at baseline and two different time points following traumatic brain injury for callosal and non-callosal cells. $n = 13$ independent fields of views (663 non callosal and 139 callosal neurons) from six mice. Baseline (B) vs 10d: callosal neurons $p = 0.029$; non-callosal neurons $p = 0.015$, two-tailed t-test. 10d vs 42d: callosal neurons $p = 0.027$, non-callosal $p = 0.047$, two-tailed t-test. **d** Cumulative distributions of calcium transient frequencies at the indicated time points following traumatic brain injury. Note a shift in the distribution toward lower frequencies at 10d following lesion and a slight recovery at 42d. Baseline vs 10d: callosal neurons $p = 0.013$, non-callosal neurons $p < 10\text{–}10$, KS test). 10d vs 42d: callosal neurons $p = 0.23$, non-callosal neurons $p = 0.012$, KS test. Baseline vs 42d non-callosal $p < 10\text{-}4$, KS test. **e** Activity change between baseline and 42d in initially active non-callosal and callosal neurons. **f** Fraction of active cells at 42d dependent on the initial activity levels at baseline in non-callosal and callosal neurons (≥1 transient/min: 'high', <1 transient/min: 'low'). Note that the initial activity levels determines the likelihood of remaining active at 42 days after the injury. Data analyzed with non-parametric bootstrapping of 10,000 iterations. Error bars represent the 95% confidence interval (CI). **g** Fate of non-callosal and callosal neurons active at baseline. **h** Activity history of non-callosal and callosal neurons active at 42d., $^{*}p < 0.05$, $^{**}p < 0.01$, $^{***}p < 0.001$. Source data are provided as a Source Data file.

the contralesional hemisphere are recruited to compensate for altered visual function[59]. One aspect of the adaptation of callosal neurons is that the spines that are lost early after the TBI lesion are replaced over time with newly formed spines that on average persist longer than the spines that are formed over the same time period in non-callosal neurons. This underlines the functional significance of callosal input circuitry plasticity. Such a re-establishment of stable spines has previously been described in response to sensory deprivation in mice[60] and might be an attempt to re-establish a response to spared inputs or to recruit new inputs. Notably the spine morphology of callosal neurons evolves in line with the changes of spine density with more immature spines appearing at acute time points after injury and more mature and stable spine morphologies emerging later on. This is interesting as it suggests a biphasic plastic and adaptive response of callosal spines after injury. It therefore demonstrates that connected neurons in the contralesional cortex are uniquely affected by and respond to the injury in specific ways. This is in line with recent results showing a specific adaptation of callosal connections to peripheral injury[17]. It is important to note, in

Table. 1 Summary table of the changes and adaptations of callosal neurons following contralateral traumatic brain injury.

Manipulation	Acute time points	Later time points	Figure panel
Sensorimotor function	Decreased	Normalized	1b
Spine density in the contralesional cortex	Decreased	_	1e
Spine density of callosal neurons	Decreased	Normalized	2c & d
Spine density of non callosal neurons	Not changed	Not changed	2e & f
Excitatory input onto callosal neurons	Decreased	_	2g & h
Inhibitory input onto callosal neurons	No changed	_	2g& h
Spine morphology of callosal neurons	Altered	Normalized	3b & c
Spine morphology of non callosal neurons	Not changed	Not changed	3d & e
Persistence of new spines on callosal neurons	_	Higher in callosal neurons compared to control neurons	4g
Connectivity ratios of callosal neurons	Decreased	Normalized	5
Activity patterns callosal neurons	Decreased	Normalized	6c
Activity patterns non callosal neurons	Decreased	Normalized	6c

addition, that the changes triggered in the contralesional hemisphere can depend on the lesion extent as previous studies have shown that the balance between adaptive and mal-adaptive responses are affected by the size of the initial brain injury. It is therefore quite possible that the structural and functional alterations of callosal neurons that we observe here as well as their contribution to recovery can be affected by the type and size of the brain injury and could well be different in case of smaller or bigger lesion sizes[26,27,61] or for lesions induced in the developing or aged CNS[58]. As the TBI destroys axonal projections of the contralesional callosal neurons, we reasoned that plasticity at the level of those axons could also occur as a response to the injury and therefore investigated this possibility. It is known that during development callosal neurons extend profuse axonal projections till about post-natal day 8, and these connections are then refined[62,63] in an activity-dependent process till p21 to obtain the adult pattern of cross-hemispheric homotopy[64]. Here we have found no additional branching of callosal axons neither at acute nor at chronic time points following TBI indicating that the plastic processes could be restricted to the dendritic remodelings in the contralesional hemisphere.

As callosal neurons are uniquely affected by and responsive to TBI, we wondered whether and how their input circuitry would re-arrange at acute and chronic time points following injury. To answer this question we made use of the rabies virus, which monosynaptically labels pre-synaptic neurons that project to callosal neurons. We took a two-step approach: we first identified the brain regions connected to contralesional callosal neurons using tissue clearing and large scale imaging. Next we then determined the connectivity ratios before and after brain injury of the connected areas identified in tissue clearing analysis. Not surprisingly, we find that the main input to the somatosensory cortex is provided by cortical areas and in particular the somatosensory cortex, the motor cortex and the auditory cortex. This is in agreement with previous studies[43,65]. We further observed remarkably little pre-synaptic input at 42d to ectopic cortical or subcortical regions, as most brain regions connected before the injury were also found to provide input at 42d. This is important as restored connectivity to somatomotory areas such as the primary or secondary somatosensory cortex and primary motor cortex might underlie favorable rather than mal-adaptive adaptations[17]. Finally, we sought out to understand the state of activity of those callosal neurons and performed functional imaging experiments using genetically encoded calcium sensors. Functional imaging revealed that the fraction of active callosal neurons initially decreased but recovered over time. This initial decrease in neuronal activity in callosal neurons is in line with the synaptic structural changes seen in those neurons early following the injury. Indeed, we demonstrate that concomitantly to the decrease in activity, callosal neurons also demonstrate a specific loss of excitatory input onto their dendrite. This structural loss of excitatory input is consistent with the functional decrease in neuronal activity also observed in other paradigms[66,67]. In addition, while the callosal neurons active at baseline mostly fail to maintain and regain activity, a large part of the activity seen at 42d is due to newly active cells. This probably reflects activity-dependent functional refinements as circuit plasticity is correlated with increased spine dynamics[43,68], which we observe during this period. In line with this, monosynaptic tracing revealed that input in discrete regions increases from 7 to 42 dpi also, supporting the notion of ongoing synapse refinement. Our functional imaging data also show that callosal neurons did not behave fundamentally differently from non-callosal neurons. Why callosal and non-callosal neurons behave similarly can probably be explained by intracortical communication, as non-callosal neurons receive input from callosal neurons and vice versa.

Taken together, our study reveals important structural and functional principles of remodeling following TBI: it identifies a specific neuronal population (callosal neurons) that are particularly responsive to contralateral lesions and are thus prime targets for therapeutic interventions. Considering the importance of cortical remodeling processes for the functional recovery not only after traumatic but also after ischemic nervous system injuries, this has important implications for many common neurological conditions.

Methods

All experiments were approved by the Regierung von Oberbayern under the protocol number AZ:55.2.1.54-2532.135-15.

Animals. GFP-M mice (24 mixed gender randomized equally per group) and 78 female C57Bl6J mice, 8–12 weeks-old, were used for this study. All animals were housed under controlled standard housing conditions (dark/light cycle of 12 h, temperature 22 ± 2 degrees and humidity of 55 ± 10%) with food and water ad libitum.

Controlled cortical impact (CCI). Mice were anaesthetized via an intraperitoneal (i.p.) injection of MMF (Medetomidin 0.5 mg/kg, Orion Pharma; Midazolam 5.0 mg/kg, Ratiopharm; Fentanyl 0.05 mg/kg, B.Braun). When pedal reflex disappeared, animals were fixed on the stereotactic frame (Precision Systems & Instrumentation, LLC). The skin was incised and a square craniotomy (4 mm × 4 mm), positioned between Lambda, Bregma, the sagittal suture and the side of the skull was made. The injury to the brain was induced using a TBI-0310 impactor (Precision Systems & Instrumentation, LLC), in the area of the somatosensory cortex (flat-edged rod of 3 mm diameter, velocity of 6 m/s, a dwell time of 150 m/s and a depth of 0.3–0.5 mm). The removed bone piece was re-positioned to its previous location and glued to the skull with Vetbond (3 M™ Vetbond™, 3 M United States). The skin was sutured. The mean apnea duration and righting reflex

duration (time for a mouse to flip onto its feet from a supine position after the injury) were recorded in order to evaluate the severity of the injury.

Evaluation of sensorimotor function. *Ladder rung test*: For assessment of fine paw placement, the ladder rung test was used[69]. In this test, the animals had to cross a 1 m horizontal grid ladder and mistakes were counted by an investigator blinded to time points based on video recordings frame-by-frame of three consecutive crossings. We evaluated the animal's ability for fine coordinated paw placements using irregular spacing of the rungs (irregular walk task). Only consecutive steps of the hindlimbs were analyzed. Therefore, the last step before or after any interruptions were not scored. Placements were considered as a mistake when mice either totally missed a rung or if they slipped from a rung (deep or slight slip). Placements were considered as correct when the mice correctly placed all the foot or only a portion of the foot on the rungs. Then the number of slips over a standard distance was calculated quantitatively.

Evaluation of neuronal density, soma size, spine density, spine morphology and synaptic input onto callosal dendrites in fixed tissue

Tracer injections. For experiments on fixed tissue imaged with the confocal microscope, we retrogradely labeled callosal projection neurons by stereotactically injecting 0.3 µl of FluoroGold; (1% in 0.1 M Cacodylate buffer, Fluorochrome LLC) in the ispilesional somatosensory cortex (coordinates from Bregma: rostrocaudal −1.5 mm, lateral 1.7 mm, depth 0.3 mm and timeline is depicted in Fig. 2). In short, a glass capillary micropipette tip was slowly inserted into the brain through a small hole drilled in the skull. In order to avoid backflow, the pipette remained in the brain for a minimum of three minutes after injection completion[70]. To retrogradely label corticospinal (CST) projection neurons, laminectomy was performed at thoracic level 8 of the spinal cord and 0.5 µl of FluoroGold were stereotactically injected with a glass capillary into the right side of the spinal cord, 2 mm lateral from spinal midline at a depth 0.3 mm. The micropipette remained in place for at least 3 min after completing the injection to minimize backflow. Subsequently, the muscles and skin were sutured and saline was administered subcutaneously. For the experiment aiming at observing the changes in synaptic input onto callosal dendrites, we injected the somatosensory cortex with 0.5 µl a retrograde AAV expressing tdTomato (Retro-AAV-tdTomato, Addgene #59462) at the following coordinates from Bregma (rostrocaudal −1.5/lateral 1.7/deepth 0.3 mm).

Tissue preparation for spine imaging. Mice were sacrificed at 7, 14, and 42 days post-injury or at 12 days after injection (control non-injured group) and perfused with 4% paraformaldehyde (PFA) in 0.1 M PBS. Brains were kept in 4% PFA for 24 h, dissected, immersed in 3% low-melting-point agarose and cut with a Leica VT 1000 s vibratome. Coronal sections (100 µm) were cut and washed three times with 1× PBS for 10 min before free-floating staining with NeuroTrace 435 (Thermo Fischer Scientific; 1:500 in 0.1% Triton PBS) at 4 °C, overnight. The next day sections were washed three times in 1 × PBS for 10 min and mounted on gelatin subbed slides, using VectaShield (Vector Laboratories).

Tissue preparation for synaptic input onto callosal dendrite quantification. For thin paraffin sections, mouse brains were paraffine embedded and cut into 2 um thin sections. After deparaffination, antigen retrieval was performed using a Pascal Citrate buffer at pH6.0. To inactivate endogenous peroxidases, slides were incubated with Dako REAL peroxidase-blocking solution (Dako, K0672) and subsequently blocked with 10% FCS in PBS.

Immunohistochemistry. To quantify neuronal density and soma size, we stained free-floating (Jacobi et al., 2015). To do so, the sections were washed for 10 min in 1× PBS three times followed by 1 h incubation in blocking buffer (1× PBS with 0,5% Triton and 10% goat serum) at room temperature. Brain sections were then incubated overnight at 4 °C in the primary antibody solution: 1× PBS containing 0.1% Triton, 1% goat serum and mouse anti-NeuN Ab (1 : 500; Thermo Fischer Scientific). The next day the tissue was washed three times for 10 min in 1× PBS 0.1% Triton before the application of the secondary antibody solution goat anti-mouse AlexaFluor® 594 Ab (1:500; Invitrogen) in 1× PBS −0.1% Triton, 1% goat serum. After overnight incubation at 4 °C the tissue was again washed three times for 10 min in 1× PBS, mounted on gelatin coated glass slides in VectaShield (Vector Labs). To quantify synaptic input onto callosal dendrites in thin paraffin-sections (2 µm thin) we first stained retrogradely-labeled callosal neurons with rabbit anti-RFP antibody (1:400; abcam, ab124754) diluted in Dako REAL antibody diluent (Dako, S2022) at 4 °C o/n. To visualize the specific signal, anti-rabbit HRP (Dako,K4003) together with Opal-570 (1:600; Akoya, FP1488001KT) was used as secondary antibody and amplification system. After washing, slides were incubated with goat-anti-mouse IgG Fab-fragments (1:100; Jackson ImmunoResearch, 115-007-003) and goat serum to avoid subsequent unspecific binding. To perform the synaptic staining the sections were incubated with mouse IgG2b anti-Gephyrin antibody (1:200; Santa Cruz, sc-25311) and mouse IgG1 anti-GAD65/67 antibody (1:100; Santa Cruz, sc-365180) or chicken anti-Homer1 antibody (1:500; Synaptic System, 1600006) and mouse IgG1 anti- BNPI antibody (1:100; Santa Cruz, sc-377425), respectively. Conjugated secondary antibodies corresponding to the species and isotype of the primary antibody-pairs were used to visualize specific staining. Nuclei were stained with DAPI (Invitrogen, D1306). Slides were mounted with Fluoromount aqueous mounting medium (Sigma-Aldrich, F4680).

Image acquisition and image processing. Callosal neurons were identified as GFP and Fluorogold positive, while GFP-positive but Fluorogold-negative neurons located in the same area than callosal neurons were considered non-callosal. CST-neurons were identified as double positive neurons for Fluorogold and GFP.

Cortical thickness, cell density and cell size. To measure the cortical thickness, cell density and soma size in the contralesional cortex, confocal stacks of 10 µm were taken (four sections per animals) with a step size of 1 µm using the FV1000 Olympus microscope (10× objective NA 0.4, zoom of 1.0 and resolution of 1024 × 1024). Fluorogold labeling was imaged using the 405 nm laser (with emission wavelength set at 610 nm), GFP with 488 nm laser and NeuN with 543 nm laser, in sequential scans.

Spine density and morphology. To measure spine density and morphology we relied on the intense and sparse labeling of GFP-M mice (essentially layer V neurons and fewer layer II/III neurons). In order to quantify the spine density/morphology of individual dendrites, we acquired z-stacks using the FV1000 Olympus microscope (60x oil objective NA 1.35, zoom of 3.5 and resolution of 800 × 800). We imaged three areas for each individual layer V neuronal dendrites and two areas for layer II/III neuronal dendrites (average length of 60 µm): proximal dendrite (at a distance of ~70–150 µm from soma), distal dendrite (at a distance of ~370–450 µm from soma, only for layer V neurons) and apical tuft (at a distance up to 75 µm below the S1 cortical surface). The images underwent deconvolution using the Huygens Essential software (16.05 Scientific Volume Imaging, NL) and Z projections of the deconvolved stacks were obtained using Neuron Studio.

Data analysis. All analysis were performed by an investigator blinded to the injury status and injury time points.

Cortical thickness. To calculate cortical thickness the distance between the bottom of Layer VI and top of Layer I, using the straight line tool in Fiji was made at three different coordinates in the medio-lateral direction (1 mm, 1.5 mm and 2 mm from midline). An average of those three measurements was then made.

Cell density and cell size. Images were processed and analyzed using the Definiens Developer XD™ software from Definiens, Version 2.7.0 which allowed a precise cell count. The cell counts were then divided by the area to obtain the cell density results.

Spine density and morphology analysis. Each deconvoluted stack containing one proximal, distal or apical tuft dendritic segment was opened in Neuronstudio (version 0.9.92) (Fig. 2.b) and the dendritic trunk was semi-automatically traced resulting in a series of green vertices superimposed on volume-rendered data. Thereafter, dendritic spines were detected and classified. This automatic quantification was manually controlled to remove falsely detected spines, add falsely undetected or reclassify misclassified spines. The resulting numbers of spines were divided by the length of the dendritic segment as calculated by the program.

Analysis of synaptic input onto callosal dendrites. Immunofluorescence staining was performed to visualize excitatory or inhibitory synaptic pairs together with RFP positive neuronal structures. Images were acquired on a Leica Malpighi TCS SP8 confocal microscope (63× oil objective, zoom of 3.5 and resolution of 1024 × 1024, z-stack of 0.3 µm). Quantification was carried as follows: the perimeter of the dendrites was outlined and measured. Then the number of excitatory or inhibitory synaptic pairs (in which both the pre-synaptic and post-synaptic markers co-localize) that co-localize with the outlined dendritic segments were counted. The density of synaptic pairs along the dendritic segments was then calculated.

Lesion volume. To characterize the lesion volume, we cut 50 µm coronal brain sections beginning from the first visibly "damaged" section to the last. Lesion volume was calculated according to Yu et al[71]. by outlying in 15–17 consecutive sections the area of the lesion 42 days following the TBI.

In vivo 2 photon imaging of spine density in the contralesional cortex

Chronic cranial window implantation. Before in vivo two-photon imaging, all animals were implanted with a chronic cranial window (CW), following a slightly modified protocol by Holtmaat et al. (2009)[72]. Mice were anaesthetized and fixed into a stereotactic frame. The skin above half of the skull was permanently removed with scissors. The remaining skin, surrounding the exposed skull was glued to the sides of the skull with Vetbond (3 M™ Vetbond™ tissue adhesive, 3 M United States). The CW (a circle of 4 mm of diameter) was positioned onto the somatosensory cortex between both coronal sutures and lambda and bregma, respectively. Then the bone was thinned until it was possible to remove the bone flap from the skull with forceps leaving the sagittal suture intact. A 4 mm diameter glass coverslip was

then positioned on top of the exposed and then glued and fixed onto to remaining skull, by applying another cyanoacrylate tissue adhesive (Histoacryl®, B.Braun) on the edges of the glass. Dental cement was then placed on the remaining skull, as well as at the edges of the glass coverslip, thereby securing the coverslip further. After the surgery, a resting period of at least 2–3 weeks before starting the imaging procedure was respected to minimize inflammation.

Two-photon microscopy. All animals were imaged using a two-photon microscope (Olympus FV1000 MPE), equipped with a Mai Tai DeepSee femto-second pulsed Ti:Sapphire laser (SpectraPhysics). In more detail, the apical dendritic tufts of GFP-labelled neurons of the somatosensory cortex were imaged. Before every imaging session animals were anaesthetized with an i.p. injection of MMF. Mice were placed under the two-photon microscope objective (Olympus XLPlan N 25X W MP). To visualize GFP-fluorescence, a green/red Olympus filter cube (FV10-MRVGR/XR; BA595-540, BA575) was used. The mice were imaged at a wavelength of 940 nm. A low-resolution overview stack was taken over regions of interest (resolution: 640 × 640 pixels; Zoom: 1; step 3 or 5 µm). This overview stack was later used to find back the same ROIs and dendrites each subsequent imaging session. In addition, the unique vascular arrangement, visible in superficial layers of the brain through the fluorescence lamp of the microscope, helped locate the same dendrites each following imaging period. For a detailed stack of individual dendrites and their spines, which were later used for spine analysis, a higher resolution image was acquired (resolution: 2048 × 2048 pixels; Zoom: 2; step 1 µm). In general, at least two detailed images with a varying number of analyzable dendrites (ranging from 3 to 20) were imaged per animal. Particular care was taken to keep a similar fluorescence intensity and laser power for each ROI, but also in between animals. Image acquisition was performed for baseline measurements and every 3 days after the induction of TBI. In total 2 baselines were acquired, baseline 1 (B1) and baseline 2 (B2), with 3 days in between each other. We imaged and followed 81 dendritic stretches from 4 animals (Fig. 1d) and a total of 10,191 spines throughout the experiment. The average length of the dendritic stretches quantified was 63.31 ± 1.54 µm.

Analysis of in vivo spine dynamics and counting criteria. Image analysis was performed only on the high resolution stacks with Fiji (ImageJ) software. Images were median filtered ("Despeckle"), and suitable dendrites for counting were determined. The length of each dendrite was traced and measured with Fiji at baseline. Dendritic spines were counted using the Fiji Cell Counter Plugin at each time point, by going through stacks manually and looking at each plane. In short, only structures clearly protruding laterally from the dendritic shaft, with a minimum protrusion length of 0.4 µm, were defined and counted as spines[72]. Structures, however, that fulfilled these criteria but coincided with another crossing dendrite and could not be distinctly attributed to the chosen dendrite were not included in the analysis. The total spine number, number of eliminated and formed spines, as well as the stable number of spines were determined. A spine was defined as eliminated, if it was not visible anymore in the next time point or as formed, if a new structure appeared, at the same location or where no spine had been counted before. Spines that were visible in successive time points at the same location were considered as stable. In addition, an elimination and formation rate was calculated by dividing the number of eliminated or formed spines at one time point by the number of total spines in the previous time point and multiplied by 100 (thus, rates were expressed as percentages). Spine density in turn was calculated relative to the length of the dendrite (number of spines/µm).

In vivo 2 photon imaging of newly formed spine persistence index. Imaging of the specific cell population of callosal and non callosal CST neurons (Fig.3) was carried out as described above. For detecting callosal neurons, we first injected the somatosensory cortex (coordinates from Bregma: rostrocaudal −1.5 mm, lateral 1.7 mm, depth 0.3 mm) with 0.5 µl of a retrograde AAV expressing GFP (Retro-AAV-GFP #37825 Addgene; Fig. 3a) and then implanted a CW 4 days later. To image non-callosal (control) neurons, we injected the dorsal column of cervical spinal cord with 0.5 µl of the same RetroAAV-GFP (Fig. 3d) and implanted the CW on the same day. Two to 3 weeks between the CW implantation and the first imaging session was given for all imaging groups in order to minimize possible inflammation. As with GFP-M animals 2 baseline measurements were done each 3 days apart before injury induction with CCI. Thereafter animals were imaged every 3 days and up to 42 days after TBI. Using this approach we could follow 23 apical dendrite stretches (8724 spines followed at each time points) for callosal neurons and 13 apical dendrite stretches (4376 spines followed at each time points) for CST neurons for dendritic lengths comprised between 62 and 88 µm

Quantification of the persistence index. To assess the stability of spines we determine the persistence index for both pre-existing spines (already present at the two baselines) and those that were newly formed after injury. Thus for pre-existing spines, single spines on dendrite stretches were followed at each imaging time-point and attributed to a binary code of either "1" when present or "0" when eliminated at every time-point individually. Then, the sum of binary code was divided by the number of all imaging time-points. For spines that were not present at baseline, but were newly formed after injury, the same persistence index was calculated[73].

Neuronal connectivity

Viral tracing. For labeling and analysis of neuronal cell connectivity using clearing we used the mono-synaptic rabies virus tracing technique. For this purpose, callosal axons on the ipsilesional side of the injury were first selectively infected with 0.5 µl of AAV expressing the cre recombinase ("AAV-cre" [AAV1.hSyn.Cre.W-PRE.hGH], titer: 5.0 e13 vg/ml supplied by the Penn Vector Core; dilution 1:6 in 1× PBS; coordinates from Bregma: rostrocaudal −1.5 mm, lateral 1.7 mm, depth 0.3 mm). For the acute time point groups (7 dpi) 0.5 µl of the helper virus AAV-TVA-G-eGFP ([AAV1-synP-DIO-sTpEpB-eGFP]; titer: 3.9×10e12 GC/ml supplied by Gene Therapy Vector Core, University of North Carolina; dilution 1:4 in 1× PBS) was injected on the same day, using the same coordinates as for AAV-cre but on the contralesional hemisphere. In contrast, chronic time point groups (42 dpi) were injected with AAV-TVA-G-eGFP, in the same way as described above, only 35 days after AAV-cre injection. In a final step, pre-synaptic partners of callosal neurons were visualized by injecting 1 µl of a rabies virus (SAD-ΔG-mcherry (EnvA); titer: 3×10^8 ffu/ml; dilution 1:1 in 1× PBS; coordinates from Bregma: rostrocaudal −1.5 mm, lateral 1.7 mm, depth 0.3 mm; kindly provided by K.K. Conzelmann)[74]. Furthermore, for acute time points, TBI was induced on the same day as the rabies virus injection (2 weeks after the AAV-cre and AAV-TVA-G-eGFP injections), while animals in the chronic time point group were injured 2 weeks after AVV-cre- injection, 1 week before the AAV-TVA-G-eGFP and 35 days before the rabies virus injection. Control unlesioned animals were generated similarly, with one early and one late injection group.

Tissue clearing. Brains underwent staining and clearing using vDISCO protocol as described in Cai et al[42]. Briefly, after perfusing the animals with 1× PBS and 4% PFA, brains were collected and post-fixed for one night in 4% PFA and the next day were washed with 1 × PBS.

Then whole brains were placed in 5 mL tubes (Eppendorf, 0030 119.401) and incubated in a permeabilization solution containing 1.5 vol/vol% goat serum (Gibco, 16210072), 0.5 vol/vol% Triton X-100 (AppliChem, A4975,1000), 0.5 mM of methyl-β –cyclodextrin (Sigma, 332615), 0.2% wt/vol% trans-1-acetyl-4-hydroxy-l-proline (Sigma-Aldrich, 441562) and 0.05 wt/vol% sodium azide (Sigma, 71290) in 1× PBS for 1 day at 37 °C in dark with gentle shaking. Then samples were incubated in 4.5 mL of a solution containing 1.5 vol/vol% goat serum, 0.5 vol/vol% Triton X-100, and 0.05 wt/vol% sodium azide in 1× PBS + 4uL of anti-RFP nanobody conjugated with Atto647N (Chromotek, rba647n-100, lot 81106002SAT2) for 14 days at 37 °C in dark with gentle shaking to stain the cells expressing mcherry. After 14 days, samples were washed with the same solution containing 1.5 vol/vol% goat serum, 0.5 vol/vol% Triton X-100, and 0.05 wt/vol% sodium azide in 1× PBS for four times every hour and finally with 1×PBS four times every hour. Both washing procedures were carried at room temperature in the dark and with gentle shaking. Samples were next cleared by incubating them in the following serial solutions for 2–3 h each step: 50 vol% THF, 70 vol% THF, 80 vol% THF in distilled water, 100 vol% THF overnight and again 1 h in 100 vol% THF, followed by 2 h in dichloromethane and finally in BABB until samples turned completely transparent after 5–6 h. All the clearing steps were performed with gentle shaking, at room temperature and by protecting the samples from light.

Light-sheet microscopy imaging and whole brain analysis. Cleared brains were imaged as tiling scans (10% overlap) with the light-sheet microscope Ultramicroscope II (LaVision BioTec) using a x2 objective Olympus MVPLAPO2XC/0.5 NA (WD = 6 mm) coupled to an Olympus MVX10 zoom body that was kept at zoom magnification ×2.5 using the filter set ex 640/40 nm, em 690/50 nm. Stitching of tile scans was performed by using Fiji's (ImageJ, v.1.52 h, https://fiji.sc/) stitching plugin[75]. Stitched images were saved in tiff format. Fiji's TrakEM2 plugin and Imglib2 library were used to correct acquisition shifting[76]. Scans were pre-processed in Fiji software for background equalization via pseudo-flat-field correction function from Bio-Voxxel toolbox, for background removal (to remove particles bigger than cells) via median option from the same toolbox, for noise reduction via two-dimensional medial filter and for signal amplification via the unsharpen mask. Cells were visualized as heatmaps after Clearmap software analysis as described by Renier et al[77]. TBI and control heatmaps colored with two different colors were overlayed over the brain atlas provided by Clearmap and merged in Fiji and displayed as image sequence in Fig. 5b and in the Supplementary movie.

Tissue processing and immunohistochemistry. For circuit connectivity analysis, mice were transcardially perfused either 7 or 42 days after TBI, as described above. Control mice were sacrificed on the same day as TBI-mice. After the 24 h period of post-fixation in 4% PFA, brains were microdissected and kept in eppendorf receptacles with 30% sucrose until sinking to the bottom. They were sectioned coronally with a cryostat (Leica CM1850) at a thickness of 60 µm. Next, a GFP-amplification-protocol combined with a NeuroTrace (NT) staining was performed on free-floating sections. To this end, sections were first washed three times with 1×PBS à 10 min. In the final washing step, 1 × PBS was replaced by blocking buffer (1 × PBS with 0.5% Triton and 10% goat serum) and sections were incubated in it for 1 h at room temperature. After removing the blocking buffer, primary antibody solution (1× PBS containing 0.1% Triton, 1% goat serum and 1:500 chicken anti-GFP Ab (Abcam)) was added. Overnight incubation at 4 °C ensued. The following

day, sections were washed three times for 10 min with 1× PBS/0.1% Triton and later incubated with the secondary antibody solution (1× PBS −0.1% Triton, 1% goat serum and 1:500, Goat Anti-Chicken Alexa Fluor® 488 Ab (Abcam); 1:500 NT435 (Invitrogen)) overnight at 4 °C. After a last washing step, three times à 10 min with 1xPBS, sections were mounted on gelatine subbed slides with Vecta-Shield (Vector Laboratories) and finally coverslipped as described above.

Imaging of cleared tissue. Images of brain sections of 2 mm thickness were acquired on a light-sheet microscope (UM II LaVision BioTec-UltraMicroscope II), with a z-step size of 3 µm, using a 4× objective (0.28 NA, Olympus XLFLURO4x), with a lens provided with a 10 mm working distance dipping cap. Images were processed with Imaris (Bitplane1) in order to generate 3D-projections, while HeatMap Histograms were created using Fiji.

Imaging. Starter cells were evaluated as follows: A total of six sections per brain, beginning from the section with the first detectable starter cells to the section with the last detectable starter cells, were scanned using a Leica SP8 confocal microscope (magnification: ×20; Zoom 1; step; 1 µm; resolution: 512 ×512 pixels). Presynaptic cells were evaluated as follows: Here, 20 sections per brain were selected according to the Allen Mouse Brain Atlas from ~1.15 to ~2.85 mm relative to Bregma[78]. All sections were imaged consecutively with a Leica DM4 B microscope (Leica Microsystems), using the MBF Stereo Investigator 2017 software and a 2.5X objective when cells were sparse. In cases where cell labelling was too dense we used a 10X objective. All 2.5 and ×10 magnification images were stitched with the Fiji Pairwise Stitching Plugin. The 20X image stacks were further processed ImageJ (Fiji).

Quantifications. Starter cells were manually quantified using the Fiji Cell Counter Plugin in all imaged sections and interpolated to the total number of sections evaluated in the whole brain. For quantification, each imaged section was subdivided into different brain areas, as defined by the Allen Mouse Brain Atlas. In total we chose 20 different brain regions, ranging from cortical to subcortical regions as well as white matter tract structures. Within those, pre-synaptic cells (mCherry positive) were manually counted with the Fiji Cell Counter Plugin. For areas in which cell aggregation was too dense and manual counting was not accurate enough we employed Fiji's Particle Analyzer Plugin for automatic quantification, after image processing for background subtraction. We then made a ratio between the total number of pre-synaptic neurons in that specific area to the total number of starter cells in the whole brain. This ratio was termed connectivity ratio, as previously described[43]. We then compared the connectivity ratios of acute and chronic injured animals with their respective controls (acute and controls generated with the respective virus injections timelines as for injured animals).

Calcium imaging experiments

Viral injections and window implantation. For in vivo calcium imaging, callosal neurons were selectively traced and labelled using viral vectors. To do so we injected mice with a retrograde adeno-associated virus (retro AAV-CAG-Td -Tomatoe, Addgene, 59462-AAVrg; Titer≥7×10^{12} vg/mL; dilution 1:3 with 1× PBS) as described above. AAV1.hSyn-GCaMP6mWPRE.SV40 (Addgene 100838, Titer ≥10^{13}vg/mL) was injected in the contralesional site at the following coordinates (rostro-caudal to Bregma: −1.8; lateral to Bregma 2.0; 0.3 mm depth) and a CW (diameter 4 mm) was implanted above as described above.

Two-photon imaging in anesthetized mice. In vivo two-photon imaging was performed on a resonant scanning two-photon microscope (Hyperscope, Scientifica, equipped with an 8 kHz resonant scanner) and a 16× water-immersion objective (Nikon), yielding frame rates of 30 Hz at a resolution of 512 × 512 pixels. We recorded 18,000 frames (10 min) within cortical layer II/III (cortical depths of 140–310 µm), covering a field of view (FOV) of 230 × 230 μm^2. Light source was a Ti:Sapphire laser with a DeepSee pre-chirp unit (Spectra Physics MaiTai eHP). GCaMP6m and tdTomato were co-excited at 930 nm, with a laser power not exceeding 40 mW (typically 10–40 mW). During imaging, mice were anesthetized with 1.0–1.5% isoflurane in pure O_2 at a flow rate of ~0.5 l/min, to maintain a respiratory rate in the range of 110–140 breaths per minute. Body temperature was maintained at 37 degrees using a physiological monitoring system (Harvard Apparatus). In total 663 non-callosal and 139 callosal neurons were analyzed within 13 experiments in 6 mice.

Image processing and data analysis. All image analyses were performed using custom-written routines in Matlab (R2018b)[79]. In brief, full frame images were corrected for potential x and y brain displacement occurred during the in vivo recording period, and regions of interests (ROIs) were manually selected based on the maximum and mean projection of all frames. Those ROIs were readjusted, if necessary, over the different recorded frames following our time course. Fluorescence signals of all pixels within a selected ROI were averaged, the intensity traces were low pass filtered at 10 Hz. Contamination from neuropil signals was accounted for, as described using the following equation: FROI_comp = FROI − 0.7 × Fneuropil + 0.7 × median (Fneuropil)

F_{ROI_comp} stands for neuropil-compensated fluorescence of the ROI, F_{ROI} and $F_{neuropil}$ represent the initial fluorescence signal of the ROI and the signal from the neuropil, respectively. A neuron was defined as 'active' if it displayed at least one prominent calcium transient over 20 frames (corresponding to ~0.7 s).

Statistical analysis. All results are given as mean ± standard error of the mean (SEM), unless otherwise stated. Statistical analysis, as well as graphs illustrating data, was carried out with GraphPad Prism 7.01 for Windows (GraphPad Software). Ladder rung behavior data were analyzed with a Friedman test followed by post-hoc test. In vivo two-photon imaging data were analyzed using one-way and two-ways RM ANOVA followed by post-hoc test. In experiments without data of a "repeated-measures-type", we performed an ordinary one-way ANOVA and post-hoc test. In addition, two-tailed *t*-test were carried out for connectivity analysis and in vivo functional imaging experiments (unless otherwise stated). To compare cumulative distributions we used the Kolmogorov–Smirnov (KS) test. When data were unparametric we used Mann–Whitney test to compare two groups. Statistical significance levels are indicated as follows: $^{*}p < 0.05$; $^{**}p < 0.01$; $^{***}p < 0.001$.

Reporting summary. Further information on research design is available in the Nature Research Reporting Summary linked to this article.

Data availability

Source data are provided with this paper and have also been deposited in the Zenodo database under https://doi.org/10.5281/zenodo.6364730 including supplementary data. Raw data are available from the corresponding author upon reasonable request.

Received: 26 February 2021; Accepted: 11 April 2022;
Published online: 12 May 2022

References

1. Nudo, R. J. Mechanisms for recovery of motor function following cortical damage. *Curr. Opin. Neurobiol.* **16**, 638–644 (2006).
2. Nudo, R. J. Neural bases of recovery after brain injury. *J. Commun. Disord.* **44**, 515–520 (2011).
3. Benowitz, L. I. & Carmichael, S. T. Promoting axonal rewiring to improve outcome after stroke. *Neurobiol. Dis.* **37**, 259–266 (2010).
4. Murphy, T. H. & Corbett, D. Plasticity during stroke recovery: from synapse to behaviour. *Nat. Rev. Neurosci.* **10**, 861–872 (2009).
5. Stoeckel, M. C. & Binkofski, F. The role of ipsilateral primary motor cortex in movement control and recovery from brain damage. *Exp. Neurol.* **221**, 13–17 (2010).
6. Ueno, M., Hayano, Y., Nakagawa, H. & Yamashita, T. Intraspinal rewiring of the corticospinal tract requires target-derived brain-derived neurotrophic factor and compensates lost function after brain injury. *Brain* **135**, 1253–1267 (2012).
7. Rehme, A. K., Fink, G. R., Von Cramon, D. Y. & Grefkes, C. The role of the contralesional motor cortex for motor recovery in the early days after stroke assessed with longitudinal fMRI. *Cereb. Cortex* **21**, 756–768 (2011).
8. Biernaskie, J., Szymanska, A., Windle, V. & Corbett, D. Bi-hemispheric contribution to functional motor recovery of the affected forelimb following focal ischemic brain injury in rats. *Eur. J. Neurosci.* **21**, 989–999 (2005).
9. Johansen-Berg, H. et al. Correlation between motor improvements and altered fMRI activity after rehabilitative therapy. *Brain* **125**, 2731–2742 (2002).
10. Bestmann, S. et al. The role of contralesional dorsal premotor cortex after stroke as studied with concurrent TMS-fMRI. *J. Neurosci.* **30**, 11926–11937 (2010).
11. Calautti, C., Leroy, F., Guincestre, J. Y., Marié, R. M. & Baron, J. C. Sequential activation brain mapping after subcortical stroke: Changes in hemispheric balance and recovery. *Neuroreport* **12**, 3883–3886 (2001).
12. Carmichael, S. T. & Chesselet, M. F. Synchronous neuronal activity is a signal for axonal sprouting after cortical lesions in the adult. *J. Neurosci.* **22**, 6062–6070 (2002).
13. Feydy, A. et al. Longitudinal study of motor recovery after stroke: Recruitment and focusing of brain activation. *Stroke* **33**, 1610–1617 (2002).
14. Biernaskie, J., Chernenko, G. & Corbett, D. Efficacy of Rehabilitative Experience Declines with Time after Focal Ischemic Brain Injury. *J. Neurosci.* **24**, 1245–1254 (2004).
15. Cramer, S. C. & Crafton, K. R. Somatotopy and movement representation sites following cortical stroke. *Exp. Brain Res.* **168**, 25–32 (2006).
16. Duering, M. et al. Acute infarcts cause focal thinning in remote cortex via degeneration of connecting fiber tracts. *Neurology* **84**, 1685–1692 (2015).
17. Petrus, E., Dembling, S., Usdin, T., Isaac, J. T. R. & Koretsky, A. P. Circuit-specific plasticity of callosal inputs underlies cortical takeover. *J. Neurosci.* **40**, 7714–7723 (2020).

18. Lu, H. et al. Transcranial magnetic stimulation facilitates neurorehabilitation after pediatric traumatic brain injury. *Sci. Rep.* **5**, 14769 (2015).
19. Napieralski, J. A., Butler, A. K. & Chesselet, M. F. Anatomical and functional evidence for lesion-specific sprouting of corticostriatal input in the adult rat. *J. Comp. Neurol.* **373**, 484–497 (1996).
20. Lenzlinger, P. M. et al. Delayed inhibition of Nogo-A does not alter injury-induced axonal sprouting but enhances recovery of cognitive function following experimental traumatic brain injury in rats. *Neuroscience* **134**, 1047–1056 (2005).
21. Liu, Z., Zhang, R. L., Li, Y., Cui, Y. & Chopp, M. Remodeling of the corticospinal innervation and spontaneous behavioral recovery after ischemic stroke in adult mice. *Stroke* **40**, 2546–2551 (2009).
22. Zai, L. et al. Inosine alters gene expression and axonal projections in neurons contralateral to a cortical infarct and improves skilled use of the impaired limb. *J. Neurosci.* **29**, 8187–8197 (2009).
23. Omoto, S., Ueno, M., Mochio, S., Takai, T. & Yamashita, T. Genetic deletion of paired immunoglobulin-like receptor B does not promote axonal plasticity or functional recovery after traumatic brain injury. *J. Neurosci.* **30**, 13045–13052 (2010).
24. McPherson, J. G. et al. Progressive recruitment of contralesional cortico-reticulospinal pathways drives motor impairment post stroke. *J. Physiol.* **596**, 1211–1225 (2018).
25. Lotze, M. et al. The role of multiple contralesional motor areas for complex hand movements after internal capsular lesion. *J. Neurosci.* **26**, 6096–6102 (2006).
26. Jones, T. A. Motor compensation and its effects on neural reorganization after stroke. *Nat. Rev. Neurosci.* **18**, 267–280 (2017).
27. Bradnam, L. V., Stinear, C. M., Barber, P. A. & Byblow, W. D. Contralesional hemisphere control of the proximal paretic upper limb following stroke. *Cereb. Cortex* **22**, 2662–2671 (2012).
28. Dancause, N., Touvykine, B. & Mansoori, B. K. Inhibition of the contralesional hemisphere after stroke: reviewing a few of the building blocks with a focus on animal models. *Prog. Brain Res.* **218**, 361–387 (2015).
29. Marzi, C. A., Bisiacchi, P. & Nicoletti, R. Is interhemispheric transfer of visuomotor information asymmetric? Evidence from a meta-analysis. *Neuropsychologia* **29**, 1163–1177 (1991).
30. Berlucchi, G., Aglioti, S., Marzi, C. A. & Tassinari, G. Corpus callosum and simple visuomotor integration. *Neuropsychologia* **33**, 923–936 (1995).
31. Stark, D. E. et al. Regional variation in interhemispheric coordination of intrinsic hemodynamic fluctuations. *J. Neurosci.* **28**, 13754–13764 (2008).
32. Toga, A. W. & Thompson, P. M. Mapping brain asymmetry. *Nat. Rev. Neurosci.* **4**, 37–48 (2003).
33. Pernici, C. D. et al. Longitudinal optical imaging technique to visualize progressive axonal damage after brain injury in mice reveals responses to different minocycline treatments. *Sci. Rep.* **10**, 7815 (2020).
34. Rowe, R. K. et al. Aging with Traumatic Brain Injury: effects of Age at Injury on Behavioral Outcome following Diffuse Brain Injury in Rats. *Dev. Neurosci.* **38**, 195–205 (2016).
35. Harrison, J. L. et al. Resolvins AT-D1 and E1 differentially impact functional outcome, post-traumatic sleep, and microglial activation following diffuse brain injury in the mouse. *Brain. Behav. Immun.* **47**, 131–140 (2015).
36. Feng, G. et al. Imaging neuronal subsets in transgenic mice expressing multiple spectral variants of GFP. *Neuron* **28**, 41–51 (2000).
37. Chovsepian, A., Empl, L., Correa, D. & Bareyre, F. M. Heterotopic transcallosal projections are present throughout the mouse cortex. *Front. Cell. Neurosci.* **11**, 36 (2017).
38. Gipson, C. D. & Olive, M. F. Structural and functional plasticity of dendritic spines – root or result of behavior? *Genes Brain Behav.* **16**, 101–117 (2017).
39. Rochefort, N. L. & Konnerth, A. Dendritic spines: from structure to in vivo function. *EMBO Rep.* **13**, 699–708 (2012).
40. Osakada, F. & Callaway, E. M. Design and generation of recombinant rabies virus vectors. *Nat. Protoc.* **8**, 1583–1601 (2013).
41. Wickersham, I. R., Finke, S., Conzelmann, K. K. & Callaway, E. M. Retrograde neuronal tracing with a deletion-mutant rabies virus. *Nat. Methods* **4**, 47–49 (2007).
42. Cai, R. et al. Panoptic imaging of transparent mice reveals whole-body neuronal projections and skull–meninges connections. *Nat. Neurosci.* **22**, 317–327 (2019).
43. Falkner, S. et al. Transplanted embryonic neurons integrate into adult neocortical circuits. *Nature* **539**, 248–253 (2016).
44. Frackowiak, R. S., Weiller, C. & Chollet, F. The functional anatomy of recovery from brain injury. *Ciba Foundation Symposium* **163**, 235–44 (1991).
45. Floel, A., Hummel, F., Duque, J., Knecht, S. & Cohen, L. G. Influence of somatosensory input on interhemispheric interactions in patients with chronic stroke. *Neurorehabil. Neural Repair* **22**, 477–485 (2008).
46. Buetefisch, C. M. Role of the contralesional hemisphere in post-stroke recovery of upper extremity motor function. *Front. Neurol.* **6**, 214 (2015).
47. Jones, T. A. et al. Motor system plasticity in stroke models intrinsically use-dependent, unreliably useful. *Stroke* **44**, S104-6 (2013).
48. Dancause, N., Touvykine, B. & Mansoori, B. K. Inhibition of the contralesional hemisphere after stroke: reviewing a few of the building blocks with a focus on animal models. in *Progress in Brain Research* vol. **218** 361–387 (Elsevier B.V., 2015).
49. Touvykine, B. et al. The effect of lesion size on the organization of the ipsilesional and contralesional motor cortex. *Neurorehabil. Neural Repair* **30**, 280–292 (2016).
50. Axelson, H. W. et al. Plasticity of the contralateral motor cortex following focal traumatic brain injury in the rat. *Restor. Neurol. Neurosci.* **31**, 73–85 (2013).
51. Yang, Z. et al. Compensatory functional connectome changes in a rat model of traumatic brain injury. *Brain Commun.* **3**, fcab244 (2021).
52. Neumann-Haefelin, T. & Witte, O. W. Periinfarct and remote excitability changes after transient middle cerebral artery occlusion. *J. Cereb. Blood Flow. Metab.* **20**, 45–52 (2000).
53. Jones, T. A., Kleim, J. A. & Greenough, W. T. Synaptogenesis and dendritic growth in the cortex opposite unilateral sensorimotor cortex damage in adult rats: A quantitative electron microscopic examination. *Brain Res.* **733**, 142–148 (1996).
54. Hsu, J. E. & Jones, T. A. Time-sensitive enhancement of motor learning with the less-affected forelimb after unilateral sensorimotor cortex lesions in rats. *Eur. J. Neurosci.* **22**, 2069–2080 (2005).
55. Calautti, C., Leroy, F., Guincestre, J. Y. & Baron, J. C. Displacement of primary sensorimotor cortex activation after subcortical stroke: A longitudinal PET study with clinical correlation. *Neuroimage* **19**, 1650–1654 (2003).
56. Ward, N. S., Brown, M. M., Thompson, A. J. & Frackowiak, R. S. J. Neural correlates of outcome after stroke: A cross-sectional fMRI study. *Brain* **126**, 1430–1448 (2003).
57. Schaechter, J. D. & Perdue, K. L. Enhanced cortical activation in the contralesional hemisphere of chronic stroke patients in response to motor skill challenge. *Cereb. Cortex* **18**, 638–647 (2008).
58. Li, N. et al. Evidence for impaired plasticity after traumatic brain injury in the developing brain. *J. Neurotrauma* **31**, 395–403 (2014).
59. Celeghin, A. et al. Intact hemisphere and corpus callosum compensate for visuomotor functions after early visual cortex damage. *Proc. Natl Acad. Sci. U. S. A.* **114**, E10475–E10483 (2017).
60. Schubert, V., Lebrecht, D. & Holtmaat, A. Peripheral deafferentation-driven functional somatosensory map shifts are associated with local, not large-scale dendritic structural plasticity. *J. Neurosci.* **33**, 9474–87 (2013).
61. Morecraft, R. J. et al. Frontal and frontoparietal injury differentially affect the ipsilateral corticospinal projection from the nonlesioned hemisphere in monkey (Macaca mulatta). *J. Comp. Neurol.* **524**, 380–407 (2016).
62. Mitchell, B. D. & Macklis, J. D. Large-scale maintenance of dual projections by callosal and frontal cortical projection neurons in adult mice. *J. Comp. Neurol.* **482**, 17–32 (2005).
63. Innocenti, G. M. & Price, D. J. Exuberance in the development of cortical networks. *Nat. Rev. Neurosci.* **6**, 955–965 (2005).
64. Wang, C. L. et al. Activity-dependent development of callosal projections in the somatosensory cortex. *J. Neurosci.* **27**, 11334–11342 (2007).
65. Deshpande, A. et al. Retrograde monosynaptic tracing reveals the temporal evolution of inputs onto new neurons in the adult dentate gyrus and olfactory bulb. *Proc. Natl. Acad. Sci. U. S. A.* **110**, E1152-61 (2013).
66. Rose, T., Jaepel, J., Hübener, M. & Bonhoeffer, T. Cell-specific restoration of stimulus preference after monocular deprivation in the visual cortex. *Science* **352**, 1319–1322 (2016).
67. Jafari, M. et al. Phagocyte-mediated synapse removal in cortical neuroinflammation is promoted by local calcium accumulation. *Nat. Neurosci.* **24**, 355–367 (2021).
68. Keck, T. et al. Massive restructuring of neuronal circuits during functional reorganization of adult visual cortex. *Nat. Neurosci.* **11**, 1162–1167 (2008).
69. Metz, G. A. & Whishaw, I. Q. The ladder rung walking task: a scoring system and its practical application. *J. Vis. Exp.* (2009) https://doi.org/10.3791/1204.
70. Bradley, P. M. et al. Corticospinal circuit remodeling after central nervous system injury is dependent on neuronal activity. *J. Exp. Med.* **216**, 2503–2514 (2019).
71. Yu, F. et al. Posttrauma cotreatment with lithium and valproate: reduction of lesion volume, attenuation of blood-brain barrier disruption, and improvement in motor coordination in mice with traumatic brain injury. *J. Neurosurg.* **119**, 766–773 (2013).
72. Holtmaat, A. et al. Long-term, high-resolution imaging in the mouse neocortex through a chronic cranial window. *Nat. Protoc.* **4**, 1128–1144 (2009).
73. Liebscher, S. et al. Chronic γ-secretase inhibition reduces amyloid plaque-associated instability of pre- and postsynaptic structures. *Mol. Psychiatry* **19**, 937–946 (2014).

74. Granier, C. et al. Formation of somatosensory detour circuits mediates functional recovery following dorsal column injury. *Sci. Rep.* **10**, 10953 (2020).
75. Preibisch, S., Saalfeld, S. & Tomancak, P. Globally optimal stitching of tiled 3D microscopic image acquisitions. *Bioinformatics* **25**, 1463–1465 (2009).
76. Pietzsch, T., Preibisch, S., Tomančák, P. & Saalfeld, S. Img lib 2-generic image processing in Java. *Bioinformatics* **28**, 3009–3011 (2012).
77. Renier, N. et al. Mapping of Brain Activity by Automated Volume Analysis of Immediate Early Genes. *Cell* **165**, 1789–1802 (2016).
78. Paxinos and Franklin's the Mouse Brain in Stereotaxic Coordinates, Compact - 5th Edition. https://www.elsevier.com/books/paxinos-and-franklins-the-mouse-brain-in-stereotaxic-coordinates-compact/franklin/978-0-12-816159-3.
79. Liebscher, S., Keller, G. B., Goltstein, P. M., Bonhoeffer, T. & Hübener, M. Selective Persistence of Sensorimotor Mismatch Signals in Visual Cortex of Behaving Alzheimer's Disease Mice. *Curr. Biol.* **26**, 956–964 (2016).

Acknowledgements

We thank B. Fiedler and L. Schödel for excellent technical assistance as well as D.Matzek and B. Stahr for animal husbandry. F.M.B. is supported by the Deutsche Forschungsgemeinschaft (DFG, SFB 870 Project ID 118803580). F.M.B. is supported by the Wings for Life Foundation, the International Foundation for Research in Paraplegia (IRP) and the DFG, TRR274 (Project ID 408885537). F.M.B. and S.L. are supported by the Munich Center for Systems Neurology (DFG, SyNergy; EXC 2145/ID 390857198). S.L. is supported by the Emmy Noether program (DFG). V.V.S. is supported by the Humboldt foundation and J.F. is supported by the Wings for Life Foundation. The authors declare no competing financial interests. We thank the Core Facility Bioimaging at the Biomedical Center (BMC) for excellent imaging support.

Author contributions

F.M.B. designed the experiments. L.E., A.C., M.C., W.Y.V.K. contributed all surgical procedures. L.E., A.C., M.C., W.Y.V.K., S.W., V.V.S., J.F., M.M. collected and analyzed data. A.G., P.B., and K.K.C. contributed rabies viruses. R.C., A.G., A.E. contributed clearing experiments. M.C., W.I.V.K., and S.L. contributed calcium imaging and analysis. I.W., M.K., and D.M. analyzed cell density in the cortex and performed paraffin-embedded immunohistochemistry. L.E., A.C., S.L., and F.M.B. wrote the paper. All authors approved the final version of the paper.

Funding

Open Access funding enabled and organized by Projekt DEAL.

Competing interests

The authors declare no competing interests.

Additional information

Supplementary information The online version contains supplementary material available at https://doi.org/10.1038/s41467-022-29992-0.

Correspondence and requests for materials should be addressed to Florence M. Bareyre.

Peer review information *Nature Communications* thanks Ramesh Raghupathi and the other, anonymous, reviewer(s) for their contribution to the peer review of this work. Peer reviewer reports are available.

Reprints and permission information is available at http://www.nature.com/reprints

Publisher's note Springer Nature remains neutral with regard to jurisdictional claims in published maps and institutional affiliations.

Study 3

Repetition of brain concussions drives microglia-mediated engulfment of presynaptic excitatory input associated with cognitive and anxiety perturbations.

Maryam Chahin, Julius Mutschler, Stephanie P Dzhuleva, Clara Dieterle, Leidy Reyes Jimenez, Valerie Van Steenbergen and Florence M Bareyre

Aim of Study 3

This study aims to investigate the cellular mechanisms underlying physiological brain dysfunction following repetitive concussions, a common consequence of traumatic brain injury (TBI) that can lead to long-term cognitive and mood impairments. Despite the prevalence of concussions, there is currently no effective therapies and treatments due to a lack of understanding the underlying pathology. Therefore, the study utilizes a mouse model of repetitive concussion to mimic human brain injury and examines the fate of glial and neuronal cells in the cortex and hippocampus. The results reveal a specific loss of presynaptic excitatory synapses in these brain regions following repetitive concussion, accompanied by structural and functional activation of microglia, the brain's immune cells. Furthermore, the study demonstrates that microglia-mediated engulfment contributes to the removal of these synapses. Additionally, cognitive and anxiety deficits are observed in association with these cortical and hippocampal changes, highlighting the importance of targeting this novel mechanism for potential treatment strategies.

My contribution to this publication in detail:

For this manuscript, I was the main researcher and have performed all animal experiments for the experiments mentioned below. Furthermore, I contributed to the writing and editing of the manuscript.

The current manuscript has been submitted to Communication Biology 2024.

Repetition of brain concussions drives microglia-mediated engulfment of presynaptic excitatory input associated with cognitive and anxiety perturbations

Maryam Chahin[1,2,3], Julius Mutschler[1,2], Stephanie P Dzhuleva[1,2], Clara Dieterle[1,2], Leidy Reyes Jimenez[1,2], Valerie Van Steenbergen[1,2] and Florence M Bareyre*[1,2,4]

1 Institute of Clinical Neuroimmunology, University Hospital, LMU Munich, 81377 Munich, Germany

2 Biomedical Center Munich (BMC), Faculty of Medicine, LMU Munich, 82152 Planegg-Martinsried, Germany

3 Graduate School of Systemic Neurosciences, LMU Munich, 82152 Planegg-Martinsried, Germany

4 Munich Cluster of Systems Neurology (SyNergy), 81377 Munich, Germany

* Corresponding author. Email: florence.bareyre@med.uni-muenchen.de

ORCID Florence M Bareyre: 0000-0002-0917-1725

Keywords: repetitive concussions, microglia, excitatory synapse engulfment.

Abstract

Concussive injuries are a current health concern, accounting for the vast majority of head trauma. While the symptoms are usually transient following a single impact, repetitive concussions, such as those often seen in sports, are responsible for sustained acute and chronic deficits. In this report, we set out to establish a model of concussive head injury in mice to determine the behavioral and anatomical differences between single and repetitive injuries. We show that a single concussion does not induce synaptic changes or alterations in microglia structure and function. We also found no motor or cognitive behavioral changes in the mice. In contrast, repetition of the injury induced a specific loss of excitatory synapses in the brain areas below the concussion sites. These changes were accompanied by a significant activation of microglia and an increase in microglia-mediated engulfment of presynaptic excitatory synapses. These changes were associated with a transient decrease in spatial memory and later changes in behavior related to fear and anxiety. This study highlights the role of concussion repetition in the emergence of pathogenic processes affecting excitatory synapses due to microglia increasing their engulfment function.

Introduction

Traumatic brain injury (TBI) is one of the most debilitating causes of disability in young adults and children, affecting approximately 70 million people worldwide each year [1]. Among all forms of TBI, concussions, often referred to as "mild TBI", account for approximately 80% of these head injuries [2,3]. Although these concussions usually result in short-term behavioral deficits, in some cases these deficits can be observed for several months [4,5]. An important factor in the development of long-lasting deficits is the repetition of these concussions, especially if they occur before the brain has fully recovered from the previous insult [6], a situation that can be seen particularly in contact sports [7]. While the practice of sport has long been recognized for its many benefits to physical and mental health, it is increasingly recognized that repetitive concussions, as in contact sports, can pose a risk to brain health [8]. In particular, several clinical reports have shown that individuals involved in these repetitive sports concussions can show short, medium and long-term consequences of these repetitive head impacts, ranging from immediate and short-term loss of cognitive function and mood changes to long-term evolving physiological changes such as dementia, progressive tauopathy or chronic encephalopathy, among others [9,10]. The management of these sport-related repetitive concussions is complicated because current return-to-play guidelines classically assume that symptom-free behavior is equivalent to a return to brain homeostasis and the loss of cellular dysfunction. However, much clinical work has shown that most people with repetitive concussions have symptoms for at least a week after the blows [11], and recent reports even suggest that symptoms worsen over time [12,13]. There is currently no treatment for single and repetitive concussions, partly because people with concussions never go to hospital, and partly because patients who do go to hospital are left to heal from their injuries and only the symptoms are treated, not the causes [9]. There is therefore an important need to better characterize these repetitive concussions in animal models and to identify the cellular and molecular checkpoints that could be targeted in order to develop new therapies to prevent the consequences of these repetitive impacts on the brain. To this end, experimental studies have

now described the pathology following experimental repetitive mild concussion, describing increased behavioral deficits and more pronounced inflammation and axonal injury following repetitive mild brain impacts [6,14,15]. Importantly, most studies reported cellular changes up to several weeks after the repetitive concussions [14-17]. The mechanisms leading to these pathophysiological changes are not yet fully understood. Therefore, in this study, we modelled repetitive concussion in mice and investigated the cellular players that contribute to physiological brain dysfunction following repetitive concussion. We established a controlled cortical impact blunt injury on the skin surface to best mimic human concussion and investigated the fate of glial and neuronal cortical and hippocampal cells following single and repetitive concussion. We show a specific loss of presynaptic excitatory synapses in the cortex and hippocampus after repetitive brain concussion. We also report that this loss is accompanied by structural and functional activation of microglia. Indeed, we show that presynaptic excitatory synapses in the cortex and hippocampus are removed by a process of microglia-mediated engulfment following repetitive concussion. Finally, we show that these cortical and hippocampal changes are associated with cognitive and anxiety deficits, but not with gross motor changes. In conclusion, we uncover a novel mechanism of damage following repetitive concussion that may become an important target for treatment.

Results

Establishment of a reproducible model of repetitive concussion without macroscopic alterations and underlying cell death

To determine the anatomical consequences of repetitive brain concussions, we used a controlled cortical impact device in which we replaced the tip with a custom made, 5-mm-diameter, pliant, silicone tip with a hardness of 55 Shore A [18] (**Fig. 1A**). We aimed at creating a model of concussion displaying no overt macroscopic changes. To do so we induced either single concussion or we repetitive the concussion three times at 48hrs interval (**Fig. 1B**) with a depth of about 0.5 mm to 3.0 mm, a velocity of 3.5m/sec and a 500-msec dwell time. We indeed could not see any macroscopic changes on the brains as defined by hematoma, hemorrhage, or bruising (**Fig.1C**). To evaluate the effects of repetitive concussion on acute physiological responses and determine if apnea and righting reflex depend on the repetition of the concussion, responses were compared among mice subjected to up to three repetitive concussions spaced of 48hrs. Apnea duration decreased as a function of the number of concussions with the apnea duration being significantly shorter after the third concussion compared to after the first concussion (**Suppl. Fig. 1A**; p=0.0005 one-way ANOVA and Dunn's test 1st vs 3rd contusions). We then evaluated the righting reflex, which is the time mice take to turn back spontaneously to a prone position. We found that the amount of time to elicit a righting reflex response was significantly reduced with the number of impact and in particular after the third concussion (**Suppl. Fig. 1B**; p<0.0001 ANOVA and Dunn's test 1st vs 3rd contusion and p=0,0429 2nd vs 3rd contusion). Those physiological responses are in accordance with previous data on repetitive concussions [18]. We controlled the weight of the mice following the repetitive injuries and could not see any statistical differences even if mice slightly lost weight after the first, second and third concussions (**Suppl. Fig.1C**). While we could not see any macroscopic anatomical changes on the brain surface following the single and repetitive concussions, we wanted to determine whether cell death would be triggered by the impact. In order to do so we performed two analyses. First, we counted the number of

neurotrace positive cells in layer II/III of the cortex (just underlying the concussion) and second, we stained for activated caspase-3 as a marker of apoptotic cell death. We could neither see any decrease in the number of neurotrace positive cells nor any increase in the number of activated caspase-3 positive cells compared to control mice indicating that our model is indeed very mild and does not trigger any death of cells in layer II/III of the cortex below the impact (**Suppl. Fig.1D,E**).

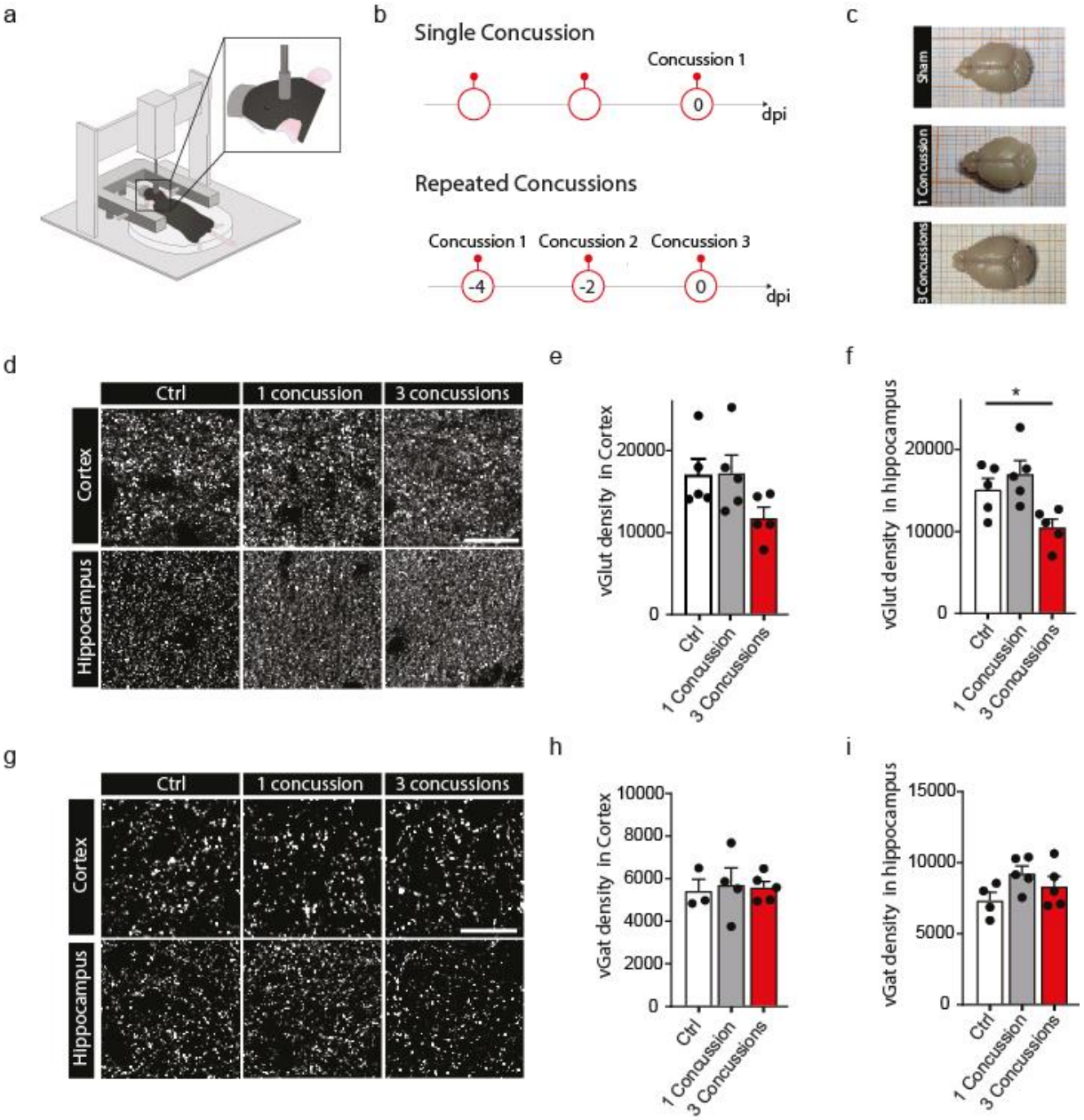

Figure 1. Repetitive concussions trigger regional loss of excitatory pre-synaptic input. (**a**) Scheme of the controlled cortical impact device used to produce repetitive closed-skull concussions in mice. (**b**) Time line of the experiment with the concussions delivered either single or repetitive at 48hrs interval. (**c**) Macroscopic view of the brains following sham injury, single concussion or repetitive

concussions (**d**) Confocal images of vGlut staining in layer II/III of the cortex (top) and hippocampus (bottom) underlying the concussion(s) at 1 week following repetitive concussions. Scale bar equals 30μm. (**e**) Quantification of vGlut puncta in layer II/III of the cortex at 1 week following single or repetitive concussions. (**f**) Quantification of vGlut puncta in the hippocampus at 1 week following single or repetitive concussions. p=0.0340 one-way ANOVA and Fisher test. (**g**) Confocal images of vGat staining in layer II/III of the cortex (top) and hippocampus (bottom) underlying the concussion(s) at 1 week following repetitive concussions. Scale bar equals 30μm. (**h**) Quantification of vGat puncta in layer II/III of the cortex at 1 week following single or repetitive concussions. (**i**) Quantification of vGat puncta in the hippocampus at 1 week following single or repetitive concussions.

Repetitive concussions trigger loss of pre-synaptic input and changes in the morphology of the post-synapse.

As we did not find any changes in neuronal survival in our model of repetitive concussion, we investigated synapse density following single and repetitive concussion (**Fig. 1D-I**). We focused on two presynaptic markers one for excitatory synapses – vGlut – and one for inhibitory synapses – vGat – at 1 and 6 weeks following single and repetitive concussions. We observed that the density of vGlut puncta is stable following single concussion while we see a marked – albeit non significant (p=0.712 one-way ANOVA and Fisher test) – decrease in synapse density in the cortex and a more pronounced and significant one in the hippocampus (p=0.0340 one-way ANOVA and Fisher test; **Fig.1D-F**). In contrast to presynaptic excitatory synapses, we could not detect any changes in presynaptic inhibitory synapse density at any time point considered, in either the cortex or the hippocampus (**Fig.1G-I**). This data indicates that repetitive concussions trigger a marked loss of presynaptic excitatory synapses in the brain area below the impact. As we detected changes using presynaptic markers, we also asked whether the post-synapse was altered. To do so we used GFP-M mice and investigated the spine density and morphology of pyramidal neurons in the cortex. We found no changes in spine density in both apical and proximal dendrites at any time points considered e.g. 1week, 3 weeks or 6 weeks following the injuries (**Suppl. Fig. 2A-F**). To further characterize the changes triggered by single and repetitive concussions to dendritic spines below the injury level, we then characterized the spine morphology as an indicator of the degree of spine maturation (**Suppl. Fig. 3A-F**).

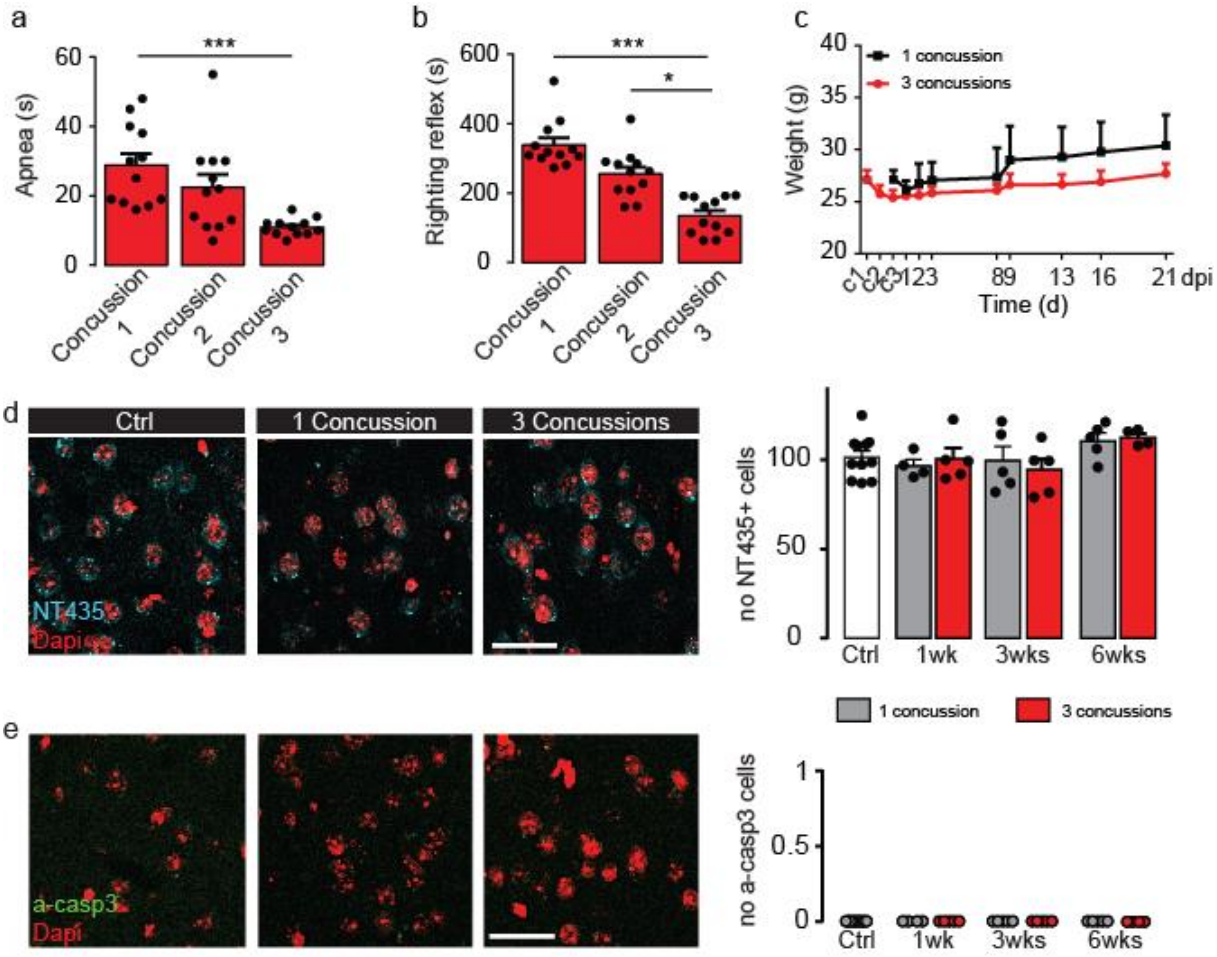

Supplementary Figure 1. Repetitive concussions do not trigger macroscopic alterations or underlying cell death. (**a**) Quantification of apnea duration following repetitive concussions. p=0.0005 one-way ANOVA and Dunn's test 1st vs 3rd contusions. (**b**) Quantification of righting reflex following repetitive concussions. p<0.0001 ANOVA and Dunn's test 1st vs 3rd contusion and p=0,0429 2nd vs 3rd contusion. (**c**) Quantification of the animal weight following single or repetitive concussions over a 21d period. (**d**) Confocal images of layer II/III of the cortex below the concussion impact point stained for neurotrace (cyan) and dapi (red) and quantification of the number of cells per field of views (FOVs). Scale bar equals 30μm. (**e**) Confocal images of layer II/III of the cortex below the concussion impact point stained for activated caspase-3 (a-casp3; green) and dapi (red) and quantification of the number of cells stained for caspase-3 per field of views (FOVs). Scale bar equals 30μm.

We divided spines into three types: mushroom, thin and stubby spines with mushroom spines generally considered as the most stable and mature structures [19-21]. We investigated spine morphology in the apical tuft and proximal dendrite of control and single or repetitively injured pyramidal neurons in GFP-M mice following single and repetitive concussions (**Suppl. Fig. 3B-C**). We found that the proportion of the more stable mushroom spines and thin spines did not change at 1 week following either the single or the repetitive concussion. In contrast, the

proportion of the more immature stubby spines transiently increased at 1 week in the apical tuft ($p = 0.0286$; One-Way Anova and Dunnett's test) and proximal dendritic part ($p = 0.0317$; One-Way Anova and Dunnett's test) following repetitive but not single concussion (**Suppl. Fig. 3D**) arguing for a shortening of the neck and a destabilization of the spines. We then investigated spine morphology in the proximal dendrites and apical tuft at 3 and 6 weeks following the injuries and could not find any lasting changes (**Suppl. Fig. 3D-E**).

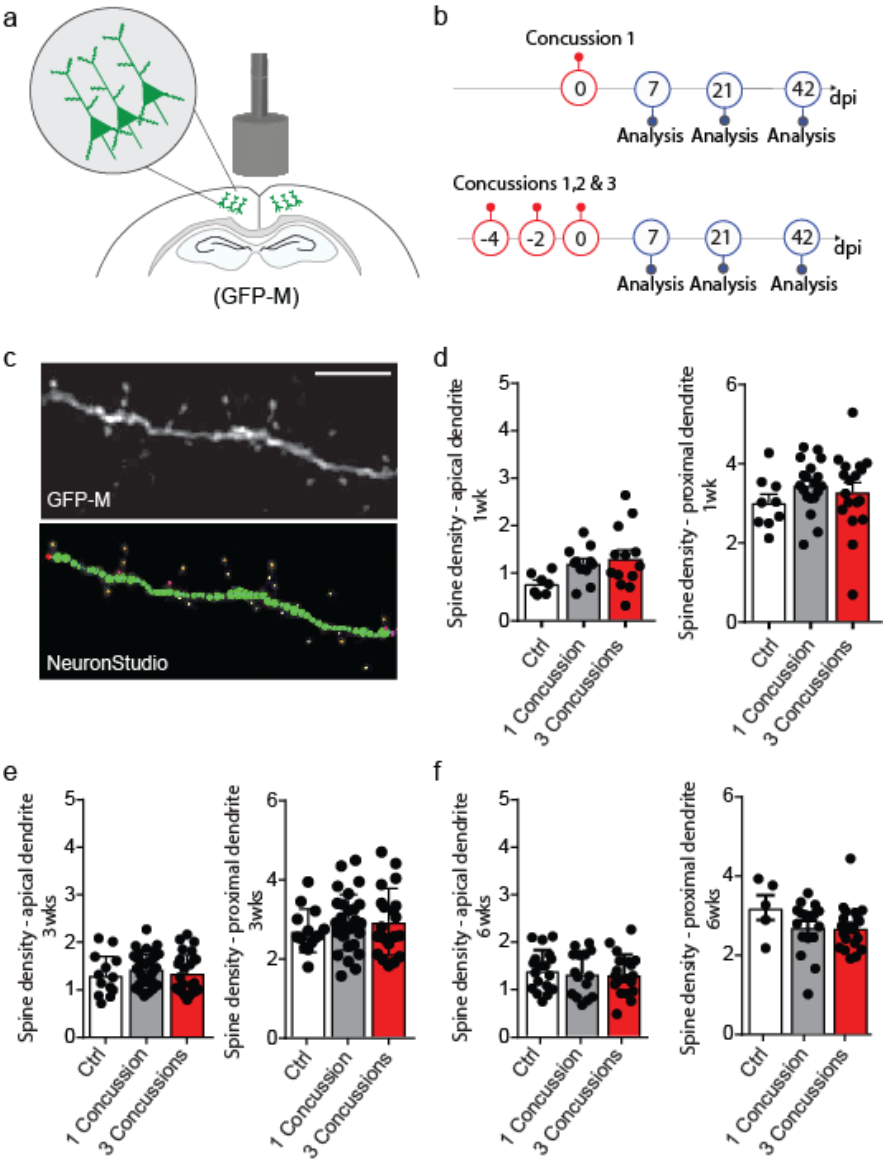

Supplementary Figure 2. Single and repetitive concussions do not trigger any changes in spine density. (**a**) Scheme of the experimental design (green: GFP positive neurons). (**b**) Timeline of the experiment. (**c**) Confocal images of a dendritic stretch (top) and representative example illustrating the spine quantification using Neuronstudio (bottom). Scale bar equals 5 µm. (**d**) Quantification of the spine density in control and following single and repetitive concussions at 1 week post-injury in the apical tuft and in the proximal dendritic stretch. n=20-28 independent dendritic stretches from 4 to 5 mice for apical and n = 20-28 independent dendritic stretches from 4 to 5 mice for proximal. (**e**) Quantification of the

spine density in control and following single and repetitive concussions at 3 weeks post-injury in the apical tuft and in the proximal dendritic stretch. . n =21-30 independent dendritic stretches from 4 to 5 mice for apical and n = 15-28 independent dendritic stretches from 4 to 5 mice for proximal. (**f**) Quantification of the spine density in control and following single and repetitive concussions at 6 weeks post-injury in the apical tuft and in the proximal dendritic stretch. n = 15-28 independent dendritic stretches from 4 to 5 mice for Apical and n = 17-28 independent dendritic stretches from 4 to 5 mice for Proximal.

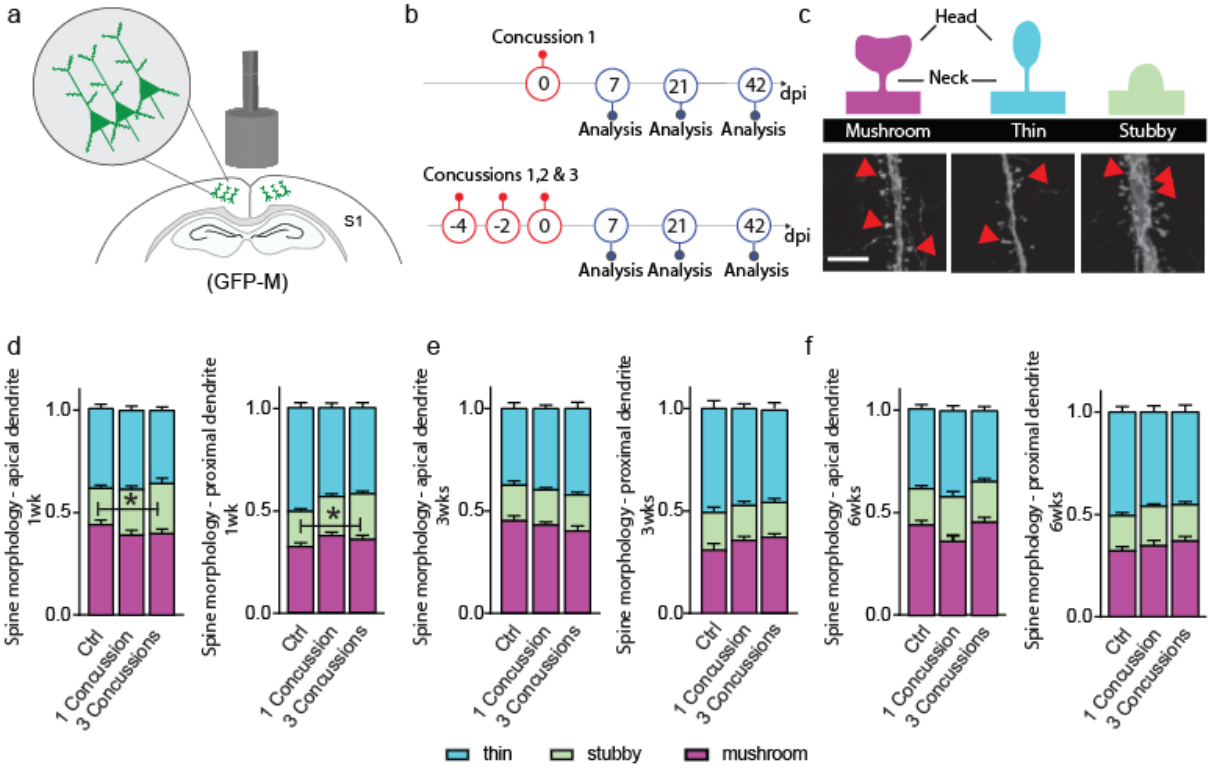

Supplementary Figure 3. Pyramidal cortical neurons display subtle changes in spine morphology following repetitive concussions. (**a**) Scheme of the experimental design (green: GFP positive neurons). (**b**) Timeline of the experiment. (**c**) Schematic representation of spine morphology and confocal images of mushroom, thin and stubby spines. Red arrowheads represent the examples of the respective spine type. Scale bar: 5 µm. (**d**) Quantification (mean ± SEM) of the fraction of mushroom, thin and stubby spines on apical tuft and proximal dendrites of layer II/III callosal neurons at 1 week post-injury. n = 20-28 independent dendritic stretches from 4-5 mice for Apical and n = 20-28 independent dendritic stretches from 4-5 mice for Proximal. Apical stubby spines: p = 0.0286 Ctrl vs 3 Concussion, One-way ANOVA and Dunnett's test. Proximal stubby spines: p = 0.0317 Ctrl vs 3 concussions, One-way ANOVA and Dunnett's test. (**e**) Quantification (mean ± SEM) of the fraction of mushroom, thin and stubby spines on apical tuft and proximal dendrites of layer II/III callosal neurons at 3 weeks post-injury. n = 24-33 independent dendritic stretches from 4-5 mice for Apical and n = 21-30 independent dendritic stretches from 4-5 mice for Proximal. (**f**) Quantification (mean ± SEM) of the fraction of mushroom, thin and stubby spines on apical tuft and proximal dendrites of layer II/III callosal neurons at 6 weeks post-injury. n = 15-28 independent dendritic stretches from 4 - 5 mice for Apical and n = 17-28 independent dendritic stretches from 4 to 5 mice for Proximal.

Important morphological and functional changes to microglia cells following single and repetitive concussions.

Since microglia have been shown to engulf synapses during the physiological refinement of circuits in the developing and mature CNS [22-28], we asked ourselves whether those cells could become reactive and engulf synapses following single or repetitive concussions. We first characterized the phagocyte response in the cortex underlying the concussions and can show a significant proliferation of Iba1+ cells – probably resident microglia and infiltrating macrophages – at 1, 3 and 6 weeks for single concussion and at 1 and 3 weeks for the repetitive concussions (**Fig. 2A,B**). We then investigated the morphology of those microglia to determine whether concussion could trigger their activation. To do so we made use of a recently published automated morphological analysis toolbox [29]. It is known that the microglial activation status is visualized by its progressive morphological transformation from a highly ramified to an amoeboid cell shape (**Fig. 2C**).

We obtained a large number of parameters from the toolbox, and hence performed a principal component analysis (PCA) to reduce dimensionality and provide a comprehensive quantification of the morphological features. We visualized morphological patterns in the two-dimensional coordinates created by PC1–2, where PC1 explains the highest variance (52.8%; **Fig. 2D**). More specifically, the mean values of PC1 scores for controls, 1 concussion and 3 concussions demonstrate that the mice receiving 3 concussions have a significantly different morphology in PC1 ($p=0.0084$ one-way ANOVA and Dunnetts'test; **Fig. 2E**). We then focused on those morphological parameters clustering with PC1 such as the betweenness, the sphericity, the number of Segments per branches or the number of nodes and could see that while single concussion did not trigger major changes in microglia morphology, repetitive concussion triggered long lasting changes and activation of microglia cells that become spheric and lose their branches to assume a amoeboid morphology (Kruskal-Wallis and Dunn's test; **Fig. 2F-I**). Interestingly those changes, while significant, were relatively subtle compared to the changes triggered by more massive injuries.

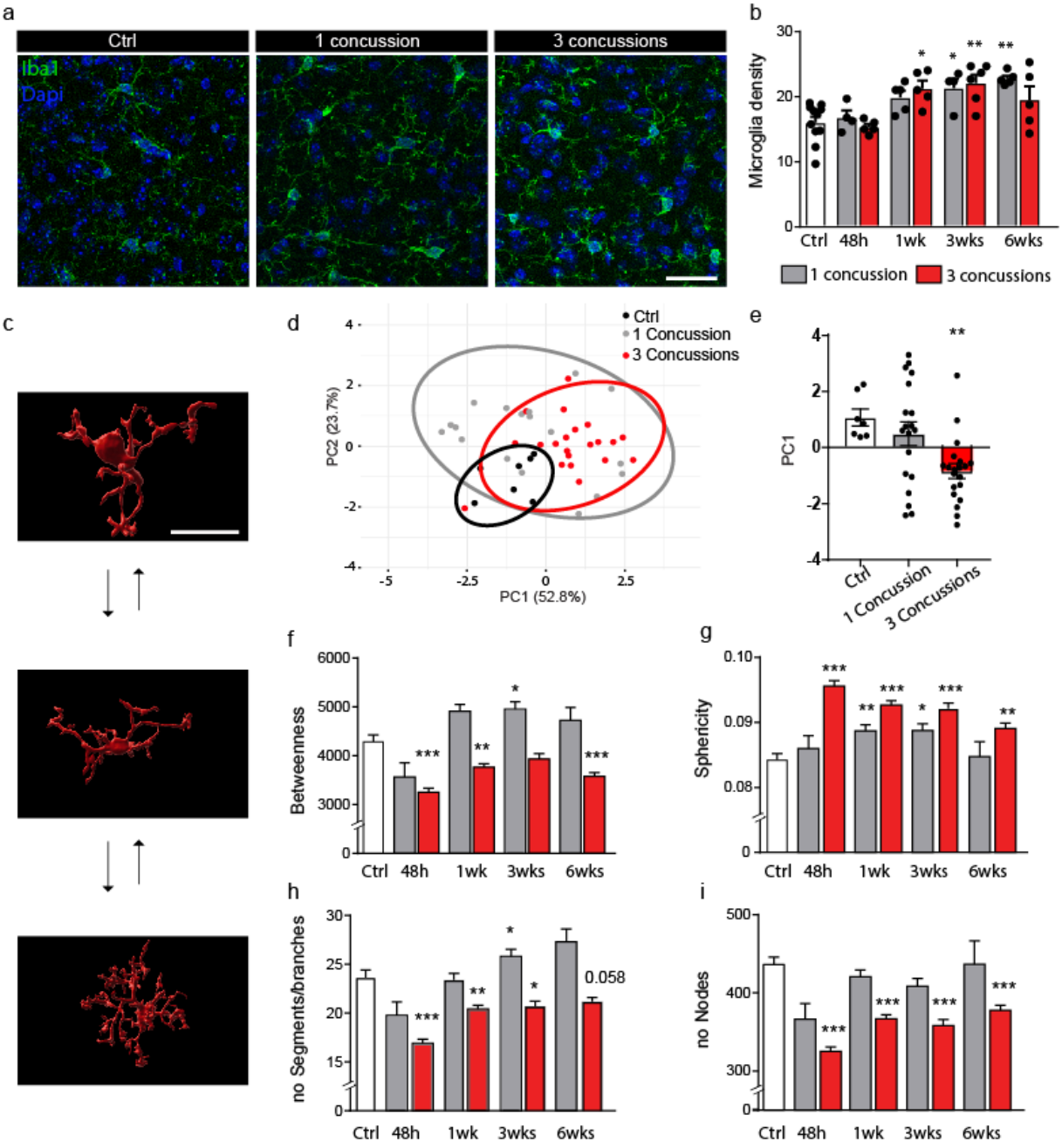

Figure 2. Microglia become ameboid in the cortex following single and repetitive concussions. (**a**) Representative confocal images of the cortex from control, 1 concussion and 3 concussions mice immunostained against Iba1 (Iba1: green; blue: dapi) 1 week after the last injury. (**b**) Quantification of the number of Iba1+ cells in the cortex at different time point 48hrs 1, 3, and 6 weeks following single (grey bars) or repetitive (red bars) concussions. n=4-7 mice per group. Scale bars: 50 µm. (**c**) 3D Imaris representations of the morphological changes in microglia following repetitive concussions. Scale bars: 20 µm (**d**) Principal component analysis of the morphological features to reduce dimensionality following single of repetitive concussions. (**e**) Quantification of average scores on principal components 1 for sham, single concussion and repetitive concussions. (**f**) Quantification of the microglia betweenness. (**g**) Quantification of the microglia sphericity. (**h**) Quantification of the microglia number of segments per branches and (**i**) Quantification of the number of nodes of microglia in the cortex at different time points 48hrs 1 , 3, and 6 weeks following single (grey bars) or repetitive (red bars) concussions. n=4-7 mice per group. Data represent mean +/- SEM. Significant differences with * $p < 0.05$, *** $p < 0.001$; 1-way ANOVA Ordinary or Kruskal-Wallis test with multiple comparison to control. Scale bar equals 5µm.

Since microglia cells are significantly activated following, in particular, repetitive concussions, we then sought to understand whether their function is also affected. To do so, we investigated if and when microglia in the cortex and hippocampus engulf presynaptic input as we determined earlier, that presynaptic input decreases in the cortex and hippocampus following repetitive concussions. We first focused on the cortex below the impact as we reasoned that this should be the region the most impacted by the trauma. To do so, we perfused mice at different time points following single and repetitive concussions and immunostained brain sections for the microglia marker Iba1, the presynaptic excitatory marker vGlut / inhibitory marker vGat and the lysosomal marker CD68 and analyzed the pattern of engulfment in the cortex (**Fig.3**) and the hippocampus (**Fig. 4**). In the cortex, our analysis of 3D reconstructions of confocal microscopy images using Imaris revealed a transient significant increase at 48 hrs and 1 week post-injury of the volume of CD68-positive lysosomes into microglia indicating an increase phagocytosis capacity of microglia following repetitive concussions (Kruskal-Wallis test with Dunn's multiple comparison test**; Fig. 3B-E**). In comparison, the volume of CD68-positive lysosomes was only increased at 1 week following single concussions. We also analyzed the number of vGlut–positive excitatory presynaptic input engulfed by cortical microglia. Interestingly, we could show that while engulfment of vGlut positive synapses was present only at 1 week following single concussion, it started earlier following repetitive concussions and was significantly prolonged up to 6 weeks e.g. for the entire study-period in the cortex (Kruskal-Wallis test with Dunn's multiple comparison test) following injury (**Fig.3B-D,F**). We then focused on the hippocampus and selected only two time points for our analysis: 1 week and 6 weeks as the first represents the early response and 6 weeks represents the lasting response in case of the repetition of the trauma. When investigating the volume of CD68 pro microglia volume, we could not find any differences at the chosen time points suggesting no changes in phagocytic capacity (Kruskal-Wallis test with Dunn's multiple comparison test**; Fig. 4A-E**). However, when we investigated the number of presynaptic excitatory input engulfed in the hippocampus, we demonstrated a significant increase at 1 week for the single concussion and at 6 weeks for the repetitive concussions indicating that the engulfment of

synapses occurs on a longer time scale following repetitive concussions (Kruskal-Wallis test with Dunn's multiple comparison test**; Fig.4F**). Notably, the inhibitory marker vGat was not significantly more engulfed by microglia at any time points in the cortex and hippocampus following single or repetitive concussions (Suppl. **Fig.4A-E**). This is in line with our vGat density data that demonstrate no decrease neither in the cortex nor in the hippocampus at any time points post-injury considered for single and repetitive concussions and underscore a specific removal of presynaptic excitatory input.

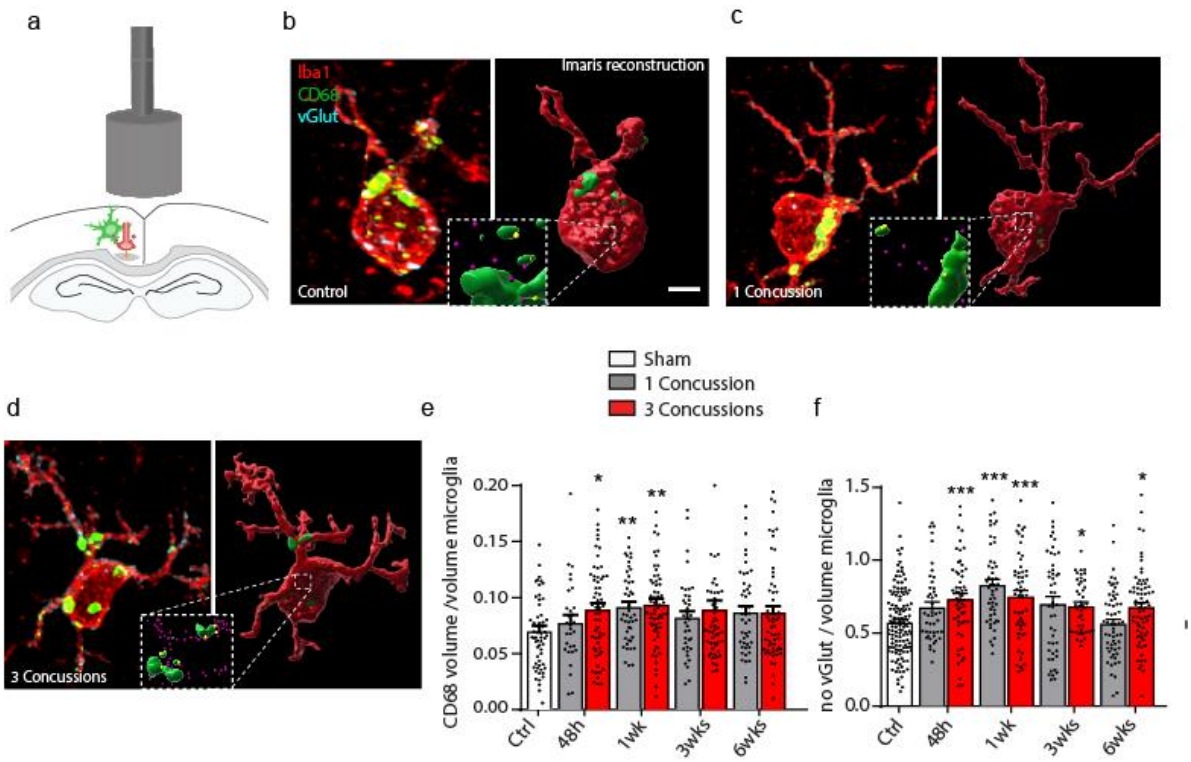

Figure 3. Increase engulfment of presynaptic excitatory input by cortical microglia following repetitive concussions. (**a**) Scheme of the experimental design investigating cortical microglia-mediated synapse engulfment in the cortex (green: microglia; red: presynaptic terminal). (**b**) Confocal images and 3D surface rendering in Imaris of synaptic marker (cyan, purple in 3D reconstructions) engulfment in lysosomes (green) of microglia (red) in controls. (**c**) Confocal images and 3D surface rendering in Imaris of synaptic marker (cyan, purple in 3D reconstructions) engulfment in lysosomes (green) of microglia (red) in single concussion at 6 weeks. (**d**) Confocal images and 3D surface rendering in Imaris of synaptic marker (cyan, purple in 3D reconstructions) engulfment in lysosomes (green) of microglia (red) in repetitive concussions at 6 weeks. (**e**) Quantification of volume of CD68–positive lysosome per volume microglia in the cortex of controls mice and at different time points following injury. n=4 (48hrs) to 5 (1wk, 3wks and 6wks) mice per group, 15 microglia on average per animal. (**f**) Quantification of the engulfment of vGlut excitatory synapses in the cortex of controls mice and at different time points following injury. n=4 (48hrs) to 5 (1wk, 3wks and 6wks) mice per group, 15 microglia on average per animal. Scale bar equals 5μm.

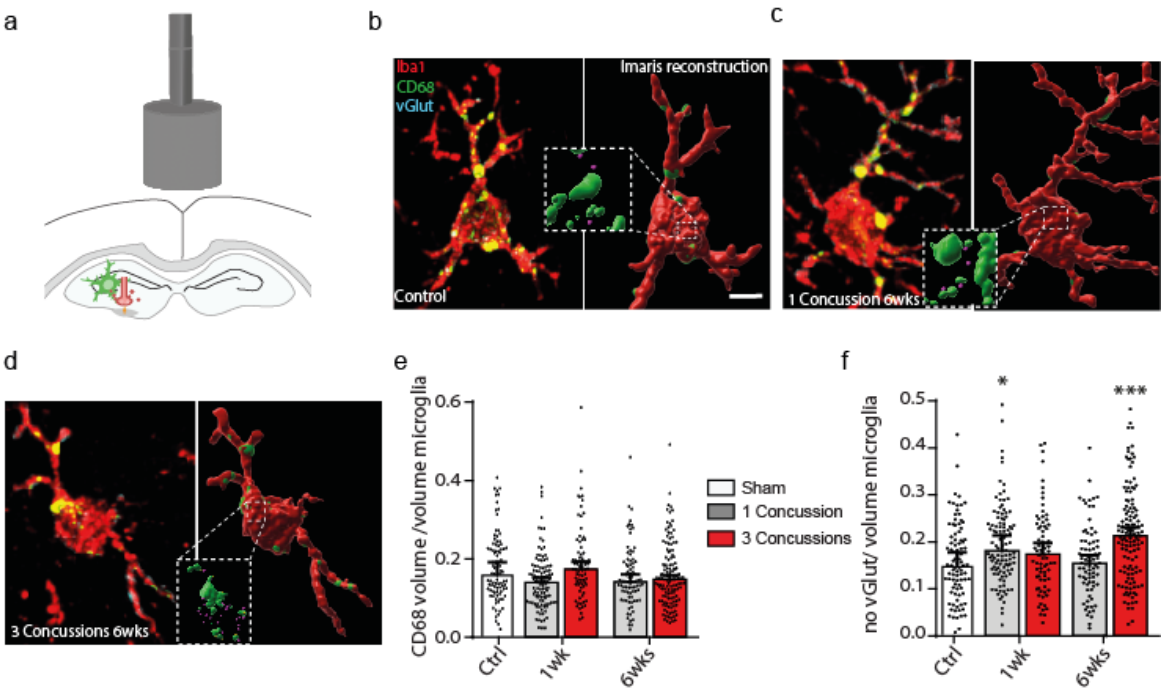

Figure 4. Increase engulfment of presynaptic excitatory input by hippocampal microglia following repetitive concussions. (**a**) Scheme of the experimental design investigating hippocampal microglia-mediated synapse engulfment in the hippocampus (green: microglia; red: presynaptic terminal). (**b**) Confocal images and 3D surface rendering in Imaris of synaptic marker (cyan, purple in 3D reconstructions) engulfment in lysosomes (green) of microglia (red) in controls. (**c**) Confocal images and 3D surface rendering in Imaris of synaptic marker (cyan, purple in 3D reconstructions) engulfment in lysosomes (green) of microglia (red) in single concussion at 6 weeks. (**d**) Confocal images and 3D surface rendering in Imaris of synaptic marker (cyan, purple in 3D reconstructions) engulfment in lysosomes (green) of microglia (red) in repetitive concussions at 6 weeks. (**e**) Quantification of volume of CD68 –positive lysosome per volume microglia in the hippocampus of controls mice and at different time points following injury. n= 5 (1wk and 6wks) mice per group, 15 microglia on average per animal. (**f**) Quantification of the engulfment of vGlut excitatory synapses in the hippocampus of controls mice and at different time points following injury. n= 5 (1wk and 6wks) mice per group, 15 microglia on average per animal.

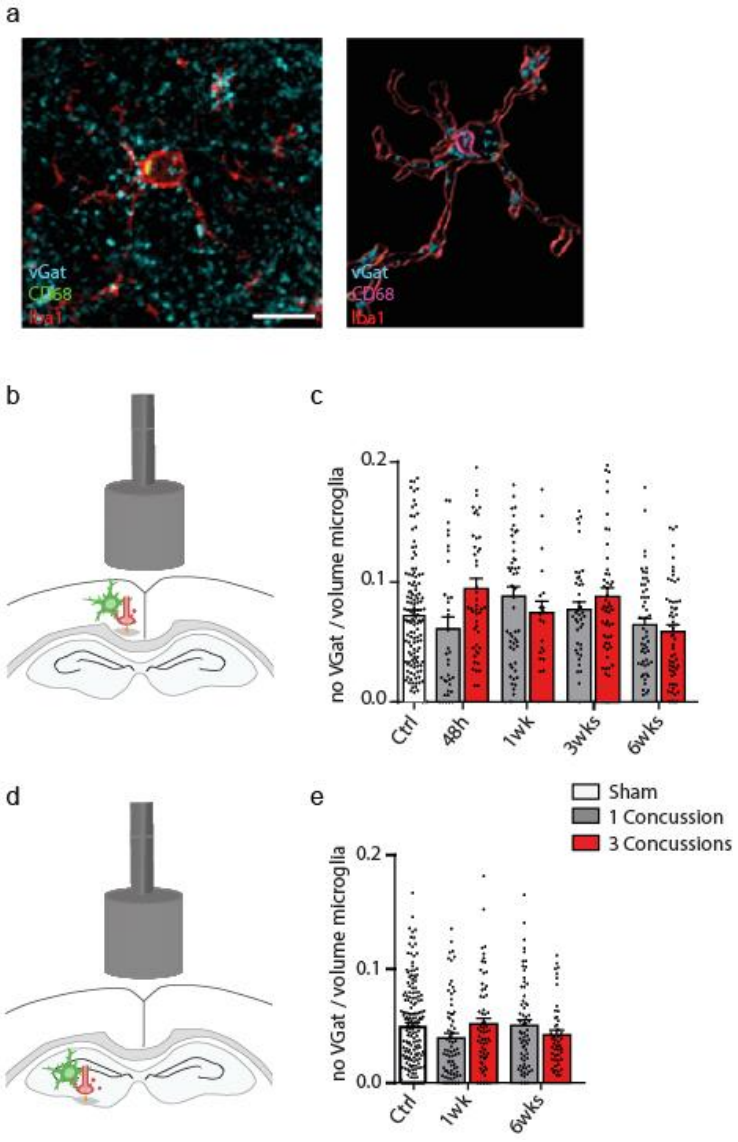

Supplementary Figure 4. Microglia do not engulf inhibitory presynaptic material following repetitive concussions. (**a**) Confocal images of vGat engulfment by microglia in the cortex**.** Scale bar equals 10μm. **(b)** Scheme of the experimental design investigating microglia-mediated synapse engulfment in the cortex (green: microglia; red: presynaptic terminal). (**c**) Quantification of the engulfment of vGat inhibitory synapses in the cortex of controls mice and at different time points following injury. n=4 (48hrs) to 5 (1wk, 3wks and 6wks) mice per group, 15 microglia on average per animal. (**d**) Scheme of the experimental design investigating microglia-mediated synapse engulfment in the hippocampus (green: microglia; red: presynaptic terminal). (**e**) Quantification of the engulfment of vGat inhibitory synapses in the hippocampus of controls mice and at different time points following injury. n= 5 (1wk and 6wks) mice per group, 15 microglia on average per animal.

Repetitive concussions trigger subtle behavioral perturbation in cognitive function and no alteration in motor behavior.

Finally, we wondered whether the consequences of those single and repetitive concussions could be distinguished at a behavioral level. To do so we designed four behavioral tests to

evaluate the motor and cognitive function as well as the anxiety level following single and repetitive concussions. To evaluate motor function, we performed the rotarod test to evaluate balance and endurance and performed the ladder rung test to evaluate locomotion [30]. We could not see any differences between sham mice and mice receiving a single concussion or repetitive contusions for any parameters evaluated (**Suppl. Fig. 5**).

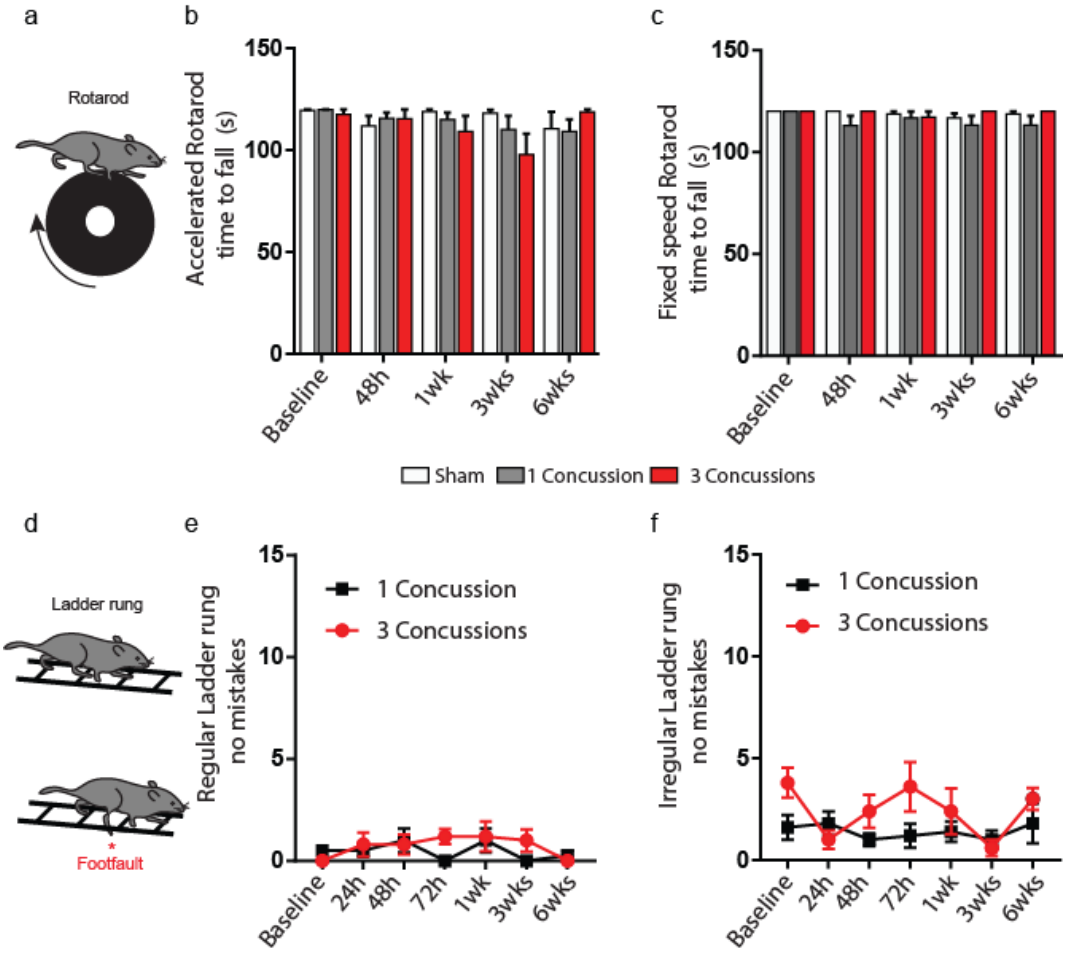

Supplementary Figure 5. Motor performance does not change following single or repetitive concussion. (**a**) Schematic representation of the rotarod test. (**b**) Quantification of the time to fall in the accelerated rotarod in sham (white box), single concussion (grey box) and repetitive concussions (red box) at different time points following injury (48hrs, 1wk, 3wks, 6wks). (**c**) Quantification of the time to fall in the fixed speed rotarod in sham (white box), single concussion (grey box) and repetitive concussions (red box) at different time points following injury (48hrs, 1wk, 3wks, 6wks). (**d**) Schematic representation of the ladder rung test. (**e**) Quantification of the number of mistakes after single concussion (black line) and repetitive concussions (red line) at different time points following injury (48hrs, 1wk, 3wks, 6wks) for the regular ladder rung. (**F**) Quantification of the number of mistakes after single concussion (black line) and repetitive concussions (red line) at different time points following injury (48hrs, 1wk, 3wks, 6wks) for the irregular ladder rung.

This underscores that motor function is not significantly altered at acute and chronic time points following the concussions as we deliver them in this study. To evaluate the cognitive function, we used the Y maze that allows the evaluation of short term memory and spatial working memory in mice (**Fig 5**). In this test, the mice are allowed to explore all three arms of the maze after one arm was previously blocked and is driven by the curiosity of rodents to explore previously unvisited areas [31]. We evaluated the preference index for the novel arm and found in control animal that this was stable throughout the study-period around 0.35 which is in accordance with the literature [32] (**Fig.5A,B**). Interestingly we saw no changes over the study period for mice subjected to a single concussion. However, mice subjected to repetitive concussions demonstrated a significant decrease in the preference index at 1 week post-injury (**Fig.5B**; Two-way ANOVA followed by Dunnett's test p=0.0480 sham vs 3 Concussions). The deficits in preference index, indicating that the spatial memory of the mice receiving 3 concussions is impaired, was transient and recovered by week 3 following injury. We also analyzed the distance ran by the mice as well as the time spent in the conditioning arm. Mice sustaining a single concussion did not show differences with sham mice are were stable over the entire study-period (**Fig.5C,D)**. In contrast, mice receiving repetitive concussions ran an increased distance 1 week following the injury and spent more time in the conditioning arm at 1 and 3 weeks indicating that they struggled more due to memory impairments. We then used the tail suspension test to evaluate behavioral despair and learned helplessness or anxiety [33,34]. We recorded the percentage of the total experimental time that the mice spent struggling, the total duration of the struggles and the mean duration of the struggles to escape the suspension. In sham animals we observed that the three evaluated parameters decreased steadily over the study-period, indicating that the animals learn that there is no escape possible (**Fig. 5E-H;** 2-way ANOVA followed by Tuckey's multiple comparisons test. % of total time struggling: p=0,0074 sham bas vs sham 3wks; p=0,0016 sham bas vs sham 6wks; Total duration of struggles: p=0,0073 sham bas vs sham 3wks; p=0,0015 sham bas vs sham 6wks; Mean duration of Struggles: p=0,0202 sham bas vs sham 3wks; p=0,0099 sham bas vs sham 6wks). Mice sustaining one concussion demonstrated the same pattern as sham mice albeit a

bit delayed and with a less pronounced decrease indicating an increase albeit subtle of anxiety (**Fig. 5E-H;** 2-way ANOVA followed by Tuckey's multiple comparisons test. % of total time struggling: p=0,0054 1concussion bas vs 1concussion 6wks; Total duration of struggles: p=0,0053 1concussion bas vs 1concussion 6wks; Mean duration of Struggles: p=0,0106 1concussion bas vs 1concussion 3wks; p=0,0049 1concussion bas vs 1 concussion 6wks). However, mice sustaining 3 consecutive concussions did not display such decrease and kept struggling similarly to baseline (**Fig.5F-H**). Moreover, at 48hrs and 1 week following the repetitive concussions mice displayed a significant increase of mean duration of struggles (**Fig 5H,** 2-way ANOVA followed by Dunnet's test; p=0,0037 Sham 48hrs vs 3 concussions 48hrs, p=0,0021 sham 1wk vs 3 concussions 1wk). As this test is indicative of learned helplessness and of anxiety, we can also conclude that mice sustaining three concussions demonstrate increased anxiety and panic as they keep struggling in the tail suspension test.

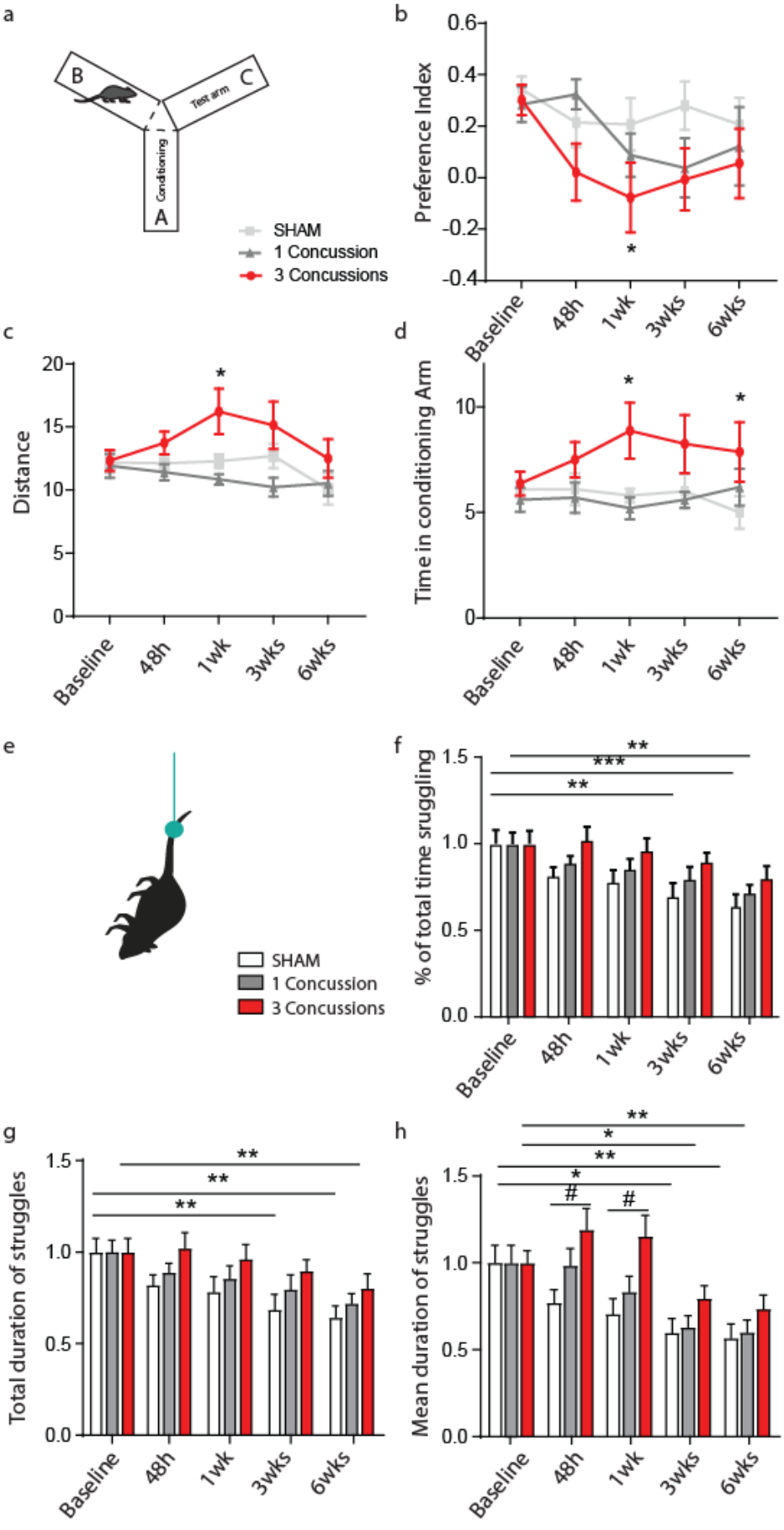
a
B
C
Test arm
Conditioning
A
SHAM
1 Concussion
3 Concussions
b
Preference Index
0.6
0.4
0.2
0.0
-0.2
-0.4
*
Baseline
48h
1wk
3wks
6wks
c
Distance
20
15
10
5
0
*
Baseline
48h
1wk
3wks
6wks
d
Time in conditioning Arm
10
5
0
*
*
Baseline
48h
1wk
3wks
6wks
e
SHAM
1 Concussion
3 Concussions
f
% of total time sruggling
1.5
1.0
0.5
0.0
**
***
**
Baseline
48h
1wk
3wks
6wks
g
Total duration of struggles
1.5
1.0
0.5
0.0
**
**
**
Baseline
48h
1wk
3wks
6wks
h
Mean duration of struggles
1.5
1.0
0.5
0.0
**
*
**
*
#
#
Baseline
48h
1wk
3wks
6wks

415

Figure 5. Repetitive concussion triggers perturbation in cognitive function and anxiety. (**a**) Schematic representation of the Y-maze test. (**b**) Quantification of the preference index in sham (light grey line), single concussion (dark grey line) and repetitive concussions (red line) at different time points following injury (48hrs, 1wk, 3wks, 6wks). p=0.0480 (Two-way ANOVA followed by Tuckey's multiple comparison test sham 1wk vs 3 concussions 1wk). (**c**) Quantification of distance ran in sham (light grey line), single concussion (dark grey line) and repetitive concussions (red line) at different time points following injury (48hrs, 1wk, 3wks, 6wks). p=0,0219 sham 1wk vs 3 concussions 1wk (Two-way ANOVA followed by Tuckey's multiple comparison test). (**d**) Quantification of time spent in the conditioning arm in sham (light grey line), single concussion (dark grey line) and repetitive concussions (red line) at different time points following injury (48hrs, 1wk, 3wks, 6wks). p=0,0230 sham 1wk vs 3 concussions 1w and p= 0,0363 sham 6wks vs 3 concussions 6wks (Two-way ANOVA followed by Tuckey's multiple comparison test). (**e**) Schematic representation of the tail suspension test. (**f**) Quantification of the percentage of total experimental time spent struggling in sham (white box), single concussion (grey box) and repetitive concussions (red box) at different time points following injury (48hrs, 1wk, 3wks, 6wks). p=0,0074 sham baseline vs sham 3wks; p=0,0016 sham baseline vs sham 6wks; p=0,0054 1concussion baseline vs 1concussion 6wks (Two-way ANOVA followed by Tukey's multiple comparison test). (**g**) Quantification of the total duration of struggles in control (white box), single concussion (grey box) and repetitive concussions (red box) at different time points following injury (48hrs, 1wk, 3wks, 6wks). p=0,0073 sham bas vs sham 3wks; p=0,0015 sham baseline vs sham 6wks; p=0,0053 1concussion baseline vs 1concussion 6wks (Two-way ANOVA followed by Tukey's multiple comparison test). (**h**) Quantification of the mean duration of struggles in sham (white box), single concussion (grey box) and repetitive concussions (red box) at different time points following injury (48hrs, 1wk, 3wks, 6wks). p=0,0202 sham baseline vs sham 3wks; p=0,0099 sham baseline vs sham 6wks; p=0,0106 1concussion baseline vs 1concussion 3wks; p=0,0049 1concussion baseline vs 1 concussion 6wks (Two-way ANOVA followed by Tukey's multiple comparison test) and p=0,0037 Sham 48hrs vs 3 concussions 48hrs, p=0,0021 sham 1wk vs 3 concussions 1wk (Two-way ANOVA followed by Dunnet's multiple comparison test).

Discussion

Here we identify a critical role of microglial cells following repetitive concussions in mice. We show that microglial cells specifically engulf presynaptic excitatory inputs for several weeks after injury. This is in contrast to the lack of engulfment following a single concussion, showing that repetition of the injury exacerbates the damage. We show that this synapse pruning is associated to behavioral changes in cognitive and anxiety function in mice subjected to repetitive concussion.

Establishment of a model of repetitive concussions

Most concussions occur in the context of sports activities where the risk of repetition is increased. In this study, based on previous reports, we developed a mouse model of repetitive concussion using a cushioned midline blow to the closed skull [18]. We designed our model to produce no macroscopic brain changes; specifically, we could not detect hemorrhage, contusion, skull fracture or cell death [6,18,35,36]. We wanted this to be representative of human concussions, where loss of consciousness may or may not occur after impact and imaging shows only minor changes [37,38]. We demonstrated that the apnea and righting reflex diminished with successive impacts. Both the righting reflex and apnea are consistent with previous reports using midline concussion [18,39,40]. While apnea does not typically occur in the clinical setting, apnea is common in rodent models of midline concussion [35], likely due to tissue deformation towards the brainstem, which transiently affects neurons involved in respiration [41]. The reduction in apnea and righting reflex duration is consistent with previous reports and probably reflects adaptive or protective mechanisms [18,42]. It is worth noting that other reports show increased or prolonged apnea duration or righting reflex responses after repetitive concussion [39,42], which are likely to be specific to injury models, sites and species.

Subtle loss of synapses and morphological changes following repetitive concussions

In this study, we observed a subtle loss of synapses in the cortex underlying the concussion and a more pronounced loss in the dentate gyrus of the hippocampus. In particular, we identified a specific loss of excitatory synapses using immunohistochemistry with a vGlut marker. Changes in synaptic strength have recently been reported in the first hours after mild brain injury [43]. Here, we also report an imbalance between excitatory and inhibitory input, which is not altered by single and repetitive concussions. This excitatory/inhibitory imbalance has been highlighted by other recent reports following mild traumatic brain injury (mTBI/concussion), in particular a persistent upregulation of excitatory hippocampal synapses, possibly through changes in postsynaptic Ca2+ signaling/regulation, has been shown in hippocampal slices one month after single and repetitive mTBI [44]. Similarly, Langlois and colleagues demonstrated in a model of 3 repetitive closed head concussions that repetitive concussions induce persistent changes in the spontaneous synaptic activity of hippocampal neurons [45]. Here, the authors suggest that repetitive concussions induce increased postsynaptic excitatory neurotransmission while inducing a shift in synaptic drive towards more inhibition in hippocampal CA1 neurons two weeks after repetitive concussions. These results are consistent with our data showing a transient decrease in presynaptic excitatory input in the hippocampus and, to a lesser extent, in the cortex following impact but no change in presynaptic inhibitory input. Our study also suggests changes at the post-synaptic level. To investigate these changes, we used CFP-M mice, which have specific labelling of a subset of pyramidal neurons in the cortex and hippocampus. We were able to show that while there was no change in spine density, there were large and transient changes in spine morphology 1 week after repetitive concussions. As the changes at the pre- and post-synaptic level can only be detected in the repetitive concussions but not in the single concussions, this highlights the vulnerability of the already injured brain to subsequent insults. In addition, the spine morphology of pyramidal neurons develops in two phases, with more immature spines at early time points after injury and more mature and stable spine morphologies later on in the case of repetitive concussions. Again, this highlights the vulnerability of the already injured brain to further injury that exacerbates the damage.

Activation of microglia cells and specific engulfment of excitatory synapses

In this study, we can now also show that microglial cells also act as important sculptors of neuronal circuits after repetitive concussion. We show that microglial cells are activated by repetitive concussion and that this activation is accompanied by specific engulfment of excitatory synapses. Contact and synapse refinement have mainly been studied during development, where glial cells have been implicated in the process of synapse removal and circuit shaping [23,26,27,46-49]. Here, we show that in a model of subthreshold injury that does not produce visible damage, the structure and function of microglia are specifically affected by repetitive concussion. Such involvement of microglia and their ability to engulf synapses after brain injury has been reported previously, albeit in a model of moderate open skull injury [50]. Here, the authors show that late after injury there is ongoing synaptic degeneration driven by microglial phagocytosis of complement-opsonized synapses in both the ipsilateral and contralateral brain, and that complement inhibition interrupted the degenerative neuroinflammatory response and reversed cognitive decline even when therapy was delayed until 2 months after TBI. Our data extend these findings and identify excitatory synapses as the major vulnerable synapse type removed by microglial cells after repetitive concussion. It is interesting to see that both microglial activation and engulfment are only visible after repetitive concussions, suggesting that microglial activation and function is dependent on the number of concussions. Whilst the complement pathway may mediate this engulfment - as previously demonstrated by Alawieh and colleagues [50] - this remains to be demonstrated following repetitive concussion and once the pathway is elucidated, one possibility would be to antagonize these pathways following the first, second or third repetition to alleviate the consequences of repetitive concussion.

Cognitive disturbances accompany the microglia-mediated loss of excitatory synapses

Finally, we show that mice subjected to repetitive concussion develop transient changes in spatial memory and longer-lasting changes in their anxiety-related behavior. These features are often observed in patients who suffer repetitive blows to the head, for example in sports,

who may develop amnesia of neuropsychological changes in the period following the repetitive concussions [4,38, 51-53]. Our findings recapitulate the clinical situation and are consistent with other experimental reports in mice showing cognitive and anxiety-related behavioral changes [54]. Not surprisingly, we found no changes in motor function as assessed by the rotarod or ladder rung test. This is also consistent with both the clinical and experimental literature on concussion [52,54]. We can therefore conclude that we have a mouse model of repetitive concussion that recapitulates the clinical situation. In this model, we could show that the loss of excitatory synapses, particularly in the hippocampus, is mediated by microglial cells engulfment and is associated with transient cognitive changes. We believe that targeting microglia engulfment following repetitive concussion may be a strategy to alleviate the consequences of these repetitive subthreshold injuries.

Materials and Methods

Animals

All the experiments were carried out under the approval of the Regierung von Oberbayern under the protocol number 20-164. Eight to twelve weeks-old C57Bl6J (Janvier Labs) and GFP-M mouse line, mixed gender randomized equally per group, were used for this study. All animals were housed under controlled standard housing conditions (dark/light cycle of 12 h, temperature 22 ± 2 degrees and humidity of 55 ± 10%) with food and water ad libitum.

Single and Repetitive concussions using the Controlled Cortical Impact (CCI)

Mice were anaesthetised using 3% isolfuorane (Piramal) delivered through a chamber (Harvard Apparatus, Holliston, USA) After being put in a stereotaxic frame (Precision Systems & Instrumentation, LLC) , mice were maintained under 1,5% isofluorane during the whole procedure until the impact. A TBI-0310 Impactor (Precision Systems & Instrumentation, LLC) using a 5 mm diameter silicone tip was used to administer an impact of a 3.5 m/s speed, 2.0 mm depth and 500 ms dwell time [18]. The landing position of the tip was positioned between Bregma and Lambda, aligned with the midline impacting both hemisphere equally. Following the impact, apnea and righting reflex duration (time needed for each mouse to get back to their prone position) were assessed on individual mouse to assure reproducibility of the injury. Mice were put back on a heating pad until completion of the experiment. The repetitive concussion group underwent 3 impacts spaced 48h apart, the single concussion group received only one impact and Sham group was subjected to the same procedure, undergoing anesthesia and subsequently put into the stereotaxic frame without any impact. No mice were excluded from the study. The weight of the mice was recorded every day for the duration of the experiments.

Behavioral tests and processing

Mice were habituated 3 times before any initial testing and were recorded for baseline before they underwent concussion. Cognitive and anxiety tests such as Y-maze, tail suspension were carried out as well as motor tests such as the Rotarod and ladder rung. All the tests have been carried out by two observers blinded in respect to injury and time points.

Y-maze test: The Y maze was used to assess the spatial memory of each mouse and their spontaneous alternation potential. The spontaneous alternation was used to test the spatial memory. In-house costume-made Y-maze was used to perform the test. Y-maze comprises 3 separate arms (8x30x15cm, at a 120° angle from one another). The test was performed in two steps: in the initial phase, the 'conditioning' phase, a random arm was closed and another was randomly picked as the 'starting' arm. The mouse was placed on the 'starting' arm and was let to explore the two arms for 5 min. In the test phase, after 30min, the mouse was returned to the 'starting' arm and was allowed to explore the entire Y-maze for 5 min. In between each conditioning and test phase, the Y-maze was cleaned with 70% ethanol. Parameters were recorded with a GoPro 8 camera at 120 frames per second. Preference Index was calculated as follows: (time in the novel arm− time in the old arm)/(time in the novel arm+ time in the old arm) [55].

Tail suspension: Tail suspension is used to assess anxiety, behavioral despair and learned helplessness [33,34]. Mice were placed individually and isolated from each other in a self-made box and suspended by their tail at 30 cm above the bench. As mice have been shown to climb on their tail during the procedure, a tube covering the mouse's tail was placed to avoid this behavior. The trial lasted 6 min and each trial was recorded with a GoPro 8 camera. The motility and immobility of each mouse were assessed using Behavioral Observation Research Interactive Software (BORIS) [56].

Ladder rung: For assessment of regular walking and fine paw placement the ladder rung test was used [21,57]. In this test, the animals have to cross a 1m horizontal grid ladder 3 times consecutively and footfalls are counted by an investigator blinded to injury and time point based on video recordings. We evaluated locomotion with evenly distributed spacing between the

rungs and the animal's ability for fine coordinated paw placements using irregular spacing of the rungs. We only analyzed consecutive steps and the last step before or after an interruption were therefore not evaluated. Footfalls were recorded when mice either totally missed a rung or if they slipped from a rung (deep or slight slip). The number of footfalls was calculated quantitatively for a given distance.

Rotarod test: To evaluate motor ability and balance, we used the rotarod test (Ugo Basile, Italy; [30]). Mice were placed on the apparatus which was kept either at a constant speed of 20 rounds/min or accelerated from 2 to 40 rounds/min. Maximum score is 120 and the device automatically records the time and velocity at which the mice fell from the rod.

Tissue processing and Immunohistochemistry

Mice were sacrificed and transcardially perfused with 4% paraformaldehyde (PFA) in 1M PBS. Tissue was postfixed overnight and then micro-dissected.

Microglia density and morphology: For the evaluation of microglia density and morphology, mice's brains were embedded in a 3% agarose solution in deionised water. Sections of 100µm were cut on a Leica VT 1000s vibratome. Sections were then stained following a two-day protocol. Initially, the sections, after being washed 3 times with 1X PBS for 10 min each, were mounted on slides. They were then incubated in a blocking solution of 10% horse serum (HS) in 0,5% (v:v) Triton X-100 in 1X PBS (T-PBS) for 1 hour at room temperature (RT). The coronal sections were then incubated overnight at room temperature in a solution 5% HS with T-PBS containing primary antibody: anti-rabbit anti-ionized calcium-binding adaptor molecule-1 [IBA-1] (1/500, Wako, N°019-19741). After an overnight incubation of the primary antibody, sections were washed 3 times, thereafter incubated for 2 hours with a solution of 5% HS with T-PBS containing Alexa-594 donkey anti-rabbit (1/500,ThermoFisher, A21207). Sections were then washed and cover slipped with VectaShield (Vector Laboratories).

Spine density and morphology: To measure spine density and morphology we relied on the intense and sparse labeling of GFP-M mice (essentially layer V neurons and fewer layer II/III neurons). No signal amplification was required. 100μm sections were made using the vibratome.Sections were then washed and cover slipped with VectaShield (Vector Laboratories).

Microglia-mediated synaptic engulfment and density of excitatory and inhibitory synapses: To evaluate the engulfment of presynaptic material by microglia and the density of excitatory and inhibitory synapses, brains were immersed in a 30% sucrose solution as cryopreservation for 48h. The samples were then positioned into a cryo-mold, coated with Optimal Cutting Temperature compound (Tissue-Tek O.C.T. medium) and 30μm thick sections were cut using a cryostat (Leica CM 1850 model). The sections were washed 1X PBS, followed by their incubation in a blocking solution (10% HS with T-PBS. The sections were then incubated with a solution of 5% HS with T-PBS containing for our first set, guinea pig anti-IBA1 (1/500, Synaptic Systems, N°234 004), rabbit anti-VGLUT1/2 (1/500, Synaptic Systems, N°135 503), rat anti-CD68 (1/500, Abcam, N°ab53444). The second set consisted of rabbit anti-IBA1 (1/500, Wako, N°019-19741), guinea pig anti-VGAT (1/500, Synaptic Systems, N°131 308), rat anti-CD68 (1/500, Abcam, N°ab53444). After being incubated overnight, the section were incubated for 2 hours containing secondary antibodies: anti-guinea pig Alexa Fluor (AF) 633 (1/500, Sigma Aldrich, N°SAB4600129), anti-rat AF594 (1/500, ThermoFisher, N° A21209), anti-rabbit AF488 (1/500, ThermoFisher, N°A21206), anti-rabbit AF647 (1/500, ThermoFisher, N°A32795), anti-guinea pig Cy3 (1/500, Jackson Immunoresearch, N°706-165-148), anti-rat AF488 (1/500, Abcam, N°ab150153) .The section were thereafter incubated with a DAPI (1:10000) 1X PBS solution for 10 min. Sections were then washed and cover slipped with VectaShield (Vector Laboratories).

Neuronal density and cell death: To assess the neuronal cell death and quantify neuron density, 30μm sections were cut using a cryostat. Immunohistochemistry was performed as stated in the paragraph above. For cell death, we used an activated Casp3 antibody

(1/250,Abcam, ab2302) coupled with an anti-rabbit AF647 (1/500, ThermoFisher, A32795): To determine neuronal density we used Neurotrace (NT; Thermofisher N21479). Sections were then washed and cover slipped with VectaShield (Vector Laboratories).

Image acquisition and processing

Spine density and morphology: In order to quantify the spine density/morphology of individual dendrites, we acquired z-stacks using the FV1000 Olympus microscope (60x oil objective NA 1.35, zoom of 3 and resolution of 1024 × 1024). We imaged two areas for each dendrites: proximal dendrite (at a distance of ~70–150 µm from soma), and apical tuft (at a distance up to 75 µm below the S1 cortical surface). The images underwent deconvolution using the Huygens Essential software (16.05 Scientific Volume Imaging, NL) and Z projections of the deconvolved stacks were obtained using Neuron Studio.

Microglia density, morphology and synapse density and engulfment: Leica SP8X WLL upright confocal microscope from the Bioimaging core facility from the biomedical centre, Martinsried-Munich was used. Excitation was obtained using a continuous 405 nm laser and a pulsed white light laser (470-670 nm). Each section was scanned in a specific cortical region defined as follows: 100µm from the midline and 20µm depth from the surface of the coronal section. Each acquired z-stack was 20µm thick each using a step size of 0,4µm (NA 1.3, 40x oil, zoom 2 resolution 2048x2048, speed 600). Three to four sections were scanned per animal.

Data analysis

Synapse density: Synapse density was quantified using Imaris software 9.6.0 version (BitPlane) in a semi-automatic manner. The spot features parameters were preset for each Vglut and Vgat spot, by defining the diameter of each the spot. Thereafter, these settings were used in a batch processing pipeline to 3D ender and quantify the the synaptic markers

accordingly. The ratios of excitatory/inhibitory markers were made to determine the imbalance of synapses following concussion.

Spine density and morphology analysis: Each deconvoluted stack containing the dendritic segment was opened in Neuronstudio (version 0.9.92) and the dendritic trunk was semi-automatically traced resulting in a series of green vertices superimposed on volume-rendered data (**Suppl. Fig.1**). Thereafter, dendritic spines were detected and classified. This automatic quantification was manually controlled to remove falsely detected spines, add falsely undetected or reclassify misclassified spines (mushroom, thin, stubby). The obtained numbers of spines were divided by the length of the dendritic segment determined by the program.

Microglia morphology: Sections stained with IBA-1 were rendered using a MATLAB (MathWorks) based script developed and published by Heindl and colleagues [29]. The script allows a rendering of the morphology of double positive IBA-1 and DAPI microglia. Parameters such as the volume, the branches length, the number of nodes or branches were extracted. The analysis has been carried out in the cortex at layer II-III as well as in the hippocampus.

Microglia synapse engulfment: Microglia engulfment was conducted using Imaris software 9.6.0 version (BitPlane). At least ten individual Iba+ cells per animal were reconstructed automatically in a stack of 5 µm. On each scanned section, each microglia was 3D reconstructed using the rendered surface feature and used as a mask on vGut and vGat channels and the spot function was used to identify the positive signals (spheres). The average intensity of five ROIs selected in the background of a random subset of images was used to define the threshold in each channel of the spheres, and used in all the images. Spheres that were not fully engulfed were manually removed. Spheres were assessed on the CD68 channel to evaluate colocalization into phagocytic lysosomes. The CD68 channel was further masked by the cell surface and the volume was automatically reconstructed to identify the CD68 volume per cell.

Neurotrace positive Cell count and cell death quantification : Neurotrace (NT) 435/455 positive cell were quantified using Fiji (ImageJ, v.1.52 h) on three individual section per mouse. This

was carried out manually by a blinded investigator. To check for the viability of those neuron, activated cleaved caspase 3 double positive cells were quantified using Fiji (ImageJ, v.1.52 h) on three individual section per mouse.

Statistical analysis

All results are given as mean ± standard error of the mean (SEM), unless otherwise stated. Prism software (GraphPad, version 9) was used for statistical analysis. All datasets were initially tested for normality using the Shapiro-Wilk test. Parametric and non-parametric tests were used accordingly and indicated. In all analyses $p < 0.05$ was considered statistically significant and all significance levels are indicated in the figure legends as follows: *$p < 0.05$; **$p < 0.01$; ***$p < 0.001$.

Acknowledgements

The authors would like to thank Bernadette Fiedler for excellent technical assistance, XiaoQian Ye for help with Matlab as well as Dana Matzek and Bianca Stahr for animal husbandry. We also thank the Core Bioimaging Facility of the Biomedical Center for their support and confocal imaging systems.

Funding declaration:

FMB is supported by grants from the Deutsche Forschungsgemeinschaft (DFG): SFB 870 Project ID 118803580; TRR274 Project ID 408885537; Munich Center for Systems Neurology (SyNergy; EXC 2145 / ID 390857198).

VVS is supported by a post-doctoral fellowship from the Humboldt foundation.

Author contributions:

Design of experiments: FB, MC, JM

Surgical procedures: MC, JM

Data collection and analysis: MC,JM,CD,LJ,SPD, VVS

Figures: FB; SPD

Manuscript writing: FB, MC. All authors validated the final version of the manuscript.

Ethics approval

All procedures were performed in accordance with the Regierung von Oberbayern under the protocol number 55.2-2532.Vet_02-20-164.

Competing interests: The authors declare no competing interests.

Data and materials availability: All datasets used and/or analyzed in this present study are available from the corresponding author upon request.

References

[1] Dewan, M. C., Rattani, A., Gupta, S., Baticulon, R. E., Hung, Y. C., Punchak, M., Agrawal, A., Adeleye, A. O., Shrime, M. G., Rubiano, A. M., Rosenfeld, J. V., & Park, K. B. (2018). Estimating the global incidence of traumatic brain injury. Journal of neurosurgery, 130(4), 1080–1097. Doi:10.3171/2017.10.JNS17352

[2] Harmon, K. G., Drezner, J. A., Gammons, M., Guskiewicz, K. M., Halstead, M., Herring, S. A., Kutcher, J. S., Pana, A., Putukian, M., & Roberts, W. O. (2013). American Medical Society for Sports Medicine position statement: concussion in sport. British journal of sports medicine, 47(1), 15–26. Doi:10.1136/bjsports-2012-091941

[3] Faul, M., & Coronado, V. (2015). Epidemiology of traumatic brain injury. Handbook of clinical neurology, 127, 3–13. Doi:10.1016/B978-0-444-52892-6.00001-5

[4] McCrea, M., Guskiewicz, K. M., Marshall, S. W., Barr, W., Randolph, C., Cantu, R. C., Onate, J. A., Yang, J., & Kelly, J. P. (2003). Acute effects and recovery time following concussion in collegiate football players: the NCAA Concussion Study. JAMA, 290(19), 2556–2563. Doi: 10.1001/jama.290.19.2556

[5] McMahon, P., Hricik, A., Yue, J. K., Puccio, A. M., Inoue, T., Lingsma, H. F., Beers, S. R., Gordon, W. A., Valadka, A. B., Manley, G. T., Okonkwo, D. O., & TRACK-TBI Investigators (2014). Symptomatology and functional outcome in mild traumatic brain injury: results from the prospective TRACK-TBI study. Journal of neurotrauma, 31(1), 26–33. Doi:10.1089/neu.2013.2984

[6] Laurer, H. L., Bareyre, F. M., Lee, V. M., Trojanowski, J. Q., Longhi, L., Hoover, R., Saatman, K. E., Raghupathi, R., Hoshino, S., Grady, M. S., & McIntosh, T. K. (2001). Mild head injury increasing the brain's vulnerability to a second concussive impact. Journal of neurosurgery, 95(5), 859–870. Doi:10.3171/jns.2001.95.5.0859

[7] Smith, D. W., Myer, G. D., Currie, D. W., Comstock, R. D., Clark, J. F., & Bailes, J. E. (2013). Altitude Modulates Concussion Incidence: Implications for Optimizing Brain Compliance to Prevent Brain Injury in Athletes. Orthopaedic journal of sports medicine, 1(6), 2325967113511588. Doi:10.1177/2325967113511588

[8] Wilson, L., Stewart, W., Dams-O'Connor, K., Diaz-Arrastia, R., Horton, L., Menon, D. K., & Polinder, S. (2017). The chronic and evolving neurological consequences of traumatic brain injury. The Lancet. Neurology, 16(10), 813–825. Doi:10.1016/S1474-4422(17)30279-X

[9] Ntikas, M., Binkofski, F., Shah, N. J., & Ietswaart, M. (2022). Repeated Sub-Concussive Impacts and the Negative Effects of Contact Sports on Cognition and Brain Integrity. International journal of environmental research and public health, 19(12), 7098. Doi:10.3390/ijerph19127098

[10] Bolton-Hall, A. N., Hubbard, W. B., & Saatman, K. E. (2019). Experimental Designs for Repeated Mild Traumatic Brain Injury: Challenges and Considerations. Journal of neurotrauma, 36(8), 1203–1221. Doi:10.1089/neu.2018.6096

[11] Marar, M., McIlvain, N. M., Fields, S. K., & Comstock, R. D. (2012). Epidemiology of concussions among United States high school athletes in 20 sports. The American journal of sports medicine, 40(4), 747–755. Doi:10.1177/0363546511435626

[12] Slobounov, S., Slobounov, E., Sebastianelli, W., Cao, C., & Newell, K. (2007). Differential rate of recovery in athletes after first and second concussion episodes. Neurosurgery, 61(2), 338–344. Doi:10.1227/01.NEU.0000280001.03578.FF

[13] McAllister, T., & McCrea, M. (2017). Long-Term Cognitive and Neuropsychiatric Consequences of Repetitive Concussion and Head-Impact Exposure. Journal of athletic training, 52(3), 309–317. Doi:10.4085/1062-6050-52.1.14

[14] Petraglia, A. L., Plog, B. A., Dayawansa, S., Chen, M., Dashnaw, M. L., Czerniecka, K., Walker, C. T., Viterise, T., Hyrien, O., Iliff, J. J., Deane, R., Nedergaard, M., & Huang, J. H. (2014). The spectrum of neurobehavioral sequelae after repetitive mild traumatic brain injury: a novel mouse model of chronic traumatic encephalopathy. Journal of neurotrauma, 31(13), 1211–1224. Doi: 10.1089/neu.2013.3255

[15] McAteer, K. M., Corrigan, F., Thornton, E., Turner, R. J., & Vink, R. (2016). Short and Long Term Behavioral and Pathological Changes in a Novel Rodent Model of Repetitive Mild Traumatic Brain Injury. PloS one, 11(8), e0160220. Doi:10.1371/journal.pone.0160220

[16] Mountney, A., Boutté, A. M., Cartagena, C. M., Flerlage, W. F., Johnson, W. D., Rho, C., Lu, X. C., Yarnell, A., Marcsisin, S., Sousa, J., Vuong, C., Zottig, V., Leung, L. Y., Deng-Bryant, Y., Gilsdorf, J., Tortella, F. C., & Shear, D. A. (2017). Functional and Molecular Correlates after Single and Repeated Rat Closed-Head Concussion: Indices of Vulnerability after Brain Injury. Journal of neurotrauma, 34(19), 2768–2789. Doi:10.1089/neu.2016.4679

[17] Mouzon, B. C., Bachmeier, C., Ferro, A., Ojo, J. O., Crynen, G., Acker, C. M., Davies, P., Mullan, M., Stewart, W., & Crawford, F. (2014). Chronic neuropathological and neurobehavioral changes in a repetitive mild traumatic brain injury model. Annals of neurology, 75(2), 241–254. Doi:10.1002/ana.24064

[18] Bolton, A. N., & Saatman, K. E. (2014). Regional neurodegeneration and gliosis are amplified by mild traumatic brain injury repeated at 24-hour intervals. Journal of neuropathology and experimental neurology, 73(10), 933–947. Doi:10.1097/NEN.0000000000000115

[19] Rochefort, N. L., & Konnerth, A. (2012). Dendritic spines: from structure to in vivo function. EMBO reports, 13(8), 699–708. Doi:10.1038/embor.2012.102

[20] Gipson, C. D., & Olive, M. F. (2017). Structural and functional plasticity of dendritic spines - root or result of behavior?. Genes, brain, and behavior, 16(1), 101–117. Doi:10.1111/gbb.12324

[21] Empl, L., Chovsepian, A., Chahin, M., Kan, W. Y. V., Fourneau, J., Van Steenbergen, V., Weidinger, S., Marcantoni, M., Ghanem, A., Bradley, P., Conzelmann, K. K., Cai, R., Ghasemigharagoz, A., Ertürk, A., Wagner, I., Kreutzfeldt, M., Merkler, D., Liebscher, S., & Bareyre, F. M. (2022). Selective plasticity of callosal neurons in the adult contralesional cortex following murine traumatic brain injury. Nature communications, 13(1), 2659. Doi:10.1038/s41467-022-29992-0

[22] Lee, E., & Chung, W. S. (2019). Glial Control of Synapse Number in Healthy and Diseased Brain. Frontiers in cellular neuroscience, 13, 42. Doi:10.3389/fncel.2019.00042

[23] Favuzzi, E., Huang, S., Saldi, G. A., Binan, L., Ibrahim, L. A., Fernández-Otero, M., Cao, Y., Zeine, A., Sefah, A., Zheng, K., Xu, Q., Khlestova, E., Farhi, S. L., Bonneau, R., Datta, S. R., Stevens, B., & Fishell, G. (2021). GABA-receptive microglia selectively sculpt developing inhibitory circuits. Cell, 184(15), 4048–4063.e32. doi:10.1016/j.cell.2021.06.018

[24] Filipello, F., Morini, R., Corradini, I., Zerbi, V., Canzi, A., Michalski, B., Erreni, M., Markicevic, M., Starvaggi-Cucuzza, C., Otero, K., Piccio, L., Cignarella, F., Perrucci, F., Tamborini, M., Genua, M., Rajendran, L., Menna, E., Vetrano, S., Fahnestock, M., Paolicelli, R. C., Matteoli, M. (2018). The Microglial Innate Immune Receptor TREM2 Is Required for Synapse Elimination and Normal Brain Connectivity. Immunity, 48(5), 979–991.e8. doi:10.1016/j.immuni.2018.04.016

[25] Lehrman, E. K., Wilton, D. K., Litvina, E. Y., Welsh, C. A., Chang, S. T., Frouin, A., Walker, A. J., Heller, M. D., Umemori, H., Chen, C., & Stevens, B. (2018). CD47 Protects Synapses from Excess Microglia-Mediated Pruning during Development. Neuron, 100(1), 120–134.e6. doi:10.1016/j.neuron.2018.09.017

[26] Paolicelli, R. C., Bolasco, G., Pagani, F., Maggi, L., Scianni, M., Panzanelli, P., Giustetto, M., Ferreira, T. A., Guiducci, E., Dumas, L., Ragozzino, D., & Gross, C. T. (2011). Synaptic pruning by microglia is necessary for normal brain development. Science (New York, N.Y.), 333(6048), 1456–1458. Doi:10.1126/science.1202529

[27] Schafer, D. P., Lehrman, E. K., Kautzman, A. G., Koyama, R., Mardinly, A. R., Yamasaki, R., Ransohoff, R. M., Greenberg, M. E., Barres, B. A., & Stevens, B. (2012). Microglia sculpt postnatal neural circuits in an activity and complement-dependent manner. Neuron, 74(4), 691–705. Doi:10.1016/j.neuron.2012.03.026

[28] Wang, C., Yue, H., Hu, Z., Shen, Y., Ma, J., Li, J., Wang, X. D., Wang, L., Sun, B., Shi, P., Wang, L., & Gu, Y. (2020). Microglia mediate forgetting via complement-dependent synaptic elimination. Science (New York, N.Y.), 367(6478), 688–694. Doi:10.1126/science.aaz2288

[29] Heindl, S., Gesierich, B., Benakis, C., Llovera, G., Duering, M., & Liesz, A. (2018). Automated Morphological Analysis of Microglia After Stroke. Frontiers in cellular neuroscience, 12, 106. Doi:10.3389/fncel.2018.00106

[30] Loy, K., Fourneau, J., Meng, N., Denecke, C., Locatelli, G., & Bareyre, F. M. (2021). Semaphorin 7A restricts serotonergic innervation and ensures recovery after spinal cord injury. Cellular and molecular life sciences : CMLS, 78(6), 2911–2927. Doi:10.1007/s00018-020-03682-w

[31] Kraeuter, A. K., Guest, P. C., & Sarnyai, Z. (2019). The Y-Maze for Assessment of Spatial Working and Reference Memory in Mice. Methods in molecular biology (Clifton, N.J.), 1916, 105–111. Doi:10.1007/978-1-4939-8994-2_10

[32] Eakin, K., Baratz-Goldstein, R., Pick, C. G., Zindel, O., Balaban, C. D., Hoffer, M. E., Lockwood, M., Miller, J., & Hoffer, B. J. (2014). Efficacy of N-acetyl cysteine in traumatic brain injury. PloS one, 9(4), e90617. Doi:10.1371/journal.pone.0090617

[33] Wu, D. W., Shen, X. Y., Dong, Q., Wang, S. P., Cheng, Z. H., & Zhang, S. J. (2000). Space medicine & medical engineering, 13(4), 244–248.

[34] Can, A., Dao, D. T., Terrillion, C. E., Piantadosi, S. C., Bhat, S., & Gould, T. D. (2012). The tail suspension test. Journal of visualized experiments : JoVE, (59), e3769. Doi:10.3791/3769

[35] Creed, J. A., DiLeonardi, A. M., Fox, D. P., Tessler, A. R., & Raghupathi, R. (2011). Concussive brain trauma in the mouse results in acute cognitive deficits and sustained impairment of axonal function. Journal of neurotrauma, 28(4), 547–563. Doi:10.1089/neu.2010.1729

[36] Huh, J. W., Widing, A. G., & Raghupathi, R. (2008). Midline brain injury in the immature rat induces sustained cognitive deficits, bihemispheric axonal injury and neurodegeneration. Experimental neurology, 213(1), 84–92. Doi:10.1016/j.expneurol.2008.05.009

[37] Hähnel, S., Stippich, C., Weber, I., Darm, H., Schill, T., Jost, J., Friedmann, B., Heiland, S., Blatow, M., & Meyding-Lamadé, U. (2008). Prevalence of cerebral microhemorrhages in amateur boxers as detected by 3T MR imaging. AJNR. American journal of neuroradiology, 29(2), 388–391. Doi:10.3174/ajnr.A0799

[38] Koerte, I. K., Lin, A. P., Willems, A., Muehlmann, M., Hufschmidt, J., Coleman, M. J., Green, I., Liao, H., Tate, D. F., Wilde, E. A., Pasternak, O., Bouix, S., Rathi, Y., Bigler, E. D., Stern, R. A., & Shenton, M. E. (2015). A review of neuroimaging findings in repetitive brain trauma. Brain pathology (Zurich, Switzerland), 25(3), 318–349. Doi:10.1111/bpa.12249

[39] Shultz, S. R., Bao, F., Omana, V., Chiu, C., Brown, A., & Cain, D. P. (2012). Repeated mild lateral fluid percussion brain injury in the rat causes cumulative long-term behavioral impairments, neuroinflammation, and cortical loss in an animal model of repeated concussion. Journal of neurotrauma, 29(2), 281–294. Doi:10.1089/neu.2011.2123

[40] Bennett, R. E., Mac Donald, C. L., & Brody, D. L. (2012). Diffusion tensor imaging detects axonal injury in a mouse model of repetitive closed-skull traumatic brain injury. Neuroscience letters, 513(2), 160–165. Doi:10.1016/j.neulet.2012.02.024

[41] Thibault, L. E., Meaney, D. F., Anderson, B. J., & Marmarou, A. (1992). Biomechanical aspects of a fluid percussion model of brain injury. Journal of neurotrauma, 9(4), 311–322. Doi:10.1089/neu.1992.9.311

[42] Mouzon, B., Chaytow, H., Crynen, G., Bachmeier, C., Stewart, J., Mullan, M., Stewart, W., & Crawford, F. (2012). Repetitive mild traumatic brain injury in a mouse model produces learning and memory deficits accompanied by histological changes. Journal of neurotrauma, 29(18), 2761–2773. Doi :10.1089/neu.2012.2498

[43] Witkowski, E. D., Gao, Y., Gavsyuk, A. F., Maor, I., DeWalt, G. J., Eldred, W. D., Mizrahi, A., & Davison, I. G. (2019). Rapid Changes in Synaptic Strength After Mild Traumatic Brain Injury. Frontiers in cellular neuroscience, 13, 166. Doi:10.3389/fncel.2019.00166

[44] McDaid, J., Briggs, C. A., Barrington, N. M., Peterson, D. A., Kozlowski, D. A., & Stutzmann, G. E. (2021). Sustained Hippocampal Synaptic Pathophysiology Following Single and Repeated Closed-Head Concussive Impacts. Frontiers in cellular neuroscience, 15, 652721. Doi:10.3389/fncel.2021.652721

[45] Langlois, L. D., Selvaraj, P., Simmons, S. C., Gouty, S., Zhang, Y., & Nugent, F. S. (2022). Repetitive mild traumatic brain injury induces persistent alterations in spontaneous synaptic activity of hippocampal CA1 pyramidal neurons. IBRO neuroscience reports, 12, 157–162. Doi :10.1016/j.ibneur.2022.02.002

[46] Chung, W. S., Clarke, L. E., Wang, G. X., Stafford, B. K., Sher, A., Chakraborty, C., Joung, J., Foo, L. C., Thompson, A., Chen, C., Smith, S. J., & Barres, B. A. (2013). Astrocytes mediate synapse elimination through MEGF10 and MERTK pathways. Nature, 504(7480), 394–400. Doi:10.1038/nature12776

[47] Freeman M. R. (2006). Sculpting the nervous system: glial control of neuronal development. Current opinion in neurobiology, 16(1), 119–125. Doi:10.1016/j.conb.2005.12.004

[48] Neniskyte, U., & Gross, C. T. (2017). Errant gardeners: glial-cell-dependent synaptic pruning and neurodevelopmental disorders. Nature reviews. Neuroscience, 18(11), 658–670. Doi:10.1038/nrn.2017.110

[49] Vainchtein, I. D., Chin, G., Cho, F. S., Kelley, K. W., Miller, J. G., Chien, E. C., Liddelow, S. A., Nguyen, P. T., Nakao-Inoue, H., Dorman, L. C., Akil, O., Joshita, S., Barres, B. A., Paz, J. T., Molofsky, A. B., & Molofsky, A. V. (2018). Astrocyte-derived interleukin-33 promotes microglial synapse engulfment and neural circuit development. Science (New York, N.Y.), 359(6381), 1269–1273. Doi:10.1126/science.aal3589

[50] Alawieh, A., Chalhoub, R. M., Mallah, K., Langley, E. F., York, M., Broome, H., Couch, C., Adkins, D., & Tomlinson, S. (2021). Complement Drives Synaptic Degeneration and Progressive Cognitive Decline in the Chronic Phase after Traumatic Brain Injury. The Journal of neuroscience : the official journal of the Society for Neuroscience, 41(8), 1830–1843. Doi:10.1523/JNEUROSCI.1734-20.2020

[51] Zhang, M. R., Red, S. D., Lin, A. H., Patel, S. S., & Sereno, A. B. (2013). Evidence of cognitive dysfunction after soccer playing with ball heading using a novel tablet-based approach. PloS one, 8(2), e57364. Doi:10.1371/journal.pone.0057364

[52] Koerte, I. K., Nichols, E., Tripodis, Y., Schultz, V., Lehner, S., Igbinoba, R., Chuang, A. Z., Mayinger, M., Klier, E. M., Muehlmann, M., Kaufmann, D., Lepage, C., Heinen, F., Schulte-Körne, G., Zafonte, R., Shenton, M. E., & Sereno, A. B. (2017). Impaired Cognitive Performance in Youth Athletes Exposed to Repetitive Head Impacts. Journal of neurotrauma, 34(16), 2389–2395. Doi:10.1089/neu.2016.4960

[53] Alosco, M. L., Tripodis, Y., Baucom, Z. H., Mez, J., Stein, T. D., Martin, B., Haller, O., Conneely, S., McClean, M., Nosheny, R., Mackin, S., McKee, A. C., Weiner, M. W., & Stern, R. A. (2020). Late contributions of repetitive head impacts and TBI to depression symptoms and cognition. Neurology, 95(7), e793–e804. Doi:10.1212/WNL.0000000000010040

[54] Honig, M. G., Dorian, C. C., Worthen, J. D., Micetich, A. C., Mulder, I. A., Sanchez, K. B., Pierce, W. F., Del Mar, N. A., & Reiner, A. (2021). Progressive long-term spatial memory loss following repeat concussive and subconcussive brain injury in mice, associated with dorsal hippocampal neuron loss, microglial phenotype shift, and vascular abnormalities. The European journal of neuroscience, 54(5), 5844–5879. Doi:10.1111/ejn.14711

[55] Dix, S. L., & Aggleton, J. P. (1999). Extending the spontaneous preference test of recognition: evidence of object-location and object-context recognition. Behavioural brain research, 99(2), 191–200. Doi:10.1016/s0166-4328(98)00079-5

[56] Friard, O. and Gamba, M. (2016) BORIS: a free, versatile open-source event-logging software for video/audio coding and live observations. Methods Ecol Evol, 7: 1325–1330. Doi: 10.1111/2041-210X.12584

[57] Metz, G. A., & Whishaw, I. Q. (2009). The ladder rung walking task: a scoring system and its practical application. Journal of visualized experiments: JoVE, (28), 1204. Doi:10.3791/1204

Discussion

From behavioural impairments to neuronal circuits adaptation as well as the involvement of microglia as an emerging protagonist of the functional changes associated with traumatic brain injury (TBI), the previous studies have, each, led to unravel certain aspects of the complexity behind the pathophysiology of TBI.

1- Refinement and implementation of appropriate behavioural testing to assess disturbances following traumatic brain injury in rodents

As a major cause of morbidity and mortality, TBI has been held accountable for the development of long-term impairments affecting, to some extent and permanently, patient's behaviour. Gaining insights into the brain's function requires an accurate evaluation of the behaviour. Experimentally, it is well known that motor dysfunction following traumatic brain injury – and even more so following mild injuries - is very difficult to detect with the current behavioural tests, particularly when mice are used as experimental animals (A. Guillot & Collet, 2008). It often also comes with the use of onerous and intricate equipment, which restrain its accessibility to certain scientific communities and reveals to be time consuming for the experimenter. Therefore, we have been able, thanks to the emergence of artificial intelligence and deep-learning paradigms, to implement our own "open-source deep learning-based toolbox" named ALMA (Automated Limb Motion Analysis) in our study 1 (study 1: Aljović et al., 2022). ALMA toolbox has not only resolved the problem encountered in terms of rodents' locomotion recording but also has simplified and automatized the analysis part. The ALMA toolbox has introduced a new and affordable way to track rodents' locomotion and gaits and enables refined analyses with significant reduced costs (study 1: Aljović et al., 2022).
We used ALMA in two contexts: the treadmill and the ladder rung. Treadmill is regularly used as a locomotion and gait analysis test and demonstrates to be reproducible as it allows the experimenter to apply fixed speed settings to a group of rodents (Pereira et al., 2006). For gait analysis, the rodents' limb joints are usually highlighted with marks in order to analyse their kinematic (Pereira et al., 2006). The labelling procedure have revealed to be a burden for the experimenter. The marks are intrusive, constantly being removed and requires for the rodent to be shaved which can cause an extra level of stress that could already alter the behaviour state, priorly to the round of experiments. The mark should also be put in a precise and constant position as it labels bilaterally the rodent's key joints which serves for longitudinal assessment of their locomotion. The use of deep learning strategies with DeepLabCut has resolved this issue by allowing a marker-free monitoring of the limb's joint as well as tracking their locomotion using DLC24 (Mathis et al., 2018). From the monitoring, ALMA extracts coordinates used to evaluate gait features of locomotion. The data support the versatility offered by

the ALMA toolbox. Not only it is compatible with DeepLabCut, but it is also compatible with other systems such as VICON, MARS, DANNCE, SLEAP and DeepPoseKit. The implementation brought to DeepLabCut by the ALMA toolbox has, after a pivotal session of model training, been able to define 44 hindlimb's parameters with an important reliability. Those parameters, originating from limbs and joints coordinates recorded with a single camera, are thereafter used to characterise gait locomotion patterns demonstrating the robustness of the analysis. Compared to established kinematic instruments such as Catwalk which are expensive and involve additional manual manipulation to extract the parameters, the ALMA toolbox is cost effective and user friendly (study 1: Aljović et al., 2022). In addition, the ALMA toolbox can allow tracking of gait parameters with a 2D side-view tracking including step height, joint angle which is impossible with a bottom view tracking as in the case of catwalk (Hamers, Koopmans, & Joosten, 2006). The ALMA toolbox also goes beyond kinematics analysis as it constitutes the first analysis of footfalls on regular and irregular ladder rung that is automated and provides crucial insights into paw placements tasks (study 1: Aljović et al., 2022). The toolbox is also adaptable and can focus on the forelimb, hindlimb and forelimb synchronisation. ALMA can also be largely used in rodents (study 1: Aljović et al., 2022).

Not only ALMA is providing a way to analyse locomotion patterns and the gait of control mice, but it can also be applied to monitor mice or globally rodents presenting deficits, such as traumatic brain injury. As previously mentioned, it has been very laborious to pick up any deficit following TBI, as severe as it could be, and especially when the impairments are considered subtle (Shultz, MacFabe, Foley, Taylor, & Cain, 2012; Zhao, Zhang, Li, Li, & Xie, 2023). The analysis of the stride length, the step height or the dynamic time warping (DTW) distance as gait coordinates, identified deficits at a very acute stage of the injury (day 1) and thereafter showed a complete recovery, similar to baseline at day 10.

However, in our study, gait analysis was based on the hindlimb only, the forelimbs were not analysed. ALMA can be broadened in order to improve the interpretability of the data while simultaneously avoiding information loss (Jolliffe & Cadima, 2016; Dever et al., 2022).

To conclude, ALMA has proven not only to provide a new reliable way to assess locomotion in an automated manner but also has brought a more standardised protocol to apply for behavioural testing, accessible to anyone at low cost (study 1: Aljović et al., 2022). ALMA helps reducing a maximum the involvement of the experimenter to remove any potential biases. It allows, as well, the prediction of disease onset in the case of Experimental autoimmune encephalomyelitis (EAE) (study 1: Aljović et al., 2022) and detects subtle impairments on acute TBI where conventional scoring methods struggle to.

As we have seen, ALMA has been able to pick up the remarkable acute recovery after moderate TBI. In our publication number 3 (study 3: Chahin M. et al.), we were interested in the locomotor behaviour of mice following a milder version of the TBI, that we also call concussions. In

this case, conventional investigations methods were carried in the acute and the subacute phase following concussions (Blennow et al., 2016; Barone et al., 2024).

Our concussion model did not induce any macroscopic changes: no skull fracture, no haemorrhage, no invasive lesion and therefore no direct cell death. Our model aims to come as close as possible to the concussions observed in humans, which often do not trigger any changes that can be picked up by imaging (Blennow et al., 2016) and might in some instances trigger some loss of consciousness. Mice undergoing a simple or repetitive concussions display minimal or sometimes, depending on the TBI model, no motor behaviour impairments (study 3: Chahin M. et al.) which goes along with previous and current studies (Bodnar, Roberts, Higgins, & Bachstetter, 2019b; Anderson, Heitger, & Macleod, 2006; Xiong, Mahmood, & Chopp, 2013; Blennow et al., 2016). However, our repetitive concussions model has shown cognitive disturbances particularly in spatial memory as well as related anxiety behaviour, revealed to be long-lasting (study 3: Chahin M. et al.), also shown in previous studies (Vasudevan, Glass, & Packel, 2014). Those characteristics are frequently noticed in individuals experiencing repetitive head impacts, such as athletes or military forces, who may undergo memory loss or neuropsychological alterations in the aftermath of repeated concussions (Petrie et al., 2014; Baxendale et al., 2019; Van Praag et al., 2019; Halalmeh et al., 2024; Complication Of Mild Traumatic Brain Injury In Veterans And Military Personnel: A Systematic Review, 2013; Younger, 2023; Karr et al., 2014). Most importantly, the impairments observed on mice subjected to concussions and its repetition demonstrate the reduction and sometimes the loss of any adaptive behaviour and furthermore learning behaviour following an environmental change (Vasudevan, Glass, & Packel, 2014). This loss of adaptation highlights the burden that a rise in concussion incidence is weighting on our society with an increasing need in caretakers and psychotherapist (Blennow et al., 2016; Van Der Vlegel et al., 2021). It is therefore interesting to see that our animal model closely mimics the human situation which allow us to conclude that our model is well suited to study cellular perturbations triggered by concussions.

However, the intricacy of the cognitive behaviours, displayed by patients subjected to concussion, implies the development of better tools to assess it on animal models. Single behaviour tests reveal to not be enough to describe a cognitive state which requires the merging of different tests to characterise the cognitive level of the rodents in that case (Tanila, 2018). One potential advancement stemming from research studies 1 and 3 could involve utilizing the ALMA toolbox for analysing motor and gait behaviour after repetitive concussions. Additionally, we may consider creating additional toolboxes for artificial intelligence (AI)-driven cognitive test analysis, such as stress-related behaviour testing or spatial memory assessment (study 1: Aljović et al., 2022; study 3: Chahin M. et al.; Lorsch et al., 2021; Kuo et al., 2022).

The perception and expectation of what mild TBI and concussion "look like" in animal models constitutes another challenge inherent in research of repetitive mild traumatic brain injury and repeated concussion. While repeated mild TBI and repeated concussion can induce long-lasting

neurological consequences clinically, the majority of individuals who suffer from mild TBI and concussion recover within days or may exhibit no notable physiological or behavioural changes. Therefore, one could debate whether an ideal model of mild TBI or concussion is one that produces consistent, albeit mild, deficits in all subjects or one that yields no damage or symptoms in most subjects with only a subset of animals showing pathology/dysfunction, more akin to the clinical situation. If mild TBI and concussion models yield only small, transient changes in a few pathological or behavioural parameters, studies would likely produce large quantities of negative data, much of which might go unpublished. This increases the chance of positive published findings reflecting type I error and, alternatively, may bias researchers toward models that produce consistent or easily measured changes.

While there are many challenges to overcome, such as complex experimental design and variability across injury models, the field of mild TBI and concussive injury can make great strides with logically formulated injury paradigms and inclusion of both acute and long-term outcome measures. Proper interpretation of the effects of repeated mild TBI and repeated concussion require careful comparisons to appropriate controls. In this way, discovery of fundamental aspects of the molecular, cellular, and behavioural responses to mild TBI and concussion TBI can be accelerated, guiding prevention and treatment efforts.

2- Adaptations of circuit plasticity and connectivity following traumatic brain injury in rodents

The effect of TBI on neuron is rather clear, they unfortunately undergo stressful episodes which lead to disruption of their intertwined networks. Impairment of brain networks' integrity is often related to diffuse axonal Injury (DAI) and direct deafferentation due to neuronal death occurring at the time of the primary injury (Raizman et al., 2020). Interestingly enough, the brain reveals to be plastic and adaptable, leading often to the recovery of subsequently impaired functions by TBI. However, the process leading to this recovery was not properly understood. Therefore, in the publication number 2, we decided to investigate a particular neuronal network that has the specificity to link both hemispheres in a rather symmetrical manner, the trans-callosal neurons. Those neurons were subjected to a hemi-cortical lesion, directly injuring the sensorimotor cortex. This resulted in behavioural changes; Impairment of the walking pattern of those mice was seen acutely after TBI, and remodelling of the neuronal circuitry was investigated to see whether it could be related to the process observed in the following weeks (study 2: Empl et al., 2022).

No changes in terms of neuronal density or shape were noticeable in the contralesional cortex as it was spared from the impact. Similar observations were made on the site of the impact following concussion/repetitive concussion. This could be explained by the lack of invasive injury, implying no

skull fracture and no breach of the blood brain barrier (BBB) as compared to the moderate TBI lesion where a penumbra surrounds the primary injury on the ipsilesional side, as shown in study 1 and study 3 ((study 1: Aljović et al., 2022; study 3: Chahin M. et al.). When we investigated neuronal spines, we could see no changes in spine density at the different dendritic levels examined after single and repetitive concussion. In comparison, moderate TBI induced an acute reduction in dendritic spine on contralesional callosal neurons (study 2: Empl et al., 2022). The spine reduction following moderate TBI is likely related to the neuronal population studied. Indeed, the transcallosal neurons have the specificity to link both hemisphere in a symmetrical way and their axons are directly damaged by the traumatic lesion. We then investigated the morphology of those spines following moderate injury and concussions, to identify their level of maturation. The dendritic spine also displays different shape/morphology which hold important structural function within the central nervous system (Gipson & Olive, 2016). According to the nomenclature established to define spine morphology, we could see that mushroom spine and stubby spine density decreased very acutely and remained decreased after moderate TBI (Pchitskaya & Bezprozvanny, 2020; study 2: Empl et al., 2022). No variation on spine morphology was observed on non-callosal neurons indicating specificity of changes on those neurons connected to the injured area. As we investigated the effect of single and repetitive concussion on neurons, we have seen an unbalance in the spine type, with more immature spine, specifically the thin spine. In the case of moderate TBI, the maintained spines seem more mature, and the newly formed spine post TBI from the transcallosal neurons are more stable as compared to the non-callosal ones (study 2: Empl et al., 2022). The morphology of spine has always been an indicator of the level of the connection establish and of the homeostasis of the brain (Fiala, Spaček, & Harris, 2002). In term of connectivity, we observed that callosal neurons initially lost their connectivity following moderate TBI but later on the lost connections were re-established (study 2: Empl et al., 2022). In the context of concussion, and more broadly mild TBI, brain connectivity is not yet fully understood. Some studies argue for hyperconnectivity which translate paradoxically as an increase in functional connectivity where other claims an overall maintenance of the functional connectivity (Woodrow et al., 2023; Simos et al., 2022; Kim et al., 2022). The hyperconnectivity that could result from concussions, has been linked to an increase in brain metabolism leading to metabolic stress and cause the brain to be vulnerable. This vulnerability has been associated with the development of neurodegenerative condition (Hillary & Grafman, 2017).

In the context of moderate TBI, we have been able to highlight a transient reduction in neuronal activity (study 2: Empl et al., 2022). Similar outcomes have been observed, mainly using fMRI and on human patients that underwent moderate/severe TBI (Hayes, Bigler, & Verfaellie, 2016) (Xiao, Yang, Xi, & Chen, 2015). Those alteration have often been associated with neurologic and functional impairments. Injured axons participate in rupturing any “conventional communication” between neurons. (Hayes, Bigler, & Verfaellie, 2016).

Finally, we were interested in the synaptic density following repetitive concussion. We observed cortical synapses loss underneath the impact site with a more pronounced loss in the dentate gyrus of the hippocampus. Interestingly, excitatory synapses are being primarily targeted, labelled by VgluT marker (Witkowski et al., 2019), but no loss was seen for the inhibitory synapses labelled by VGAT marker, after a single or repetitive concussions. The loss is maintained overtime in case of repetitive concussion.

Following traumatic brain injury, there is an initial surge in extracellular glutamate and a subsequent decrease in glutamate uptake due to alterations in excitatory amino acid transporter (EAAT) isoform expression (McGuire et al., 2018). Shortly thereafter, reductions in NMDA receptor subunits and changes in AMPA receptor subunit composition occur. Over time, there is a sustained depression in glutamate signalling coupled with alterations in postsynaptic receptor composition, a decreased astroglia EAAT expression and shifts in the relative expression of neuronal and glial transporters (McGuire et al., 2018). GABA signalling undergoes an acute shift in receptor balance post-injury, leading to chronic dysregulation of GABAergic tone, with region-specific variations contributing to potential epileptogenesis (McGuire et al., 2018).

After experiencing traumatic brain injury, there are indications that cellular processes controlling glutamatergic and GABAergic signalling suggest a changed balance between excitation and inhibition (McGuire et al., 2018). Utilizing preclinical models allows for the direct assessment of neural circuit activity following injury (McGuire et al., 2018). The effects of TBI extend beyond the immediate site of injury, influencing various brain circuits. In cortical regions, diverse responses are observed post-injury, including alterations in firing patterns. In the hippocampus, there is a shift in the balance between excitatory and inhibitory activity, leading to impaired plasticity (McGuire et al., 2018). This disruption in excitatory/inhibitory balance persists and evolves over time. Following injuries, there is an exaggeration of GABAergic inhibition in the frontal cortex, which can be reversible, but chronic hypo-excitation indicates neuron shrinkage (McGuire et al., 2018). In the dentate gyrus, there is a gradual loss of GABAergic inhibition in the dentate gyrus, which becomes bilateral over time. Additionally post-TBI, responses to extra synaptic GABAR agonists diminish. Remodelling of hippocampal circuits after severe TBI favours excitatory inputs, tilting the balance towards excitation (McGuire et al., 2018).

3- Microglia a player not to overlook when it comes to inflammatory response following traumatic brain injury in rodents

We have seen that an impact to the brain, regardless of its severity level, triggers behavioural tampering in mice in particular cognitive deficits and in some cases locomotion impairment when the injury is more invasive (study 3: Chahin M. et al., submitted; study 1: Aljović et al., 2022).

We also have shown that TBI triggers impairment in synaptic units leading to a reduction in synapse density as well as subtle changes in dendritic spines (study 3: Chahin M. et al., submitted; study 2: Empl et al., 2022). Previous studies have linked synapses disappearance and their loss of function with the development of neurodegenerative diseases such AD or PD as well as neurodevelopmental diseases such as schizophrenia (Sheng, Sabatini, & Südhof, 2012; Griffiths & Grant, 2023; Subramanian, Savage, & Tremblay, 2020; Holmes et al., 2024; Obi-Nagata, Temma, & Hayashi-Takagi, 2019; Howes & Onwordi, 2023). Neuroinflammatory response, seen in cases of TBI, participates or has been held accountable for the loss of synapses (Zheng et al., 2022). In this context, we looked at the microglia cells, a significant cell type of the central nervous system that may be accountable for the synaptic loss. Microglia have been shown to be responsible for circuit refinement, during development, by engulfing synapses (Andoh & Koyama, 2021; T. Li et al., 2020; Kettenmann, Kirchhoff, & Verkhratsky, 2013).

Therefore, we directed our investigation toward this category of glial cells, in order to understand their responsibility and the mechanism behind the loss of synapses. First, we identified an increase in Iba1 positive cells, likely microglia, transient after a single concussion and long-lasting following repetitive concussion. Using the automated morphological pipeline developed by Heindl et al., we then observed that following concussion, microglia displayed an activated morphology (Heindl et al., 2018). They evolved from a ramified to a more amoeboid body (Wolf et al., 2017). However, the activation of those microglial cells revealed to be injury dependent. Their activation was maintained overtime following the repetitive concussions as compared to a single concussion after which microglia activation faded overtime. Not only the microglia cells evolve in term of shape, but they also acquire certain functions associated to the morphology they adopt (Nimmerjahn, Kirchhoff, & Helmchen, 2005). This change in morphology is usually associated with phagocytosis features subsequently to their migration to the site of injury (Leyh et al., 2021). In order to determine their level of activation and therefore their phagocytic level, microglia cells were co-labelled with a lysosomal marker, Cluster of Differentiation 68 marker (CD68). The increase and maintenance over time in CD68 positive lysosomes is seen following repetitive concussion and is in line with microglia activation. We have been also able to demonstrate that microglia cells were responsible for the loss of excitatory synaptic input via engulfment. Microglia engulfed, in a higher rate, pre-synaptic elements following repetitive concussion. However, a major characteristic of this engulfment is its specificity in targeting a certain type of synapses. Indeed, microglia cells will engulf preferentially excitatory synapses labelled with VGlut in the cortex as well as in the hippocampus, after repetitive concussion. After a single concussion, similar observations were made however the time extent of the engulfment was rather limited.

During development, microglia are essential as they are responsible for permanent circuit refinement (T. Li et al., 2020; Wu, Dissing-Olesen, MacVicar, & Stevens, 2015; Wu et al., 2015; C. Li et al., 2022). As previously mentioned, the lack of appropriate synaptic pruning, notably by microglia, could be one

potential lead to explain certain neurodevelopmental conditions that persist through life. For instance ASD, displaying an overabundance of synapses with atypical network functions, may be explained by a deficiency in synaptic pruning originating from the mutations of genes responsible for synaptic formation and structure (Bourgeron, 2009; Sheng, Sabatini, & Südhof, 2012; Griffiths & Grant, 2023; Subramanian, Savage, & Tremblay, 2020; Holmes et al., 2024; Obi-Nagata, Temma, & Hayashi-Takagi, 2019; Howes & Onwordi, 2023). This synapse excess leads to irregular functional connectivity. In a 2021 study, Pagani et al. have been able to show a subtle mechanism involving mammalian target of rapamycin (mTOR), a key factor in macro-autophagy, that would be responsible for the lack of synaptic pruning leading then to abnormal signalling and finally to the development of ASD (Pagani et al., 2021). The importance of synaptic pruning in the development of neurological disorders has also been demonstrated by Tang et al., in an innovative study, also exposing the responsibility of impaired mTOR in the deficit of synaptic pruning (Tang et al., 2014).

In the adult brain, the alteration of microglia functions can lead to an excessive engulfment contributing to brain related pathologies such as PD or AD (Colonna and Butovsky, 2017; Li and Barres, 2018; Prinz et al., 2019). The microglia phagocytosis process of the synapses, also referred as synaptic pruning/ engulfment, is possible through receptor present externally on microglia, such as the complement cascade C1q or the complement component 3 receptor (CR3) (Werneburg et al., 2020; Schafer et al., 2012; Hong et al., 2016), TREM2 (Jay et al., 2019), CXRCR1 (Gunner et al., 2019). For example, IL-33, a transcriptional regulator, is thought to promote microglia engulfment of synapses during development (Sun et al., 2021). The interest on the complement cascade has been constantly increasing over the years, demonstrating not only its importance in the innate immune system (Warwick, Keyes, Woodruff, & Usachev, 2021) but also in the central nervous system as a non-negligible player in mediating synaptic pruning/engulfment (Werneburg et al., 2020; Schafer et al., 2012; Hong et al., 2016). As an example, synapses expressing C3 will be recognized by C3R (C3 receptor), present on microglia, that will trigger the engulfment. Deficit in the complement cascade could lead to a deficiency in synapse engulfment leading to inflammatory responses in the CNS and the development of degenerative pathologies (Schafer et al., 2012; Hong et al., 2016). Similar outcomes are expected with a deficit in microglia which, in a different way, would lead to an excessive or a lack in synaptic engulfment leading to cognitive decline, as seen in our concussion model (Alawieh et al., 2020). To prevent any abnormal synaptic engulfment, complement cascade constitute a potential target. In 2020, Werneburg et al. blocked synaptic C3 using an adeno-associated virus to overexpress complement inhibitor Crry, which inhibits C3 (Werneburg et al., 2020). This led to the restoration and the protection of the visual functions.

In future experiments, this approach could be a potential way to limit phagocytic microglia to overly engulf synapses and participate in the attenuation of the cognitive consequences of repetitive concussion.

Conclusions and remarks

While certain questions are still unanswered, the studies presented in this thesis have helped us understand the intricacy of what traumatic brain injury is and have outlined how further studies will help find new strategies and therapies to alleviate the consequences of it. The development of new analysis with the ALMA toolbox brought us a step forward in the evaluation of the behaviour of TBI models. The analysis of the connectivity of neuronal circuits highlighted the importance of brain rewiring and its adaptability in the recovery process following moderate TBI. Finally, investigating the impact of repetitive concussion versus a single concussion on the brain has led us to highlight the loss of excitatory synapses in key areas of the brain, notably the hippocampus. This excessive loss of synapses was mediated through activated microglia over a long period of time. In addition, maintained cognitive impairments and anxiety-related behaviour were pinpointed which could correlate with the loss of synapses and the activation of those microglia. However, the mechanisms leading to those pathophysiological changes are yet not fully elucidated.

Thus far no therapies nor treatment were found to alleviate the related symptoms. The lack in proper diagnosis, notably linked to a lack of proper biomarkers, hinders the chance as well to treat properly a patient. Prevention remains, so far, the only way to reduce the numbers of victims. Therefore, the identification of the cellular and molecular mechanisms contributing physiologically to the brain dysfunction following repetitive concussion is significant and paramount to further our knowledge on the subject.

References

Adams, J. H., Doyle, D., Ford, I., Gennarelli, T. A., Graham, D. I., & Mclellan, D. R. (1989). Diffuse axonal injury in head injury: Definition, diagnosis and grading. *Histopathology*, *15*(1), 49–59. https://doi.org/10.1111/j.1365-2559.1989.tb03040.x

Adams, J. H., Graham, D. I., & Gennarelli, T. (1981). Acceleration Induced Head Injury in the Monkey. II. Neuropathology. Dans *Acta neuropathologica. Supplementum* (p. 26-28). https://doi.org/10.1007/978-3-642-81553-9_8

Aguilar-Fuentes, V., Orozco-Puga, P., & Jiménez-Ruiz, A. (2024). The Glasgow Coma Scale: 50-year anniversary. *Neurological Sciences*. https://doi.org/10.1007/s10072-024-07432-9

Ajami, B., Bennett, J., Krieger, C., Tetzlaff, W., & Rossi, F. (2007). Local self-renewal can sustain CNS microglia maintenance and function throughout adult life. *Nature Neuroscience*, *10*(12), 1538–1543. https://doi.org/10.1038/nn2014

Alawieh, A., Langley, E. F., & Tomlinson, S. (2018). Targeted complement inhibition salvages stressed neurons and inhibits neuroinflammation after stroke in mice. *Science Translational Medicine*, *10*(441). https://doi.org/10.1126/scitranslmed.aao6459

Alawieh, A., Langley, E. F., Weber, S., Adkins, D., & Tomlinson, S. (2018). Identifying the Role of Complement in Triggering Neuroinflammation after Traumatic Brain Injury. *˜the œJournal of Neuroscience/˜the œJournal of Neuroscience*, *38*(10), 2519–2532. https://doi.org/10.1523/jneurosci.2197-17.2018

Albert-Weissenberger, C., & Sirén, A. (2010). Experimental traumatic brain injury. *Experimental & Translational Stroke Medicine*, *2*(1). https://doi.org/10.1186/2040-7378-2-16

Aljovic, A., Zhao, S., Chahin, M., De La Rosa, C., Van Steenbergen, V., Kerschensteiner, M., & Bareyre, F. M. (2022). A deep learning-based toolbox for Automated Limb Motion Analysis (ALMA) in murine models of neurological disorders. *Communications Biology*, *5*(1). https://doi.org/10.1038/s42003-022-03077-6

Altman, J., & Sudarshan, K. (1975). Postnatal development of locomotion in the laboratory rat. *Animal Behaviour*, *23*, 896–920. https://doi.org/10.1016/0003-3472(75)90114-1

Anderson, T., Heitger, M., & Macleod, A. (2006). Concussion and mild head injury. *Practical Neurology*, *6*(6), 342-357. https://doi.org/10.1136/jnnp.2006.106583

Andoh, M., & Koyama, R. (2021). Microglia regulate synaptic development and plasticity. *Developmental Neurobiology*, *81*(5), 568-590. https://doi.org/10.1002/dneu.22814

Andrews, R. J. (1965). Treadmill for small laboratory animals. *Journal of Applied Physiology*, *20*(3), 572–574. https://doi.org/10.1152/jappl.1965.20.3.572

Andriessen, T. M. J. C., Jacobs, B., & Vos, P. E. (2010). Clinical characteristics and pathophysiological mechanisms of focal and diffuse traumatic brain injury. *Journal of Cellular and Molecular Medicine*, *14*(10), 2381–2392. https://doi.org/10.1111/j.1582-4934.2010.01164.x

Annegers, J. F., Hauser, W. A., Coan, S. P., & Rocca, W. A. (1998). A Population-Based Study of Seizures after Traumatic Brain Injuries. *New England Journal Of Medicine/˜The œNew England Journal Of Medicine*, *338*(1), 20-24. https://doi.org/10.1056/nejm199801013380104

Arac, A., Zhao, P., Dobkin, B. H., Carmichael, S. T., & Golshani, P. (2019). DeepBehavior: a deep learning toolbox for automated analysis of animal and human behavior imaging data. *Frontiers in Systems Neuroscience*, *13*. https://doi.org/10.3389/fnsys.2019.00020

Ashman, T., Cantor, J., Gordon, W. A., Spielman, L., Flanagan, S. R., Ginsberg, A.,. . . Greenwald, B. D. (2009). A Randomized Controlled Trial of Sertraline for the Treatment of Depression in

Persons With Traumatic Brain Injury. *Archives Of Physical Medicine And Rehabilitation*, *90*(5), 733-740. https://doi.org/10.1016/j.apmr.2008.11.005

Babcock, A., Kuziel, W. A., Rivest, S., & Owens, T. (2003). Chemokine expression by glial cells directs leukocytes to sites of axonal injury in the CNS. *˜the œJournal of Neuroscience/˜the œJournal of Neuroscience*, *23*(21), 7922–7930. https://doi.org/10.1523/jneurosci.23-21-07922.2003

Banisadr, G., Rostène, W., Kitabgi, P., & Parsadaniantz, S. M. (2005). Chemokines and brain functions. *Current Drug Targets. Inflammation & Allergy*, *4*(3), 387–399. https://doi.org/10.2174/1568010054022097

Banisadr, G., Rostène, W., Kitabgi, P., & Parsadaniantz, S. M. (2005). Chemokines and brain functions. *Current Drug Targets. Inflammation & Allergy*, *4*(3), 387–399. https://doi.org/10.2174/1568010054022097

Barone, V., De Koning, M. E., Van Der Horn, H. J., Van Der Naalt, J., Eertman-Meyer, C. J., & Van Putten, M. J. A. M. (2024). Neurophysiological signatures of mild traumatic brain injury in the acute and subacute phase. *Neurological Sciences*. https://doi.org/10.1007/s10072-024-07364-4

Baxendale, S., Heaney, D., Rugg-Gunn, F., & Friedland, D. (2019). Neuropsychological outcomes following traumatic brain injury. *Practical Neurology (Print)*, *19*(6), 476-482. https://doi.org/10.1136/practneurol-2018-002113

Bayır, H., Pd, A., Wisniewski, S. R., Shore, P. M., Lai, Y., Brown, D. S.,. . . Kochanek, P. M. (2009). Therapeutic hypothermia preserves antioxidant defenses after severe traumatic brain injury in infants and children*. *Critical Care Medicine*, *37*(2), 689-695. https://doi.org/10.1097/ccm.0b013e318194abf2

Bennett, F. C., Bennett, M. L., Yaqoob, F., Mulinyawe, S. B., Grant, G. A., Gephart, M. H., Plowey, E. D., & Barres, B. A. (2018). A combination of ontogeny and CNS environment establishes microglial identity. *Neuron*, *98*(6), 1170-1183.e8. https://doi.org/10.1016/j.neuron.2018.05.014

Berry, K. P., & Nedivi, E. (2017). Spine dynamics: Are they all the same? *Neuron*, *96*(1), 43–55. https://doi.org/10.1016/j.neuron.2017.08.008

Bhatt, D. H., Zhang, S., & Gan, W. (2009). Dendritic spine dynamics. *Annual Review of Physiology*, *71*(1), 261–282. https://doi.org/10.1146/annurev.physiol.010908.163140

Bieniek, K. F., Ross, O. A., Cormier, K. A., Walton, R. L., Soto-Ortolaza, A., Johnston, A. E., DeSaro, P., Boylan, K. B., Graff-Radford, N. R., Wszolek, Z. K., Rademakers, R., Boeve, B. F., McKee, A. C., & Dickson, D. W. (2015). Chronic traumatic encephalopathy pathology in a neurodegenerative disorders brain bank. *Acta Neuropathologica*, *130*(6), 877–889. https://doi.org/10.1007/s00401-015-1502-4

Blennow, K., Brody, D. L., Kochanek, P. M., Levin, H. S., McKee, A. C., Ribbers, G. M., Yaffe, K., & Zetterberg, H. (2016). Traumatic brain injuries. *Nature Reviews. Disease Primers*, *2*(1). https://doi.org/10.1038/nrdp.2016.84

Bodnar, C. N., Roberts, K., Higgins, E. K., & Bachstetter, A. D. (2019). A Systematic Review of Closed Head Injury Models of Mild Traumatic Brain Injury in Mice and Rats. *Journal Of Neurotrauma*, *36*(11), 1683-1706. https://doi.org/10.1089/neu.2018.6127

Bohlen, M., Cameron, A., Metten, P., Crabbe, J. C., & Wahlsten, D. (2009). Calibration of rotational acceleration for the rotarod test of rodent motor coordination. *Journal of Neuroscience Methods*, *178*(1), 10–14. https://doi.org/10.1016/j.jneumeth.2008.11.001

Bohman, L., & Schuster, J. M. (2013). Decompressive craniectomy for Management of Traumatic Brain Injury: an update. *Current Neurology and Neuroscience Reports*, *13*(11). https://doi.org/10.1007/s11910-013-0392-x

Bohman, L., & Schuster, J. M. (2013). Decompressive craniectomy for Management of Traumatic Brain Injury: an update. *Current Neurology and Neuroscience Reports*, *13*(11). https://doi.org/10.1007/s11910-013-0392-x

Bolton-Hall, A. N., Hubbard, W. B., & Saatman, K. E. (2019). Experimental designs for Repeated Mild Traumatic Brain Injury: Challenges and considerations. *Journal of Neurotrauma*, *36*(8), 1203–1221. https://doi.org/10.1089/neu.2018.6096

Bouët, V., Borel, L., Harlay, F., Gahéry, Y., & Lacour, M. (2004). Kinematics of treadmill locomotion in rats conceived, born, and reared in a hypergravity field (2 g). *Behavioural Brain Research*, *150*(1–2), 207–216. https://doi.org/10.1016/s0166-4328(03)00258-4

Bourgeron, T. (2009). A synaptic trek to autism. *Current Opinion in Neurobiology*, *19*(2), 231–234. https://doi.org/10.1016/j.conb.2009.06.003

Bourne, J. N., & Harris, K. M. (2008). Balancing structure and function at hippocampal dendritic spines. *Annual Review of Neuroscience*, *31*(1), 47–67. https://doi.org/10.1146/annurev.neuro.31.060407.125646

Bramlett, H. M., Dietrich, W. D., Dixon, C. E., Shear, D. A., Schmid, K., Mondello, S.,. . . Kochanek, P. M. (2016). Erythropoietin Treatment in Traumatic Brain Injury : Operation Brain Trauma Therapy. *Journal Of Neurotrauma*, *33*(6), 538-552. https://doi.org/10.1089/neu.2015.4116

Bražinová, A., Rehorčíková, V., Taylor, M., Bučková, V., Majdán, M., Psota, M., Peeters, W., Feigin, V. L., Theadom, A., Holkovic, L., & Synnot, A. (2021). Epidemiology of Traumatic Brain Injury in Europe: A Living Systematic Review. *Journal of Neurotrauma*, *38*(10), 1411–1440. https://doi.org/10.1089/neu.2015.4126

Brooks, S. P., & Dunnett, S. B. (2009). Tests to assess motor phenotype in mice: a user's guide. *Nature Reviews. Neuroscience*, *10*(7), 519–529. https://doi.org/10.1038/nrn2652

Bullock, R., Maxwell, W. L., Graham, D. I., Teasdale, G. M., & Adams, J. H. (1991). Glial swelling following human cerebral contusion: an ultrastructural study. *Journal of Neurology, Neurosurgery and Psychiatry*, *54*(5), 427–434. https://doi.org/10.1136/jnnp.54.5.427

Caire, M. J., Reddy, V., & Varacallo, M. (2023, March 27). *Physiology, synapse*. StatPearls - NCBI Bookshelf. https://www.ncbi.nlm.nih.gov/books/NBK526047/

Can, A., Dao, D. T., Terrillion, C. E., Piantadosi, S. C., Bhat, S., & Gould, T. D. (2011). The tail suspension test. *Journal of Visualized Experiments*, *58*. https://doi.org/10.3791/3769

Cane, M., Maco, B., Knott, G., & Holtmaat, A. (2014). The Relationship between PSD-95 Clustering and Spine StabilityIn Vivo. *˜the œJournal of Neuroscience/˜the œJournal of Neuroscience*, *34*(6), 2075–2086. https://doi.org/10.1523/jneurosci.3353-13.2014

Cardona, A. E., Pioro, E. P., Sasse, M. E., Kostenko, V., Cardona, S. M., Dijkstra, I. M., Huang, D. R., Kidd, G. J., Dombrowski, S. M., Dutta, R., Lee, J. C., Cook, D. N., Jung, S., Lira, S. A., Littman, D. R., & Ransohoff, R. M. (2006). Control of microglial neurotoxicity by the fractalkine receptor. *Nature Neuroscience*, *9*(7), 917–924. https://doi.org/10.1038/nn1715

Carroll, M. (2004). The complement system in regulation of adaptive immunity. *Nature Immunology*, *5*(10), 981–986. https://doi.org/10.1038/ni1113

Chen, C., & Regehr, W. G. (2000). Developmental remodeling of the retinogeniculate synapse. *Neuron*, *28*(3), 955–966. https://doi.org/10.1016/s0896-6273(00)00166-5

Chen, K., Gu, H., Zhu, L., & Feng, D. (2020). A new model of repetitive traumatic brain injury in mice. *Frontiers in Neuroscience*, *13*. https://doi.org/10.3389/fnins.2019.01417

Choi, D. (1988). Glutamate neurotoxicity and diseases of the nervous system. *Neuron*, *1*(8), 623–634. https://doi.org/10.1016/0896-6273(88)90162-6

Chung, W., Clarke, L., Wang, G., Stafford, B. K., Sher, A., Chakraborty, C.,. . . Barres, B. A. (2013). Astrocytes mediate synapse elimination through MEGF10 and MERTK pathways. *Nature*, *504*(7480), 394-400. https://doi.org/10.1038/nature12776

Colonna, M., & Butovsky, O. (2017). Microglia function in the central nervous system during health and neurodegeneration. *Annual Review of Immunology*, *35*(1), 441–468. https://doi.org/10.1146/annurev-immunol-051116-052358

Complications of Mild Traumatic Brain Injury in Veterans and Military Personnel : A Systematic Review [Internet]. (2013, 1 janvier). Consulté à l'adresse https://pubmed.ncbi.nlm.nih.gov/24600749/

Compston, A., & Coles, A. (2002). Multiple sclerosis. *Lancet*, *359*(9313), 1221–1231. https://doi.org/10.1016/s0140-6736(02)08220-x

Crusio, W. E. (2012). Heritability estimates in behavior genetics: Wasn't that station passed long ago? *Behavioral and Brain Sciences*, *35*(5), 361–362. https://doi.org/10.1017/s0140525x12000970

Crusio, W. E. (2012). Mouse behavioural testing. How to use mice in behavioural research - by Douglas Wahlsten. *Genes, Brain And Behavior*, *12*(2), 288. https://doi.org/10.1111/j.1601-183x.2012.00864.x

Cryan, J. F., Mombereau, C., & Vassout, A. (2005). The tail suspension test as a model for assessing antidepressant activity: Review of pharmacological and genetic studies in mice. *Neuroscience & Biobehavioral Reviews/Neuroscience and Biobehavioral Reviews*, *29*(4–5), 571–625. https://doi.org/10.1016/j.neubiorev.2005.03.009

Davalos, D., Grutzendler, J., Yang, G., Kim, J. V., Zuo, Y., Jung, S., Littman, D. R., Dustin, M. L., & Gan, W. (2005). ATP mediates rapid microglial response to local brain injury in vivo. *Nature Neuroscience*, *8*(6), 752–758. https://doi.org/10.1038/nn1472

Dever, A., Powell, D., Graham, L., Mason, R., Das, J., Marshall, S. J.,. . . Stuart, S. (2022). Gait Impairment in Traumatic Brain Injury : A Systematic Review. *Sensors*, *22*(4), 1480. https://doi.org/10.3390/s22041480

Dewan, M. C., Rattani, A., Gupta, S., Baticulon, R. E., Hung, Y., Punchak, M., Agrawal, A., Adeleye, A. O., Shrime, M. G., Rubiano, A. M., Rosenfeld, J. V., & Park, K. B. (2019). Estimating the global incidence of traumatic brain injury. *Journal of Neurosurgery*, *130*(4), 1080–1097. https://doi.org/10.3171/2017.10.jns17352

Dharani, K. (n.d.). *The Biology of Thought: A Neuronal Mechanism in the Generation of Thought - A New Molecular Model*. Academic Press.

Di Filippo, M., Portaccio, E., Mancini, A., & Calabresi, P. (2018). Multiple sclerosis and cognition : synaptic failure and network dysfunction. *Nature Reviews. Neuroscience*, *19*(10), 599-609. https://doi.org/10.1038/s41583-018-0053-9

Diogo, C. C., Da Costa, L. M., Pereira, J. E., Filipe, V., Couto, P. A., Geuna, S., Armada-Da-Silva, P. A., Maurício, A. C., & Varejão, A. S. (2019). Kinematic and kinetic gait analysis to evaluate functional recovery in thoracic spinal cord injured rats. *Neuroscience & Biobehavioral Reviews/Neuroscience and Biobehavioral Reviews*, *98*, 18–28. https://doi.org/10.1016/j.neubiorev.2018.12.027

Döbrössy, M. D., & Dunnett, S. B. (2004). Environmental enrichment affects striatal graft morphology and functional recovery. *European Journal of Neuroscience/EJN. European Journal of Neuroscience*, *19*(1), 159–168. https://doi.org/10.1111/j.1460-9568.2004.03105.x

Doorn, K. J., Goudriaan, A., Blits-Huizinga, C., Bol, J. G. J. M., Rozemüller, A. J., Hoogland, P. V., Lucassen, P. J., Drukarch, B., Van De Berg, W. D. J., & Van Dam, A. (2013). Increased amoeboid microglial density in the olfactory bulb of Parkinson's and Alzheimer's patients. *Brain Pathology*, *24*(2), 152–165. https://doi.org/10.1111/bpa.12088

Duan, H. (2003). Age-related dendritic and spine changes in corticocortically projecting neurons in macaque monkeys. *Cerebral Cortex*, *13*(9), 950–961. https://doi.org/10.1093/cercor/13.9.950

Dunham, N., & Miya, T. (1957). A note on a simple apparatus for Detecting Neurological Deficit in Rats and Mice**College of Pharmacy, University of Nebraska, Lincoln 8. *Journal of the American Pharmaceutical Association*, *46*(3), 208–209. https://doi.org/10.1002/jps.3030460322

Dunkerson, J., Moritz, K. E., Young, J. M., Pionk, T., Fink, K. D., Rossignol, J., Dunbar, G., & Smith, J. S. (2014). Combining enriched environment and induced pluripotent stem cell therapy results in improved cognitive and motor function following traumatic brain injury. *Restorative Neurology and Neuroscience*, *32*(5), 675–687. https://doi.org/10.3233/rnn-140408

Elder, G. A., Mitsis, E., Ahlers, S. T., & Cristian, A. (2010). Blast-induced mild traumatic brain injury. *Psychiatric Clinics Of North America/˜The œPsychiatric Clinics Of North America*, *33*(4), 757-781. https://doi.org/10.1016/j.psc.2010.08.001

El-Khodor, B. F., Edgar, N., Chen, A., Winberg, M. L., Joyce, C., Brunner, D., Suárez-Fariñas, M., & Heyes, M. P. (2008). Identification of a battery of tests for drug candidate evaluation in the SMNΔ7 neonate model of spinal muscular atrophy. *Experimental Neurology*, *212*(1), 29–43. https://doi.org/10.1016/j.expneurol.2008.02.025

Empl, L., Chovsepian, A., Chahin, M., Kan, W. Y. V., Fourneau, J., Van Steenbergen, V.,. . . Bareyre, F. M. (2022). Selective plasticity of callosal neurons in the adult contralesional cortex following murine traumatic brain injury. *Nature Communications*, *13*(1). https://doi.org/10.1038/s41467-022-29992-0

Eyo, U. B., & Wu, L. (2013). Bidirectional Microglia-Neuron communication in the healthy brain. *Neural Plasticity*, *2013*, 1–10. https://doi.org/10.1155/2013/456857

Eyo, U. B., Peng, J., Swiatkowski, P., Mukherjee, A., Bispo, A., & Wu, L. (2014). Neuronal Hyperactivity Recruits Microglial Processes via Neuronal NMDA Receptors and Microglial P2Y12 Receptors after Status Epilepticus. *˜the œJournal of Neuroscience/˜the œJournal of Neuroscience*, *34*(32), 10528–10540. https://doi.org/10.1523/jneurosci.0416-14.2014

Farr, T. D., Liu, L., Colwell, K. L., Whishaw, I. Q., & Metz, G. A. (2006). Bilateral alteration in stepping pattern after unilateral motor cortex injury: A new test strategy for analysis of skilled limb movements in neurological mouse models. *Journal of Neuroscience Methods*, *153*(1), 104–113. https://doi.org/10.1016/j.jneumeth.2005.10.011

Faust, T. E., Gunner, G., & Schafer, D. P. (2021). Mechanisms governing activity-dependent synaptic pruning in the developing mammalian CNS. *Nature Reviews. Neuroscience*, *22*(11), 657–673. https://doi.org/10.1038/s41583-021-00507-y

Feeney, D. M., Boyeson, M. G., Linn, R. T., Murray, H. M., & Dail, W. G. (1981). Responses to cortical injury: I. Methodology and local effects of contusions in the rat. Brain Research, 211(1), 67–77. https://doi.org/10.1016/0006-8993(81)90067-6

Fehlings, M. G., Tetreault, L. A., Riew, K. D., Middleton, J. W., Aarabi, B., Arnold, P. M., Brodke, D. S., Burns, A. S., Carette, S., Chen, R., Chiba, K., Dettori, J. R., Furlan, J. C., Harrop, J. S., Holly, L. T., Kalsi-Ryan, S., Kotter, M., Kwon, B. K., Martin, A. R., . . . Wang, J. C. (2017). A Clinical Practice Guideline for the Management of Patients with Degenerative Cervical Myelopathy: Recommendations for patients with mild, moderate, and severe disease and nonmyelopathic patients with evidence of cord compression. *Global Spine Journal*, *7*(3_suppl), 70S-83S. https://doi.org/10.1177/2192568217701914

Feinberg, I. (1982). Schizophrenia: Caused by a fault in programmed synaptic elimination during adolescence? *Journal of Psychiatric Research*, *17*(4), 319–334. https://doi.org/10.1016/0022-3956(82)90038-3

Fesharaki-Zadeh, A. (2019). Chronic Traumatic Encephalopathy: A brief overview. *Frontiers in Neurology*, *10*. https://doi.org/10.3389/fneur.2019.00713

Fiala, J. C., Feinberg, M., Popov, V., & Harris, K. M. (1998). Synaptogenesis via dendritic filopodia in developing hippocampal area CA1. *˜the œJournal of Neuroscience/˜the œJournal of Neuroscience*, *18*(21), 8900–8911. https://doi.org/10.1523/jneurosci.18-21-08900.1998

Figueiro-Silva, J., Gruart, A., Clayton, K. B., Podlesniy, P., Abad, M. A., Gasull, X., Delgado-García, J. M., & Trullas, R. (2015). Neuronal pentraxin 1 negatively regulates excitatory synapse density and synaptic plasticity. *˜the œJournal of Neuroscience/˜the œJournal of Neuroscience*, *35*(14), 5504–5521. https://doi.org/10.1523/jneurosci.2548-14.2015

Fishman, R. A. (1975). Brain edema. *New England Journal of Medicine/˜the œNew England Journal of Medicine*, *293*(14), 706–711. https://doi.org/10.1056/nejm197510022931407

Flierl, M. A., Stahel, P. F., Beauchamp, K. M., Morgan, S. J., Smith, W. R., & Shohami, E. (2009). Mouse closed head injury model induced by a weight-drop device. *Nature Protocols*, *4*(9), 1328–1337. https://doi.org/10.1038/nprot.2009.148

Fonseca, M. I., Chu, S., Hernandez, M., Fang, M., Modarresi, L., Selvan, P.,. . . Tenner, A. J. (2017). Cell-specific deletion of C1qa identifies microglia as the dominant source of C1q in mouse brain. *Journal Of Neuroinflammation*, *14*(1). https://doi.org/10.1186/s12974-017-0814-9

Franco, R., & Fernández-Suárez, D. (2015). Alternatively activated microglia and macrophages in the central nervous system. *Progress in Neurobiology*, *131*, 65–86. https://doi.org/10.1016/j.pneurobio.2015.05.003

Frankowski, J. C., Tierno, A., Pavani, S., Cao, Q., Lyon, D. C., & Hunt, R. (2022). Brain-wide reconstruction of inhibitory circuits after traumatic brain injury. *Nature Communications*, *13*(1). https://doi.org/10.1038/s41467-022-31072-2

Franks, N. P. (2006). Molecular targets underlying general anaesthesia. *British Journal of Pharmacology*, *147*(S1). https://doi.org/10.1038/sj.bjp.0706441

Frey, L. C. (2003). Epidemiology of Posttraumatic Epilepsy : A Critical Review. *Epilepsia*, *44*(s10), 11-17. https://doi.org/10.1046/j.1528-1157.44.s10.4.x

Fujimoto, S. T., Longhi, L., Saatman, K. E., & McIntosh, T. K. (2004). Motor and cognitive function evaluation following experimental traumatic brain injury. *Neuroscience & Biobehavioral Reviews/Neuroscience and Biobehavioral Reviews*, *28*(4), 365–378. https://doi.org/10.1016/j.neubiorev.2004.06.002

Fumagalli, S., Perego, C., Ortolano, F., & De Simoni, M. G. (2013). CX3CR1 deficiency induces an early protective inflammatory environment in ischemic mice. *GLIA*, *61*(6), 827–842. https://doi.org/10.1002/glia.22474

Gabbe, B., Cameron, P., & Finch, C. F. (2003). The status of the Glasgow Coma Scale. *Emergency Medicine*, *15*(4), 353–360. https://doi.org/10.1046/j.1442-2026.2003.00474.x

Gaetz, M. (2004). The neurophysiology of brain injury. *Clinical Neurophysiology*, *115*(1), 4–18. https://doi.org/10.1016/s1388-2457(03)00258-x

Galgano, M., Toshkezi, G., Qiu, X., Russell, T. M., Chin, L. S., & Zhao, L. (2017). Traumatic brain injury. *Cell Transplantation*, *26*(7), 1118-1130. https://doi.org/10.1177/0963689717714102

Gennarelli, T. A. (1993). Mechanisms of brain injury. *PubMed*, *11 Suppl 1*, 5–11. https://pubmed.ncbi.nlm.nih.gov/8445204

Gennarelli, T. A., Thibault, L. E., Adams, J. H., Graham, D. I., Thompson, C., & Marcincin, R. P. (1982). Diffuse axonal injury and traumatic coma in the primate. *Annals Of Neurology*, *12*(6), 564-574. https://doi.org/10.1002/ana.410120611

Ghajar, J. (2000). Traumatic brain injury. *Lancet*, *356*(9233), 923–929. https://doi.org/10.1016/s0140-6736(00)02689-1

Ginhoux, F., Greter, M., Leboeuf, M., Nandi, S., See, P., Gökhan, Ş., Mehler, M. F., Conway, S. J., Ng, L. G., Stanley, E. R., Samokhvalov, I. M., & Mérad, M. (2010). Fate Mapping Analysis

Reveals That Adult Microglia Derive from Primitive Macrophages. *Science*, *330*(6005), 841–845. https://doi.org/10.1126/science.1194637

Gipson, C. D., & Olive, M. F. (2016). Structural and functional plasticity of dendritic spines – root or result of behavior ? *Genes, Brain And Behavior*, *16*(1), 101-117. https://doi.org/10.1111/gbb.12324

Glausier, J., & Lewis, D. (2013). Dendritic spine pathology in schizophrenia. *Neuroscience*, *251*, 90–107. https://doi.org/10.1016/j.neuroscience.2012.04.044

Glynn, M. W., Elmer, B. M., Garay, P. A., Liu, X., Needleman, L. A., El-Sabeawy, F., & McAllister, A. K. (2011). MHCI negatively regulates synapse density during the establishment of cortical connections. *Nature Neuroscience*, *14*(4), 442–451. https://doi.org/10.1038/nn.2764

Gould, T. D., Dao, D. T., & Kovacsics, C. E. (2009). The open field test. In *Neuromethods* (pp. 1–20). https://doi.org/10.1007/978-1-60761-303-9_1

Griffiths, J., & Grant, S. G. N. (2023). Synapse pathology in Alzheimer's disease. *Seminars In Cell & Developmental Biology*, *139*, 13-23. https://doi.org/10.1016/j.semcdb.2022.05.028

Grutzendler, J., Kasthuri, N., & Gan, W. (2002). Long-term dendritic spine stability in the adult cortex. *Nature*, *420*(6917), 812–816. https://doi.org/10.1038/nature01276

Guillot, A., & Collet, C. (2008). Construction of the Motor Imagery Integrative Model in Sport : a review and theoretical investigation of motor imagery use. *International Review Of Sport And Exercise Psychology*, *1*(1), 31-44. https://doi.org/10.1080/17509840701823139

Hall, C. S. (1934). The method of open field. *J. Comparative Psychology N*, *18*, 385-403.

Hall, C., & Ballachey, E. L. (1932). *A study of the rat's behavior in a field : a contribution to method in comparative psychology*. https://ci.nii.ac.jp/ncid/BA06072824

Hall, E. D., Sullivan, P. G., Gibson, T. R., Pavel, K. M., Thompson, B. M., & Scheff, S. W. (2005). Spatial and Temporal Characteristics of Neurodegeneration after Controlled Cortical Impact in Mice: More than a Focal Brain Injury. *Journal of Neurotrauma*, *22*(2), 252–265. https://doi.org/10.1089/neu.2005.22.252

Hamers, F. P., Koopmans, G. C., & Joosten, E. A. (2006). CatWalk-Assisted Gait Analysis in the Assessment of Spinal Cord Injury. *Journal Of Neurotrauma*, *23*(3-4), 537-548. https://doi.org/10.1089/neu.2006.23.537

Hånell, A., & Marklund, N. (2014). Structured evaluation of rodent behavioral tests used in drug discovery research. *Frontiers in Behavioral Neuroscience*, *8*. https://doi.org/10.3389/fnbeh.2014.00252

Hardy, W. N., Khalil, T. B., & King, A. I. (1994). Literature review of head injury biomechanics. *International Journal Of Impact Engineering*, *15*(4), 561-586. https://doi.org/10.1016/0734-743x(94)80034-7

Harris, K., Jensen, F., & Tsao, B. (1992). Three-dimensional structure of dendritic spines and synapses in rat hippocampus (CA1) at postnatal day 15 and adult ages: implications for the maturation of synaptic physiology and long-term potentiation [published erratum appears in J Neurosci 1992 Aug;12(8):following table of contents]. *˜the œJournal of Neuroscience/˜the œJournal of Neuroscience*, *12*(7), 2685–2705. https://doi.org/10.1523/jneurosci.12-07-02685.1992

Hayes, J. P., Bigler, E. D., & Verfaellie, M. (2016). Traumatic Brain Injury as a Disorder of Brain Connectivity. *Journal Of The International Neuropsychological Society*, *22*(2), 120-137. https://doi.org/10.1017/s1355617715000740

Haynes, S. E., Hollopeter, G., Yang, G., Kurpius, D., Dailey, M. E., Gan, W., & Julius, D. (2006). The P2Y12 receptor regulates microglial activation by extracellular nucleotides. *Nature Neuroscience*, *9*(12), 1512–1519. https://doi.org/10.1038/nn1805

He, C. X., & Portera-Cailliau, C. (2013). The trouble with spines in fragile X syndrome: density, maturity and plasticity. *Neuroscience*, *251*, 120–128. https://doi.org/10.1016/j.neuroscience.2012.03.049

Heindl, S., Gesierich, B., Benakis, C., Llovera, G., Duering, M., & Liesz, A. (2018). Automated morphological analysis of microglia after stroke. Frontiers in Cellular Neuroscience, 12. https://doi.org/10.3389/fncel.2018.00106

Heneka, M. T., Carson, M. J., Khoury, J. E., Landreth, G. E., Brosseron, F., Feinstein, D. L., Jacobs, A. H., Wyss-Coray, T., Vitórica, J., Ransohoff, R. M., Herrup, K., Frautschy, S. A., Finsen, B., Brown, G. C., Verkhratsky, A., Yamanaka, K., Koistinaho, J., Latz, E., Halle, A., . . . Kummer, M. P. (2015). Neuroinflammation in Alzheimer's disease. *Lancet Neurology*, *14*(4), 388–405. https://doi.org/10.1016/s1474-4422(15)70016-5

Heneka, M. T., Nadrigny, F., Regen, T., Martinez-Hernandez, A., Dumitrescu-Ozimek, L., Terwel, D., Jardanhazi-Kurutz, D., Walter, J., Kirchhoff, F., Hanisch, U., & Kummer, M. P. (2010). Locus ceruleus controls Alzheimer's disease pathology by modulating microglial functions through norepinephrine. *Proceedings of the National Academy of Sciences of the United States of America*, *107*(13), 6058–6063. https://doi.org/10.1073/pnas.0909586107

Hering, H., & Sheng, M. (2001). Dentritic spines : structure, dynamics and regulation. *Nature Reviews. Neuroscience*, *2*(12), 880–888. https://doi.org/10.1038/35104061

Hillary, F. G., & Grafman, J. (2017). Injured Brains and Adaptive Networks : The Benefits and Costs of Hyperconnectivity. *Trends In Cognitive Sciences*, *21*(5), 385-401. https://doi.org/10.1016/j.tics.2017.03.003

Holmes, S., Honhar, P., Tinaz, S., Naganawa, M., Hillmer, A. T., Gallezot, J.,. . . Matuskey, D. (2024). Synaptic loss and its association with symptom severity in Parkinson's disease. *NPJ Parkinson's Disease*, *10*(1). https://doi.org/10.1038/s41531-024-00655-9

Hölter, S. M., Garrett, L., Einicke, J., Sperling, B., Dirscherl, P., Zimprich, A., Fuchs, H., Gailus-Durner, V., De Angelis, M. H., & Wurst, W. (2015). Assessing cognition in mice. *Current Protocols in Mouse Biology*, *5*(4), 331–358. https://doi.org/10.1002/9780470942390.mo150068

Holtmaat, A. J., Trachtenberg, J. T., Wilbrecht, L., Shepherd, G. M., Zhang, X., Knott, G. W., & Svoboda, K. (2005). Transient and persistent dendritic spines in the neocortex in vivo. *Neuron*, *45*(2), 279–291. https://doi.org/10.1016/j.neuron.2005.01.003

How neurons talk to each other. (2016, September 21). Max Planck Gesellschaft. https://www.mpg.de/10743509/how-neurons-talk-to-each-other

Howes, O., & Onwordi, E. C. (2023). The synaptic hypothesis of schizophrenia version III : a master mechanism. *Molecular Psychiatry*, *28*(5), 1843-1856. https://doi.org/10.1038/s41380-023-02043-w

Hua, J. Y., & Smith, S. J. (2004). Neural activity and the dynamics of central nervous system development. *Nature Neuroscience*, *7*(4), 327–332. https://doi.org/10.1038/nn1218

Huang, H., Tohme, S., Al-Khafaji, A. B., Tai, S., Loughran, P., Chen, L., Wang, S., Kim, J., Billiar, T. R., Wang, Y., & Tsung, A. (2015). Damage-associated molecular pattern–activated neutrophil extracellular trap exacerbates sterile inflammatory liver injury. *Hepatology*, *62*(2), 600–614. https://doi.org/10.1002/hep.27841

Hubel, D. H., Wiesel, T. N., & Stryker, M. P. (1977). Orientation columns in macaque monkey visual cortex demonstrated by the 2-deoxyglucose autoradiographic technique. *Nature*, *269*(5626), 328-330. https://doi.org/10.1038/269328a0

Huiskamp, M., Kiljan, S., Kulik, S. D., Witte, M. E., Jonkman, L. E., Bol, J. G. J. M.,. . . Geurts, J. J. G. (2022). Inhibitory synaptic loss drives network changes in multiple sclerosis : An ex vivo

to in silico translational study. *Multiple Sclerosis*, *28*(13), 2010-2019. https://doi.org/10.1177/13524585221125381

Hutsler, J. J., & Zhang, H. (2010). Increased dendritic spine densities on cortical projection neurons in autism spectrum disorders. *Brain Research*, *1309*, 83–94. https://doi.org/10.1016/j.brainres.2009.09.120

Iadecola, C., & Anrather, J. (2011). The immunology of stroke: from mechanisms to translation. *Nature Medicine*, *17*(7), 796–808. https://doi.org/10.1038/nm.2399

Jain S, Iverson LM. Glasgow Coma Scale. 2023 Jun 12. In: StatPearls [Internet]. Treasure Island (FL): StatPearls Publishing; 2024 Jan–. PMID: 30020670.

Jamnia, N., Urban, J. H., Stutzmann, G. E., Chiren, S. G., Reisenbigler, E., Marr, R., Peterson, D. A., & Kozlowski, D. A. (2017). A clinically relevant Closed-Head model of single and repeat concussive injury in the adult rat using a controlled cortical impact device. *Journal of Neurotrauma*, *34*(7), 1351–1363. https://doi.org/10.1089/neu.2016.4517

Jay, T. R., Von Saucken, V. E., Muñoz, B., Codocedo, J. F., Atwood, B. K., Lamb, B. T., & Landreth, G. E. (2019). TREM2 is required for microglial instruction of astrocytic synaptic engulfment in neurodevelopment. *GLIA*, *67*(10), 1873-1892. https://doi.org/10.1002/glia.23664

Jolliffe, I. T., & Cadima, J. (2016). Principal component analysis : a review and recent developments. *Philosophical Transactions - Royal Society. Mathematical, Physical And Engineering Sciences/Philosophical Transactions - Royal Society. Mathematical, Physical And Engineering Sciences*, *374*(2065), 20150202. https://doi.org/10.1098/rsta.2015.0202

Jones, B. J., & Roberts, D. J. (1968). The quantitative measurement of motor inco-ordination in naive mice using an accelerating rotarod. *Journal of Pharmacy and Pharmacology*, *20*(4), 302–304. https://doi.org/10.1111/j.2042-7158.1968.tb09743.x

Kane, M. J., Angoa-Pérez, M., Briggs, D. I., Viano, D. C., Kreipke, C. W., & Kuhn, D. M. (2012). A mouse model of human repetitive mild traumatic brain injury. *Journal of Neuroscience Methods*, *203*(1), 41–49. https://doi.org/10.1016/j.jneumeth.2011.09.003

Kapalka, G. M. (2010). Collaborative treatment of disruptive and mood disorders. In *Springer eBooks* (pp. 135–151). https://doi.org/10.1007/978-1-4419-7780-9_8

Karr, J. E., Areshenkoff, C. N., & García-Barrera, M. A. (2014). The neuropsychological outcomes of concussion : A systematic review of meta-analyses on the cognitive sequelae of mild traumatic brain injury. *Neuropsychology*, *28*(3), 321-336. https://doi.org/10.1037/neu0000037

Katz, L. C., & Shatz, C. J. (1996). Synaptic activity and the construction of cortical circuits. *Science*, *274*(5290), 1133–1138. https://doi.org/10.1126/science.274.5290.1133

Kawaguchi, Y., Karube, F., & Kubota, Y. (2005). Dendritic branch typing and spine expression patterns in cortical nonpyramidal cells. *Cerebral Cortex*, *16*(5), 696–711. https://doi.org/10.1093/cercor/bhj015

Kettenmann, H., Kirchhoff, F., & Verkhratsky, A. (2013). Microglia : New Roles for the Synaptic Stripper. *Neuron*, *77*(1), 10-18. https://doi.org/10.1016/j.neuron.2012.12.023

Kiely, K. M. (2014). Cognitive function. In Springer eBooks (pp. 974–978). https://doi.org/10.1007/978-94-007-0753-5_426

Kierdorf, K., & Prinz, M. (2013). Factors regulating microglia activation. *Frontiers in Cellular Neuroscience*, *7*. https://doi.org/10.3389/fncel.2013.00044

Kierdorf, K., & Prinz, M. (2017). Microglia in steady state. *˜the œJournal of Clinical Investigation/˜the œJournal of Clinical Investigation*, *127*(9), 3201–3209. https://doi.org/10.1172/jci90602

Kierdorf, K., Erny, D., Goldmann, T., Sander, V., Schulz, C., Perdiguero, E. G., Wieghofer, P., Heinrich, A., Riemke, P., Hölscher, C., Müller, D., Luckow, B., Brocker, T., Debowski, K., Fritz, G., Opdenakker, G., Diefenbach, A., Biber, K., Heikenwälder, M., . . . Prinz, M. (2013).

Microglia emerge from erythromyeloid precursors via Pu.1- and Irf8-dependent pathways. *Nature Neuroscience*, *16*(3), 273–280. https://doi.org/10.1038/nn.3318

Kim, E., Seo, H. G., Seong, M. Y., Kang, M., Kim, H., Lee, M. Y.,. . . Oh, B. M. (2022). An exploratory study on functional connectivity after mild traumatic brain injury : Preserved global but altered local organization. *Brain And Behavior*, *12*(9). https://doi.org/10.1002/brb3.2735

King, A. I. (2000). Fundamentals of Impact Biomechanics : Part I - Biomechanics of the Head, Neck, and Thorax. *Annual Review Of Biomedical Engineering*, *2*(1), 55-81. https://doi.org/10.1146/annurev.bioeng.2.1.55

Knapp, J. M. (2005). Hyperosmolar Therapy in the Treatment of Severe Head Injury in Children. *AACN Clinical Issues*, *16*(2), 199-211. https://doi.org/10.1097/00044067-200504000-00011

Knott, G., & Holtmaat, A. (2008). Dendritic spine plasticity—Current understanding from in vivo studies. *Brain Research Reviews*, *58*(2), 282–289. https://doi.org/10.1016/j.brainresrev.2008.01.002

Koch, C., & Zador, A. (1993). The function of dendritic spines: devices subserving biochemical rather than electrical compartmentalization. *˜the œJournal of Neuroscience/˜the œJournal of Neuroscience*, *13*(2), 413–422. https://doi.org/10.1523/jneurosci.13-02-00413.1993

Kochanek, P. M., Hendrich, K. S., Dixon, C. E., Schiding, J. K., Williams, D. S., & Ho, C. (2002). Cerebral Blood Flow at One Year after Controlled Cortical Impact in Rats: Assessment by Magnetic Resonance Imaging. *Journal of Neurotrauma*, *19*(9), 1029–1037. https://doi.org/10.1089/089771502760341947

Kolb, B., & Whishaw, I. Q. (1998). BRAIN PLASTICITY AND BEHAVIOR. *Annual Review of Psychology*, *49*(1), 43–64. https://doi.org/10.1146/annurev.psych.49.1.43

Kondo, A., Shahpasand, K., Mannix, R., Qiu, J., Moncaster, J. A., Chen, C., Yao, Y., Lin, Y., Driver, J. A., Sun, Y., Wei, S., Luo, M., Albayram, Ö., Huang, P., Rotenberg, A., Ryo, A., Goldstein, L. E., Pascual-Leone, Á., McKee, A. C., . . . Lu, K. P. (2015). Antibody against early driver of neurodegeneration cis P-tau blocks brain injury and tauopathy. *Nature*, *523*(7561), 431–436. https://doi.org/10.1038/nature14658

Kongsui, R., Beynon, S. B., Johnson, S., & Walker, F. R. (2014). Quantitative assessment of microglial morphology and density reveals remarkable consistency in the distribution and morphology of cells within the healthy prefrontal cortex of the rat. *Journal of Neuroinflammation*, *11*(1). https://doi.org/10.1186/s12974-014-0182-7

Kovács, R. Á., Vadászi, H., Bulyáki, É., Török, G., Tóth, V., Mátyás, D., Kun, J., Hunyadi-Gulyás, É., Fedor, F. Z., Csincsi, Á., Medzihradszky, K., Homolya, L., Juhász, G., Kékesi, K. A., Józsi, M., Györffy, B. A., & Kardos, J. (2021). Identification of neuronal pentraxins as synaptic binding partners of C1Q and the involvement of NP1 in synaptic pruning in adult mice. *Frontiers in Immunology*, *11*. https://doi.org/10.3389/fimmu.2020.599771

Kraeuter, A., Guest, P. C., & Sarnyai, Z. (2018). The Y-Maze for assessment of spatial working and reference memory in mice. In *Methods in molecular biology* (pp. 105–111). https://doi.org/10.1007/978-1-4939-8994-2_10

Kuhlman, S. J., & Huang, Z. J. (2008). High-Resolution labeling and functional manipulation of specific neuron types in mouse brain by CRE-Activated viral gene expression. *PloS One*, *3*(4), e2005. https://doi.org/10.1371/journal.pone.0002005

Kuo, J. Y., Denman, A. J., Beacher, N. J., Glanzberg, J. T., Zhang, Y., Li, Y., & Lin, D. (2022). Using deep learning to study emotional behavior in rodent models. *Frontiers in Behavioral Neuroscience*, *16*. https://doi.org/10.3389/fnbeh.2022.1044492

Lai, S., Panarese, A., Spalletti, C., Alia, C., Ghionzoli, A., Caleo, M., & Micera, S. (2014). Quantitative kinematic characterization of reaching impairments in mice after a stroke.

Neurorehabilitation and Neural Repair, *29*(4), 382–392. https://doi.org/10.1177/1545968314545174

Langlois, J., Rutland-Brown, W., & Wald, M. M. (2006). The epidemiology and impact of traumatic Brain injury. *˜the œJournal of Head Trauma Rehabilitation/Journal of Head Trauma Rehabilitation*, *21*(5), 375–378. https://doi.org/10.1097/00001199-200609000-00001

Lee, K. F., Soares, C., Thivierge, J., & Béïque, J. (2016). Correlated Synaptic Inputs Drive Dendritic Calcium Amplification and Cooperative Plasticity during Clustered Synapse Development. *Neuron*, *89*(4), 784–799. https://doi.org/10.1016/j.neuron.2016.01.012

Lehnardt, S. (2009). Innate immunity and neuroinflammation in the CNS: The role of microglia in Toll-like receptor-mediated neuronal injury. *GLIA*, *58*(3), 253–263. https://doi.org/10.1002/glia.20928

Lehrman, E. K., Wilton, D. K., Litvina, E. Y., Welsh, C. A., Chang, S. T., Frouin, A., Walker, A. J., Heller, M. D., Umemori, H., Chen, C., & Stevens, B. (2018). CD47 Protects Synapses from Excess Microglia-Mediated Pruning during Development. *Neuron*, *100*(1), 120-134.e6. https://doi.org/10.1016/j.neuron.2018.09.017

Lemke, G., & Burstyn-Cohen, T. (2010). TAM receptors and the clearance of apoptotic cells. *Annals of the New York Academy of Sciences*, *1209*(1), 23–29. https://doi.org/10.1111/j.1749-6632.2010.05744.x

Leuner, B., & Shors, T. (2013). Stress, anxiety, and dendritic spines: What are the connections? *Neuroscience*, *251*, 108–119. https://doi.org/10.1016/j.neuroscience.2012.04.021

Levy, M. N., Berson, A., Cook, T., Bollegala, N., Seto, E., Tursanski, S.,. . . Bhalerao, S. (2005). Treatment of agitation following traumatic brain injury : A review of the literature. *NeuroRehabilitation*, *20*(4), 279-306. https://doi.org/10.3233/nre-2005-20405

Leyh, J., Paeschke, S., Mages, B., Michalski, D., Nowicki, M., Bechmann, I., & Winter, K. (2021). Classification of Microglial Morphological Phenotypes Using Machine Learning. *Frontiers In Cellular Neuroscience*, *15*. https://doi.org/10.3389/fncel.2021.701673

Li, C., Wang, Y., Xing, Y., Han, J., Zhang, Y., Zhang, A.,. . . Yang, B. (2022). Regulation of microglia phagocytosis and potential involvement of exercise. *Frontiers In Cellular Neuroscience*, *16*. https://doi.org/10.3389/fncel.2022.953534

Li, T., Chiou, B., Gilman, C. K., Luo, R., Koshi, T., Yu, D.,. . . Piao, X. (2020). A splicing isoform of GPR56 mediates microglial synaptic refinement via phosphatidylserine binding. *EMBO Journal*, *39*(16). https://doi.org/10.15252/embj.2019104136

Li, W. (2012). Eat-me signals : Keys to molecular phagocyte biology and “Appetite” control. *Journal Of Cellular Physiology (Print)*, *227*(4), 1291-1297. https://doi.org/10.1002/jcp.22815

Li, Y., Long, W., Gao, M., Jiao, F., Chen, Z., Liu, M., & Yu, L. (2021). TREM2 regulates high Glucose-Induced microglial inflammation via the NLRP3 signaling pathway. *Brain Sciences*, *11*(7), 896. https://doi.org/10.3390/brainsci11070896

Liao, G. P., Harting, M. T., Hetz, R. A., Walker, P. A., Shah, S. K., Corkins, C. J., Hughes, T. G., Jiménez, F., Kosmach, S., Day, M. C., Tsao, K. J., Lee, D. A., Worth, L. L., Baumgartner, J. E., & Cox, C. S. (2015). Autologous bone marrow mononuclear cells reduce therapeutic intensity for severe traumatic brain injury in children*. *Pediatric Critical Care Medicine*, *16*(3), 245–255. https://doi.org/10.1097/pcc.0000000000000324

Lindgren, S., & Rinder, L. (1965). Experimental studies in head injury. I. Some factors influencing results of model experiments. Biophysik 2(5), 320−329

Lighthall, J. W. (1988). Controlled cortical Impact: a new experimental brain injury model. *Journal of Neurotrauma*, *5*(1), 1–15. https://doi.org/10.1089/neu.1988.5.1

Liu, Y., Spangenberg, E. E., Tang, B., Holmes, T. C., Green, K. N., & Xu, X. (2020). Microglia elimination increases neural circuit connectivity and activity in adult mouse cortex. *˜the*

œJournal of Neuroscience/˜the œJournal of Neuroscience, *41*(6), 1274–1287. https://doi.org/10.1523/jneurosci.2140-20.2020

Liu, Y., Ying, Y., Li, Y., Eyo, U. B., Chen, T., Zheng, J., Umpierre, A. D., Zhu, J., Bosco, D. B., Dong, H., & Wu, L. (2019). Neuronal network activity controls microglial process surveillance in awake mice via norepinephrine signaling. *Nature Neuroscience*, *22*(11), 1771–1781. https://doi.org/10.1038/s41593-019-0511-3

Loane, D. J., & Kumar, A. (2016). Microglia in the TBI brain: The good, the bad, and the dysregulated. *Experimental Neurology*, *275*, 316–327. https://doi.org/10.1016/j.expneurol.2015.08.018

Logroscino, G., & Tortelli, R. (2015). Epidemiology of neurodegenerative diseases. In *Oxford University Press eBooks* (pp. 3–19). https://doi.org/10.1093/med/9780199671618.003.0001

Lorsch, Z. S., Ambesi-Impiombato, A., Zenowich, R., Morganstern, I., Bansal, M., Nestler, E. J., & Hanania, T. (2021). Computational analysis of multidimensional behavioral alterations after Chronic Social Defeat stress. *Biological Psychiatry*, *89*(9), 920–928. https://doi.org/10.1016/j.biopsych.2020.10.010

Lowery, R. L., Tremblay, M., Hopkins, B. E., & Majewska, A. K. (2017). The microglial fractalkine receptor is not required for activity-dependent plasticity in the mouse visual system. *GLIA*, *65*(11), 1744–1761. https://doi.org/10.1002/glia.23192

Lueptow, L. M. (2017). Novel Object Recognition test for the investigation of learning and memory in mice. Journal of Visualized Experiments, 126. https://doi.org/10.3791/55718

Ma, X., Aravind, A., Pfister, B. J., Chandra, N., & Haorah, J. (2019). Animal models of traumatic brain injury and assessment of injury severity. *Molecular Neurobiology*, *56*(8), 5332–5345. https://doi.org/10.1007/s12035-018-1454-5

Mandolesi, G., Gentile, A., Musella, A., Fresegna, D., De Vito, F., Bullitta, S.,. . . Centonze, D. (2015). Synaptopathy connects inflammation and neurodegeneration in multiple sclerosis. *Nature Reviews. Neurology*, *11*(12), 711-724. https://doi.org/10.1038/nrneurol.2015.222

Margolick, J., Dandurand, C., Duncan, K. C., Chen, W., Evans, D. C., Sekhon, M. S.,. . . Hameed, S. M. (2018). A Systematic Review of the Risks and Benefits of Venous Thromboembolism Prophylaxis in Traumatic Brain Injury. *Canadian Journal Of Neurological Sciences*, *45*(4), 432-444. https://doi.org/10.1017/cjn.2017.275

Marklund, N., Bellander, B., Godbolt, A. K., Levin, H. S., McCrory, P., & Thelin, E. P. (2019). Treatments and rehabilitation in the acute and chronic state of traumatic brain injury. *Journal Of Internal Medicine*, *285*(6), 608-623. https://doi.org/10.1111/joim.12900

Markram, H., Toledo-Rodriguez, M., Wang, Y., Gupta, A., Silberberg, G., & Wu, C. (2004). Interneurons of the neocortical inhibitory system. *Nature Reviews. Neuroscience*, *5*(10), 793–807. https://doi.org/10.1038/nrn1519

Marmarou, A., Foda, M. A., Van Den Brink, W., Campbell, J., Kita, H., & Demetriadou, K. (1994). A new model of diffuse brain injury in rats. *Journal of Neurosurgery*, *80*(2), 291–300. https://doi.org/10.3171/jns.1994.80.2.0291

Mathis, A., Mamidanna, P., Cury, K. M., Abe, T., Murthy, V. N., Mathis, M. W., & Bethge, M. (2018). DeepLabCut : markerless pose estimation of user-defined body parts with deep learning. *Nature Neuroscience*, *21*(9), 1281-1289. https://doi.org/10.1038/s41593-018-0209-y

McAteer, K. M., Corrigan, F., Thornton, E., Turner, R. J., & Vink, R. (2016). Short and long term behavioral and pathological changes in a novel rodent model of repetitive mild traumatic brain injury. *PloS One*, *11*(8), e0160220. https://doi.org/10.1371/journal.pone.0160220

McCrory, P., Meeuwisse, W., Aubry, M., Cantu, B., Dvořák, J., Echemendía, R. J., Engebretsen, L., Johnston, K., Kutcher, J. S., Raftery, M., Sills, A. K., Benson, B. W., Davis, G. A., Ellenbogen, R. G., Guskiewicz, K. M., Herring, S. A., Iverson, G. L., Jordan, B., Kissick, J., . .

. Turner, M. S. (2013). Consensus statement on concussion in sport: the 4th International Conference on Concussion in Sport held in Zurich, November 2012. *British Journal of Sports Medicine*, *47*(5), 250–258. https://doi.org/10.1136/bjsports-2013-092313

McGinn, M. J., & Povlishock, J. T. (2016). Pathophysiology of traumatic brain injury. *Neurosurgery Clinics of North America*, *27*(4), 397–407. https://doi.org/10.1016/j.nec.2016.06.002

McGuire, J., Ngwenya, L. B., & McCullumsmith, R. E. (2018). Neurotransmitter changes after traumatic brain injury: an update for new treatment strategies. *Molecular Psychiatry*, *24*(7), 995–1012. https://doi.org/10.1038/s41380-018-0239-6

McKee, A. C., & Daneshvar, D. H. (2015). The neuropathology of traumatic brain injury. In *Handbook of clinical neurology* (pp. 45–66). https://doi.org/10.1016/b978-0-444-52892-6.00004-0

McVea, D. A., & Pearson, K. G. (2009). Object avoidance during locomotion. In *Advances in experimental medicine and biology* (pp. 293–315). https://doi.org/10.1007/978-0-387-77064-2_15

Mecha, M., Carrillo-Salinas, F., Feliú, A., Mestre, L., & Guaza, C. (2016). Microglia activation states and cannabinoid system: Therapeutic implications. *Pharmacology & Therapeutics*, *166*, 40–55. https://doi.org/10.1016/j.pharmthera.2016.06.011

Medana, I. M., & Esiri, M. M. (2003). Axonal damage : a key predictor of outcome in human CNS diseases. *Brain*, *126*(3), 515-530. https://doi.org/10.1093/brain/awg061

Mendes, M., & Majewska, A. K. (2021). An overview of microglia ontogeny and maturation in the homeostatic and pathological brain. *European Journal of Neuroscience/EJN. European Journal of Neuroscience*, *53*(11), 3525–3547. https://doi.org/10.1111/ejn.15225

Menon, D., Schwab, K., Wright, D. W., & Maas, A. I. R. (2010). Position Statement: Definition of Traumatic Brain Injury. *Archives of Physical Medicine and Rehabilitation*, *91*(11), 1637–1640. https://doi.org/10.1016/j.apmr.2010.05.017

Metz, G. A., & Whishaw, I. Q. (2009). The Ladder Rung Walking Task: A Scoring System and its Practical Application. *Journal of Visualized Experiments*, *28*. https://doi.org/10.3791/1204

Meythaler, J. M., Brunner, R., Johnson, A., & Novack, T. A. (2002). Amantadine to Improve Neurorecovery in Traumatic Brain Injury–Associated Diffuse Axonal Injury. *˜The œJournal Of Head Trauma Rehabilitation/Journal Of Head Trauma Rehabilitation*, *17*(4), 300-313. https://doi.org/10.1097/00001199-200208000-00004

Mildner, A., Huang, H., Radke, J., Stenzel, W., & Priller, J. (2016). P2Y12receptor is expressed on human microglia under physiological conditions throughout development and is sensitive to neuroinflammatory diseases. *GLIA*, *65*(2), 375–387. https://doi.org/10.1002/glia.23097

Mollayeva, T., Mollayeva, S., & Colantonio, A. (2018). Traumatic brain injury: sex, gender and intersecting vulnerabilities. *Nature Reviews. Neurology*, *14*(12), 711–722. https://doi.org/10.1038/s41582-018-0091-y

Montenigro, P. H., Ml, A., Bm, M., Daneshvar, D. H., J, M., Ce, C., Cj, N., Au, R., Ac, M., Cantu, R., McClean, Ra, S., & Tripodis, Y. (2017). Cumulative head impact exposure predicts Later-Life depression, apathy, executive dysfunction, and cognitive impairment in former high school and college football players. *Journal of Neurotrauma*, *34*(2), 328–340. https://doi.org/10.1089/neu.2016.4413

Monville, C., Torres, E. M., & Dunnett, S. B. (2006). Comparison of incremental and accelerating protocols of the rotarod test for the assessment of motor deficits in the 6-OHDA model. *Journal of Neuroscience Methods*, *158*(2), 219–223. https://doi.org/10.1016/j.jneumeth.2006.06.001

Morales, D., Marklund, N., Lebold, D., Thompson, H., Pitkanen, A., Maxwell, W., Longhi, L., Laurer, H., Maegele, M., Neugebauer, E., Graham, D., Stocchetti, N., & McIntosh, T. (2005).

Experimental models of traumatic brain injury: Do we really need to build a better mousetrap? *Neuroscience*, *136*(4), 971–989. https://doi.org/10.1016/j.neuroscience.2005.08.030

Moretti, L., Cristofori, I., Weaver, S. M., Chau, A., Portelli, J. N., & Grafman, J. (2012). Cognitive decline in older adults with a history of traumatic brain injury. *Lancet Neurology*, *11*(12), 1103–1112. https://doi.org/10.1016/s1474-4422(12)70226-0

Morganti, J. M., Riparip, L., & Rosi, S. (2016). Call Off the Dog(ma): M1/M2 Polarization Is Concurrent following Traumatic Brain Injury. *PloS One*, *11*(1), e0148001. https://doi.org/10.1371/journal.pone.0148001

Murthy, V. N. (1998). Synaptic plasticity: Step-wise strengthening. *CB/Current Biology*, *8*(18), R650–R653. https://doi.org/10.1016/s0960-9822(07)00414-9

National Institute of Neurological Disorders and Stroke & National Institutes of Health. (n.d.). Traumatic brain injury. In *Hope Through Research*. https://catalog.ninds.nih.gov/sites/default/files/publications/traumatic-brain-injury-hope-through-research_1.pdf

Navlakha, S., Barth, A. L., & Bar-Joseph, Z. (2015). Decreasing-Rate Pruning Optimizes the Construction of Efficient and Robust Distributed Networks. *PLOS Computational Biology/PLoS Computational Biology*, *11*(7), e1004347. https://doi.org/10.1371/journal.pcbi.1004347

Nehring, S. M., Tadi, P., & Tenny, S. (2023, July 3). *Cerebral edema*. StatPearls - NCBI Bookshelf. https://www.ncbi.nlm.nih.gov/books/NBK537272/

Newell, K., Quinn, J., Sparrow, W., & Walter, C. (1983). Kinematic information feedback for learning a rapid arm movement. *Human Movement Science*, *2*(4), 255–269. https://doi.org/10.1016/0167-9457(83)90021-0

Nguyen, R. H., Fiest, K. M., McChesney, J., Kwon, C., Jetté, N., Frolkis, A., Atta, C., Mah, S. M., Dhaliwal, H., Reid, A. Y., Pringsheim, T., Dykeman, J., & Gallagher, C. (2016). The International Incidence of Traumatic Brain Injury: A Systematic Review and Meta-Analysis. *Canadian Journal of Neurological Sciences*, *43*(6), 774–785. https://doi.org/10.1017/cjn.2016.290

Nikolaev, A., McLaughlin, T., O'Leary, D. D. M., & Tessier-Lavigne, M. (2009). APP binds DR6 to trigger axon pruning and neuron death via distinct caspases. *Nature*, *457*(7232), 981–989. https://doi.org/10.1038/nature07767

Nikoo, M., Gadermann, A., To, M. J., Krausz, M., Hwang, S. W., & Palepu, A. (2017). Incidence and associated risk factors of traumatic brain injury in a cohort of homeless and vulnerably housed adults in 3 Canadian cities. *˜the œJournal of Head Trauma Rehabilitation/Journal of Head Trauma Rehabilitation*, *32*(4), E19–E26. https://doi.org/10.1097/htr.0000000000000262

Nimchinsky, E. A., Sabatini, B. L., & Svoboda, K. (2002). Structure and function of dendritic spines. *Annual Review of Physiology*, *64*(1), 313–353. https://doi.org/10.1146/annurev.physiol.64.081501.160008

Nimmerjahn, A. (2012). Two-Photon imaging of microglia in the mouse cortex in vivo. *Cold Spring Harbor Protocols*, *2012*(5), pdb.prot069294. https://doi.org/10.1101/pdb.prot069294

Nimmerjahn, A., Kirchhoff, F., & Helmchen, F. (2005). Resting Microglial Cells Are Highly Dynamic Surveillants of Brain Parenchyma in Vivo. *Science*, *308*(5726), 1314-1318. https://doi.org/10.1126/science.1110647

Nolan, S. (2005). Traumatic brain injury. *Critical Care Nursing Quarterly*, *28*(2), 188–194. https://doi.org/10.1097/00002727-200504000-00010

Nudi, E., Jacqmain, J., Dubbs, K., Geeck, K., Salois, G., Searles, M. A., & Smith, J. S. (2015). Combining Enriched Environment, Progesterone, and Embryonic Neural Stem Cell Therapy Improves Recovery after Brain Injury. *Journal of Neurotrauma*, *32*(14), 1117–1129. https://doi.org/10.1089/neu.2014.3618

Nyein, M. K., Jérusalem, A., Radovitzky, R., Moore, D. F., & Noels, L. (2008). Modeling Blast-Related Brain Injury. *The 26th Army Science Conference*. Consulté à l'adresse https://apps.dtic.mil/dtic/tr/fulltext/u2/a504193.pdf

O'Connor, W., Smyth, A., & Gilchrist, M. D. (2011). Animal models of traumatic brain injury: A critical evaluation. *Pharmacology & Therapeutics*, *130*(2), 106–113. https://doi.org/10.1016/j.pharmthera.2011.01.001

O'Donnell, J., Zeppenfeld, D., McConnell, E., Peña, S., & Nedergaard, M. (2012). Norepinephrine: a neuromodulator that boosts the function of multiple cell types to optimize CNS performance. *Neurochemical Research*, *37*(11), 2496–2512. https://doi.org/10.1007/s11064-012-0818-x

Obi-Nagata, K., Temma, Y., & Hayashi-Takagi, A. (2019). Synaptic functions and their disruption in schizophrenia : From clinical evidence to synaptic optogenetics in an animal model. *Proceedings Of The Japan Academy. Series B, Physical And Biological Sciences*, *95*(5), 179-197. https://doi.org/10.2183/pjab.95.014

Olsen, O., Kallop, D. Y., McLaughlin, T., Huntwork-Rodriguez, S., Wu, Z., Duggan, C. D., Simon, D. J., Lu, Y., Easley-Neal, C., Takeda, K., Hass, P. E., Jaworski, A., O'Leary, D. D., Weimer, R. M., & Tessier-Lavigne, M. (2014). Genetic Analysis Reveals that Amyloid Precursor Protein and Death Receptor 6 Function in the Same Pathway to Control Axonal Pruning Independent of β-Secretase. *˜ the œJournal of Neuroscience/˜ the œJournal of Neuroscience*, *34*(19), 6438–6447. https://doi.org/10.1523/jneurosci.3522-13.2014

Omalu, B. I., DeKosky, S. T., Minster, R. L., Kamboh, M. I., Hamilton, R. L., & Wecht, C. H. (2005). Chronic traumatic encephalopathy in a National Football League player. *Neurosurgery/Neurosurgery Online*, *57*(1), 128–134. https://doi.org/10.1227/01.neu.0000163407.92769.ed

Ommaya, A. K., Thibault, L. E., & Bandak, F. A. (1994). Mechanisms of impact head injury. *International Journal Of Impact Engineering*, *15*(4), 535-560. https://doi.org/10.1016/0734-743x(94)80033-6

Orihuela, R., McPherson, C. A., & Harry, G. J. (2015). Microglial M1/M2 polarization and metabolic states. *British Journal of Pharmacology*, *173*(4), 649–665. https://doi.org/10.1111/bph.13139

Ozcan, A. S. (2017). Filopodia: a rapid structural plasticity substrate for fast learning. *Frontiers in Synaptic Neuroscience*, *9*. https://doi.org/10.3389/fnsyn.2017.00012

Pagani, M. P., Barsotti, N., Bertero, A., Trakoshis, S., Ulysse, L., Locarno, A., Misevičiūtė, I., De Felice, A., Canella, C., Supekar, K., Galbusera, A., Menon, V., Tonini, R., Deco, G., Lombardo, M., Pasqualetti, M., & Gozzi, A. (2021). mTOR-related synaptic pathology causes autism spectrum disorder-associated functional hyperconnectivity. *Nature Communications*, *12*(1). https://doi.org/10.1038/s41467-021-26131-z

Païdassi, H., Tacnet-Delorme, P., Garlatti, V., Darnault, C., Ghebrehiwet, B., Gaboriaud, C.,. . . Frachet, P. (2008). C1q Binds Phosphatidylserine and Likely Acts as a Multiligand-Bridging Molecule in Apoptotic Cell Recognition. *˜The œJournal Of Immunology/˜The œJournal Of Immunology*, *180*(4), 2329-2338. https://doi.org/10.4049/jimmunol.180.4.2329

Paolicelli, R. C., Bolasco, G., Pagani, F., Maggi, L., Scianni, M., Panzanelli, P., Giustetto, M., Ferreira, T. A., Guiducci, E., Dumas, L., Ragozzino, D., & Gross, C. (2011). Synaptic pruning by microglia is necessary for normal brain development. *Science*, *333*(6048), 1456–1458. https://doi.org/10.1126/science.1202529

Parnass, Z., Tashiro, A., & Yuste, R. (2000). Analysis of spine morphological plasticity in developing hippocampal pyramidal neurons. *Hippocampus*, *10*(5), 561–568. https://doi.org/10.1002/1098-1063(2000)10:5

Pchitskaya, E., & Bezprozvanny, I. (2020). Dendritic Spines Shape Analysis—Classification or Clusterization ? Perspective. *Frontiers In Synaptic Neuroscience*, *12*. https://doi.org/10.3389/fnsyn.2020.00031

Pereira, J. E., Cabrita, A. M., Filipe, V. M., Bulas-Cruz, J., Couto, P. A., Melo-Pinto, P., Costa, L. M., Geuna, S., Maurício, A. C., & Varejão, A. S. (2006). A comparison analysis of hindlimb kinematics during overground and treadmill locomotion in rats. *Behavioural Brain Research*, *172*(2), 212–218. https://doi.org/10.1016/j.bbr.2006.04.027

Pérez-Cerdá, F., Sánchez-Gómez, M. V., & Matute, C. (2015). Pío del Río Hortega and the discovery of the oligodendrocytes. *Frontiers in Neuroanatomy*, *9*. https://doi.org/10.3389/fnana.2015.00092

Perry, V. H., & Teeling, J. L. (2013). Microglia and macrophages of the central nervous system: the contribution of microglia priming and systemic inflammation to chronic neurodegeneration. *Seminars in Immunopathology*, *35*(5), 601–612. https://doi.org/10.1007/s00281-013-0382-8

Peters, A., & Kaiserman-Abramof, I. R. (1970). The small pyramidal neuron of the rat cerebral cortex. The perikaryon, dendrites and spines. *American Journal of Anatomy*, *127*(4), 321–355. https://doi.org/10.1002/aja.1001270402

Petrie, E. C., Cross, D., Yarnykh, V. L., Richards, T. L., Martin, N., Pagulayan, K. F.,. . . Peskind, E. R. (2014). Neuroimaging, behavioural, and Psychological Sequelae of Repetitive Combined Blast/Impact Mild Traumatic Brain Injury in Iraq and Afghanistan War Veterans. *Journal Of Neurotrauma*, *31*(5), 425-436. https://doi.org/10.1089/neu.2013.2952

Plesnila, N. (2007). Decompression craniectomy after traumatic brain injury : recent experimental results. Dans *Progress in brain research* (p. 393-400). https://doi.org/10.1016/s0079-6123(06)61028-5

Ponce, L. L., Navarro, J. C., Ahmed, O., & Robertson, C. S. (2013). Erythropoietin neuroprotection with traumatic brain injury. *Pathophysiology*, *20*(1), 31-38. https://doi.org/10.1016/j.pathophys.2012.02.005

Porsolt, R. D., Anton, G., Blavet, N., & Jalfre, M. (1978). Behavioural despair in rats: A new model sensitive to antidepressant treatments. *European Journal of Pharmacology*, *47*(4), 379–391. https://doi.org/10.1016/0014-2999(78)90118-8

Post, A., & Hoshizaki, T. B. (2012). Mechanisms of brain impact injuries and their prediction : A review. *Trauma*, *14*(4), 327-349. https://doi.org/10.1177/1460408612446573

Povlishock, J. T., & Katz, D. I. (2005). Update of neuropathology and neurological recovery after traumatic brain injury. *˜the œJournal of Head Trauma Rehabilitation/Journal of Head Trauma Rehabilitation*, *20*(1), 76–94. https://doi.org/10.1097/00001199-200501000-00008

Prieur, E., & Jadavji, N. (2019). Assessing spatial working memory using the spontaneous alternation Y-maze test in aged male mice. *Bio-protocol*, *9*(3). https://doi.org/10.21769/bioprotoc.3162

Prins, M., Greco, T., Alexander, D., & Giza, C. C. (2013). The pathophysiology of traumatic brain injury at a glance. *Disease Models & Mechanisms*. https://doi.org/10.1242/dmm.011585

Prinz, M., Jung, S., & Priller, J. (2019). Microglia Biology: One Century of Evolving Concepts. *Cell*, *179*(2), 292–311. https://doi.org/10.1016/j.cell.2019.08.053

Prinz, M., Tay, T. L., Wolf, Y., & Jung, S. (2014). Microglia: unique and common features with other tissue macrophages. *Acta Neuropathologica*, *128*(3), 319–331. https://doi.org/10.1007/s00401-014-1267-1

Puccio, A. M., Fischer, M., Jankowitz, B. T., Yonas, H., Darby, J. M., & Okonkwo, D. O. (2009). Induced Normothermia Attenuates Intracranial Hypertension and Reduces Fever Burden after Severe Traumatic Brain Injury. *Neurocritical Care*, *11*(1), 82-87. https://doi.org/10.1007/s12028-009-9213-0

Purves, D., Augustine, G., Fitzpatrick, D., Hall, W. C., LaMantia, A., Mooney, R., & White, L. E. (2018). *Neuroscience*. Sinauer..

Purves. (n.d.). *Neuroscience 6th Edition*. Oxford University Press, USA.

R, V. F., Za, C., Jg, H., Jh, H., Wg, S., & Hl, L. (1972). The mononuclear phagocyte system: a new classification of macrophages, monocytes, and their precursor cells. *PubMed*, *46*(6), 845–852. https://pubmed.ncbi.nlm.nih.gov/4538544

Raizman, R., Tavor, I., Biegon, A., Harnof, S., Hoffmann, C., Tsarfaty, G.,. . . Livny, A. (2020). Traumatic Brain Injury Severity in a Network Perspective : A Diffusion MRI Based Connectome Study. *Scientific Reports*, *10*(1). https://doi.org/10.1038/s41598-020-65948-4

Ransohoff, R. M. (2016). How neuroinflammation contributes to neurodegeneration. *Science*, *353*(6301), 777–783. https://doi.org/10.1126/science.aag2590

Ransohoff, R. M., & Perry, V. H. (2009). Microglial physiology: unique stimuli, specialized responses. *Annual Review of Immunology*, *27*(1), 119–145. https://doi.org/10.1146/annurev.immunol.021908.132528

Rauchman, S. H., Placantonakis, D. G., & Reiss, A. B. (2023). Editorial: Manifestations of mild-to-moderate traumatic brain injury. *Frontiers in Neuroscience*, *17*. https://doi.org/10.3389/fnins.2023.1266355

Reeves, T. M., Lyeth, B. G., & Povlishock, J. T. (1995). Long-term potentiation deficits and excitability changes following traumatic brain injury. *Experimental Brain Research*, *106*(2). https://doi.org/10.1007/bf00241120

Reeves, T., Phillips, L., & Povlishock, J. (2005). Myelinated and unmyelinated axons of the corpus callosum differ in vulnerability and functional recovery following traumatic brain injury. *Experimental Neurology*, *196*(1), 126–137. https://doi.org/10.1016/j.expneurol.2005.07.014

Ren, F., Desbordes, S. C., Xie, H., Tilló, E. S., Pixley, F. J., Stanley, E. R., & Graf, T. (2008). PU.1 and C/EBPα/β convert fibroblasts into macrophage-like cells. *Proceedings of the National Academy of Sciences of the United States of America*, *105*(16), 6057–6062. https://doi.org/10.1073/pnas.0711961105

Riccomagno, M. M., & Kolodkin, A. L. (2015). Sculpting neural circuits by axon and dendrite pruning. *Annual Review of Cell and Developmental Biology*, *31*(1), 779–805. https://doi.org/10.1146/annurev-cellbio-100913-013038

Risher, W. C., Patel, S., Kim, I. H., Uezu, A., Bhagat, S., Wilton, D. K., Pilaz, L., Alvarado, J. S., Calhan, O. Y., Silver, D. L., Stevens, B., Calakos, N., Soderling, S. H., & Eroglu, C. (2014). Astrocytes refine cortical connectivity at dendritic spines. *eLife*, *3*. https://doi.org/10.7554/elife.04047

Roberts, I., & Sydenham, E. (2012). Barbiturates for acute traumatic brain injury. *Cochrane Library*. https://doi.org/10.1002/14651858.cd000033.pub2

Roozenbeek, B., Maas, A. I. R., & Menon, D. (2013). Changing patterns in the epidemiology of traumatic brain injury. *Nature Reviews. Neurology*, *9*(4), 231–236. https://doi.org/10.1038/nrneurol.2013.22

Rosen, C. D., & Gerring, J. P. (1986). *Head trauma: Educational Reintegration*.

Rubiano, A. M., Carney, N., Chesnut, R. M., & Puyana, J. C. (2015). Global neurotrauma research challenges and opportunities. *Nature*, *527*(7578), S193–S197. https://doi.org/10.1038/nature16035

Rule, G., Bocchieri, R., Burns, J., & Young, L. (2015). Biophysical mechanisms of traumatic brain injuries. *Seminars in Neurology*, *35*(01), 005–011. https://doi.org/10.1055/s-0035-1544242

Runge, K., Cardoso, C., & De Chevigny, A. (2020). Dendritic spine plasticity: function and mechanisms. *Frontiers in Synaptic Neuroscience*, *12*. https://doi.org/10.3389/fnsyn.2020.00036

Sakai, J. (2020). How synaptic pruning shapes neural wiring during development and, possibly, in disease. *Proceedings Of The National Academy Of Sciences Of The United States Of America*, *117*(28), 16096-16099. https://doi.org/10.1073/pnas.2010281117

Salamanca, L., Mechawar, N., Murai, K. K., Balling, R., Bouvier, D., & Skupin, A. (2019). MIC-MAC: An automated pipeline for high-throughput characterization and classification of three-dimensional microglia morphologies in mouse and human postmortem brain samples. *GLIA*, *67*(8), 1496–1509. https://doi.org/10.1002/glia.23623

Sande, A., & West, C. (2010). Traumatic brain injury: a review of pathophysiology and management. *Journal of Veterinary Emergency and Critical Care*, *20*(2), 177–190. https://doi.org/10.1111/j.1476-4431.2010.00527.x

Sanes, J. R., & Lichtman, J. W. (1999). DEVELOPMENT OF THE VERTEBRATE NEUROMUSCULAR JUNCTION. *Annual Review of Neuroscience*, *22*(1), 389–442. https://doi.org/10.1146/annurev.neuro.22.1.389

Santiago, L. Â. M., Oh, B. C., Dash, P. K., Holcomb, J. B., & Wade, C. E. (2012). A clinical comparison of penetrating and blunt traumatic brain injuries. *Brain Injury*, *26*(2), 107–125. https://doi.org/10.3109/02699052.2011.635363

Sawyer, E., Mauro, L. S., & Ohlinger, M. J. (2008). Amantadine Enhancement of Arousal and Cognition After Traumatic Brain Injury. *Annals Of Pharmacotherapy/˜The œAnnals Of Pharmacotherapy*, *42*(2), 247-252. https://doi.org/10.1345/aph.1k284

Schafer, D. P., Lehrman, E. K., & Stevens, B. (2012). The “quad-partite” synapse: Microglia-synapse interactions in the developing and mature CNS. *GLIA*, *61*(1), 24–36. https://doi.org/10.1002/glia.22389

Schafer, D. P., Lehrman, E. K., Kautzman, A. G., Koyama, R., Mardinly, A. R., Yamasaki, R., Ransohoff, R. M., Greenberg, M. E., Barres, B. A., & Stevens, B. (2012). Microglia sculpt postnatal neural circuits in an activity and Complement-Dependent manner. *Neuron*, *74*(4), 691–705. https://doi.org/10.1016/j.neuron.2012.03.026

Schecter, R. W., Maher, E. E., Welsh, C. A., Stevens, B., Erişir, A., & Bear, M. F. (2017). Experience-Dependent Synaptic Plasticity in V1 Occurs without Microglial CX3CR1. *˜ the œJournal of Neuroscience/˜ the œJournal of Neuroscience*, *37*(44), 10541–10553. https://doi.org/10.1523/jneurosci.2679-16.2017

Scott-Hewitt, N., Perrucci, F., Morini, R., Erreni, M., Mahoney, M., Witkowska, A., Carey, A., Faggiani, E., Schuetz, L. T., Mason, S., Tamborini, M., Bizzotto, M., Passoni, L., Filipello, F., Jahn, R., Stevens, B., & Matteoli, M. (2020). Local externalization of phosphatidylserine mediates developmental synaptic pruning by microglia. *EMBO Journal*, *39*(16). https://doi.org/10.15252/embj.2020105380

Sellgren, C. M., Sheridan, S. D., Gracias, J., Dong, X., Fu, T., & Perlis, R. H. (2016). Patient-specific models of microglia-mediated engulfment of synapses and neural progenitors. *Molecular Psychiatry*, *22*(2), 170-177. https://doi.org/10.1038/mp.2016.220

Sevenich, L. (2018). Brain-Resident microglia and Blood-Borne macrophages orchestrate central nervous system inflammation in neurodegenerative disorders and brain cancer. *Frontiers in Immunology*, *9*. https://doi.org/10.3389/fimmu.2018.00697

Shatz, C. J. (1990). Impulse activity and the patterning of connections during cns development. *Neuron*, *5*(6), 745–756. https://doi.org/10.1016/0896-6273(90)90333-b

Sheng, M., Sabatini, B. L., & Südhof, T. C. (2012). Synapses and Alzheimer's Disease. *Cold Spring Harbor Perspectives In Biology*, *4*(5), a005777. https://doi.org/10.1101/cshperspect.a005777

Shepherd, G. M. (1996). The dendritic spine: a multifunctional integrative unit. *Journal of Neurophysiology*, *75*(6), 2197–2210. https://doi.org/10.1152/jn.1996.75.6.2197

Shi, X., Bai, H., Wang, J., Wang, J., Huang, L., He, M., Zheng, X., Duan, Z., Chen, D., Zhang, J., Chen, X., & Wang, J. (2021). Behavioral assessment of sensory, motor, emotion, and cognition in rodent models of intracerebral hemorrhage. *Frontiers in Neurology*, *12*. https://doi.org/10.3389/fneur.2021.667511

Shiotsuki, H., Yoshimi, K., Shimo, Y., Funayama, M., Takamatsu, Y., Ikeda, K., Takahashi, R., Kitazawa, S., & Hattori, N. (2010). A rotarod test for evaluation of motor skill learning. *Journal of Neuroscience Methods*, *189*(2), 180–185. https://doi.org/10.1016/j.jneumeth.2010.03.026

Shultz, S. R., MacFabe, D. F., Foley, K. A., Taylor, R., & Cain, D. P. (2012). Sub-concussive brain injury in the Long-Evans rat induces acute neuroinflammation in the absence of behavioral impairments. *Behavioural Brain Research*, *229*(1), 145–152. https://doi.org/10.1016/j.bbr.2011.12.015

Silver, J. M., MD, McAllister, T. W., MD, & Arciniegas, D. B., MD. (2018). *Textbook of Traumatic Brain Injury, third edition*. American Psychiatric Pub.

Silver, J., McAllister, T. W., & Arciniegas, D. B. (2018). *Textbook of Traumatic Brain injury*. https://doi.org/10.1176/appi.books.9781615372645

Silverberg, N. D., & Iverson, G. L. (2011). Etiology of the post-concussion syndrome: Physiogenesis and psychogenesis revisited. *NeuroRehabilitation*, *29*(4), 317–329. https://doi.org/10.3233/nre-2011-0708

Simos, N. J., Manolitsi, K., Luppi, A. I., Kagialis, A., Antonakakis, M., Zervakis, M.,. . . Papadaki, E. (2022). Chronic Mild Traumatic Brain Injury : Aberrant Static and Dynamic Connectomic Features Identified Through Machine Learning Model Fusion. *Neuroinformatics*, *21*(2), 427-442. https://doi.org/10.1007/s12021-022-09615-1

Sipe, G. O., Lowery, R. L., Tremblay, M., Kelly, E., Lamantia, C., & Majewska, A. K. (2016). Microglial P2Y12 is necessary for synaptic plasticity in mouse visual cortex. *Nature Communications*, *7*(1). https://doi.org/10.1038/ncomms10905

Sivčo, P., Plančíková, D., Melichová, J., Rusňák, M., Hereitova, I., Beránek, V., Cibulka, R., & Majdán, M. (2023). Traumatic brain injury related deaths in residents and non-residents of 30 European countries: a cross-sectional study. *Scientific Reports*, *13*(1). https://doi.org/10.1038/s41598-023-34560-7

Soulet, D., & Rivest, S. (2008). Microglia. *CB/Current Biology*, *18*(12), R506–R508. https://doi.org/10.1016/j.cub.2008.04.047

Sozda, C. N., Hoffman, A. N., Olsen, A. S., Cheng, J. P., Zafonte, R., & Kline, A. E. (2010). Empirical Comparison of Typical and Atypical Environmental Enrichment Paradigms on Functional and Histological Outcome after Experimental Traumatic Brain Injury. *Journal of Neurotrauma*, *27*(6), 1047–1057. https://doi.org/10.1089/neu.2010.1313

Spence, K. W., & Lippitt, R. (1946). An experimental test of the sign-gestalt theory of trial and error learning. *Journal of Experimental Psychology*, *36*(6), 491–502. https://doi.org/10.1037/h0062419

Spiteri, C., Ponsford, J. L., Jones, H. L., & McKay, A. (2020). Comparing the Westmead Posttraumatic Amnesia Scale, Galveston Orientation and Amnesia Test, and Confusion Assessment protocol as measures of acute recovery following traumatic brain injury. *˜the œJournal of Head Trauma Rehabilitation/Journal of Head Trauma Rehabilitation*, *36*(3), 156–163. https://doi.org/10.1097/htr.0000000000000607

Stence, N., Waite, M., & Dailey, M. E. (2001). Dynamics of microglial activation: A confocal time-lapse analysis in hippocampal slices. *GLIA*, *33*(3), 256–266. https://doi.org/10.1002/1098-1136(200103)33:3

Stephan, A., Barres, B. A., & Stevens, B. (2012). The complement system: an unexpected role in synaptic pruning during development and disease. *Annual Review of Neuroscience*, *35*(1), 369–389. https://doi.org/10.1146/annurev-neuro-061010-113810

Steru, L., Chermat, R., Thierry, B., & Simon, P. (1985). The tail suspension test: A new method for screening antidepressants in mice. *Psychopharmacology/Psychopharmacologia*, *85*(3), 367–370. https://doi.org/10.1007/bf00428203

Stevens, B., Allen, N. J., Porta, L., Howell, G. R., Christopherson, K. S., Nouri, N., Micheva, K. D., Mehalow, A. K., Huberman, A. D., Stafford, B. K., Sher, A., Litke, A. M., Lambris, J. D., Smith, S. J., John, S. W. M., & Barres, B. A. (2007). The classical complement cascade mediates CNS synapse elimination. *Cell*, *131*(6), 1164–1178. https://doi.org/10.1016/j.cell.2007.10.036

Stopper, L., Bălşeanu, T. A., Cătălin, B., Rogoveanu, O. C., Mogoantă, L., & Scheller, A. (2018). Microglia morphology in the physiological and diseased brain - from fixed tissue to in vivo conditions. *PubMed*, *59*(1), 7–12. https://pubmed.ncbi.nlm.nih.gov/29940606

Stowell, R., Sipe, G. O., Dawes, R. P., Batchelor, H. N., Lordy, K. A., Whitelaw, B. S., Stoessel, M. B., Bidlack, J. M., Brown, E. A., Sur, M., & Majewska, A. K. (2019). Noradrenergic signaling in the wakeful state inhibits microglial surveillance and synaptic plasticity in the mouse visual cortex. *Nature Neuroscience*, *22*(11), 1782–1792. https://doi.org/10.1038/s41593-019-0514-0

Stratton, H. J., & Khanna, R. (2020). Sculpting Dendritic Spines during Initiation and Maintenance of Neuropathic Pain. *˜the œJournal of Neuroscience/˜the œJournal of Neuroscience*, *40*(40), 7578–7589. https://doi.org/10.1523/jneurosci.1664-20.2020

Subramanian, J., Savage, J. C., & Tremblay, M. (2020). Synaptic Loss in Alzheimer's Disease: Mechanistic Insights Provided by Two-Photon in vivo Imaging of Transgenic Mouse Models. *Frontiers In Cellular Neuroscience*, *14*. https://doi.org/10.3389/fncel.2020.592607

Sudwarts, A., & Thinakaran, G. (2023). Alzheimer's genes in microglia: a risk worth investigating. Molecular Neurodegeneration, 18(1). https://doi.org/10.1186/s13024-023-00679-4

Sun, L., & Barres, B. A. (2016). Glia get neurons in shape. *Cell*, *165*(4), 775–776. https://doi.org/10.1016/j.cell.2016.04.052

Sundaramurthy, A., Alai, A., Ganpule, S., Holmberg, A., Plougonven, E., & Chandra, N. (2012). Blast-Induced Biomechanical Loading of the rat: An experimental and anatomically accurate computational blast injury model. *Journal of Neurotrauma*, *29*(13), 2352–2364. https://doi.org/10.1089/neu.2012.2413

Suresh, S., Rajvanshi, P. K., & Noguchi, C. T. (2020). The Many Facets of Erythropoietin Physiologic and Metabolic Response. *Frontiers In Physiology*, *10*. https://doi.org/10.3389/fphys.2019.01534

Szalay, G., Martinecz, B., Lénárt, N., Környei, Z., Orsolits, B., Judák, L., Császár, E., Fekete, R., West, B. L., Katona, G., Rózsa, B., & Dénes, Á. (2016). Microglia protect against brain injury and their selective elimination dysregulates neuronal network activity after stroke. *Nature Communications*, *7*(1). https://doi.org/10.1038/ncomms11499

Tang, G., Gudsnuk, K., Kuo, S., Cotrina, M. L., Rosoklija, G., Sosunov, A. A., Sonders, M. S., Kanter, E., Castagna, C., Yamamoto, A., Yue, Z., Arancio, O., Peterson, B. S., Champagne, F. A., Dwork, A. J., Goldman, J. E., & Sulzer, D. (2014). Loss of MTOR-Dependent macroautophagy causes autistic-like synaptic pruning deficits. *Neuron*, *83*(5), 1131–1143. https://doi.org/10.1016/j.neuron.2014.07.040

Tani, J., Wen, Y., Hu, C., & Sung, J. (2022). Current and Potential Pharmacologic Therapies for Traumatic Brain Injury. *Pharmaceuticals*, *15*(7), 838. https://doi.org/10.3390/ph15070838

Tanila, H. (2018). Testing cognitive functions in rodent disease models : Present pitfalls and future perspectives. *Behavioural Brain Research*, *352*, 23-27. https://doi.org/10.1016/j.bbr.2017.05.040

Taylor, C. A., Bell, J. M., Breiding, M. J., & Xu, L. (2017). Traumatic Brain Injury–Related Emergency Department visits, hospitalizations, and deaths — United States, 2007 and 2013. *Morbidity and Mortality Weekly Report. Surveillance Summaries*, *66*(9), 1–16. https://doi.org/10.15585/mmwr.ss6609a1

Taylor, P. A., Ludwigsen, J. S., & Ford, C. C. (2014). Investigation of blast-induced traumatic brain injury. *Brain Injury*, *28*(7), 879–895. https://doi.org/10.3109/02699052.2014.888478

Taylor, S. E., Morganti-Kossmann, M. C., Lifshitz, J., & Ziebell, J. M. (2014). Rod Microglia: A morphological Definition. *PloS One*, *9*(5), e97096. https://doi.org/10.1371/journal.pone.0097096

Teasdale, G. M., Maas, A. I., Lecky, F., Manley, G. T., Stocchetti, N., & Murray, G. D. (2014). The Glasgow Coma Scale at 40 years: standing the test of time. *Lancet Neurology*, *13*(8), 844–854. https://doi.org/10.1016/s1474-4422(14)70120-6

Thierry, B., StRu, L., Simon, P., & Porsolt, R. (1986). The tail suspension test: Ethical considerations. *Psychopharmacology/Psychopharmacologia*, *90*(2). https://doi.org/10.1007/bf00181261

Thomas, D. G., Apps, J. N., Hoffmann, R. G., McCrea, M., & Hammeke, T. A. (2015). Benefits of Strict Rest After Acute Concussion : A Randomized Controlled Trial. *Pediatrics*, *135*(2), 213-223. https://doi.org/10.1542/peds.2014-0966

Titus, D. J., Furones, C., Atkins, C. M., & Dietrich, W. D. (2015). Emergence of cognitive deficits after mild traumatic brain injury due to hyperthermia. *Experimental Neurology*, *263*, 254–262. https://doi.org/10.1016/j.expneurol.2014.10.020

Tønnesen, J., Katona, G., Rózsa, B., & Nägerl, U. V. (2014). Spine neck plasticity regulates compartmentalization of synapses. *Nature Neuroscience*, *17*(5), 678–685. https://doi.org/10.1038/nn.3682

Tremblay, M., Lowery, R. L., & Majewska, A. K. (2010). Microglial Interactions with Synapses Are Modulated by Visual Experience. *PLoS Biology*, *8*(11), e1000527. https://doi.org/10.1371/journal.pbio.1000527

Tremblay, M., Stevens, B., Sierra, A., Wake, H., Bessis, A., & Nimmerjahn, A. (2011). The role of microglia in the healthy brain: figure 1. *˜the œJournal of Neuroscience/˜the œJournal of Neuroscience*, *31*(45), 16064–16069. https://doi.org/10.1523/jneurosci.4158-11.2011

Tucker, L. B., Burke, J. F., Fu, A. H., & McCabe, J. T. (2017). Neuropsychiatric Symptom Modeling in Male and Female C57BL/6J Mice after Experimental Traumatic Brain Injury. *Journal of Neurotrauma*, *34*(4), 890–905. https://doi.org/10.1089/neu.2016.4508

Tucker, L. B., Fu, A. H., & McCabe, J. T. (2016). Performance of male and female C57BL/6J mice on motor and cognitive tasks commonly used in Pre-Clinical Traumatic Brain Injury research. *Journal of Neurotrauma*, *33*(9), 880–894. https://doi.org/10.1089/neu.2015.3977

Ueno, M., & Yamashita, T. (2011). Kinematic analyses reveal impaired locomotion following injury of the motor cortex in mice. *Experimental Neurology*, *230*(2), 280–290. https://doi.org/10.1016/j.expneurol.2011.05.006

Van Der Vlegel, M., Polinder, S., Mikolić, A., Kaplan, R., Von Steinbüechel, N., Plass, A. M.,. . . Haagsma, J. A. (2021). The Association of Post-Concussion and Post-Traumatic Stress Disorder Symptoms with Health-Related Quality of Life, Health Care Use and Return-to-

Work after Mild Traumatic Brain Injury. *Journal Of Clinical Medicine*, *10*(11), 2473. https://doi.org/10.3390/jcm10112473

Van Praag, D., Cnossen, M. C., Polinder, S., Wilson, L., & Maas, A. I. (2019). Post-Traumatic Stress Disorder after Civilian Traumatic Brain Injury : A Systematic Review and Meta-Analysis of Prevalence Rates. *Journal Of Neurotrauma*, *36*(23), 3220-3232. https://doi.org/10.1089/neu.2018.5759

Van Spronsen, M., & Hoogenraad, C. C. (2010). Synapse pathology in Psychiatric and Neurologic disease. *Current Neurology and Neuroscience Reports*, *10*(3), 207–214. https://doi.org/10.1007/s11910-010-0104-8

Vasudevan, E., Glass, R. N., & Packel, A. (2014). Effects of Traumatic Brain Injury on Locomotor Adaptation. *Journal Of Neurologic Physical Therapy*, *38*(3), 172-182. https://doi.org/10.1097/npt.0000000000000049

Wahab, R. A., Neuberger, E. J., Lyeth, B. G., Santhakumar, V., & Pfister, B. J. (2015). Fluid percussion injury device for the precise control of injury parameters. *Journal of Neuroscience Methods*, *248*, 16–26. https://doi.org/10.1016/j.jneumeth.2015.03.010

Waites, C. L., Craig, A. M., & Garner, C. C. (2005). MECHANISMS OF VERTEBRATE SYNAPTOGENESIS. *Annual Review of Neuroscience*, *28*(1), 251–274. https://doi.org/10.1146/annurev.neuro.27.070203.144336

Wake, H., Moorhouse, A. J., Jinno, S., Kohsaka, S., & Nabekura, J. (2009). Resting microglia directly monitor the functional state of SynapsesIn vivoand determine the fate of ischemic terminals. *˜the œJournal of Neuroscience/˜the œJournal of Neuroscience*, *29*(13), 3974–3980. https://doi.org/10.1523/jneurosci.4363-08.2009

Walcott, B. P., Kahle, K. T., & Simard, J. M. (2012). Novel treatment targets for cerebral edema. *Neurotherapeutics*, *9*(1), 65–72. https://doi.org/10.1007/s13311-011-0087-4

Walsh, R. N., & Cummins, R. A. (1976). The open-field test: A critical review. *Psychological Bulletin*, *83*(3), 482–504. https://doi.org/10.1037/0033-2909.83.3.482

Warkentin, J., & Carmichael, L. (1939). A study of the development of the Air-Righting reflex in cats and rabbits. *˜the œPedagogical Seminary and Journal of Genetic Psychology*, *55*(1), 67–80. https://doi.org/10.1080/08856559.1939.10533184

Warwick, C. A., Keyes, A., Woodruff, T. M., & Usachev, Y. M. (2021). The complement cascade in the regulation of neuroinflammation, nociceptive sensitization, and pain. *Journal Of Biological Chemistry/˜The œJournal Of Biological Chemistry*, *297*(3), 101085. https://doi.org/10.1016/j.jbc.2021.101085

Wasilczuk, A. Z., Maier, K. L., & Kelz, M. B. (2018). The mouse as a model organism for assessing anesthetic sensitivity. In *Methods in enzymology on CD-ROM/Methods in enzymology* (pp. 211–228). https://doi.org/10.1016/bs.mie.2018.01.008

Weinhard, L., Di Bartolomei, G., Bolasco, G., Machado, P., Schieber, N. L., Neniskyte, U., Exiga, M., Vadisiute, A., Raggioli, A., Schertel, A., Schwab, Y., & Gross, C. (2018). Microglia remodel synapses by presynaptic trogocytosis and spine head filopodia induction. *Nature Communications*, *9*(1). https://doi.org/10.1038/s41467-018-03566-5

Witkowski, E., Gao, Y., Gavsyuk, A. F., Maor, I., DeWalt, G. J., Eldred, W. D.,. . . Davison, I. G. (2019). Rapid Changes in Synaptic Strength After Mild Traumatic Brain Injury. *Frontiers In Cellular Neuroscience*, *13*. https://doi.org/10.3389/fncel.2019.00166

Wolf, S., Boddeke, H., & Kettenmann, H. (2017). Microglia in physiology and disease. *Annual Review of Physiology*, *79*(1), 619–643. https://doi.org/10.1146/annurev-physiol-022516-034406

Woodrow, R., Winzeck, S., Luppi, A. I., Kelleher-Unger, I., Spindler, L. R. B., Wilson, J. T. L.,. . . Stamatakis, E. A. (2023). Acute thalamic connectivity precedes chronic post-concussive

symptoms in mild traumatic brain injury. *Brain*, *146*(8), 3484-3499. https://doi.org/10.1093/brain/awad056

Wu, Y., Dissing-Olesen, L., MacVicar, B. A., & Stevens, B. (2015). Microglia : Dynamic Mediators of Synapse Development and Plasticity. *Trends In Immunology*, *36*(10), 605-613. https://doi.org/10.1016/j.it.2015.08.008

Xiao, H., Yang, Y., Xi, J., & Chen, Z. (2015). Structural and functional connectivity in traumatic brain injury. *Neural Regeneration Research/Neural Regeneration Research*, *10*(12), 2062. https://doi.org/10.4103/1673-5374.172328

Xiong, Y., Mahmood, A., & Chopp, M. (2013). Animal models of traumatic brain injury. *Nature Reviews. Neuroscience*, *14*(2), 128–142. https://doi.org/10.1038/nrn3407

y Cajal, S. R. (1888). *Estructura de los centros nerviosos de las aves*.

Young, L. A., Rule, G., Bocchieri, R. T., & Burns, J. M. (2015). Biophysical Mechanisms of Traumatic Brain Injuries. *Seminars In Neurology*, *35*(01), 005-011. https://doi.org/10.1055/s-0035-1544242

Younger, D. S. (2023). Mild traumatic brain injury and sports-related concussion. Dans *Handbook of clinical neurology (Print)* (p. 475-494). https://doi.org/10.1016/b978-0-323-98817-9.00001-6

Yuste, R., & Majewska, A. (2001). Book review: On the Function of Dendritic Spines. *Neuroscientist*, *7*(5), 387–395. https://doi.org/10.1177/107385840100700508

Zagórska, A., Través, P. G., Lew, E. D., Dransfield, I., & Lemke, G. (2014). Diversification of TAM receptor tyrosine kinase function. *Nature Immunology*, *15*(10), 920–928. https://doi.org/10.1038/ni.2986

zHalalmeh, D. R., Salama, H. Z., LeUnes, E., Feitosa, D., Ansari, Y., Sachwani-Daswani, G., & Moisi, M. (2024). The Role of Neuropsychology in Traumatic Brain Injury: Comprehensive Literature Review. *World Neurosurgery*, *183*, 128-143. https://doi.org/10.1016/j.wneu.2023.12.069

Zhao, Q., Zhang, J., Li, H., Li, H., & Xie, F. (2023). Models of traumatic brain injury-highlights and drawbacks. *Frontiers In Neurology*, *14*. https://doi.org/10.3389/fneur.2023.1151660

Zheng, R., Lee, K., Qi, Z., Wang, Z., Xu, Z., Wu, X., & Mao, Y. (2022). Neuroinflammation Following Traumatic Brain Injury : Take It Seriously or Not. *Frontiers In Immunology*, *13*. https://doi.org/10.3389/fimmu.2022.855701

Zhu, F., Skelton, P. M., Chou, C. C., Mao, H., Yang, K. H., & King, A. I. (2012). Biomechanical responses of a pig head under blast loading : a computational simulation. *International Journal For Numerical Methods In Biomedical Engineering*, *29*(3), 392-407. https://doi.org/10.1002/cnm.2518

Ziebell, J. M., Taylor, S. E., Cao, T., Harrison, J. L., & Lifshitz, J. (2012). Rod microglia: elongation, alignment, and coupling to form trains across the somatosensory cortex after experimental diffuse brain injury. *Journal of Neuroinflammation*, *9*(1). https://doi.org/10.1186/1742-2094-9-247

Ziv, N. E., & Smith, S. J. (1996). Evidence for a role of dendritic filopodia in synaptogenesis and spine formation. *Neuron*, *17*(1), 91–102. https://doi.org/10.1016/s0896-6273(00)80283-4

Zuo, Y., Lin, A., Chang, P., & Gan, W. (2005). Development of Long-Term dendritic spine stability in diverse regions of cerebral cortex. *Neuron*, *46*(2), 181–189. https://doi.org/10.1016/j.neuron.2005.04.001

Заорска, A., Través, P. G., Lew, E. D., Dransfield, I., & Lemke, G. (2014). Diversification of TAM receptor tyrosine kinase function. *Nature Immunology*, *15*(10), 920-928. https://doi.org/10.1038/ni.2986

List of publications

Almir Aljovic*, Shuqing Zhao***, Maryam Chahin**, Clara de la Rosa, Valerie Van Steenbergen, Martin Kerschensteiner & Florence M. Bareyre. A deep learning-based toolbox for Automated Limb Motion Analysis (ALMA) in murine models of neurological disorders. Commun Biol. 2022;5(1):131.

Laura Empl*, Alexandra Chovsepian*, **Maryam Chahin**, Wing Yin Vanessa Kan, Julie Fourneau, Valérie Van Steenbergen, Sanofer Weidinger, Maite Marcantoni, Alexander Ghanem, Peter Bradley, Karl Klaus Conzelmann, Ruiyao Cai, Alireza Ghasemigharagoz, Ali Ertürk, Ingrid Wagner, Mario Kreutzfeldt, Doron Merkler, Sabine Liebscher & Florence M. Bareyre. Selective plasticity of callosal neurons in the adult contralesional cortex following murine traumatic brain injury. Nat Commun. 2022;13(1):2659.

Valérie Van Steenbergen, Laura Burattini*, Michelle Trumpp*, Julie Fourneau, Almir Aljović, **Maryam Chahin**, Hanseul Oh, Marta D'Ambra, Florence M. Bareyre; Coordinated neurostimulation promotes circuit rewiring and unlocks recovery after spinal cord injury. *J Exp Med* 6 March 2023; 220 (3)

Maryam Chahin, Julius Mutschler, Stephanie P Dzhuleva, Clara Dieterle, Leidy Reyes Jimenez, Valerie Van Steenbergen and Florence M Bareyre. Repetition of brain concussions drives microglia-mediated engulfment of presynaptic excitatory input associated with cognitive and anxiety perturbations. Submitted 2024

** These authors contributed equally to the manuscript*

(in Munich/München, date/ Datum) (Unterschrift/ Signature)

Author contributions

Article 1

Almir Aljovic*, Shuqing Zhao***, Maryam Chahin**, Clara de la Rosa, Valerie Van Steenbergen, Martin Kerschensteiner & Florence M. Bareyre. A deep learning-based toolbox for Automated Limb Motion Analysis (ALMA) in murine models of neurological disorders. Commun Biol. 2022;5(1):131.

** These authors contributed equally to the manuscript*

Author contributions:

F.B., A.A., and S.Z. designed the experiments. A.A., C.R., and M.C. performed all surgical procedures. A.A., S.Z., and V.V. collected and analyzed the data. F.B., A.A., S.Z., and M.K. wrote the manuscript.

My contribution to this publication in detail:

For this paper, I was involved in generating mice model of moderate traumatic brain injury and in the performance of all required surgical procedures. To be more specific, I carried the anaesthesia of those mice, the craniotomy, the brain injury using an impactor directly onto the brain parenchyma, the awakening and the monitoring of the mice subsequently to the injury.

Article 2

Laura Empl*, Alexandra Chovsepian*, Maryam Chahin, Wing Yin Vanessa Kan, Julie Fourneau, Valérie Van Steenbergen, Sanofer Weidinger, Maite Marcantoni, Alexander Ghanem, Peter Bradley, Karl Klaus Conzelmann, Ruiyao Cai, Alireza Ghasemigharagoz, Ali Ertürk, Ingrid Wagner, Mario Kreutzfeldt, Doron Merkler, Sabine Liebscher & Florence M. Bareyre. Selective plasticity of callosal neurons in the adult contralesional cortex following murine traumatic brain injury. Nat Commun. 2022;13(1):2659.

** These authors contributed equally to the manuscript*

Author contributions:

F.M.B. designed the experiments. L.E., A.C., M.C., W.Y.V.K. contributed all surgical procedures. L.E., A.C., M.C., W.Y.V.K., S.W., V.V.S., J.F., M.M. collected and analyzed data. A.G., P.B., and K.K.C. contributed rabies viruses. R.C., A.G., A.E. contributed clearing experiments. M.C., W.I.V.K., and S.L. contributed calcium imaging and analysis. I.W., M.K., and D.M. analyzed cell density in the cortex and performed paraffin-embedded immunohistochemistry. L.E., A.C., S.L., and F.M.B. wrote the paper.

My contribution to this publication in detail:

For this paper, I was involved in designing experiments as well as contributing to the surgical procedures, inducing moderate traumatic brain injury on mice through a craniotomy and the placement of cranial windows. The injured mice also underwent chronic in vivo recording with the use of two-photon microscope in order to record dendritic spine dynamic. I also performed the analysis of the dendritic spine morphology using NeuronStudio. I also did stereotaxic brain viral tracer injection to label transcallosal neuron and CST neurons. Apart from data collection, I contributed to analysis and data quantifications. The data collection consisted of sacrificing the mice that underwent injuries as well as their controls to extract their brain. I participated in the brain tissue processing that was used for immunohistochemistry, notably to evaluate the lesion volume following moderate TBI. With the generation of calcium imaging two-photon recording of mice that underwent moderate TBI, I analysed, using a custom-written matlab code, calcium intensity within integral neuron using manually drawn regions of interest (ROIs).

Article 3

Repetition of brain concussions drives microglia-mediated engulfment of presynaptic excitatory input associated with cognitive and anxiety perturbations.

Maryam Chahin, Julius Mutschler, Stephanie P Dzhuleva, Clara Dieterle, Leidy Reyes Jimenez, Valerie Van Steenbergen and Florence M Bareyre

The current manuscript was submitted to Cellular and Molecular Life Science in April 2024.

Author contributions:

Design of experiments: FB, MC, JM 748 Surgical procedures: MC, JM 749 Data collection and analysis: MC,JM,CD,LJ,SPD, VVS 750 Figures: FB; SPD 751 Manuscript writing: FB, MC.

My contribution to this publication in detail:

For this manuscript, I was the main researcher and have performed all animal experiments for the experiments mentioned below. Furthermore, I contributed to the writing and editing of the manuscript.

Article 4

Valérie Van Steenbergen, Laura Burattini*, Michelle Trumpp*, Julie Fourneau, Almir Aljović, **Maryam Chahin**, Hanseul Oh, Marta D'Ambra, Florence M. Bareyre; Coordinated neurostimulation promotes circuit rewiring and unlocks recovery after spinal cord injury. *J Exp Med* 6 March 2023; 220 (3)

** These authors contributed equally to the manuscript*

Author contributions:

Van Steenbergen: Conceptualization, methodology, validation, formal analysis, investigation, writing—original draft, writing—review and editing, visualization, supervision, funding acquisition. L. Burattini: Validation, formal analysis, investigation, writing—review and editing. M. Trumpp: Validation, formal analysis, investigation, writing—review and editing. J. Fourneau: Methodology, validation, formal analysis, investigation, writing—review and editing, funding acquisition. A. Aljović: Methodology, data curation, validation, formal analysis, investigation, writing—review and editing. M. Chahin: Validation, formal analysis, investigation, writing—review and editing. H. Oh: Validation, formal analysis, investigation, writing—review and editing. M. D'Ambra: Validation, formal analysis, investigation, writing—review and editing. F.M. Bareyre: Conceptualization, methodology, validation, resources, writing—original draft, writing—review and editing, visualization, supervision, project administration, funding acquisition.

My contribution to this publication in detail:

For this study, my participation included the writing, the reviewing and the editing of the manuscript. Beforehand, I contributed to the surgery implying brain injection for the labelling of the CST.

Eidesstattliche Versicherung/Affidavit

Maryam Chahin
(Studierende/Student)

Hiermit versichere ich an Eides statt, dass ich die vorliegende Dissertation Traumatic brain injury: a binding condition in search of solutions selbstständig angefertigt habe, mich außer der angegebenen keiner weiteren Hilfsmittel bedient und alle Erkenntnisse, die aus dem Schrifttum ganz oder annähernd übernommen sind, als solche kenntlich gemacht und nach ihrer Herkunft unter Bezeichnung der Fundstelle einzeln nachgewiesen habe.

I hereby confirm that the dissertation Traumatic brain injury: a binding condition in search of solutions is the result of my own work and that I have only used sources or materials listed and specified in the dissertation.

München/ Munich

02/07/2024 **Maryam Chahin**

Licences and Copyrights

ELSEVIER LICENSE
TERMS AND CONDITIONS

Sep 10, 2024

This Agreement between Maryam Chahin ("You") and Elsevier ("Elsevier") consists of your license details and the terms and conditions provided by Elsevier and Copyright Clearance Center.

License Number	5834140990947
License date	Jul 22, 2024
Licensed Content Publisher	Elsevier
Licensed Content Publication	Brain Research Reviews
Licensed Content Title	Dendritic spine plasticity—Current understanding from in vivo studies
Licensed Content Author	Graham Knott,Anthony Holtmaat
Licensed Content Date	Aug 1, 2008
Licensed Content Volume	58
Licensed Content Issue	2
Licensed Content Pages	8
Start Page	282
End Page	289
Type of Use	reuse in a thesis/dissertation
Portion	figures/tables/illustrations
Number of figures/tables/illustrations	1
Format	both print and electronic
Are you the author of this Elsevier article?	No
Will you be translating?	No
Title of new work	TRAUMATIC BRAIN INJURY: A BINDING CONDITION IN SEARCH OF SOLUTIONS
Institution name	LMU Munich
Expected presentation date	Sep 2024
Order reference number	2
Portions	Fig.3
The Requesting Person / Organization to Appear on the License	Maryam Chahin
Requestor Location	Mrs. Maryam Chahin an der würmleiten 5B Gräfelfing, 82166 Germany Attn: Mrs. Maryam Chahin
Publisher Tax ID	GB 494 6272 12
Total	**0.00 EUR**
Terms and Conditions	

INTRODUCTION

1. The publisher for this copyrighted material is Elsevier. By clicking "accept" in connection with completing this licensing transaction, you agree that the following terms and conditions apply to this transaction (along with the Billing and Payment terms

ELSEVIER LICENSE TERMS AND CONDITIONS

Sep 10, 2024

This Agreement between Maryam Chahin ("You") and Elsevier ("Elsevier") consists of your license details and the terms and conditions provided by Elsevier and Copyright Clearance Center.

License Number	5865271424210
License date	Sep 10, 2024
Licensed Content Publisher	Elsevier
Licensed Content Publication	The Lancet Neurology
Licensed Content Title	Cognitive decline in older adults with a history of traumatic brain injury
Licensed Content Author	Laura Moretti,Irene Cristofori,Starla M Weaver,Aileen Chau,Jaclyn N Portelli,Jordan Grafman
Licensed Content Date	Dec 1, 2012
Licensed Content Volume	11
Licensed Content Issue	12
Licensed Content Pages	10
Start Page	1103
End Page	1112
Type of Use	reuse in a thesis/dissertation
Portion	figures/tables/illustrations
Number of figures/tables/illustrations	1
Format	both print and electronic
Are you the author of this Elsevier article?	No
Will you be translating?	No
Title of new work	TRAUMATIC BRAIN INJURY: A BINDING CONDITION IN SEARCH OF SOLUTIONS
Institution name	LMU Munich
Expected presentation date	Sep 2024
Order reference number	4
Portions	Figure 1.
The Requesting Person / Organization to Appear on the License	Maryam Chahin

SPRINGER NATURE LICENSE TERMS AND CONDITIONS

Sep 10, 2024

This Agreement between Maryam Chahin ("You") and Springer Nature ("Springer Nature") consists of your license details and the terms and conditions provided by Springer Nature and Copyright Clearance Center.

License Number	5834141428621
License date	Jul 22, 2024
Licensed Content Publisher	Springer Nature
Licensed Content Publication	Nature Reviews Neuroscience
Licensed Content Title	Mechanisms governing activity-dependent synaptic pruning in the developing mammalian CNS
Licensed Content Author	Travis E. Faust et al
Licensed Content Date	Sep 20, 2021
Type of Use	Thesis/Dissertation
Requestor type	academic/university or research institute
Format	print and electronic
Portion	figures/tables/illustrations
Number of figures/tables/illustrations	1
Would you like a high resolution image with your order?	no
Will you be translating?	no
Circulation/distribution	1 - 29
Author of this Springer Nature content	no
Title of new work	TRAUMATIC BRAIN INJURY: A BINDING CONDITION IN SEARCH OF SOLUTIONS
Institution name	LMU Munich
Expected presentation date	Sep 2024
Order reference number	3
Portions	Fig.4
The Requesting Person / Organization to Appear on the License	Maryam Chahin

SPRINGER NATURE LICENSE TERMS AND CONDITIONS

Sep 10, 2024

This Agreement between Maryam Chahin ("You") and Springer Nature ("Springer Nature") consists of your license details and the terms and conditions provided by Springer Nature and Copyright Clearance Center.

License Number	5834140735453
License date	Jul 22, 2024
Licensed Content Publisher	Springer Nature
Licensed Content Publication	Nature Reviews Neuroscience
Licensed Content Title	Animal models of traumatic brain injury
Licensed Content Author	Ye Xiong et al
Licensed Content Date	Jan 18, 2013
Type of Use	Thesis/Dissertation
Requestor type	academic/university or research institute
Format	print and electronic
Portion	figures/tables/illustrations
Number of figures/tables/illustrations	1
Would you like a high resolution image with your order?	no
Will you be translating?	no
Circulation/distribution	1 - 29
Author of this Springer Nature content	no
Title of new work	TRAUMATIC BRAIN INJURY: A BINDING CONDITION IN SEARCH OF SOLUTIONS
Institution name	LMU Munich
Expected presentation date	Sep 2024
Order reference number	1
Portions	Figure1.a Figure1.d Figure1.e
The Requesting Person / Organization to Appear on the License	Maryam Chahin

SPRINGER NATURE LICENSE TERMS AND CONDITIONS

Sep 02, 2025

This Agreement between Maryam Chahin ("You") and Springer Nature ("Springer Nature") consists of your license details and the terms and conditions provided by Springer Nature and Copyright Clearance Center.

License Number	6100781389780
License date	Sep 02, 2025
Licensed Content Publisher	Springer Nature
Licensed Content Publication	Nature Reviews Disease Primers
Licensed Content Title	Traumatic brain injuries
Licensed Content Author	Kaj Blennow et al
Licensed Content Date	Nov 17, 2016
Type of Use	Thesis/Dissertation
Requestor type	academic/university or research institute
Format	print and electronic
Portion	figures/tables/illustrations
Number of figures/tables/illustrations	1
Would you like a high resolution image with your order?	no
Will you be translating?	no
Circulation/distribution	1 - 29
Author of this Springer Nature content	no
Title of new work	TRAUMATIC BRAIN INJURY: A BINDING CONDITION IN SEARCH OF SOLUTIONS
Institution name	LMU Munich
Expected presentation date	Sep 2025
Portions	Box 1 in page 3
The Requesting Person / Organization to Appear on the License	Maryam Chahin

Outlook

Re: Permission to republish material

From permissions <permissions@thejns.org>
Date Tue 02/09/2025 16:33
To Maryam Chahin

Dear Maryam,

> Non-exclusive permission is granted to Maryam Chahin at no charge for use in their thesis, provided proper credit is given as determined by style guidelines of the publisher of the new work, or by some accepted style such as AP or Chicago. Please save this communication as proof of permission grant.

Please be aware—in addition to the reference to our publication, the figure legend requires the inclusion of the below language:

> "Regarding maps, reproduced with permission from OpenStreetMap Contributors, CC BY-SA 2.0 (http://www.openstreetmap.org/copyright). "

Best of luck on your thesis!

Gillian

Gillian Shasby
permissions@thejns.org

> On Sep 2, 2025, at 9:35 AM, Maryam Chahin
>
> Dear JNS journal,
>
> I am a phd student and I am requesting the permission to use a figure from this article :**Dewan, M. C., Rattani, A., Gupta, S., Baticulon, R. E., Hung, Y., Punchak, M., Agrawal, A., Adeleye, A. O., Shrime, M. G., Rubiano, A. M., Rosenfeld, J. V., & Park, K. B. (2019). Estimating the global incidence of traumatic brain injury.** ***Journal of Neurosurgery*****, *130*(4), 1080-1097. https://doi.org/10.3171/2017.10.JNS17352**

Acknowledgements

This doctoral journey has been a transformative experience, and I owe my deepest gratitude to all the people who have supported me along the way.

First and foremost, I am very grateful to my supervisor, PD. Dr. Florence Bareyre, for the chance that was given to me to work in her lab. Her guidance has been instrumental in shaping both my research and personal growth which have challenged me to thrive for more. I thank her for her expertise, constant availability, which is not given to most of the students. And I would like to especially thank her for helping me in the last steps towards handing my thesis, which was very helpful.

I would like to thank Prof. Dr. Martin Kerschensteiner for allowing me to be part of his institute and for the wise feedback given during the lab meetings and institute meetings presentation of my PhD project.

I would like to thank all my TAC members for accepting to be part of my TAC committee, for your feedback and clear guidance on my project and for your availability.

I would like to express my deepest gratitude to the GSN office, Stephanie, Karin and the other members, for being extremely helpful and understanding, especially at the end stage of my PhD. Thank you very much. I would like to thank the CAM facility for their help throughout my whole PhD.

A special thanks goes to Clara, Julius, Stephanie, Leonard, whose dedication and hard work have had a tremendous impact on the progress of this project. As interns, your contributions went above and beyond. Your innovative ideas and diligent efforts played a crucial role in advancing the research of this project. The progress we achieved together is a testimony to your assets and commitment.

I would like to thank my former and current colleagues from the Bareyre's lab. Thank you to Almir, Julie for their collaborative spirit and support during all those years. Thank you to Luca and Max for being great colleagues but even better friends. I also extend my gratitude to the people that are currently and have once been part of the Kerschensteiner Lab; Paula, Daniel, Yi-Heng and all my fellow researchers who have created a supportive and enjoyable atmosphere throughout this journey. Thank you to XiaoQian and Vanessa for being supportive and kind to help me for IT related matters, your invaluable help will never be forgotten.

A very special thanks goes to Valerie. You tremendously contributed to my journey and helped me reach this significant milestone in my academic career. You helped me awaken and sharpen my scientific critical mind and my ethic. Your support, guidance, and encouragement have been invaluable, and I am truly blessed to have encountered you and to have made a friend for life.

Thanks to Leidy for becoming such a precious friend and a motivation. You always have made yourself available for me and I cannot be enough thankful for that.

I extend my heartfelt appreciation to Ida, Tino, Elise, Meryem, Ali, and all those whose names may not be mentioned here but have nonetheless played a significant role in my journey. Whether through a word of encouragement, a gesture of kindness, or a moment of inspiration, your contributions have not gone unnoticed and have made a lasting impact on my academic and personal growth.

To my friends Segolene, Aminata, and Houda, my heartfelt thanks go out to each of you for your constant support since many years now. Thank you for always being there when I needed it the most. From our 3-hour phone calls to our memorable trips, thank you for always bringing me to tears of laughter and joy, even if we were apart. That has been truly priceless. I cherish our bond and sincerely trust that our friendship lasts forever.

Ich möchte Sabine Mader meinen tiefsten und herzlichsten Dank aussprechen. Sie sind ein einzigartiger und außergewöhnlicher Mensch. Ich hätte nie gedacht, dass ich, als ich nach Deutschland kam, eine so wunderbare Person treffen würde, und wie wir uns oft gegenseitig sagen, war es vorherbestimmt, dass wir uns über den Weg laufen. Ich werde dir nie genug für die Hilfe, die Unterstützung, die Ermutigung und das Vertrauen danken können, dass du mir entgegengebracht hast. Du bist selbst eine solche Inspiration und ich bin gesegnet, dich in meinem Leben zu haben. Du wirst immer in meinem Herzen sein und immer zu meiner Familie gehören. Ich danke dir aus tiefstem Herzen für alles.

Dominik, ich bin zutiefst dankbar, dass ich dich kennengelernt habe und für deine unerschütterliche Unterstützung während der letzten Jahre meiner Doktorarbeit. Ihre Anwesenheit und Ermutigung während des gesamten Prozesses der Erstellung der Dissertation waren von unschätzbarem Wert. Du hast mir Mut gemacht und mir geholfen, Hindernisse zu überwinden. Für all das danke ich Ihnen von ganzem Herzen und Ich werde dich immer in meinem Herzen tragen.

I would like to thank my family for always being supportive in every step I have undertaken. Thank you to my sister for inspiring me, at her young age, to thrive for more and for always being there throughout the years. Thank you to my brothers for you unwavering support and your joyfulness. I love you all and will forever carry you in my heart.

Et pour conclure, Papa, Maman, je ne pourrais jamais vous remercier assez pour tous les sacrifices que vous ayez pu faire à notre égard. Quitter un pays, ces racines avec des rêves pour en adopter un autre et reconstruire une nouvelle vie n'a pas était facile mais vous vous êtes battus et vous êtes parvenues aux aspirations que vous vous étiez fixés. Merci de nous avoir montrer et appris à être tolérant, bienveillant, patient et à être résilient. Comme le dit si bien François Rabelais 'tout vient à point à qui sait attendre'. Papa, Maman je suis immensément fière de vous, fière de l'éducation que vous nous avez octroyé, fière que vous ayez eu une confiance aveugle quant à mes choix et mes ambitions, et fière que vous ayez tout simplement cru en moi. Je vous aime.

Merci pour tout